

Dissertation zur Erlangung des Doktorgrades der  
Fakultät für Chemie und Pharmazie der Ludwig-Maximilians-Universität München

---

# **Cytoplasmic protein aggregates interfere with nucleo-cytoplasmic transport of protein and RNA**

*Designed  $\beta$ -sheet proteins and their structural properties  
reveal novel toxicity mechanisms  
in a gain-of-function model of protein misfolding diseases*

---

**Andreas Christian Wörner**

*aus Stuttgart, Germany*

2016



## **Erklärung**

Diese Dissertation wurde im Sinne von § 7 der Promotionsordnung vom 28. November 2011 von Herrn Prof. Dr. Franz Ulrich Hartl betreut.

## **Eidesstattliche Versicherung**

Diese Dissertation wurde eigenständig und ohne unerlaubte Hilfe erarbeitet.

München, den 23. Juni 2016

Andreas Wörner

Dissertation eingereicht am 23. Juni 2016

1. Gutachter: Prof. Dr. Franz Ulrich Hartl

2. Gutachter: PD Dr. Dietmar Martin

Mündliche Prüfung am 11. Juli 2016







# Acknowledgements

Studying in your laboratory, Prof. Dr. F. Ulrich Hartl, was a great experience and privilege. I highly appreciate to have worked in such an excellent environment, offering such a highly international atmosphere and profound expertise. I admire your overwhelming curiosity and persisting search for answers to great scientific questions and hidden challenges. Thank you for your trust and great freedom, which allowed me to develop and pursue this project over so many years.

Especially, I want to thank my supervisors Dr. Mark-Steffen Hipp and Dr. Martin Vabulas for so many valuable discussions, and for your scientific, experimental, and editorial guidance.

The scientific Munich offers a great multi-disciplinary and collaborative environment. I am very grateful for the close, complementing cooperation with Prof. Dr. Jörg Tatzelt and Prof. Konstanze Winklhofer, as well as for your steady scientific support. I thank Prof. Dr. Matthias Mann and Daniel Hornburg for your expertise in proteome analysis. Prof. Dr. Wolfgang Baumeister, Dr. Harald Engelhardt, and Oana Mihalache, thank you for your support in recording electron micrographs and FTIR spectra of our amyloid fibrils. I want to express my gratitude to Prof. Dr. Rüdiger Klein, Dr. Irina Dudanova, and Katharina Schulz-Trieglaff, for your experience in neuronal systems and your support in the preparation of neuronal samples.

Dr. Heidi Olzscha, you have already worked intensely on the  $\beta$  proteins before I joined the team. Thank you for your great collegiality and the supportive working atmosphere. Dr. Li Rebekah Feng, thank you for your persevering effort to transfer our experiments into neuronal systems. I thank Dr. Frédéric Frottin, for your spontaneous efforts during the revision of our publication. Thank you, Dr. Ulrike Resenberger and Dr. Maria Patra, for your interest in the  $\beta$  proteins, and for giving me the chance to participate in your studies on the human prion protein.

Thank you, Dr. Dietmar Martin, for co-referring this dissertation. I further thank Prof. Dr. Walter Neupert, Prof. Dr. Jörg Tatzelt, Prof. Dr. Dieter Edbauer, Prof. Dr. Klaus Förstemann, and Prof. Dr. Nediljko Budisa, Prof. Dr. Matthias Mann, and Prof. Dr. Karl-Peter Hopfner, for your dedicated participation in my dissertation and thesis advisory committees.

I want to express my gratitude to Emmanuel Burghardt, Albert Ries, Nadine Wischnewski, Verena Marcus, Ana Jungclaus, Romy Lange, Elisabeth Schreil, Peter Nagy, Andreas Scaia, and Bernd Grampp for your skilled technical support in all possible situations we experienced together in the laboratory. Dr. Stephan Uebel, Dr. Martin Spitaler, Ralf Zenke, and Elisabeth Wehyer-Stingl from the core facility, thank you for your technical experience and helpful support. A big thank you for your administrative support to Evelyn Frey-Royston, Darija Pompino, Silke Leuze-Bütün, and Andrea Obermayr-Rauter.

I was very glad for having such great “co-perpetrators”, thank you Florian Rübmann, Matthias Antonin, Christian Löw, Yury Kukushkin, Sneha Kumar, Itika Saha, Rajat Gupta, Lisa Vinzenz-Donnelly, Swasti Raychaudhuri, Karsten Klage, Young-Jun Choe, Rashmi Gupta and Sathish Kumar Lakshmiopathy, Kristina Popova, Min Zheng, Andreas Bracher, Courtney Klaips, Niti Kumar, and Hannah Girstmair, for creating the atmosphere that finally made our daily lab-life enjoyable. Thanks to all members of the scientific community inside and outside of the Hartl department I met during those years during plentiful discussions and numerous evenings of fun and laughter.

For the opportunity to meet so many new colleagues and friends through the various IMPRS events I thank Dr. Hans Joerg Schaeffer, Dr. Ingrid Wolf, Maximiliane Reif, and Dr. Amy Gerc, as well as for the organization of retreats, workshops, seminars, lectures, barbecues and get-togethers.

Ganz besonders herzlichen Dank an Leslie Ripaud, meinen Eltern Dr. Jörg und Irmgard Wörner, sowie meiner ganzen Familie für Eure vorbehaltlose Ermutigung, Unterstützung und Geduld über all die Jahre hinweg.

# Abstract

Protein misfolding and aggregation are linked to various forms of dementia and amyloidoses, such as Alzheimer's, Parkinson's, and Creutzfeldt Jakob diseases. Although the primary misfolding proteins are disease-specific and structurally diverse, the related disorders share numerous symptoms and cellular malfunctions. A sustainable cure remains so far out of reach.

The highly complex nature of the associated cellular deficiencies challenges our understanding of primary causes and consequences in the disease progression. To focus on the toxic properties and pathogenic gain-of-function mechanisms of misfolded structures in cells, we applied a set of artificial  $\beta$  proteins directly folding into amyloid-like oligomers and fibrils. Amyloid-related proteotoxicity appeared sequence-dependently in human, murine neuronal, fungal, and bacterial cells. The interplay between elevated surface hydrophobicity and structural disorder among the  $\beta$  proteins and their cellular interactors was critical for toxicity. Small distributed oligomers correlated to elevated toxicity.

Protein-rich plaques or misfolded assemblies appear in patients often simultaneously in different cellular compartments and in the extracellular space. To analyze site-specific toxicities and vulnerabilities, we targeted the  $\beta$  proteins specifically into distinct compartments. Aggregation in the cytoplasm was highly toxic and interfered with active nucleo-cytoplasmic transport in both directions, including the translocation of NF- $\kappa$ B and mRNA. We compared our results to human disease-associated mutants of Huntingtin, TDP-43, and Parkin, causing comparable transport defects. Remarkably, toxicity of the  $\beta$  proteins was strongly reduced when targeted to the nucleus. Aggregates localized in dense nucleolar foci caused no transport inhibition. Only protein aggregation in the cytoplasm led to sequestration and mislocalization of numerous proteins with extended disordered regions, including factors involved in nucleo-cytoplasmic transport of proteins and mRNA (importin  $\alpha$  and THOC proteins). Nuclear  $\beta$  proteins in contrast behaved very inert, potentially being shielded by nucleolar factors such as nucleophosmin (NPM-1).

In presence of cytoplasmic aggregation vital signaling processes were impaired, further destabilizing cellular homeostasis. The mRNA accumulated in enlarged "nuclear RNA bodies". Depletion of cytoplasmic mRNA consequently resulted in a reduction of protein synthesis. Impairment of nucleo-cytoplasmic transport caused by cytoplasmic protein aggregation may thus seriously aggravate the cellular pathology initiated by misfolding and aggregation in human amyloid diseases. Our findings suggest that novel therapeutic strategies may improve nucleo-cytoplasmic transport, utilize the nuclear proteostasis for aggregate removal, or increase the cellular resilience towards misfolded structures in general.



# Zusammenfassung

Proteinmissfaltung und -aggregation wird mit neurodegenerativen Krankheiten wie Alzheimer, Parkinson und der Creutzfeldt-Jakob-Krankheit, sowie mit systemischen Amyloidosen in Verbindung gebracht. Auch wenn sich anfangs die Hauptbestandteile der Proteinaggregate krankheitsspezifisch unterscheiden, so kommt es bei den verschiedenen Demenzerkrankungen doch oft zu ähnlichen Symptomen und zellulären Fehlfunktionen. Eine nachhaltige Heilung ist bisher nicht möglich.

Die Komplexität der auftretenden zellulären Fehlfunktionen erschwert eine klare Unterscheidung von primären Ursachen sowie deren Folgen und Nebenwirkungen. Um uns auf die toxischen Eigenschaften und die toxische Wirkung von missgefalteten Strukturen in Zellen zu konzentrieren, setzen wir eine Reihe von künstlichen  $\beta$  Proteinen ein, welche direkt amyloide Oligomere und Aggregate bilden. Die Toxizität der  $\beta$  Proteine trat sequenzabhängig in menschlichen, neuronalen, Pilz- und Bakterienzellen auf. Erhöhte Hydrophobie an der Proteinoberfläche und unstrukturierte Sequenzbereiche wurden als kritische strukturelle Merkmale der  $\beta$  Proteine und ihrer zellulären Interaktionspartner im Zusammenhang zur Toxizität identifiziert. Auch korrelierten kleinere, über das Zytoplasma verteilte Oligomere mit hoher Toxizität.

Proteinaggregate treten in Patienten in verschiedenen Kompartimenten der Zelle und im extrazellulären Raum auf, oft an mehreren Stellen gleichzeitig. Um die Toxizität in verschiedenen Kompartimenten und deren Sensibilitäten zu untersuchen, schickten wir die  $\beta$  Proteine mittels Signalsequenzen gezielt in bestimmte zelluläre Kompartimente. Aggregation im Zytoplasma war hochtoxisch und störte den aktiven Transport zwischen Zytoplasma und Zellkern, einschließlich der Translokation von NF- $\kappa$ B und mRNA. Wir reproduzierten unsere Ergebnisse mit krankheitsassoziierten Mutanten von Huntingtin, TDP-43 und Parkin, welche vergleichbare Transportdefekte verursachten. Bemerkenswerterweise reduzierte sich die Toxizität der  $\beta$  Proteine stark, wenn sie in den Zellkern geschickt wurden. Hier sammelten sich die  $\beta$  Proteine in dichten Aggregaten in den Nukleoli. Dabei traten keine Transportprobleme auf. Nur Proteinaggregation im Zytoplasma verursachte (Ko-)Aggregation und Fehllokalisation zahlreicher zellulärer Proteine, besonders von solchen mit längeren unstrukturierten Bereichen. Dazu zählten auch Faktoren, welche den Transport von Proteinen und mRNA zwischen Zytoplasma und Zellkern vermitteln (Importin  $\alpha$  und THOC Proteine). Die  $\beta$  Proteine im Zellkern verhielten sich im Gegensatz sehr unauffällig. Anscheinend wurden sie zusätzlich durch nukleoläre Faktoren wie Nukleophosmin (NPM-1) abgeschirmt.

Aggregation im Zytoplasma beeinträchtigte die Übermittlung lebenswichtiger zellulärer Signale, was die zelluläre Homöostase weiter destabilisierte. Die mRNA hat sich dabei in vergrößerten „nukleären RNA Körperchen“ angesammelt. Die fehlende mRNA im Zytoplasma führte zu einer Abnahme der Proteinsynthese. Die von Proteinaggregaten verursachten Defekte im molekularen Transport zwischen Zytoplasma und Zellkern könnten so ernsthaft zur Verschlimmerung der zellulären Funktionsfähigkeit in neurodegenerativen und anderen Proteinfehlfaltungserkrankungen beitragen. Neue Therapieansätze könnten in einer Verbesserung des Kerntransports, in einer Verminderung von Aggregaten durch Proteostasisysteme im Zellkern, oder in einer generellen Stärkung der zellulären Resilienz gegenüber fehlgefalteten Proteinen zu finden sein.



# Table of contents

<b>ABSTRACT</b>	<b>VIII</b>
<b>ZUSAMMENFASSUNG</b>	<b>IX</b>
<b>FOREWORD</b>	<b>1</b>
<b>INTRODUCTION</b>	<b>3</b>
<b>Molecular forces in protein folding</b>	<b>3</b>
Ionic bonds	3
Van der Waals forces	3
Hydrogen bonds	3
Covalent bonds	4
<b>Water structure and hydrophobic effect – key drivers of protein folding</b>	<b>5</b>
The hydrophobic effect	6
Stability-flexibility equilibrium of protein structures	6
<b>Cellular protein folding – and its challenges</b>	<b>8</b>
Proteins fold into three-dimensional structures	8
Diversity of folding – superfast folders, molten globules, complex folding pathways	9
Molecular chaperones promote protein folding in a cellular environment	10
Protein misfolding causes toxicity in cells – loss- and gain-of-function	11
<b>Structural features of misfolded assemblies: oligomers &amp; amyloid fibrils</b>	<b>13</b>
Functional amyloids and non-chromosomal inheritance by prions	13
Sequence effects on amyloid formation	13
Oligomeric assemblies and the multiplicity of protein states	14
<b>Molecular chaperones</b>	<b>16</b>
Cellular protein biosynthesis	16
Chaperones guarding the nascent chain	16
Chaperone networks for folding, maintenance, and degradation	17
The multifunctional Hsp 70/Hsp40 system	17
Chaperonins – single molecule folding chambers	18
The Hsp90 chaperone family of activators and regulators	19
Disaggregases – chaperones reversing aggregation	19
Small heat shock proteins	20
<b>Protein degradation as part of the proteostasis network</b>	<b>21</b>
The ubiquitin-proteasome-system (UPS)	21
A multifaceted network of ubiquitin ligases rules over the fate of proteins	21
The proteasome – regulated protein destruction	22
Endoplasmic reticulum-associated degradation (ERAD)	23
Bulk and chaperone-mediated autophagy	24
<b>Maintaining and restoring proteostasis under misfolding stress</b>	<b>25</b>
Heat shock response	25
Unfolded protein response (UPR)	25

The mitochondrial unfolded protein response (UPRmt)	26
<b>Neurodegenerative protein misfolding diseases</b>	<b>27</b>
Dementia	27
Alzheimer's disease	28
Signaling and structural functions of the amyloid precursor protein (APP)	28
Processing of APP, production of A $\beta$ variants, and related pathophysiology	28
Cytoplasmic neurofibrillary tangles and cytoplasmic APP cleavage products	29
Amyloid cascade hypothesis	30
The impact of cholesterol and other lipids on Alzheimer's disease	30
Missing links in Alzheimer's disease	30
Huntington's disease	31
Biological function of full length Huntingtin and amyloid formation	33
Parkinson's disease	33
<b>Nucleo-cytoplasmic transport of proteins and RNAs</b>	<b>35</b>
Subcellular compartmentalization and proteostasis	35
Nuclear envelope and nuclear pores	35
Nucleo-cytoplasmic targeting of proteins	37
Nuclear import	37
Nuclear export	37
The Ran cycle	38
Messenger RNA processing and nuclear export	38
<b>Designed <math>\beta</math> proteins as experimental model to investigate molecular mechanisms behind neurodegenerative diseases</b>	<b>41</b>
<b>AIMS OF THIS STUDY</b>	<b>43</b>
<b>RESULTS</b>	<b>44</b>
<b>Designed <math>\beta</math> proteins</b>	<b>44</b>
<b>Artificial <math>\beta</math> proteins are cytotoxic in <i>E. coli</i></b>	<b>44</b>
Structural modifications affect toxicity	45
<b><math>\beta</math> proteins are purified from <i>E. coli</i> inclusion bodies</b>	<b>47</b>
Concentration and purity of the $\beta$ proteins	48
<b>Structural properties of the <math>\beta</math> proteins</b>	<b>49</b>
Amyloid-like oligomers and fibrils revealed by transmission electron microscopy	49
CD spectroscopy demonstrates $\beta$ -sheet secondary structure	51
FTIR spectroscopy confirms amyloid-like nature	53
<b>Amyloid properties and aggregation kinetics</b>	<b>55</b>
$\beta$ proteins bind classical and novel amyloid sensors – in correlation with toxicity	55
$\beta$ proteins contain hydrophobic surface patches – in correlation with toxicity	57
$\beta$ proteins refold rapidly and spontaneously – with highly similar kinetics	58
ANS, Thioflavin T, and NIAD-4 differentiate between monomers, oligomers, and fibrils	61
$\beta$ proteins bind anti-amyloid oligomer (A11) antibody	63
$\beta$ proteins interact directly with Hsp110 – quantitatively correlating with toxicity	64

<b>Purified <math>\beta</math> proteins are cytotoxic on addition to human cells</b>	<b>65</b>
Sonicated $\beta$ proteins are more hydrophobic	66
Extracellular $\beta$ proteins induce neurotoxic signaling by the cellular prion protein	67
<b><math>\beta</math> proteins are highly toxic in the human cytoplasm</b>	<b>69</b>
$\beta$ proteins are highly toxic in the cytoplasm, and less toxic in the nucleus	69
$\beta$ protein-EGFP fusions remain toxic	71
Nuclear $\beta$ protein levels are slightly higher than cytoplasmic	72
<b>Diverse cytoplasmic aggregates distort the nuclear pore complex</b>	<b>73</b>
<b>Nuclear <math>\beta</math> proteins associate with nucleoli and scatter around the nuclear envelope</b>	<b>76</b>
Nuclear $\beta$ protein aggregates remain intact during cell division	78
<b>Increased solubility of <math>\beta</math> proteins in the cytoplasm</b>	<b>80</b>
Oligomers of intermediate-molecular-weight in the cytoplasm	82
Major aggregates are stable and immobile in cytoplasm and nucleus (FRAP)	84
Structural differences of $\beta$ protein assemblies forming in cytoplasm or nucleus	85
<b>Cytoplasmic <math>\beta</math> proteins suppress induction of the cytosolic stress response – nuclear <math>\beta</math> proteins (partially) induce a response</b>	<b>86</b>
<b>Interactions between proteostasis sensors and <math>\beta</math> proteins in the cytoplasm, molecular exclusion in the nucleus</b>	<b>88</b>
<b>Inhibition of the proteasome causes a collapse of nuclear proteostasis</b>	<b>91</b>
<b>Cytoplasmic <math>\beta</math> proteins, Htt96Q, TDP-F4, and Parkin<math>\Delta</math>C inhibit nuclear translocation of NF-<math>\kappa</math>B</b>	<b>93</b>
Processing upstream of NF- $\kappa$ B is functional in cells expressing $\beta$ proteins	96
<b>Cytoplasmic <math>\beta</math> proteins, Huntingtin96Q, and Parkin<math>\Delta</math>C interfere with general nucleo-cytoplasmic protein transport</b>	<b>97</b>
<b>Cytoplasmic aggregation of importin <math>\alpha</math> proteins</b>	<b>101</b>
<b>Nuclear mRNA accumulation in cells with cytoplasmic protein aggregation</b>	<b>102</b>
Isolation and quantification confirms diminished cytoplasmic mRNA	106
Proteasomal inhibition induces nuclear mRNA accumulation	107
mRNA disturbances in the R6/2 Huntington's disease mouse model	108
Low apoptosis signaling in 9 week old R6/2 mice	111
<b>Cytoplasmic mislocalization and aggregation of RNA exporter THOC2</b>	<b>112</b>
siRNA-induced silencing of the transcriptional export complex protein THOC2	114
Aggravated nuclear mRNA bodies in cells with pathogenic protein aggregation	115
<b>Cytoplasmic <math>\beta</math> proteins inhibit the cellular protein synthesis</b>	<b>117</b>
<b>Translation initiation factors (eIFs) are trapped into cytoplasmic <math>\beta</math> protein aggregates</b>	<b>118</b>
<b>Outlook: <math>\beta</math> proteins targeted to mitochondria are toxic and cause mitochondrial swelling</b>	<b>119</b>

<b>DISCUSSION</b>	<b>122</b>
Rationally designed $\beta$ proteins are inherently toxic for cellular life	122
$\beta$ proteins structurally resemble natural amyloid proteins	123
Hydrophobic surfaces, conformational flexibility, and low-molecular-weight structures correlate with cellular toxicity	125
Aggregation and toxicity in cytoplasm and nucleus	128
Inhibition of NF- $\kappa$ B by cytoplasmic protein aggregation may shift the balance between neuronal life and death	129
General defects in nucleo-cytoplasmic protein transport	131
Interferences with nuclear mRNA export	131
Reduced cytoplasmic RNA and nucleolar volumes in dementia patients	133
Localization of Huntingtin aggregates in cell cultures, mouse models, and human patients	134
Cytoplasmic proteostasis – how does it promote misfolding and toxicity?	136
Protein folding environment in the cytoplasm – keeping unstable structures alive?	137
Efficient degradation or secluded deposition – a new role of the nucleus in proteostasis	137
Cellular transport systems – high susceptibility towards misfolding?	138
What makes neurons especially vulnerable?	140
Therapeutic strategies	142
A new role for the nucleus in the prevention of toxic protein aggregation?	142
Increasing proteostatic resilience	143
<b>EXPERIMENTAL PROCEDURES</b>	<b>144</b>
<b>Molecular genetics</b>	<b>144</b>
Expression systems	144
Sequence design	144
Agarose gel electrophoresis	145
Polymerase chain reaction (PCR)	145
Site-directed mutagenesis (mutations, insertions, and fusion proteins)	146
Molecular cloning (restriction, ligation)	147
Preparation and transformation of chemically competent <i>E. coli</i> cells	147
Plasmid preparation	147
<b>Protein purification</b>	<b>148</b>
De novo $\beta$ proteins	148
De novo $\alpha$ -helical protein $\alpha$ S824	148
Hsp110 (Hsp105)	148
<b>Protein analytics</b>	<b>149</b>
Determination of protein concentration	149
Discontinuous, denatured SDS-PAGE	149
Coomassie Brilliant Blue staining	150

Immunoblotting	150
Native dot blots for immunodetection of A11 reactive species	150
<b>Spectroscopy</b>	<b>151</b>
Fluorescence spectroscopy	151
Circular dichroism (CD) spectroscopy	151
Fourier transform infrared spectroscopy (FTIR)	151
Electron microscopy	152
<b>Human cells: culture and transfection</b>	<b>152</b>
Cultivation and passage of human cells	152
Cryopreservation	152
Determining cell numbers	152
Transient transfection by electroporation	153
Transient transfection by lipofection	153
<b>Confocal fluorescence microscopy</b>	<b>153</b>
Fixation and immunostaining of human cells	153
Confocal immunofluorescence and image acquisition	154
Fluorescence in situ hybridization (RNA FISH)	154
Fluorescence in situ hybridization on murine brain sections (RNA FISH)	154
Fixation and staining of mitochondrial matrix proteins	155
<b>Cellular experiments and assays</b>	<b>155</b>
Cytotoxicity measurements by MTT assay	155
Intracellular expression of $\beta$ proteins	155
Extracellular addition of purified $\beta$ proteins to the culture medium	155
<i>E. coli</i> growth inhibition	155
NF- $\kappa$ B activation and translocation	156
Compartmental quantification of S-GFP	156
THOC2 knockdown by siRNA	156
Cellular distribution of mRNA after proteasome inhibition by MG132	156
Single cell quantification of total polyA RNA	157
Absolute quantification of cytoplasmic mRNA	157
Solubility of cytoplasmic and nuclear $\beta$ proteins	158
Size exclusion chromatography of HEK293T lysates	158
Proteostasis sensors	158
FRAP (fluorescence recovery after photo bleaching)	158
<sup>35</sup> S-Met radioactive pulse labeling of newly translated proteins	159
Hsp70 promoter activation	159
Observing mitotic cells	159
<b>Statistics</b>	<b>159</b>
<b>Antibodies</b>	<b>160</b>
<b>Sequences of utilized constructs</b>	<b>161</b>
<b>LITERATURE</b>	<b>163</b>
<b>PUBLICATIONS</b>	<b>184</b>





# Foreword

Cells are the elementary units of life, comprising all forms of uni- and multicellular organisms, from bacteria and archaea over fungi and plants to animals. A healthy cell or organism contains the entire hereditary information to regulate all vital cellular functions in its natural environment, and for passing on this information to the next generation.

Cells originate from preexisting cells and create new life through cellular division (Robert Remak, Rudolf Virchow; Magner 2002). The first primordial cells, surrounded by a lipid membrane, formed presumably around 4 billion years ago on earth in terrestrial, anoxic fields (Mulkidjanian 2012). Basic inorganic chemicals and electric discharges were most likely enough to produce the first organic molecules of life: amino acids and nucleobases (Miller 1953, Miller 1959, Oro 1961).

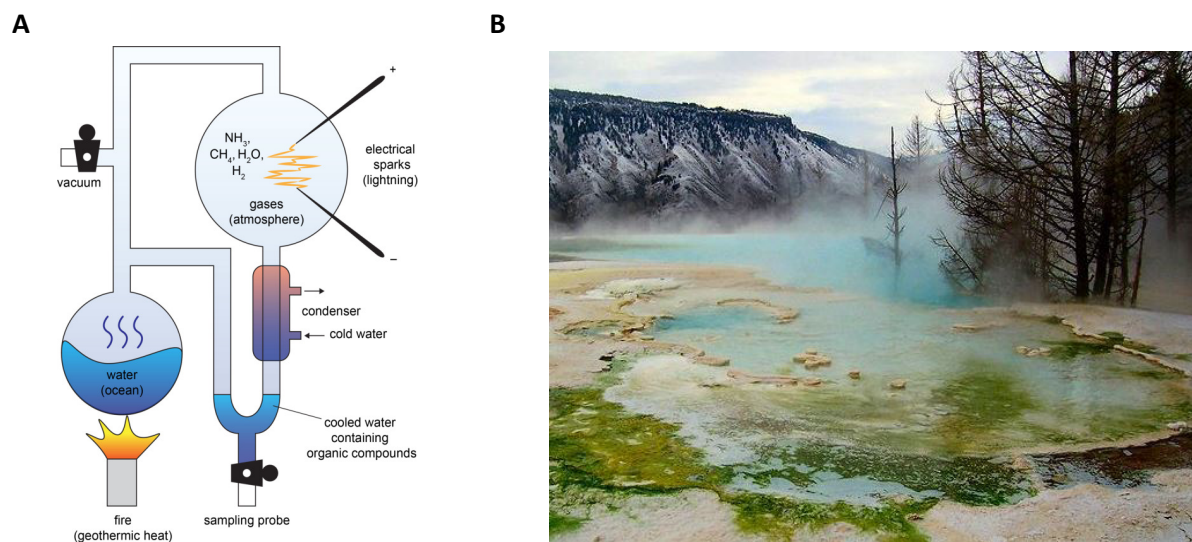


**Figure 1 | Creation of the first elements of life on earth in hot volcanic vents. (A)** Stanley Miller simulated in his famous “primordial soup” experiment conditions prevailing at hot geothermal springs on the young earth around four billion years ago. Heating water created a humid atmosphere containing methane, ammonia, water and hydrogen. Electrical discharges were run resembling those present on the forming earth. Intense UV-light created free radicals reacting further into small organic molecules. In the condensate, Miller found four amino acids (glycine, alanine, aspartic and glutamic acid) and a couple of organic molecules, such as formic acid, acetic acid, lactic acid, and urea (Miller, Science, 1953 and 1959). Later, improved electrical discharge experiments found a much higher variety of amino acids and organic chemicals (Johnson 2008 Science), including the ones discovered on a meteorite falling in Australia in 1969 (Ring 1972). **(B)** A volcanic vent in the Yellowstone National Park with geothermal springs similar to those, where presumably the first biomolecules and primordial cells originated billions of years ago (photo by Jeremy Doorten, stockxchng, 2007).

Cells assemble from different classes of biomolecules. The cellular DNA (deoxyribonucleic acid) contains the inheritable sequence information that is transcribed into different types of RNAs (ribonucleic acids). A part of them is subsequently translated into functional and structural proteins. In addition to the nucleic acid sequence, information is embodied in cells through the localization and activity of cellular factors (King 1999, Zhou 2004). Proteins are complex biomolecules synthesized by ribosomes that translate the sequence information encoded in an mRNA molecule into a polypeptide chain. Thereby, amino acids are polymerized in a linear chain like pearls in a necklace, selecting from more than 20 natural amino acids harboring different physicochemical properties in their side chains. As biochemical catalysts, proteins modify the cell by synthesis of

biomolecules, such as lipids, carbohydrates, and metabolites. Proteins are involved in sensing, transmitting, and regulating extra- and intracellular information. And proteins are cellular building blocks on their own (e.g. in membranes, cytoskeleton).

Unlike a pearl necklace, polypeptide chains are in large part not unstructured, flexible chains. Most proteins fold into defined three-dimensional structures in which they are active. Protein folding is caused by the molecular forces between the individual amino acids and their cellular environment. The density of factors within a cell is extremely high (around 300 mg/mL), perpetually resulting in interactions between the mostly solvated molecules.

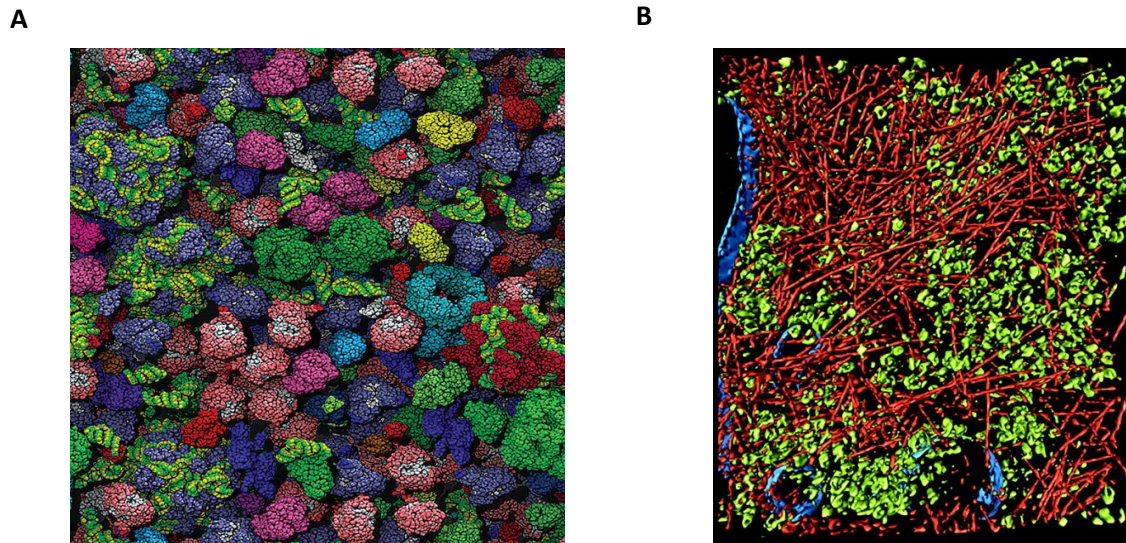


**Figure 2 | Crowding of biological macromolecules inside of a cell. (A)** Computer model of a bacterial cytoplasm including the most abundant macromolecules at experimentally determined concentrations (figure from McGuffee 2010). **(B)** Cytoplasmic macromolecular complexes (green), cytoskeleton (red) and membranes (blue) of a eukaryotic cell visualized by cryoelectron tomography (figure from Medalia 2002).

The high density of proteins and other biomolecules in a cell poses a permanent challenge to its proteome. Specific interactions permanently execute the elementary actions of life. Productive interactions have been selected during billions of years of evolution. At the same time, undesirable erroneous interactions need to be prevented, which is one major task of molecular chaperones.

Evolution, however, has not come to an end. Spontaneous genetic mutations occur constantly, introducing mostly adverse modifications into protein sequences. On some areas of life, evolution has less direct influence, such as at high, post-reproductive age (Lahdenpera 2004). Mutations and aging phenomena leading to protein misfolding and deleterious cellular interactions are believed to set the ground for numerous forms of dementia and other amyloidoses. In how many ways misfolded protein accumulations are harmful, and which mechanisms enable cells to keep aggregation under control, still remains insufficiently understood. I hope the insights gained in this study may contribute to a better understanding of the fundamental biology of proteins and proteotoxicity. At best, it may inspire future research on the therapy of prevalent human disorders, to provide human health and wellbeing.

# Introduction

## Molecular forces in protein folding

The molecular forces playing a role in protein folding are the same fundamental forces as for any other forms of molecular interactions within a cell. The mainly non-covalent interactions comprise electrostatic bonds, van der Waals forces, and hydrogen bonds, and are individually relatively weak and transient. As the free energy of protein folding usually lies in the range of a few non-covalent interactions (10-40 kJ/mol), every individual of them is very important and contributes to the final conformation of a folded protein (Pace 1975, Dill 1990).

### Ionic bonds

A number of amino acids contain charged chemical groups, which electrostatically attract or repulse each other. The force and the energy of these interactions are weakened immensely by the high polarity of water and the presence of salt ions in a cell. However, they can become very strong in the interior of a protein fold, or within cellular membranes. Shielding charged groups from the surrounding aqueous solvent can strengthen electrostatic forces up to 20 fold in biological systems. The energy of an ionic bond is described by  $E = q^+q^- / (\epsilon_0\epsilon_r r)$  ( $E$  = energy;  $q$  = charge;  $r$  = distance;  $\epsilon_0$  = electric field constant;  $\epsilon_r$  = relative dielectric field constant, in water 78.5 at 298K, within a protein down to  $\sim 4$ ). The strength of ionic bonds lies between 10-30 kJ/mol (Winter/Noll 1998, p. 5f). Posttranslational modifications of proteins, such as phosphorylation, acetylation, or methylation, can modify local charges and  $pK_A$  values and thereby induce conformational changes.

### Van der Waals forces

Van der Waals forces are an order of magnitude weaker than electrostatic interactions (1-4kJ/mol). They originate from fluctuations of electron density around atomic nuclei, creating temporary electrical dipole moments. These induce a similar asymmetry in neighboring atoms, leading to attractive interactions. Van der Waals forces are especially important when a number of atoms come very close together ( $r^6$  dependence,  $r$  = distance between dipoles). The forces integrate over many densely packed, sterically matching structures, as they occur inside a folded protein or in the carbohydrate chains of membrane lipids (Winter/Noll 1998. p. 6-8).

### Hydrogen bonds

Hydrogen bonds are a major stabilizer of secondary structures in proteins, and they coordinate the pairing of nucleotides in DNA and RNA structures (Winter/Noll 1998. p. 8f). Looking closer, hydrogen bonds originate in the relatively high electronegativity of an atom (in biomolecules mainly oxygen and nitrogen) covalently bound to hydrogen, creating a dipole along the bond. The partially positively charged hydrogen attracts partially negatively charged hydrogen bond acceptors. In proteins, hydrogen bonds are formed between the amide and carboxyl group of peptide bonds, but also among side chain residues. The hydrogen bonding potential of most donors and acceptors are satisfied in many natively folded structures (Stickle 1992).

In contrast to electrostatic interactions, the strength and energy of hydrogen bonds are highly angle- and distance-dependent, providing directionality during protein folding, in protein structures and among the interactions of proteins and ligands. Optimized during evolution, energetics and kinetics of hydrogen bond formation therefore allow the rapid folding of most proteins, conferring stability and providing specificity required for selective macromolecular interactions (Hubbard 2010).

## Covalent bonds

Cystein residues are able to covalently link different side chains within one or between two polypeptide chains. With the help of a reversible oxidizing agent (glutathione) two thiol groups (-SH) are coupled to disulfide bonds and thereby covalently link and conformationally restrict two otherwise much more flexible polypeptide regions. Disulfide bonds especially play a role in proteins residing within the endoplasmic reticulum, mitochondrial intermembrane space and the extracellular space, as in the cytoplasm reducing conditions are prevalent.

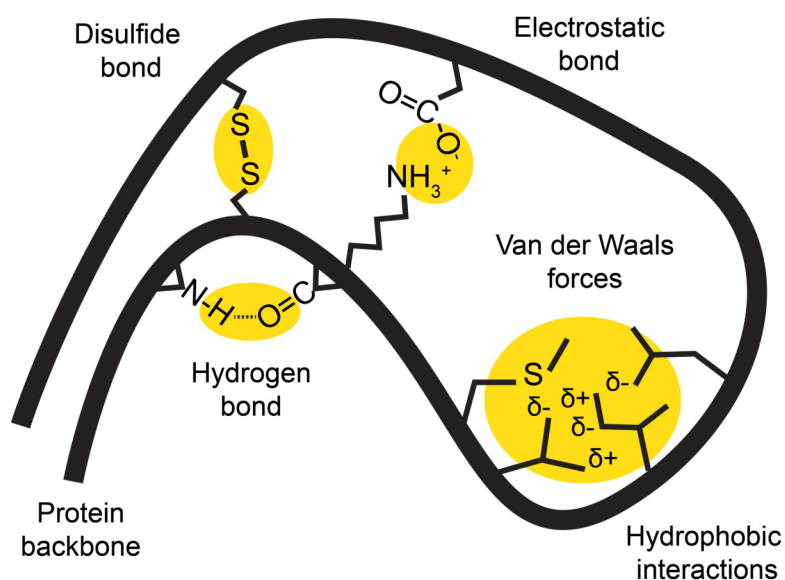


**Figure 3 | Molecular forces and bonds between amino acid residues of a polypeptide chain.** The intramolecular forces determine the conformational fold and the stability of a protein or a complex. This three-dimensional structure lays the foundation for enzymatic reactivity and interactions with other biomolecules in a cell.

## Water structure and hydrophobic effect – key drivers of protein folding

Life originated in water, presumably in anoxic geothermal fields containing high concentrations of  $K^+$ ,  $Zn^{2+}$ ,  $Mn^{2+}$ , and phosphate, resembling the internal milieu of present day cells (Mulikidjanian 2011). Water is the natural solvent, surrounding most biomolecules. The surfaces of proteins are in permanent contact to their water shells. Water even plays a coordinating or catalytic role in enzymes. Serine proteases have catalytically active water molecules in their active center (Perona 1993), and contain water channels securing substrate specificity due to the formation of hydrogen-bonded networks (Krem 1998). In the active center of Rubisco, water molecules coordinate an  $Mg^{2+}$  ion important for the stability of the overall structure (Matsumura 2012).

Water is a very special molecule. Its high polarity and its ability to form hydrogen bonded networks results in an unusually large heat capacity, elevated melting and boiling temperatures, an increased density after melting, a high thermal conductivity, and the phenomenon of surface tension (Levy 2006). When water forms hydrogen bonds (water-water or water-protein), energy is released in form of enthalpy, but the change in entropy is negative, since the free movement of water molecules becomes restricted (at room temperature  $\sim 80\%$  of possible hydrogen bonds are maintained). Similarly, a protein lowers its Gibbs energy upon folding into the native structure, but its own entropy decreases. However, proteins fold surrounded by water molecules that are very restricted in motion on the protein surface, but released upon compaction of the structure into higher entropy states. Protein folding energetics are therefore a complex balance act of the whole system, and often can be directed by external influences in one or another direction (Bryan 1992).

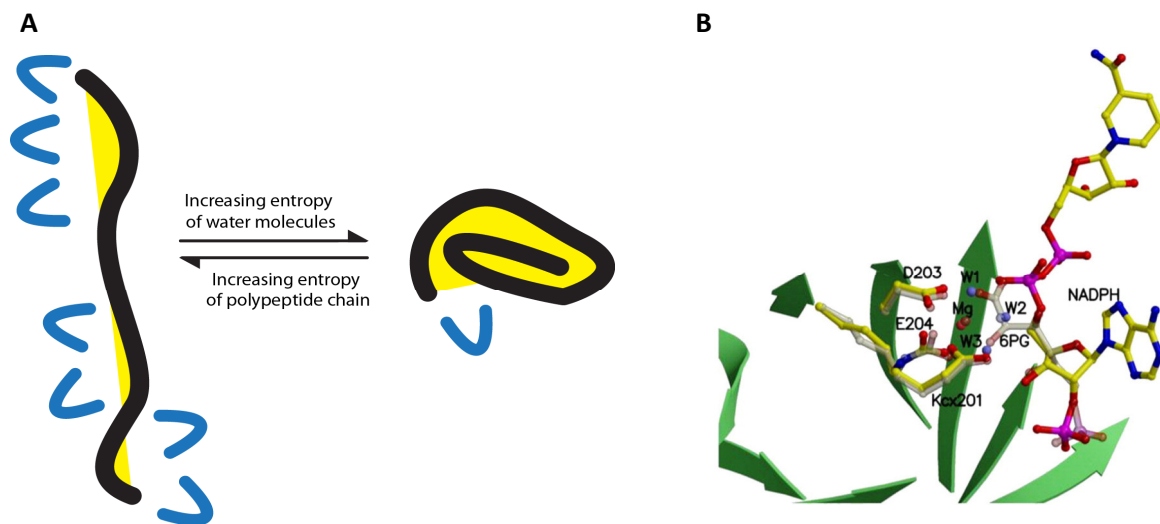


**Figure 4 | Entropy of water molecules and a polypeptide chain in the unfolded and in the folded state, and conserved structured water molecules in the center of Rubisco, coordinating substrate molecules. (A)** An unfolded polypeptide chain contains many surface accessible hydrophobic side chains, which disturb the water structure and create a shell of conformationally restricted water molecules. Upon folding, the hydrophobic amino acid residues are buried in the interior of the protein and release many structured water molecules into states of higher entropy, providing free energy for the folding process. **(B)** Twenty structured water molecules in the active center of Rubisco coordinate the binding of NADPH. Three of these water molecules (W1, W2, and W3) are thereby coordinated by a central  $Mg^{2+}$ -ion, which stabilizes the activated Rubisco structure, and directly interacts with bound 6-phosphogluconate (figure from Matsumura 2012).

## The hydrophobic effect

Water can form up to four hydrogen bonds in a tetrahedral fashion, leading to its ability to form three-dimensional hydrogen bonded networks and to its liquid nature under atmospheric pressure. In direct contact to nonpolar side chains or solutes, water loses its hydrogen bonding partners and orientates itself in a way to minimize the loss or distortion of residual hydrogen bonds. In the first and second hydration shell around such hydrophobic molecules, water therefore arranges in a constrained, entropically very unfavorable way, which consequently leads to the removal of hydrophobic molecules or groups from the water surface. This exclusion of hydrophobic surfaces from water is widely known as “hydrophobic effect”, and it is a major driver of protein folding (Bolen 2008, Dill 1990).

The hydrophobic effect directs extended amino acid chains to fold in a way that clusters its hydrophobic groups in the interior of a protein structure, which thereby compacts into its native three-dimensional conformation. The importance of the hydrophobic effect is further demonstrated by intrinsically unstructured proteins or protein segments that usually lack hydrophobic groups, but largely consist of charged and polar residues (Dyson 2005, Dunker 2008). However, water seems to be a poor solvent for the protein backbone itself (or polyglycine as a model system), driving even purely polar polypeptides into molten globule or folded states, which also contributes to the collapse of e.g. polyglutamine polypeptides (Tran 2008).

The importance of water structure for protein folding is furthermore demonstrated by both chaotropic reagents and water structure enhancers. Guanidinium hydrochloride or urea disturb the water structure and weaken the hydrophobic effect and backbone hydrogen bonding up to a point where proteins start to unfold (Zou 1998). TMAO (trimethylamine-N-oxide) enhances water structure and long-range spatial order, increasing the number and strength of hydrogen bonds per water molecule, which further discourages water-backbone interactions and stabilizes protein structures (Zou 2002).

## Stability-flexibility equilibrium of protein structures

Finally, temperature plays an important role in protein folding, as it affects water structure. The native fold of proteins usually evolved to be stable around the physiological temperatures of its organism. The stability-flexibility equilibrium is specifically balanced to allow precise conformational alterations during molecular recognition, catalysis, and degradation, and to facilitate the functional evolution of protein sequences (Somero 1995, Bloom 2004).

With higher temperature, higher kinetic energy states become accessible and entropy becomes more important ( $\Delta G = \Delta H - T\Delta S$ ). Entropy generally favors disorder, and proteins unfold usually cooperatively at their specific melting temperature. Lower temperature increases water structure, influencing the strength of the hydrophobic effect, which initially may stabilize protein structures, but also leads to cold denaturation of proteins (Dias 2010). Nature uses the different, although often compensating and yet only partially understood temperature dependences of enthalpy and entropy to specifically adapt protein stability and flexibility to the physiological conditions of its respective organisms.

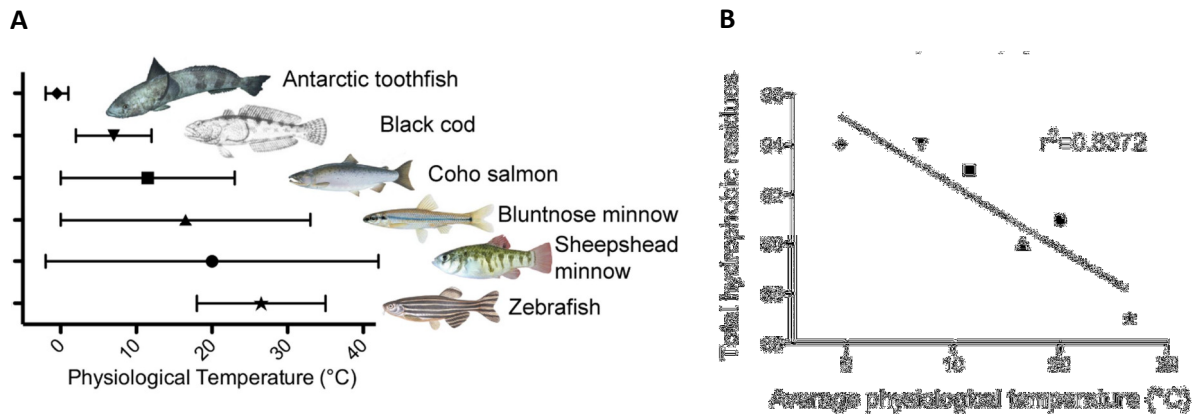


**Figure 5 | The number of hydrophobic residues within a protein ( $\alpha$ A-crystallin) correlates to the environmental temperature of different teleost fish species, adapting the thermal stability of the protein and its chaperone-like activity.** The number of hydrophobic residues reflects both, the stability of the protein influenced by the temperature dependent hydrophobic effect, as well as the surface hydrophobicity necessary for the chaperone-like activity of  $\alpha$ A-crystallin. **(A)** Physiological temperature ranges of different fish species (figure from Posner 2012). **(B)** Negative correlation between the total number of hydrophobic residues within  $\alpha$ A-crystallin and the average physiological temperature of the respective fishes (figure from Posner 2012).

Water structure and the hydrophobic effect are elementary for biological structures and interactions. The key drivers form phospholipid bilayers surrounding cells and cellular compartments, but they also cause the assembly of protein fibrils and aggregates, a usually undesirable side effect in living cells (Lazaridis 2013).

The physical forces explained here are simulated by “forcefields” in computer algorithms, describing specific energy potentials. Protein folding and dynamics is studied *in silico* with the ultimate goal of predicting three-dimensional structures, conformational dynamics, or the effect of small molecule drugs on protein structure and function (Dill 2012).

# Cellular protein folding – and its challenges

## Proteins fold into three-dimensional structures

Proteins, although being synthesized as a linear chain of amino acids, adopt specific three-dimensional structures to become active in a cellular environment. These functional structures are called the “native state”. In principal, the complete information about the three-dimensional arrangement is already present in the DNA sequence, encoding the exact amino acid sequence of a protein (Anfinsen’s dogma). As proteins are synthesized from 20 proteinogenic amino acids, the theoretical number of possible conformations of a polypeptide is enormous, way too large to fold into them serially (described by Cyrus Levinthal in 1969).

The folding of proteins, however, does not occur as a random process, but is directed by local molecular forces. These forces act within the protein itself, between the protein and its solvent, and, during its biogenesis *in vivo*, come from the ribosome, from molecular chaperones as well as the entire cellular surroundings. This includes other proteins, metabolites, salts, and water (Bryan 1992). Protein folding is therefore highly dependent on the local environment, on molecular crowding, and the local ionic composition (Zimmerman 1991; see Levy 2006 p. 9). Excluded volume effects influence protein folding rates and equilibria. Molecular crowding and confinement generally increase the rates of slow, transition-state-limited associations and decreasing the rates of fast, diffusion-limited association reactions (Zimmerman 1991, Zhou 2008).

The amino acid sequence itself, therefore, determines the structure of a protein only in context of the prevailing conditions.

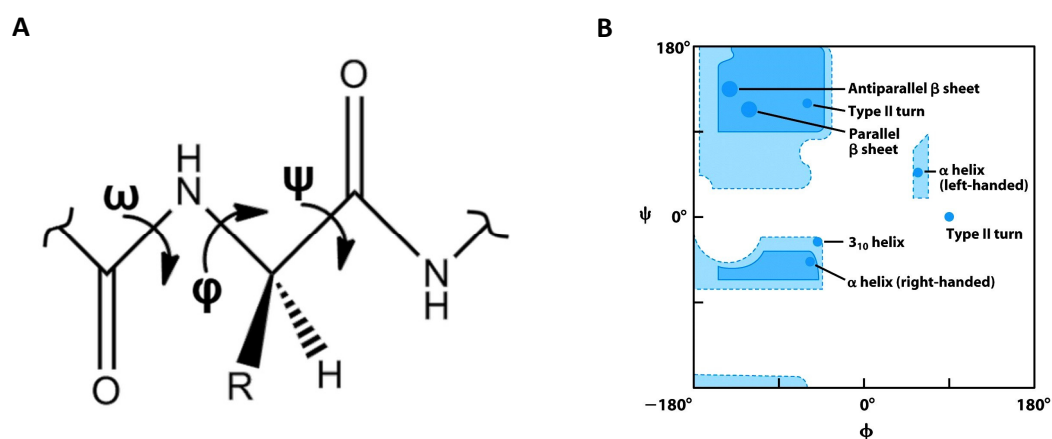


**Figure 6 | Steric confinements of the polypeptide torsion angles result in favorable regular conformations. (A)** Next to the planar peptide bond ( $\omega = 180^\circ$ ), torsion angles of  $\pm 60^\circ$  and  $\pm 45^\circ$  for  $\phi$  and  $\psi$  are sterically most favored (Siegel 2011; figure from <https://www.quora.com/Why-are-most-alpha-helices-in-proteins-right-handed>). **(B)** Naturally occurring  $\phi$  and  $\psi$  angles are plotted in a Ramachandran plot and reveal common secondary structures (figure from Principles of Biochemistry, Pearson Prentice Hall, 2006). The chiral nature of L- amino acids mostly hinders the formation of left-handed  $\alpha$ -helices due to bulky residues (besides glycine). Planar  $\beta$ -sheets exist in a parallel or antiparallel alignment.

A fully flexible polypeptide chain could in principle fold into an almost indefinite number of conformations. However, polypeptide chains sterically and energetically prefer specific orientations, which lead to a limited number of common geometrical secondary structures. Due to the planar peptide bond ( $\omega = 180^\circ/0^\circ$ ), every amino acid in a polypeptide chain orientates itself by two torsion angles ( $\phi$ ,  $\psi$ ) towards the previous and the following residue. Steric limitations within the chain



energetically favor distinct bond angles, others only rarely occur. Conformations of neighboring residues from protein crystal structures are summarized in a Ramachandran plot (Ramachandran 1963). The right-handed  $\alpha$ -helix as well as parallel and antiparallel  $\beta$ -sheets are the most common secondary structures, next to special conformations such as the collagen triple-helix, the left-handed  $\alpha$ -helix, the  $3_{10}$ - or the  $\pi$ -helix.

Energy landscapes describe the conformational space and the kinetic barriers of a protein under its specific conditions. Changes in the local environment modify the folding pathways, creating new downhill routes or altering kinetic barriers, so that proteins fold into different accessible states. Modifying local chemistry influences the conformational directions of a protein fold. Thereby, molecular chaperones can change the energetic landscape and the downhill routes towards states of lower energy. Changes in the energy landscapes are realized through the elementary forces described above. This can happen through direct cellular interactions, influences on water structure and dynamics, or the local ion composition. Chaperones modulate folding directions by mechanisms such as binding and release, iterative annealing, or steric confinement (Brinker 2001, Jewett 2004, Kovacs 2005).

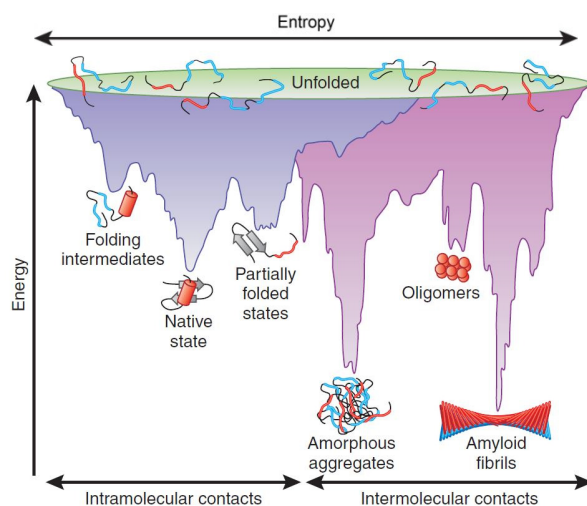


**Figure 7 | Energy landscape of protein folding and aggregation.** An ensemble of unfolded, fluctuating conformations at high energy levels are found at the top of the folding funnel. The polypeptides quickly collapse into states of lower energy, such as molten globules. Partially folded states and folding intermediates reside in local energy minima, before they successively adjust their intramolecular contacts into the native state. Achieving intermolecular contacts, especially between incompletely folded polypeptides, may cause misfolding into oligomeric states, amorphous aggregates, or very stable, highly ordered amyloid fibrils. All these misfolded structures might be more or less toxic to a cell (Chiti 2006). Chaperones influence protein folding by smoothing energy landscapes, decreasing high energy barriers towards the native structure, preventing misfolding and aggregation, and thereby optimizing the efficiency of productive folding (figure modified from Hartl 2009).

## Diversity of folding – superfast folders, molten globules, complex folding pathways

Most natural protein structures combine  $\alpha$ -helical and  $\beta$ -sheet conformations connected via turns and linker regions. Except for short polypeptides, protein folding is usually not a one-step process. Rather, proteins fold stepwise from a structurally very unstable unfolded state through one or more folding intermediates into their native conformation. An unfolded polypeptide is not a completely extended, but rather a dynamic disordered state that *in vivo* is often stabilized by chaperones. Folding intermediates appear in the energy landscape as valleys down the road to the native state. Rather compact conformations with many intramolecular contacts close to the native state, but increased conformational dynamics are called “molten globules” (Haynie 1993, Bartlett 2009, Redfield 2004).

For many proteins, an initial hydrophobic collapse buries hydrophobic residues in the core of a molten globule structure, which progressively readjusts contacts and bond angles into the stable and defined native state. While the hydrophobic collapse often happens within milliseconds (Kim 2008),

refinement and progression into the final structure varies from submilliseconds for very small polypeptides with simple folds up to seconds, minutes, hours, or days (Bryan 1992, Aronsson 1997). Superfast folders include the all-helical  $\lambda$ -repressor (Huang 1995), but also the small  $\beta$ -barrel cold shock protein CspB (Schindler 1995, Zeeb 2005). Long folding times are rather typical for complex multidomain proteins, especially those containing mixed  $\alpha$ -helical/ $\beta$ -sheet architectures with numerous long-range interactions (Aronsson 1997, Zhou 2002). Intrinsic structural properties including proline *cis-trans* isomerizations, formation of long-distance hydrogen bonds, or buried polar interactions in a hydrophobic environment can furthermore cause slow folding (Waldenburger 1996).

## **Molecular chaperones promote protein folding in a cellular environment**

The rate-limiting steps in protein folding *in vitro* often slow down the process of folding into native structures due to energetic reasons. Kinetically trapped folding intermediates accumulate in energy wells. Kinetics with folding half-times of minutes, hours, or days observed *in vitro* obviously explain the need for promoting efficient protein folding in cells. This enhancement in cellular protein folding is carried out by specialized folding catalysts, the molecular chaperones.

Mechanistically, chaperones support protein folding through binding and stabilization of partially folded intermediates, partial unfolding and release of the polypeptide chain, creation of a protein folding environment with defined biophysical properties (e.g. hydrophobic, polar, or charged surfaces), and through steric confinement and application of mechanical forces on the polypeptide chains (Hartl 2009, Kim 2013). In terms of energy landscape, chaperones create an efficient folding pathway by smoothening the downhill road towards the native state, or by increasing the energetic barriers towards off-pathway intermediates and misfolded states (Mashagi 2013). Thereby chaperones are able to direct folding pathways to functional native conformations and to avoid routes leading to misfolding and aggregation. In many cases, efficient folding is achieved through a collaborative network of different structural and functional classes of chaperones on a substrate protein (Young 2004).

However, in the crowded environment of a cell, efficient protein folding is not only a problem of achieving correct intramolecular interactions. Not yet properly folded polypeptide chains engage easily in unspecific interactions with other cellular factors. Stretches from different protein molecules encountering each other may mutually disturb their folding pathways and induce misfolding. Especially hydrophobic stretches are prone to cluster among each other. Transiently interacting molecules might finally assemble in higher molecular weight oligomers and aggregates. To prevent misfolding and aggregation is the second major function of molecular chaperones. These recognize and bind to polypeptide stretches which are prone to unspecific interactions and usually become buried in the native state. Chaperones hold these structures in a folding competent state and shield them from potential disturbances. Repeated cycles of binding and release and folding in isolated chambers give proteins the chance to fold into their native conformation. Proteins that were unsuccessful in folding correctly are rebound or delivered to downstream chaperones, mechanistically described as *kinetic partitioning* in protein folding (Rothman 1989, Hardy 1991, Hartl 2011).

Further chaperon functions lie in intracellular protein transport, oligomeric assembly, conformational maintenance, refolding of denatured proteins, and assistance in degradation (Hartl 2009).

## Protein misfolding causes toxicity in cells – loss- and gain-of-function

Proteins need to fold efficiently into stable and functional structures, putting opposing pressures on the evolution of optimal sequences (Bartlett 2009). Proteins exposing unspecific interaction surfaces that are potentially deleterious to the cell have been removed or adapted to safe conformations (e.g. Monsellier 2007). In addition, molecular chaperones evolved to promote proper folding and rescue unsuccessful folding attempts. Chaperones thereby increase the available sequence space of a cellular proteome and buffer phenotypic variation (Rutherford 2003).

Nevertheless, (partially) unfolded proteins expose regions susceptible to unspecific interactions. As protein folding pathways are very dependent on surrounding forces and conditions, it may happen that a folding polypeptide chain leaves its routes to the native state and follows an off-pathway downhill route into a kinetically trapped state, or into a stable misfolded conformation with stable nonnative intramolecular interactions. These under normal conditions inaccessible states may be of similar or even higher thermodynamic stability than the native state (Hartl 2009).

Protein function is strongly dependent on native structure. Misfolded proteins are therefore in most cases unable to fulfill their cellular activity. This loss-of-function phenomenon is being discussed as one major origin of cellular toxicity: incapable of tolerating or substituting the activity of an essential protein, a cell may lose its ability to sustain. Toxicity occurring due to this loss-of-function principle is expected to be highly sequence-dependent, since a specific functional loss would lead to a characteristic disease phenotype.

Parkin, an E3 ubiquitin ligase, promotes mostly degradation-independent ubiquitination of proteins involved in signal transduction, transcriptional regulation, DNA repair, endocytosis, and cellular trafficking. In Parkinson's disease, mutations within the polypeptide sequence of Parkin or high levels of oxidation stress seem to cause the protein to misfold and aggregate, rendering Parkin's native function inactive. The respective defects at least contribute to neuronal toxicity (Winklhofer 2008).

Beyond their functional loss, misfolded protein structures continuously expose nonnative regions on their surface, which represents a permanent hazard in cells. Such stretches carry the potential to engage in unspecific aberrant interactions, especially with other misfolded proteins, but also with native cellular factors (Hortschansky 2005, Olzscha 2011). The initial formation of misfolded structures (monomers, dimers, small oligomers) and the subsequent growth are described by a nucleation and growth mechanism. Oligomeric species that appear early during an aggregation process are often considered as transient. However, they may reorganize further into stable, highly ordered amyloids (Auer 2007), the microscopically visible hallmarks of neurodegenerative diseases.

The self-propagating mechanism of misfolded conformations by templating, which has been described for prion proteins before (Creutzfeldt-Jakob disease), seems to apply for a number of neurodegenerative disease proteins as well. Proposed proteins include A $\beta$ , tau,  $\alpha$ -synuclein, and mutant SOD (Kretschmar 2013, Münch 2011, Aguzzi 2009, Kraus 2013). Misfolded structures coming into contact to other cellular molecules may engage in unspecific interactions, induce and propagate misfolding, and recruit a growing number of other molecules into misfolded assemblies. The A $\beta$  fragment A $\beta$ (25-35) has been shown *in vitro* to strongly promote misfolding and aggregation of firefly luciferase. Moreover a wide variety of native proteins co-precipitated in amorphous aggregates along with A $\beta$ (25-35) (Konno 2001). Similarly, in human cells, especially vulnerable sequences or metastable proteins were sequestered into growing cellular aggregates (Olzscha 2011, Suhr 2001).

Non-native, misfolded protein conformations therefore gain potentially harmful functions that were not present in their native conformation, which is described by the “toxic gain-of-function hypothesis” (Winklhofer 2008). Together, loss- and gain-of-function contribute to the pathogenesis of neurodegenerative diseases, although their individual contribution undoubtedly varies depending on the sequence and associated disease and remains to be defined in many cases.

The loss-of-function phenotype of a disease protein is expected to be very protein and disease specific. For signaling and transcription factors, it has been shown that small alterations of their fine-balanced levels can determine cell fate. In neural stem cells, transcription factors control cell proliferation, multipotency, neurogenesis, and the generation of specific neuronal classes at the correct time and location, ultimately deciding about life or death of a cell. For example, minor changes in the relative levels of the transcription factors Pax6, Hes1, and Neurog2 are crucial for neural stem cell self-renewal and the generation of cortical neurons or basal progenitor cells (Sansom 2009). Alterations in the levels of other, e.g. non-essential proteins might be rather tolerated by cells under normal conditions. Parkin is involved in cellular stress responses, promoting cell survival and further aggravating pathogenic effects upon misfolding (Henn 2007). However, the native functions of many neurodegenerative disease associated proteins and the consequences of their respective functional losses remain still unclear.

The toxic gain-of-function of misfolded protein conformations on the other hand is discussed to underlie the many common symptoms observed among the various protein misfolding diseases. Misfolded proteins of unrelated sequences accumulate into similar molecular assemblies (oligomers, aggregates, fibrils), which suggests similar mechanisms behind their toxic effects on cells. Toxicity may arise from protein sequestration, signaling malfunctions, membrane permeabilization (Lashuel 2002, Soto 2003), or increased appearance of radicals. Multiple malfunctions crossing tolerable thresholds finally pile up in proteostasis collapse and cell death (Hipp 2014, Labbadia 2015).

Toxic loss-of-function and toxic gain-of-function may contribute to disease pathology to variable degrees in different forms of dementia or amyloidoses. Toxicity ultimately becomes multifactorial, complex in its nature, and tremendously challenging to analyze and understand.

## Structural features of misfolded assemblies: oligomers & amyloid fibrils

Microscopically visible protein deposits and inclusions are the hallmark of neurodegenerative and other protein misfolding diseases. These proteinaceous aggregates consist of one or a few major protein components in addition to a mixture of other misfolded proteins, metal ions, glycosaminoglycans, and other biomolecules (Armstrong 2008).

Isolated from patients, such aggregates have been shown to consist of protein fibrils (the amyloids), which similarly can be produced *in vitro* from most proteins under specific, often mildly denaturing conditions. Isolated amyloids were highly structured and ordered. They usually assembled from protofilaments of 2-5 nm in diameter, which can twist together forming rope-like higher fibrils, or associate laterally to long and narrow ribbons. For many fibrils, X-ray fiber diffraction has revealed  $\beta$ -sheet strands running perpendicular to the long axis of the fibrils, consequently termed “cross  $\beta$ -sheet” structures. These fibrils bind amyloid specific dyes, such as Thioflavin T and Congo Red, despite their unrelated sequences. Solid-state NMR has demonstrated first atomic details on the example of transthyretin, showing extended  $\beta$ -strands and a crystal-like uniformity (Jaroniec 2002). Cryo-electron microscopy and Fourier transform infrared spectroscopy furthermore revealed the presence of highly planar  $\beta$ -sheets in amyloids (Zandomenighi 2004), opposed to more twisted  $\beta$ -sheet structures in native proteins (Chothia 1981). Forcing the  $\beta$ -strands into a planar conformation limits their length in amyloid cores, where the  $\beta$ -strands run perpendicular to the fibril axis (Chiti 2006).

## Functional amyloids and non-chromosomal inheritance by prions

Rarely, functional amyloid structures have been found *in vivo*. In such cases, the amyloid conformation constitutes the native state of certain proteins. *Escherichia coli* functionalize curlin fibrils to mediate binding to host proteins and inert surfaces. Mammalian melanosomes, lysosome-related organelles in melanin pigment producing epidermal cells, store a highly aggregation-prone protein (Pmel17) in functional amyloid structures that are involved in melanosome biogenesis. Also, peptide hormones in secretory granules of the endocrine system are stored in a fibrillary form (Maji 2009). Thus, native amyloid conformations exist in cells, even though nucleation and assembly has to be highly regulated and controlled in these systems (Fowler 2007).

Other proteins associated with functional amyloids are the prion proteins Ure2p and Sup35p from *Saccharomyces cerevisiae*. They exist in either a soluble or an aggregated state, giving rise to distinct phenotypes that are inherited to daughter cells. Sup35 is involved in termination of mRNA translation, facilitating the read-through of stop codons in [PSI<sup>+</sup>] cells (Krishnan 2005 nature). Ure2p only binds the transcription factor Gln3p in its native state, whereas its conversion to amyloid results in the activation of a series of associated genes in [URE3] cells. As prions, these proteins transfer this conformation through contact to equal sequences in their soluble conformation. Switching between a soluble and an amyloid conformation therefore enables these proteins to regulate gene expression and transmit an epigenetic phenotype (Chiti 2006).

## Sequence effects on amyloid formation

Amyloid formation is likely a common property of proteins and peptides. This may be explained by the properties of protein backbones comparable to simple artificial polymers. However, the protein

sequence crucially influences the stability of a native state, its susceptibility to and rate of misfolding, or in other words, the energetics of multiple accessible conformations and the kinetics of their conversion.

A high hydrophobicity, a low net charge, and a high propensity to convert from  $\alpha$ -helical to  $\beta$ -sheet structure have been described as major factors leading to a high aggregation propensity of partially unfolded states (Chiti 2003, Calamai 2003). At the same time, most of the natively unstructured proteins comprise a low hydrophobicity and a low net charge (Uversky 2000). Hydrophobic patches on proteins especially promote unspecific interactions in an aqueous environment (hydrophobic effect). Substitutions in sequence regions playing a central role for nucleation or formation of amyloid cores can reduce or increase the aggregation propensity of proteins. Longer hydrophobic stretches are less frequent and are usually buried inside of a protein fold, however regularly present at interaction surfaces. Here they are often surrounded by polar or charged “gatekeeper” residues that decrease the overall aggregation propensity, and at the same time represent recognition signals for the cellular quality control machinery (Beerten 2012, Sant'Anna 2014).

High global or local net charge may hinder self-association. Decreasing charge by substitutions within a sequence or by binding of macromolecules with a high compensatory net charge usually facilitates aggregation (Konno 2001, Krishnan 2005). The net charge of 84% of sequences noted in the Protein Data Bank (PDB) falls within a range of  $\pm 10$  (Lawrence 2007). Thus, extreme net charge is rather rare in native proteins, likely due to requirements of folding, engaging in specific interactions, and degradability.

Beyond hydrophobicity and charge, a low propensity of forming  $\alpha$ -helices, a high propensity of forming  $\beta$ -sheet structure, or, related to that, certain patterns of hydrophilic and hydrophobic residues can promote the formation of amyloid structures. Especially polypeptide segments that are sterically self-compatible and offer enough flexibility assemble into zipper-like repeating patterns (Sawaya 2007). The entire human proteome has been analyzed for segments able to form tightly complementary interfaces with itself, permitting the formation of steric zippers as a central core of a fibril. In this amyloyme, nearly all proteins have been found to contain certain self-complementary regions, which therefore need to be constrained through folding or by chaperon interactions within a cell (Goldschmidt 2010).

The described sequence features influencing amyloid formation have been rationalized in algorithms for aggregation propensity predictions, such as the Zyggregator (Tartaglia 2008).

## **Oligomeric assemblies and the multiplicity of protein states**

Research of the past decades has revealed that next to native globular states and insoluble amyloids, a polypeptide chain can adopt a multitude of intermediate conformations. Not all proteins form stable folds, some exist in very dynamic unfolded states, and many proteins with a stable globular core contain longer disordered regions. Various forms of oligomeric species have been observed. Proteins carrying specific mutations, distinct peptide fragments, or a general decline in protein folding maintenance were associated to low-molecular-weight oligomers forming on- or off-pathway to amyloids (Chiti 2006).

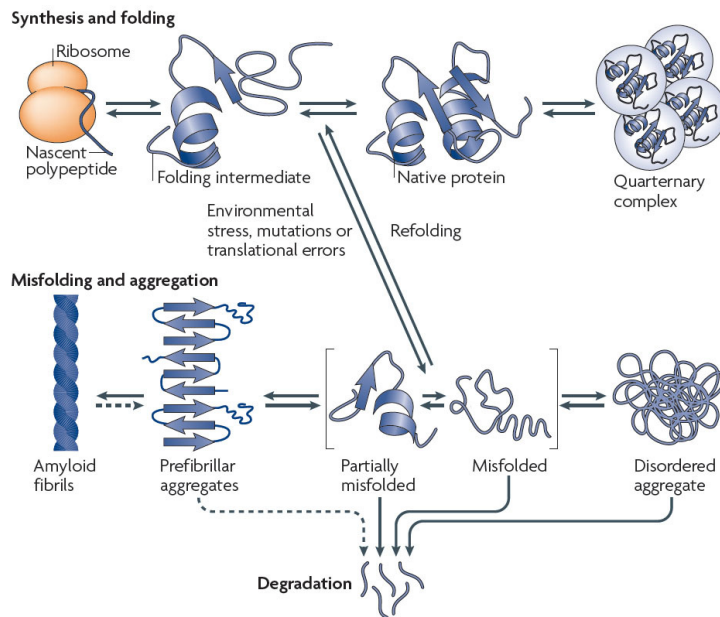


**Figure 8 | Overview over cellular protein folding and misfolding, the multiplicity of conformational states, and pathways of interconversion.** Nascent chains emerging from ribosomes are initially slowed-down in folding. Initial secondary structure elements start to form, protected by chaperones, until the nascent chain is fully released from the ribosome. From here, proteins can fold into their native state. Misfolded conformations appear transiently and reverse into native states, are degraded to peptides and free amino acids, or stabilize in forms of ordered, amyloid-like fibrils or amorphous aggregates. The cellular quality control system guards and regulates all these processes. Only if misfolding and aggregation overwhelm the cellular folding and degradation system, they may become a challenge for cellular maintenance and survival (figure from Tyedmers 2010).

Low-molecular-weight oligomers can exist in equilibrium with monomers and fibers, or they can precede fibril formation. Such spherical or chain-like protofibrillar structures have been described for  $\alpha$ -synuclein,  $A\beta$  peptides, amylin, polyQ sequences, transthyretin, immunoglobulin light chains, and others. Certain antibodies specifically recognize oligomers, independently of their sequence, suggesting that such assemblies can be defined by common structural features (Kayed 2006, Mamikonyan 2007).

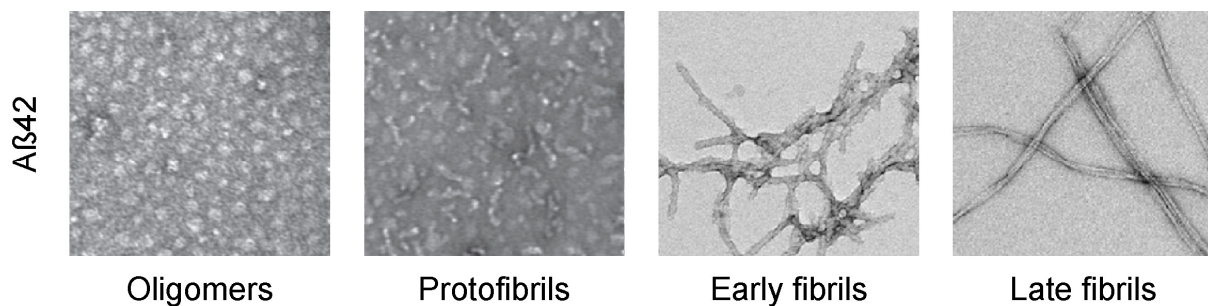


**Figure 9 | Transmission electron micrographs of  $A\beta_{42}$  oligomers and fibrils.** In vitro generated oligomers of  $A\beta_{42}$  (related to Alzheimer's disease) formed disc-shaped pentamers or hexamers of rather disordered structure, showing a higher toxicity on primary cultures of mouse cortical neurons than  $\beta$ -sheeted protofibrils or fibrils (Ahmed 2010). Early fibrils are twisted around each other and become highly ordered after longer times of incubation. Thickness of oligomers and fibrils varied between 2-10 nm. Figures from Ahmed 2010 (left two images) and Finder 2010 (right two images).

Oligomer levels correlated much more to toxicity in cells or to the disease pathology of Alzheimer's disease patients than large fibrils, which might even act as sink of misfolded structures (Lue 1999, Haass 2007). Of course, toxicity is not necessarily caused exclusively by a single structure, but may integrate effects of several distinct states, leading to a highly complex problem. Identification, isolation, and characterization of such metastable oligomers or protofibrils are highly challenging, but would certainly help to understand the nature and influences of such assemblies in cells (Chiti 2006, Knowles 2014).

## Molecular chaperones

A molecular chaperone has been defined as any interacting protein that promotes folding and assembly into functionally active conformations without being present in the final structure (Hartl 1996). Molecular chaperones are involved in every aspect of protein synthesis, maintenance, and degradation. Guarding of newly synthesized proteins begins when these emerge at the ribosome and ends when protein structures need to be unfolded for degradation.

### Cellular protein biosynthesis

$\alpha$ -helices may form within nanoseconds *in vitro*. *In vivo*, the translational speed of ribosomes is considerably slower (~4 amino acids per second for eukaryotes, ~20 amino acids per second in bacteria; Hartl 2009). As soon as peptide bonds are formed, initial folding interactions begin within the ribosome. However, the limited space restricts growing polypeptides to  $\alpha$ -helical conformations within the 10 nm long and 2 nm wide exit tunnel. Interactions with ribosomal RNA (rRNA) may already promote conformational compaction (Lu 2005, Bhushan 2010). However, structural rearrangements might occur once the N-terminus emerges from the exit tunnel (Bhushan 2005). Incomplete chains usually do not achieve any stable fold or are prone to aggregation (Parker 1981). Only complete proteins or domains offer the necessary information and thermodynamic energy to stabilize native conformations. Especially large  $\beta$ -sheet rich domains and complex  $\alpha/\beta$ -folds contain long-distance interactions, and the respective interaction sites may not be available yet. Nascent chains therefore expose peptide segments lacking their native interaction partners, which makes them prone to participate in unspecific interactions. Especially in a highly crowded environment of a cell (300 mg/mL protein), cotranslational protection is highly necessary, which is provided by the first instance of chaperones.

### Chaperones guarding the nascent chain

The ribosomal exit tunnel prevents non-native interactions of the emerging polypeptide chain. Interestingly, in *E. coli*, ribosomes themselves have been suggested to exert a chaperon-like refolding activity, especially the 23S rRNA, as they promote folding and mediate refolding of denatured proteins (Kudlicki 1997). Emerging nascent chains need to be shielded from unfavorable intra- and intermolecular interactions. This is achieved by ribosome-associated chaperones such as trigger factor (TF) in prokaryotes and specialized Hsp70 and nascent chain-associated complexes (NAC) in mammals.

TF (~50 kDa) consists of a ribosome and a nascent chain binding domain, next to its peptidylprolyl *cis/trans* isomerase (PPIase). The PPIase recognizes stretches of eight amino acids enriched in basic and aromatic residues (Ferbitz 2004, Lakshmiathy 2007). Every domain of TF can take part in nascent chain binding, which enables TF to accommodate a wide range of polypeptides. TF primarily shields emerging hydrophobic chains from non-native interactions. Its subsequent release from the nascent chain promotes folding of the polypeptide and provides energy for this ATP-independent process. Then TF dimerizes, partially masking its substrate-binding regions (Kaiser 2006). TF does not exist in eukaryotes, but the heterodimeric  $\alpha/\beta$ -NAC complex (33/22 kDa) might fulfill a similar function. NAC associates with ribosomes and short nascent chains (del Alamo 2011, Preissler 2012) and most likely functions in parallel with MPP11/Hsp70L1 (Otto 2005, Jaiswal 2011). NAC knockouts in yeast have resulted in a strong upregulation of stress inducible chaperones (del Alamo 2011).



Combinatorial knockouts of NAC and Ssb strongly enhanced aggregation of newly synthesized proteins (Koplin 2010).

A subset of proteins is capable of autonomous folding. This is often true for small  $\alpha$ -helical proteins, which straightforwardly fold into their native states. Chaperone dependence increases strongly with the length of polypeptide chains and the distance of long-range interactions. Chaperons ease folding for bacterial proteins with an average size of  $\sim 30$  kDa in *E. coli*, while the average human protein reaches over 50 kDa (Wolff 2014).

## Chaperone networks for folding, maintenance, and degradation

Downstream of the ribosome, the cellular chaperone systems form a complex network of factors, which guarantee proper protein folding, quality control, and maintenance of a healthy proteostasis (Hartl 2009). Already as the nascent chain emerges, Hsp70s and their Hsp40 cochaperones (DnaJ/DnaK in *E. coli*) cooperate with TF in shielding the polypeptide from harmful interactions. Specific chaperone functions partially overlap, as single knockouts of e.g. TF or DnaK in *E. coli* are tolerated by cells under non-stress conditions, and the remaining chaperones widen their substrate spectrum (Deuerling 1999). However, under stress or upon multiple chaperon deletions (e.g. TF and DnaK), cells experience enhanced protein aggregation up to their inability to synthesize and fold new proteins (Calloni 2012).

## The multifunctional Hsp 70/Hsp40 system

“The constitutively expressed Hsc70 and stress-inducible forms of Hsp70 are central players in protein folding and proteostasis control” (Hartl 2011). They shield the cellular proteome from hazardous interactions, prevent misfolding and aggregation, and promote folding through cycles of binding and release. DnaK, the bacterial Hsp70, recognizes hydrophobic strands surrounded by positive charges, which are often buried in the core of folded proteins (Rüdiger 1997), but which become prone to aggregate when exposed. Hsp70s perform an ATP-dependent reaction cycle. ATP binding, hydrolysis, and ADP release in the nucleotide-binding domain of Hsp70 are allosterically coupled to substrate binding and release. ATP binding opens the peptide-binding pocket allowing substrates to enter. ATP hydrolysis leads to a closed binding pocket with low substrate on and off rates (Kim 2013, Hartl 2011).

Hsp70 is regulated by cochaperones and nucleotide exchange factors (more than 40 Hsp40s in humans; DnaJ, GrpE in *E. coli*), primarily through stimulating ATP hydrolysis that stabilizes Hsp70-substrate interactions (Qiu 2006). ADP release becomes accelerated by Hsp110 (Polier 2010) and Hsp170. A new cycle of ATP binding results in substrate release, which is either properly folded, or rebound to Hsp70 or further downstream chaperones (Mayer 2010).

Hsp40s bind with their conserved J-domains to the nucleotide-binding domain of Hsp70. Specialized Hsp40s function as chaperones themselves and recruit nonnative substrates to Hsp70. Mammalian DnaJB1 and yeast Sis1p mediate the transport of misfolded proteins into the nucleus, where they become degraded by the proteasome (Park 2013). This process currently seems to arise as an important cellular pathway for removal and degradation of aggregation prone structures from the cytosol.

Hsp70s are furthermore of major importance for protein targeting. Mitochondrial proteins encoded by the nuclear genome are synthesized in the cytoplasm tagged by a mitochondrial targeting signal. Hsp70 guards (partially) unfolded mitochondrial precursor proteins through the cytoplasm to mitochondria. As the proteins become imported through the mitochondrial import complexes (TOM, TIM), they are immediately grasped by mtHsp70 with its open substrate binding site (Neupert 2007).

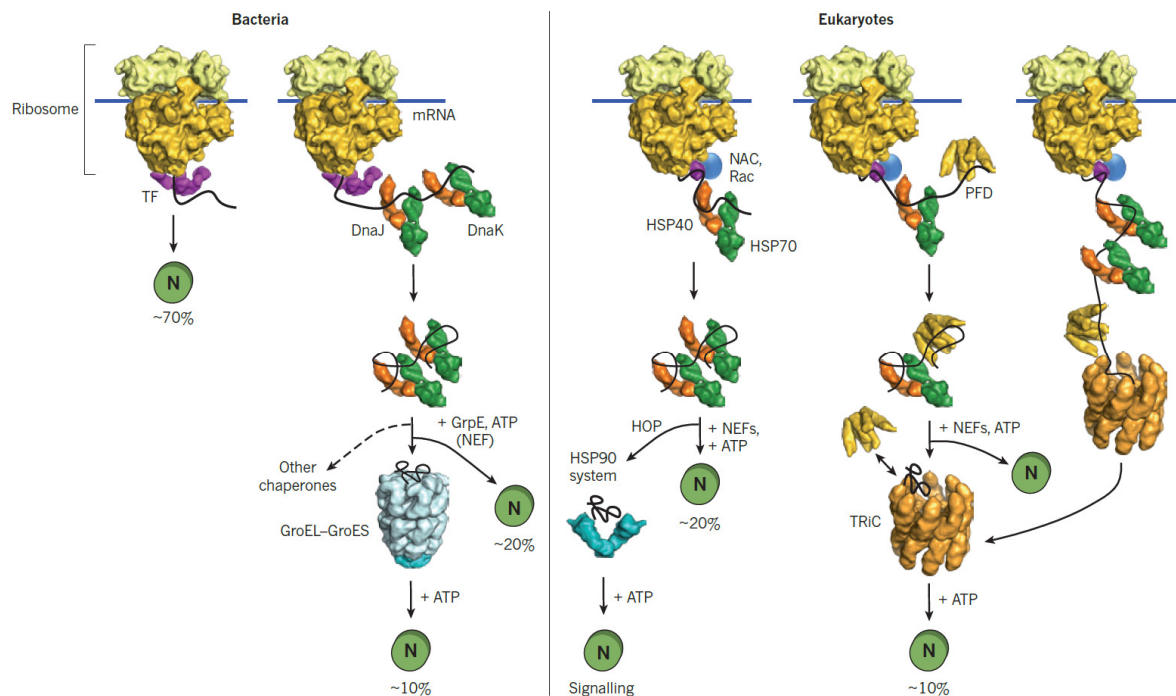


**Figure 10 | Overview of chaperones in the bacterial and eukaryotic cytoplasm, stabilizing the nascent chain and promoting folding of their substrates to the native state.** The nascent chains interact with trigger factor (TF) or NAC in conjunction with specialized Hsp70 complexes. Members of the DnaJ/K or Hsp70/40 family mediate co- or posttranslational folding or distribute proteins to downstream chaperones. Depending on the sequence, the protein substrates are delivered to the chaperonins GroEL/ES or TRiC, or chaperones of the Hsp90 family. Numerous cofactors support the folding process (such as nucleotide exchange factors, NEFs) or mediate substrate recognition (such as the Hsp70-Hsp90 organizing protein, HOP). The numbers indicate the percentage of interacting proteins as part of the total proteome (figure from Hartl 2011).

## Chaperonins – single molecule folding chambers

Chaperonins (Hsp60s) are large double-ring complexes (7-9 subunits of ~60kDa) with a central cavity. They offer substrate proteins an isolated chamber with a dynamic and active surface. Chaperonins create an optimal folding environment and allow proteins to fold independently from surrounding factors that risk their misfolding and aggregation.

GroEL from bacteria, Hsp60 in mitochondria, and Cpn60 in Chloroplasts are chaperonins that encapsulate proteins with lid-shaped cochaperones (GroES, Hsp10, Cpn10/20). The archaeal thermosome and the eukaryotic TRiC (TCP-1 Ring Complex) contain a built-in lid with an iris-like opening mechanism. The chaperonins offer a chamber to enclose proteins or domains of up to 60-70 kDa size. In case of TRiC, partial encapsulation of single domains with successful folding has been shown for proteins of >100 kDa (Rüßmann 2012).

The chaperonins interact with about 10% of newly synthesized proteins. Obligate GroEL substrates (around 85 *E.coli* proteins) are typically proteins with complex  $\alpha/\beta$ -folds being kinetically trapped in folding intermediates that need to be resolved (Kerner 2005). Well-established TRiC substrates include the cytoskeletal actin and tubulin as well as proteins with  $\beta$ -propeller/WD40 domains (Dekker 2008, Yam 2008). Upon substrate binding, GroEL forms a hydrophobic folding chamber encapsulating mostly molten-globule like structures that partially lack native long-distance interactions. ATP-dependent GroES binding leads to a conformational transition, resulting in a hydrophilic, negatively net charged inner surface (Hartl 2011). The substrate protein has now  $\sim 10$  sec for folding along an undisturbed, folding-optimized energy landscape. The chaperonins promote rather compact, native-like conformations (Brinker 2001, Chakraborty 2010). Rebinding of not yet folded structures allows multiple rounds of folding within the chaperonins, before a still misfolded protein might ultimately be delivered to degradation (Hartl 2011).

Interestingly, the eukaryotic chaperonin TRiC has been shown to modify oligomeric species of polyQ expanded versions of the Huntingtin's disease protein in cooperation with Hsp70, rendering them less toxic in a yeast model (Behrends 2006).

### **The Hsp90 chaperone family of activators and regulators**

Hsp90 chaperones are a highly conserved essential chaperone family promoting the maturation of a wide range of substrate proteins. Hsp70s transfer many substrates to Hsp90 for the completion of folding and for functional activation with the help of HOP (Hsp90 organizing protein), which bridges the two chaperones with its TPR (tetratricopeptide repeat) domains (Scheuffler 2000). Substrates include a variety of proteins involved in signal transduction, protein trafficking, receptor maturation, especially kinases and receptor proteins, assigning Hsp90 chaperones the role of an important cellular regulator (Taipale 2010). Applying Hsp90 inhibitors simultaneously inhibited multiple cellular signaling pathways important for cancer growth (Neckers 2007), however concurrently induced a general stress response (Labbadia 2015).

Hsp90 itself has been found to preferentially recognize intrinsically unstable kinases rather than binding to distinct sequence motives on their substrates. Its cochaperone CDC37 serves as an adaptor that binds to kinase folds and recruits Hsp90. Hsp90-kinase associations decrease after stabilization of the kinases by folding or by binding to stabilizing small molecules or natural ligands (Taipale 2012).

### **Disaggregases – chaperones reversing aggregation**

Beyond promoting folding and refolding, certain chaperones are able to disassemble and remodel misfolded protein oligomers and aggregates.

Hsp104 is a hexameric ring AAA+ ATPase with a central pore, through which misfolded substrate proteins are (presumably) translocated and thereby disentangled. Hsp104 from yeast is driven by ATP hydrolysis and collaborates with Hsp70 and Hsp40 (Doyle 2009). The disaggregase complex resolves disordered aggregates as well as amyloids. Homologues of Hsp104 are found in bacteria, fungi, protozoa, chromista, and plants, however not in metazoan (animals). The bacterial homologue ClpB lacks the ability to disaggregate amyloid fibrils with stable "cross- $\beta$ " cores (DeSantis 2012). Reasons for the loss of Hsp104 from metazoan are unclear (Shorter 2011). A generally advanced

proteostasis network may have decreased the selective pressure to keep the disaggregase during evolution. Alternatively, the potential risk of producing soluble misfolded species by Hsp104 through disassembly of rather “safe” amyloid species might have been disadvantageous.

Recently Hsp110, so far known as a nuclear exchange factor (NEF) of Hsp70, has been found to disaggregate disordered aggregates (of Luciferase or GFP) in the mammalian cytoplasm and *in vitro* in collaboration with Hsp70 and Hsp40. However, this complex failed to remodel amyloid forms of  $\alpha$ -synuclein or the yeast prion Sup35 (Shorter 2011). Hsp110 seems to accelerate Hsp70 kinetics by its NEF activity, and Hsp70 relies on numerous cofactors for efficient disaggregation. Putative substrate interactions of Hsp110 remain unclear (Rampelt 2012). Metazoan disaggregases are so far poorly understood, although their contribution to the proteostasis network would be highly interesting regarding the appearance of amyloid diseases.

### **Small heat shock proteins**

Small heat shock proteins contain a highly conserved “ $\alpha$ -crystallin” domain of 100 amino acids. This common core is flanked by extensions that mediate dynamic oligomerization and client recognition (Eyles 2010). Small heat shock proteins prevent aggregation through binding and/or release of unfolded or misfolded structures. These can then be transferred in a soluble state via other chaperones for functional reactivation or degradation. Small heat shock proteins do not require ATP hydrolysis, although they may be regulated by ATP binding (Bakthisaran 2015).

Many small heat shock proteins have been found in the deposits associated to protein misfolding diseases. Moreover, chaperones prevented nucleation and aggregation of amyloid fibril formation of A $\beta$  peptides, polyglutamine sequences, and other aggregation prone proteins (see below; Bakthisaran 2015). Overexpression of small heat shock proteins has been associated with stabilization of tumor cells (Bakthisaran 2015). This circumstance demonstrates the importance of a factor-specific fine-tuning and a proteostasis network-wide orchestration to create a healthy folding environment within a cell.

## Protein degradation as part of the proteostasis network

A multiplicity of factors cooperates in promoting protein homeostasis (proteostasis). Together they form the cellular proteostasis machinery or proteostasis network (PN). The mammalian proteostasis network consists of ~400 proteins involved in biosynthesis, ~300 proteins involved in conformational maintenance, and ~700 proteins involved in degradation (Kim 2013). Imbalances within the network due to cell stress or aging may lead to an overload of the cellular proteostasis capacity, which in turn results in aberrant misfolding and aggregation. However, cells monitor and sense local disturbances and react with compartment-specific stress response pathways to increase their stress tolerance. Responses include an increase in chaperone levels, a decreased protein synthesis, or the activation of degradation pathways. Ultimately, if stress becomes too strong or persistent, cellular proteostasis might collapse, and cells with defective essential functions undergo cell death. A proteostasis collapse is thought to underlie numerous human protein misfolding diseases (Balch 2008, Kim 2013, Hipp 2014). An efficient removal of misfolded structures is therefore essential to maintain a healthy cellular environment.

### The ubiquitin-proteasome-system (UPS)

Proteins have specific cellular lifetimes, before they are hydrolyzed into peptides and amino acids. Proteins that cannot be successfully folded by the chaperone system are targeted for degradation earlier. The major cellular signal for the specific degradation of proteins consists of a polyubiquitin chain. The small globular ubiquitin (8.5 kDa) is ligated to specific lysine residues on target proteins for mono- or polyubiquitination (Vijai-Kumar 1987). All possible linkages were found in cells, such as mixed and branched ubiquitin chains, whereby the ubiquitination is interpreted protein- and context-specific (Malette 2012, Zhang 2013 J, Komander 2012). Membrane proteins are monoubiquitinated or K63-linked for endocytic uptake and lysosomal degradation (Mukhopadhyay 2007).

### A multifaceted network of ubiquitin ligases rules over the fate of proteins

Ubiquitin is transferred on substrate proteins via ubiquitin-activating enzymes (E1, accompanied by hydrolysis of ATP), ubiquitin-conjugating enzymes (E2), and ubiquitin ligases (E3). E3 ligases transfer ubiquitin from E2 to substrate proteins, mostly directly or via a thioester bonds (Pickart 2001). Ubiquitin is covalently attached to substrate proteins mostly via isopeptide bonds between Ubiquitin's carboxyl terminus and the lysine side chain amine on substrate proteins. Linkage also occurs to cysteine or methionine residues. The human genome encodes more than 600 E3 ligases accounting for the high flexibility and specificity of the UPS. Most E3 ligases comprise of a RING domain, a cysteine- and histidine-rich sequence binding two zinc ions, which stabilizes the entire protein structure. Other domains increase the variety beyond the RING domains, among them the huge family of cullin-RING ubiquitin ligases (CRLs) with almost 300 members, SH2, SH3, ankyrin repeat, or ubiquitin-like domains (Deshaies 2009, Sarikas 2011, Hua 2011).

A prominent E3 ligase is CHIP (carboxyl terminus of Hsc70-interacting protein). CHIP ubiquitinates fatally misfolded Hsp70 and Hsp90 substrates (Ballinger 1999, Connell 2001) and mediates stress recovery by targeting Hsp70 and a broad range of other chaperones for proteasomal degradation (Qian 2006). CHIP plays a role in aggresome formation. Together with Hsp70 and BAG3, CHIP interacts with the microtubule motor dynein, demonstrating an organized process involving chaperones and the transport machinery in the cellular aggresome formation (Zhang 2011).

## The proteasome – regulated protein destruction

Polyubiquitinated proteins are targeted to the 26S proteasome for degradation ( Ciehanover 1978). The eukaryotic proteasome contains a 20S core supplemented by one or two 19S regulatory caps. The barrel-shaped core complex with proteolytic activities degrades proteins into peptides ranging from 4 to 25 residues. The 19S caps recognize ubiquitinated proteins, unfold their substrates powered by AAA ATPases, and target the polypeptide chains into the proteolytic 20S core. Otherwise, the proteolytic centers are inaccessible for folded proteins outside of the central cavity. Studies employing proteasome inhibitors have shown that 80-90% of cellular proteins are degraded by proteasomes (Rock 1994). The degradation machineries are distributed over cytoplasm and nucleus, where they either remain present after cell division or become actively imported. ER proteins are retro-translocated to the cytoplasm for proteasomal degradation (ERAD pathway). Deubiquitinating enzymes (DUBs) recycle ubiquitin molecules by cleaving the  $\epsilon$ -amide before degradation of a substrate (Voges 1999).

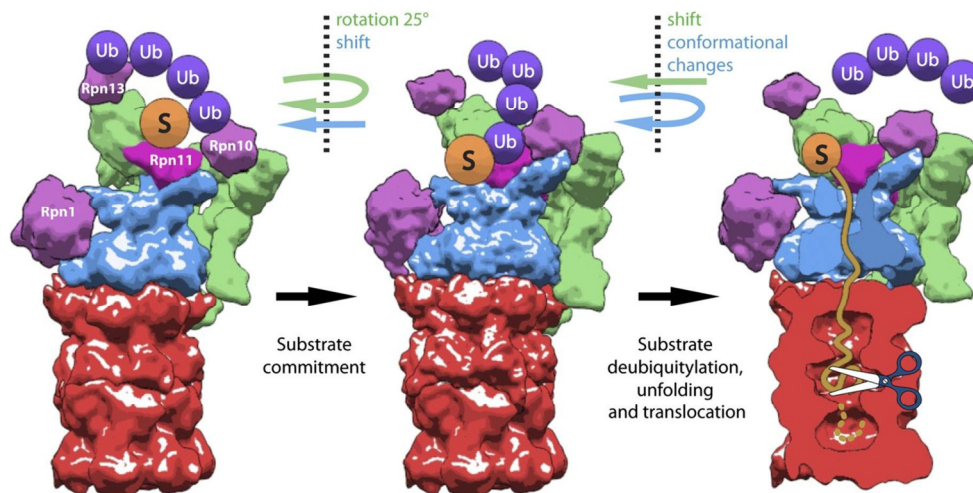


**Figure 11 | Cryo-electron microscopy structures of the 26S proteasome in a functional model of substrate degradation.** Polyubiquitinated (Ub) substrates (S) are bound by ubiquitin receptors (Rpn10, Rpn13) on the 19S regulatory subunit. A conformational switch, performing a 25° rotation of the Rpns and a shift of the AAA ATPase (blue), may transfer the substrate to the opening cleft and activate Rpn11, followed by deubiquitination of the substrate protein. Further conformational changes of the AAA ATPase enable unfolding of the substrate protein and its movement into the core particle (red), harboring the proteolytic activities and cleaving the protein into short polypeptides (figure from Unverdorben 2014).

A significantly increased proteasome activity was found to accelerate protein degradation in human embryonic stem cells that replicate continuously without signs of aging (Vilchez 2012). A distinct proteasomal core subunit with a large hydrophobic pocket is expressed in activated T cells. It produces peptides with hydrophobic, bulky C-termini, optimal anchor motifs for MHC-I (major histocompatibility complex I) presentation. An optimized oxyanion furthermore increases substrate processing (Huber 2012). Bulky aromatic surfaces improve the immune defense, non-immune cells however produce peptides that are potentially less challenging for cellular proteostasis (Kalim 2012).

## Endoplasmic reticulum-associated degradation (ERAD)

Secretory and transmembrane proteins are recognized by the signal recognition particle (SRP). Consequently, they become translocated cotranslationally through the heterotrimeric Sec61 channel (translocon) into the membrane or lumen of the endoplasmic reticulum (ER). Secretory proteins fold in the ER lumen, where they may acquire disulfide bonds, N-linked glycans, or oligomerize into higher complexes. Proteins that do not achieve their native state are retained in the ER or recycled from downstream compartments (e.g. Golgi). From here, they are retrotranslocated to the cytoplasm for proteasomal degradation (McCracken 1996). The ER specific Hsp70 chaperone BiP (binding immunoglobulin protein) recognizes hydrophobic stretches on the surface of misfolded structures, prevents their aggregation, allows for additional rounds of folding, or keeps the structures soluble for degradation.

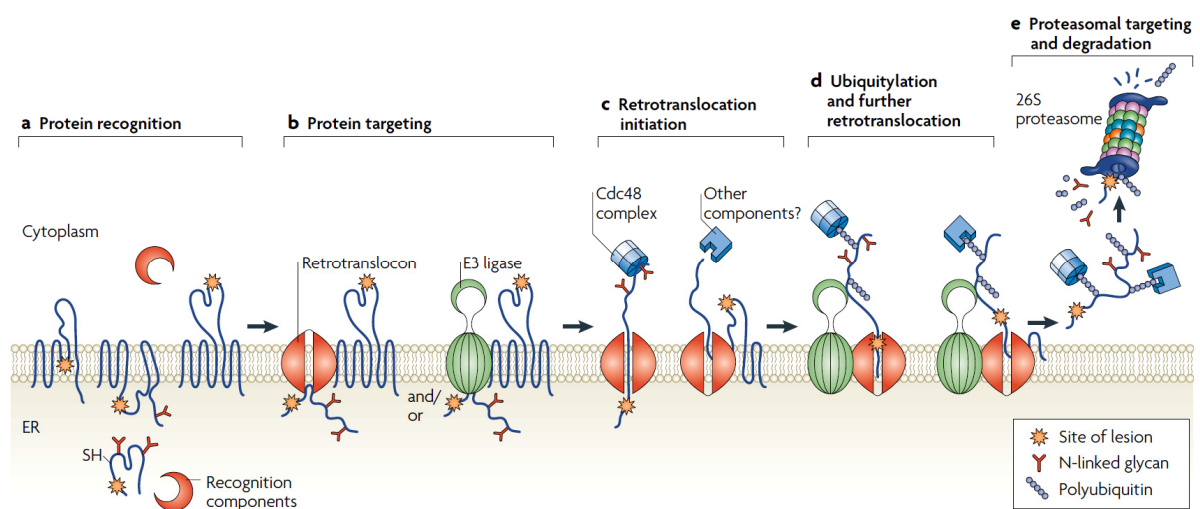


**Figure 12 | Overview over the individual steps of ER-associated protein degradation (ERAD).** Misfolded membrane or ER-luminal proteins are recognized by chaperones, such as BiP (Hsp70 family) and are targeted to retro-translocation. They are extracted to the cytoplasm by AAA ATPases, such as p97 (cdc48) or the 19S regulatory particle of the proteasome. Ubiquitylation by associated Ubiquitin E3 ligases releases ERAD substrates from the membrane, followed by proteasomal uptake and degradation (figure from Vembar 2008).

Luminal ERAD substrates are then retrotranslocated most likely through Sec61 to the cytoplasm by AAA ATPases. p97 (cdc48 in yeast) potentially disentangles proteins from other bound factors and extracts ERAD substrates with force, driven by ATP hydrolysis (Rape 2001, Richly 2005). For some substrates, the 19S regulatory particle, comprising six nonequivalent AAA ATPases, has been shown to be sufficient for substrate export from the ER (Lee 2004). A significant fraction of cellular proteasomes is ER associated. Arriving in the cytoplasm, ERAD substrates are ubiquitinated and released from the ER membrane. Finally, they become degraded by the proteasome with or without previous deglycosylation (Römisch 2005).

## Bulk and chaperone-mediated autophagy

The UPS degrades single proteins after unfolding one by one and contributes a major part to regular protein turnover in cells. Beyond this, mammalian cells utilize autophagy to degrade whole organelles and harder-to-unfold or aggregated proteins, but also lipids, nucleic acids, and polysaccharides. Two trafficking pathways deliver substrates into the lysosomal lumen, where an array of hydrolytic enzymes mediates degradation at an acidic pH. The endocytic route recycles integral and peripheral membrane proteins and lipids. And upon inhibition of autophagy in cells and mice, protein aggregates start to form (Yamamoto 2014, Rubinsztein 2011).

Substrate delivery to lysosomes can appear highly specific mediated by receptors (chaperone-mediated autophagy, CMA) or in form of macroautophagy. Here, a complex machinery of proteins forms cytoplasmic membrane-surrounded vesicles that envelope cargo, which consists of surrounding cytoplasmic material, but also selectively enriched substrates. These include ubiquitinated, non-ubiquitinated, and aggregated proteins, mitochondria, peroxisomes, and invading pathogens.

Autophagic clearance of aggregated proteins relies on Alfy, p62, and NBR1. By multimerizing, p62 forms an “inclusion” to initiate a macroautophagic site that sequesters specific adaptor proteins, such as Alfy. Loss of Alfy was found to prevent the clearance of intracellular inclusions, and Alfy overexpressions decreased polyglutamine toxicity (Filimonenko 2010). Together with NBR1, such a complex interacts with autophagic effectors (among them Atg5, Atg12, Atg16L, and LC3) to form autophagosomes. These fuse with hydrolytic endosomes or lysosomes. Alfy is a nuclear protein that becomes exported to the cytoplasm in response to cellular stress in a Crm1-dependent manner. Alfy overexpression enhanced the clearance of misfolded proteins, such as polyQ-expanded Huntingtin or  $\alpha$ -synuclein (Filimonenko 2010).

CMA relies on the direct import of proteins into the lysosomal lumen. Chaperones that recognize a specific pentapeptide motif (KFERQ or similar) traffic such substrates to the lysosomal membrane, from where LAMP2A directly translocates the cargo into the lysosomal lumen (Yamamoto 2014).  $\alpha$ -synuclein is a substrate to CMA and apparently able to block lysosomal protein import, especially when mutated (see below, Cuervo 2005).

Autophagy seems to play a special role in neurons. The autophagic response under starvation or inhibition of mTor signaling is robust in most organs, but observed rarely in the mouse brain. Macroautophagy was deleterious under neuronal stress, and its inhibition protected neurons and promoted recovery. Autophagic vesicles have to travel long distances through neurites for lysosomal fusion in the soma. Autophagy may therefore protect from an accumulation of misfolded structures, but, when overactive, also disturb the highly complex architecture of differentiated neurons. More knowledge about autophagic fine-tuning in the central nervous system and specific autophagic pathways is therefore desirable to elaborate potential therapeutic strategies for neurodegenerative disorders (Yamamoto 2014).



## Maintaining and restoring proteostasis under misfolding stress

Successful protein folding and conformational maintenance are essential for cellular survival. Although many key players have been identified, research is far from understanding how individual components of the proteostasis network (PN) are interconnected, and how this network is orchestrated during specific forms of cellular stress. Several stress response pathways have been described including the cytosolic heat shock response (HSR), the unfolded protein response (UPR) in the endoplasmic reticulum, and the mitochondrial UPR. Other forms of cellular stress may furthermore challenge the cell with increased appearance of misfolded structures and induce related responses, as in case of inflammation, starvation, or oxidative stress. Activating cellular stress response pathways induces cellular PN factors (chaperones, UPS, autophagic and antioxidative factors), increasing the cellular capacity to cope with misfolded and damaged structures (Fulda 2010, Hipp 2014).

### Heat shock response

The heat shock response was originally discovered as a cellular response to mild heat stress. The response increases the tolerance against otherwise lethal conditions. These include misfolding and oxidative stress, toxic substances, or starvation, demonstrating the broader scope of the cellular mechanism. During its initiation, general transcription and translation are halted to alleviate the burden of newly synthesized structures. The main mediator activated under such conditions is heat shock factor 1 (Hsf1). Released from associated chaperones, Hsf1 binds to heat shock elements in the promoter regions of effector genes. Some “heat shock proteins” are constitutively expressed, others are strongly activated in response to cellular stress, such as Hsp27 and Hsp70. Inducible heat shock proteins promote cellular regeneration together with various cofactors (such as Hsp40s, CHIP). They increase the cellular folding capacity or target misfolded structures for degradation (Fulda 2010). Controlled activation of Hsf1 was shown to promote longevity by maintaining proteostasis, whereas its downregulation reduced lifespan and accelerated the formation of protein aggregates in *C. elegans* (Hsu 2003).

### Unfolded protein response (UPR)

The endoplasmic reticulum is responsible for the biosynthesis and posttranslational modification of all secretory and transmembrane proteins. This is especially challenging in secretory cells of the pancreas or the hypophysis, or in neuronal cells with complex membrane architectures (Ramirez 2011). The unfolded protein response (UPR) is generally transmitted through activation of ER resident factors (Fulda 2010, Schröder 2005). The transcription factors are presumably bound by the Hsp70 chaperone BiP and become released once BiP is overwhelmed by (mis-)folding substrates. IRE1 and PERK are transmembrane kinases, dimerizing, and autophosphorylating in response to ER stress. IRE1 splices an mRNA encoding the transcription factor XBP1 (Yoshida 2001). PERK phosphorylates eIF2 $\alpha$ , resulting in translational suppression, but allowing translation of specific UPR response genes (Teske 2011). The Golgi transmembrane protein ATF6 releases its cytoplasmic transcriptionally active domain upon stress to the nucleus (Okada 2003). The UPR response generally aims at balancing ER protein load and folding capacity. Factors include chaperones, oxidoreductases (PDI), and proteins of the ERAD pathway.

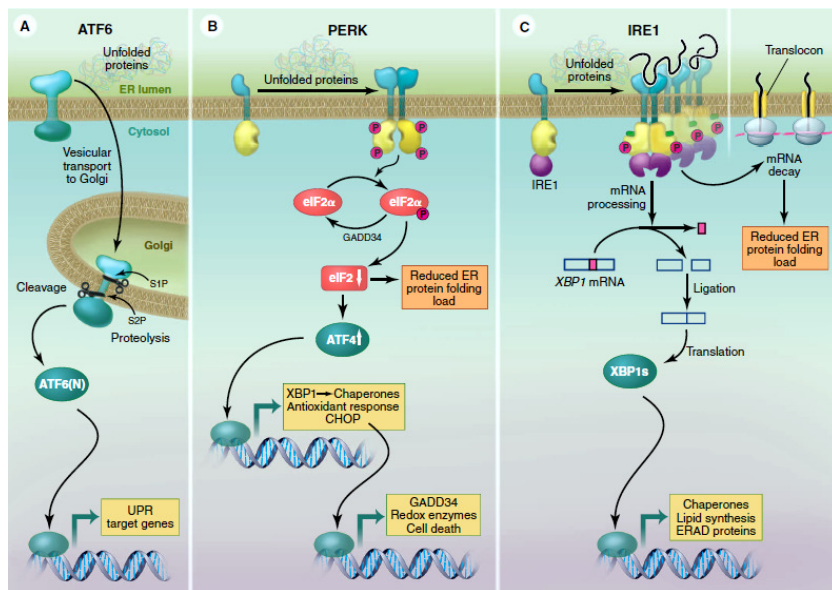


**Figure 13 | Three branches of the unfolded protein response (UPR).** Stress sensors and signal transducers ATF6, PERK, and IRE1 become activated upon appearance of misfolded proteins within the ER or other stressors. The responses are transmitted by different mechanisms: ATF6 by proteolysis and phosphorylation, PERK by oligomerization and mRNA cleavage, and IRE1 by site-specific mRNA splicing. Whereas all three pathways serve to increase the ER folding capacity, PERK and IRE1 additionally slow down protein synthesis rates to restore proteostasis in the ER (figure from Walter 2011).

The UPR is regulated by negative feedback mechanisms. Several phosphatases dephosphorylate eIF2 $\alpha$ , among them protein phosphatase 1 (PP1), induced in late ER response by ATF4. In addition, PERK is inhibited by binding to the Hsp40 cochaperone P58IPK, which is induced by IRE1/XBP1 during ER stress (Yan 2002). Duration and intensity of the stress response pathways play a critical role in the decision between cell survival and apoptosis (Marciniak 2004). However, also in unstressed cells a weak UPS activation can be detected (spliced mRNA), most likely adjusting the folding capacity to the protein synthesis load (Schröder 2005).

### The mitochondrial unfolded protein response (UPR<sup>mt</sup>)

Only a small number of mitochondrial proteins are encoded by the mitochondrial genome. Most mitochondrial proteins are transcribed from nuclear DNA. Proteins translated in the cytoplasm are then imported in an unfolded, Hsp70 bound state through TIM and TOM complexes in the inner and outer mitochondrial membranes (Neupert 2007, Neupert 2012). Folding is supported by mitochondrial chaperons, such as Hsp60/Hsp10 and Hsp70 (Hartl 1987, Cheng 1989). Mitochondria monitor their own proteostasis and control their own unfolded protein response (UPR<sup>mt</sup>; Haynes 2010, Jovaisaite 2014). The mitochondrial electron transport chain consists of large protein complexes. Disruption of their stoichiometry may be one source of mitochondrial protein folding challenges (Yoneda 2004). Increased production of reactive oxygen species (ROS) also triggers the UPR<sup>mt</sup> (Runkel 2013). During times of rapid growth, the UPR<sup>mt</sup> has been shown to promote mitochondrial proliferation (in *C. elegans*; Tsang 2002).

The UPR<sup>mt</sup> is a stress-response pathway that expands the folding capacity and prevents deleterious protein aggregation under normal physiology and in disease. Misfolded structures of the mitochondrial matrix are degraded to peptides by ClpP, which activates transcription factors such as ATFS-1. The peptides are then exported to the cytoplasm (Haynes 2010). ATFS-1 induces transcription of mitochondrial chaperones, proteases, genes involved in ROS detoxification and mitochondrial protein import. Parkin and PINK1 have been furthermore implicated in inducing mitophagy (Geisler 2010).

## Neurodegenerative protein misfolding diseases

Numerous human neurodegenerative diseases are related to protein misfolding and aggregation. The inclusions observed in different parts of the brain are disease-dependent. They contain one or a small number of major protein(s) that drive(s) the sequestration of other factors into the accumulations.

### Dementia

Alzheimer's, Huntington's and Parkinson's disease, amyotrophic lateral sclerosis (ALS), and the prion disorder Creutzfeldt-Jakob disease are all different forms of dementia. The term describes a collection of symptoms comprising a decline of memory, reason, communication skills, and motoric control. The symptoms are caused by a progressive shrinkage of disease specific neurons and brain regions.

The cognitive and physical decline is not only a huge burden for patients, but affects partners and families. As human populations age, incidences of neurodegenerative diseases increase dramatically, and the burden of cognitive decline constitutes a significant social and economic factor. In 2010, 36 million people were affected worldwide by various forms of dementia, a number predicted to double within the next 20 years (Prince 2013). Global costs were estimated to amount to US \$600 billion, comprising direct medical costs, social and informal care (Wimo 2013). This sum corresponds to 1% of global GDP (World Development Indicators database, World Bank, July 1<sup>st</sup> 2011).

Various forms of dementia are diagnosed by cognitive assessment. Similar symptoms impede a definite diagnosis. Genetic diagnostics exist for hereditary cases such as Huntington. Magnetic resonance imaging (MRI) is applied to examine shrinkage of specific cortical regions (Frisoni 2010). Young people can be affected by neurodegenerative disorders, but the prevalence of dementia

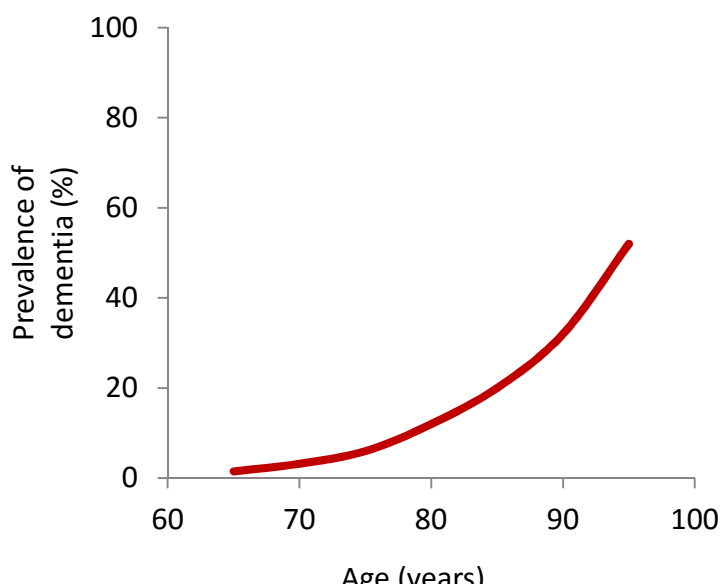


**Figure 14 | Exponential increase of dementia in human patients of higher age** (UK Dementia report 2007, Borjesson-Hanson 2004).

increases severely with age. As a Swedish study examined, around 30% of 85 years old and 50% of 95 years old suffer from dementia (Borjesson-Hanson 2004). For prevention or reversion, there are no effective treatments available yet. Therapies mainly attempt to slow down the disease progression by mental and physical activity. Avoidance of potential risk factors, such as obesity, diabetes, high cholesterol, inflammation, or high blood pressure, may improve health in general and delay symptoms of dementia at higher age.

## Alzheimer's disease

Alzheimer's disease (AD) is a chronic neurodegenerative disorder characterized by a progressive loss of cognitive functions, appearance of psychiatric symptoms (depressions, hallucinations), and increasing difficulties in physical activities that often occur incrementally. AD is accompanied by a huge loss of brain volume mainly caused by neuronal shrinkage and loss of processes and synapses. Patients in an early phase already lost around 40% of their synapses in neocortex hippocampus. This decline in connectivity correlates highly with the cognitive decline of Alzheimer patients, much better than with the pure burden of aggregates (Scheff 2006 *Neurobiol Aging/J Alz Dis*, Palop 2003, Knobloch 2008, Gomez-Isla 1996).

However, quantifications of neurons and synaptic connections are still a challenge in the human brain. AD is a very complex disease, most likely caused by multiple genetic and environmental factors defining a lifetime risk in the background of a general physiological decline during aging. Even a continuum between "normal aging" with asymptomatic lesions and developing AD based dementia seems plausible (Serrano-Pozo 2011).

On the molecular level, the two pathological hallmarks of AD are extracellular amyloid plaques and intracellular neurofibrillary tangles (NFTs). The extracellular plaques are highly enriched in aggregated forms of A $\beta$ , the amyloid  $\beta$  peptide (Glenner 1984).

### Signaling and structural functions of the amyloid precursor protein (APP)

APP is a highly conserved transmembrane protein with a large ectodomain, a single transmembrane region (partially overlapping with the A $\beta$  sequence), and a short cytoplasmic tail. Homologs of the APP have been found in invertebrates and vertebrates. The latter encode two more APP like proteins (APLP1, APLP2) without A $\beta$ -like sequence. While APLP1 is predominantly expressed in the human brain, APP is ubiquitously expressed in all cells in humans, APLP2 rather in peripheral tissues (Huang 2011).

The family members proposedly function as cell surface receptors and play key roles in neuronal development, cell adhesion, synaptic plasticity, and long-term memory (Huang 2011, Zheng 2011). Interestingly, only double knockouts including APLP2 are lethal, indicating partially overlapping functions (Huang 2011). APP binds to intra- and extracellular factors and is enriched at synaptic sites, allowing APP to engage in interactions between different cells. Knockout mice showed defects in long-term potentiation and poorly formed neuromuscular synapses (Huang 2011, Zheng 2011). The cellular interactions of individual domains and cleavage products still need to be investigated in more detail to reveal a better picture of their biological significance.

### Processing of APP, production of A $\beta$ variants, and related pathophysiology

A $\beta$  is produced by sequential cleavage of APP (Kang 1987) by  $\beta$ -secretases (BACE1) and  $\gamma$ -secretases. A competing  $\alpha$ -secretase cleaves APP in the middle of the A $\beta$  sequence and thereby prevents A $\beta$  production. In AD patients,  $\beta$ -secretase activity was found to be increased to 185% of non-AD individuals, whereas  $\alpha$ -secretase activity declined to 81% (Tyler 2002).

$\gamma$ -secretase is an integral membrane protein complex with a membrane-embedded aspartyl protease. It cleaves APP within the hydrophobic part of the membrane, releasing A $\beta$  into the ER

lumen, extracellular space, and endosomes. Due to its conformational flexibility,  $\gamma$ -secretase is able to produce different A $\beta$  peptides of varying length, from A $\beta_{37}$  to A $\beta_{46}$ . The usually predominant species is A $\beta_{40}$ , next to A $\beta_{42}$  (5-15% of the total pool, extended by Ile and Ala; Steiner 2008, Masters 2012). Increasing the A $\beta_{42}$ /A $\beta_{40}$  ratio caused e.g. by mutations in  $\gamma$ -secretase is implicated in early onset of familial AD and in increased disease progression. A $\beta_{42}$  is more aggregation prone and was found to form the initial inclusions in the brain, from which aggregation starts to seed (Findeis 2007).



**Figure 15 | A $\beta$  sequence including proteolytic cleavage sites within the amyloid precursor protein (APP).**  $\alpha$ -secretase cleaves in the middle of the A $\beta$  sequence, preventing A $\beta$  production. The combined cleavage of  $\beta$ - and  $\gamma$ -secretases creates A $\beta_{40}$  or A $\beta_{42}$  (figure adapted from Findeis 2007). Longer hydrophobic stretches are labeled in yellow, the A $\beta$  “aggregation core” (A $\beta_{16-22}$ ) is surrounded by two charged residues (blue) and forms highly ordered  $\beta$ -sheet fibrils *in vitro* (Balbach 2000). The C-terminal hydrophobic stretch corresponds mainly to the membrane spanning helix of APP.

Distinct mutations in APP and presenilin 1 and 2 (part of the  $\gamma$ -secretase complex) cause an early onset of AD (<60 years; Tanzi 2012). Most of the found mutations were associated with an increased appearance of A $\beta_{42}$  and other neurotoxic A $\beta$  products. A deletion of a single glutamate within A $\beta$ , E693 $\Delta$ , completely prevents the formation of insoluble amyloid plaques in favor of soluble A $\beta$  oligomers. Despite the fact that amyloid imaging revealed not more amyloid depositions than in age-matched healthy controls, patients carrying the E693 $\Delta$  mutant closely resembled AD symptoms (Tomiya 2008).

Susceptibility for late-onset AD (>65 years) is influenced by a very common gene polymorphism. Lipoproteins (HDL, LDL) transport lipids and cholesterol in form of soluble protein-lipid particles through the circulatory and lymphatic systems. Apolipoprotein E4 (ApoE4) binds and complexes A $\beta$  in the cerebrospinal fluid with 20-fold lower affinity than ApoE3, and thereby decreases A $\beta$  clearance by 40%. The ApoE4 variant has a negative influence on the AD risk factor cholesterol and decreases the age of AD onset in a dose-dependent manner (heterozygous, homozygous; Tanzi 2012). Recently, a strong protective but rare mutation was found close to the aspartyl protease  $\beta$ -site in APP. The A673T allele decreases the peptide deposition, whereas other mutations at the same site (such as A673V) strengthened AD symptoms. The result supports the hypothesis that lowering A $\beta$  levels are protective. The A673T allele also protects against cognitive decline in elderly people not suffering from Alzheimer’s disease, suggesting similar mechanisms behind various forms of cognitive decline (Jonsson 2012).

### Cytoplasmic neurofibrillary tangles and cytoplasmic APP cleavage products

Besides the amyloid plaques, cytoplasmic neurofibrillary tangles were already mentioned by Alois Alzheimer in his original autopsy case report. Neurofibrillary tangles consist of the microtubule stabilizing Tau protein (MAPT), which in a hyperphosphorylated form dissociates from the microtubules (Baner 1989). Consequently, microtubules start to depolymerize and Tau oligomerizes and aggregates into paired helical filaments (PHFs) in the cytoplasm (Alonso 1996, Alonso 2001).

Cytotoxic properties have also been described for the short C-terminal APP intracellular domain (AICD), which is released into the cytoplasm during protease processing of APP. In absence of the

respective caspase cleavage site in mutant APP transgenic mice, A $\beta$ -related phenotypes such as synaptic, behavioral, and electrophysiological abnormalities were absent in spite of abundant amyloid deposits (Galvan 2006, Saganich 2006). Such findings demonstrate the still poor understanding of the primary molecular causes of AD, despite of the many correlations and associations that have been described.

### Amyloid cascade hypothesis

Tau exists in six splicing isoforms of 352-441 amino acids length and contains at least 30 phosphorylation sites. Under normal conditions, tau is a soluble, most likely unstructured protein. It resides predominantly in axons and the residual neuronal cytoplasm (Huang 2009, Mandelkow 2012). Several mutations within the Tau gene can cause frontotemporal dementia with Parkinsonism, affecting e.g. the microtubule-binding repeat domains. Interestingly, this form of dementia is characterized by intense neurofibrillary tangle formation without elevated amyloid depositions (Hutton 1998, Poorkaj 1998). On the contrary, A $\beta$ -induced neurodegeneration depends on cytoplasmic tau. Tau depleted neurons in presence of A $\beta$  do not show neurodegeneration (Rapoport 2002). In mice, knockout of Hsp110, a potential disaggregase or holdase, led to hyperphosphorylation of tau and to neurodegeneration (Eroglu 2010). Aggregated A $\beta$  has been shown to induce hyperphosphorylation of tau accumulating mostly in the neuronal soma and dendrites (Zheng 2002). The potential of mutated tau causing dementia on its own and the requirement of tau for transmitting the toxic impact of A $\beta$  led to the “amyloid cascade hypothesis”: abnormal cleavage of APP combined with insufficient A $\beta$  clearance results in senile plaque accumulation, which triggers tau hyperphosphorylation and tangle formation within cells (Hardy 2002).

### The impact of cholesterol and other lipids on Alzheimer’s disease

Cholesterol is highly enriched in human brains, especially in insulating myelin sheath surrounding nerve fibers. Cholesterol concentrates within “lipid rafts”, increases the order in membranes, and affects membrane fluidity. Non-amyloidogenic APP processing by  $\alpha$ -secretase happens outside of lipid rafts and is promoted by low cholesterol levels (Kojro 2001). In contrast,  $\beta$ - and  $\gamma$ -secretases colocalize at least transiently with APP in lipid rafts, and high cholesterol stimulates their activity. The specificity of the intramembrane cleavage of  $\gamma$ -secretase is remarkably sensitive to membrane thickness. Varying the lipid components towards a lowered thickness leads to an increased A $\beta_{42/43}$  production (Winkler 2012).

The essential  $\omega$ -3 polyunsaturated fatty acid docosahexaenoic acid (DHA) was ascribed to mediate the inverse correlation between increased fish intake and dementia (Grimm 2013). DHA reduces intra-neuronal A $\beta$  levels as well as tau phosphorylation by inhibiting  $\beta$ - and  $\gamma$ -secretase activities in a dose-dependent manner. Overall, the lipid environment appears as a critical parameter at the origin of distinct A $\beta$  species (Grimm 2013). Early treatments with statins that lower cholesterol levels could offer preventive functions, as demonstrated in mice (Refolo 2001, Kurata 2012).

### Missing links in Alzheimer’s disease

The discovery of associated mutations to AD strengthens the notion of a causative role of A $\beta$  and Tau in neurodegeneration. How toxicity is transferred from extracellular A $\beta$  plaques into cells and translated into hyperphosphorylation and fibrillarization of Tau in the cytoplasm is still rather

unclear. Extracellular A $\beta$  was shown to potentially erroneously modulate important membrane receptors, such as the nicotinic acetylcholine receptors (nAChR; Buckingham 2009). It was demonstrated on postmortem AD brains that fibrillar A $\beta$  binds in nanomolar concentrations to the  $\alpha$ 7-nAChR subtype, an interaction that could be blocked by specific antagonists (Ni 2012). Disturbing signaling pathways across the cellular membrane and intracellular compartments could be one plausible way of transmitting extracellular protein misfolding into intracellular toxicity. However, pharmaceutical treatments that inhibit acetylcholinesterase performed only modestly in slowing AD progression (Raina 2008).

But extracellular A $\beta$  seeds are potentially not the only or major initiator of cell death in AD. In hippocampal rat neurons, the direct transfer of microinjected A $\beta$  oligomers between connected cells demonstrated the potential pathogenicity of intracellular A $\beta$  species. Transmission of A $\beta$  oligomers was dependent on dendritic and axonal contacts between the neurons and caused disruption of tubulin structures and cytotoxicity (Nath 2012). The ambiguity about A $\beta$  species affecting neurons primarily in form of extracellular plaques or intracellular oligomers reveals how less is still known about the pathogenic roles of various misfolded species and the sequence of pathological events that have been described for distinct neurodegenerative diseases.

## Huntington's disease

Huntington's disease (HD) is the most common inherited neurodegenerative disorder with a prevalence of 1 per 17,500 inhabitants in Europe, North America and Australia, but only 1 per 250,000 in Asia (Pringsheim 2012). Patients suffer from uncontrolled motor movements as well as cognitive and emotional deficits. Preferentially, cortical and striatal brain regions are affected by shrinking and cell death. Cytotoxicity in HD is ascribed to the appearance of protein aggregates in patients carrying an extended CAG repeat in the Huntingtin gene. CAG encodes extended polyglutamine (polyQ) sequences within the N-terminal region of the ~350 kDa Huntingtin protein (Htt). The repeats explain not only the inheritability of the disease, but their number is directly correlated to the age of HD onset. While the majority of the population contains less than 24, most HD patients carry 40-65 CAG repeats (The Huntington's Disease Collaborative Research Group 1993). The Htt gene is composed of around 70 separated exons with alternative splicing variants. N-terminal Htt fragments with an extended polyQ tract, preceded by a 17 amino acid stretch (N17) and followed by a polyproline and glutamine rich region, are most often found in intraneuronal inclusions (DiFiglia 1997). N17 has been shown to contain a switchable ER-targeting and a nuclear export signal. These signals are controlled by stress-dependent phosphorylation and acetylation, modulating the localization and the toxicity of Htt and its fragments (Atwal 2011, Maiuri 2013).

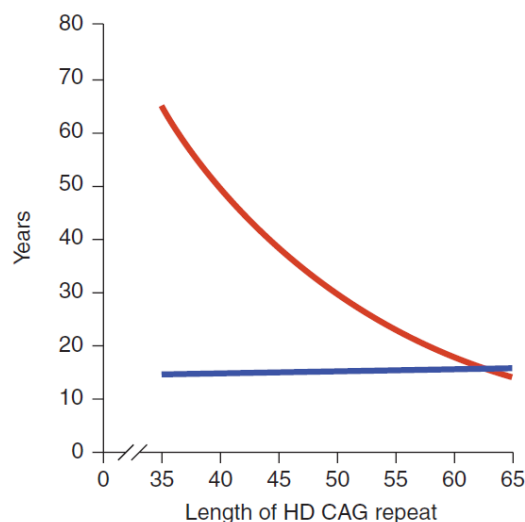


**Figure 16 | Negative relationship of CAG repeat length and age of disease onset of HD patients.** Age of neurological onset is directly inversely correlated to the age of onset (red). Duration of disease from onset to death remains fairly constant between 15-18 years (blue curve; figure from Finkbeiner 2011).

The polyproline stretch forms a flexible helix that influences solubility and aggregate formation (Dehay 2006). Localization, solubility, and conformational stability of the entire fragment in turn affect its cellular toxicity.

Nuclear aggregates of ubiquitinated, truncated Htt in the brains of patients appeared as a hallmark of HD. Lacking a C-terminal nuclear export sequence of the full-length protein, Htt fragments may increasingly enter the nucleus and form inclusions (Xia 2003). However, already early on a study examining adult HD patient brain tissues described a majority of cytoplasmic aggregates in dystrophic neurites (neuronal projections, axons, and dendrites). Only in young patients, nuclear inclusions were predominant (DiFiglia 1997). Despite the fact that cytoplasmic aggregates were often found in coexistence with intranuclear inclusions, often the latter made it into the title of publications (“Huntington’s Disease intranuclear inclusions contain truncated, ubiquitinated Huntingtin protein”, Sieradzan 1999). Using an improved antibody against the N-terminal sequence, Gutekunst et al. discovered “that neuropil aggregates are much more common than nuclear aggregates” (Gutekunst 1999). These Htt aggregates again appeared especially in dendrites and dendritic spines in the brains of HD patients.

The first transgenic Huntington’s disease mice expressing polyQ extended Htt exon 1 (including the R6/2 line analyzed in this study) displayed a progressive neurological phenotype between 9 and 12 weeks of age, dying 2-3 weeks later (Mangiarini 1996). In human cell culture experiments, mutant Htt exon 1 containing polyQ tracts of various lengths mostly accumulated in the cytoplasm of e.g. HEK293T or SH-SY5Y neuroblastoma cells. In primary neuronal cell cultures, such Htt fragments are rather imported into the nucleus, indicating a cell-type and fragment specific localization. The 17 N-terminal amino acids preceding the polyQ tract of human Htt have been described to contain a leucine-rich nuclear export sequence, which is recognized by the exportin CRM1 (Leptomycin B sensitive; Maiuri 2013). This export sequence may compete with e.g. cellular attempts to transfer misfolded fragments to the nucleus for degradation (Park 2013), which may thus be one reason for the different localizations in distinct cellular environments.

Besides the presence of microscopically visible aggregates in different cellular (sub-)compartments, their presence and selective visibility (due to e.g. specific antibodies applied) does not necessarily describe a causative link to neuronal shrinkage or disease progression. Large aggregates might be a source or a sink for less visible and rather transient structures that can harm cells at different sites, which leads us to central questions of this study: which misfolded structures are especially toxic, where and how do they severely damage living cells?

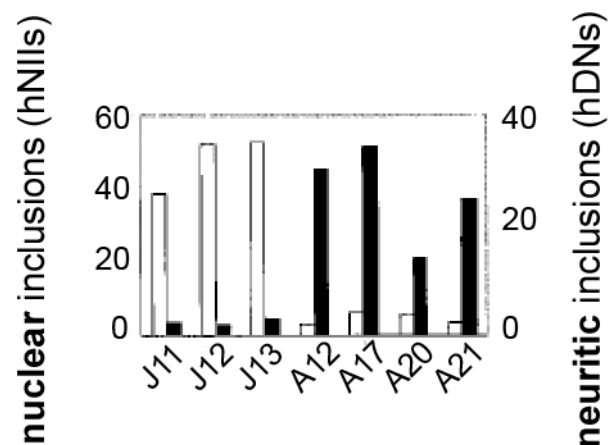


**Figure 17 | Nuclear (○) and neuritic (●) inclusions in juvenile and adult patients.** Whereas huntingtin aggregates of young HD patients were mainly detected in the nucleus, most aggregates were found in neurites (cytoplasm) of cerebral neurons in adult HD patients (figure from DiFiglia 1997).



## Biological function of full length Huntingtin and amyloid formation

Full length Htt is a multidomain protein with a C-terminal nuclear export signal (Xia 2003) that is not present in the aggregated N-terminal fragments found in inclusion bodies. Full length Htt is completely soluble and has no homology to other proteins. Htt is expressed within cytoplasm, ER and Golgi, at the highest levels in neurons of the central nervous system (Cattaneo 2005).

Htt is essential during embryogenesis as demonstrated in mice. In embryonic and adult mice and in cell culture, Htt has been shown to protect from apoptotic cell death after various apoptotic stimuli (Leavitt 2006, Zeitlin 1995). Htt is found in neurites and at synapses, where it associates with vesicular structures and microtubules and seems to be involved in vesicle trafficking (Cattaneo 2005). Heterozygous animals carrying only one Htt gene display no phenotype. However, they display motor and cognitive dysfunctions if an N-terminal fragment (Htt exon 1-4) is being expressed (Duyao 1995, Nasir 1995, Zeitlin 1995). Overall, various native functions of Htt are still intensely investigated.

Htt fragments form to cross  $\beta$ -sheet structures. In contrast to the hydrophobic aggregation cores of most other amyloid fibrils, the polar nature of the glutamine side chain is thought to form hydrogen-bonded polar zippers through linkages between main-chain and side-chain amides (Perutz 1994). However, the polyglutamine flanking sequences (N17 and C-terminal polyproline region) play an important role for the assembly of nonfibrillar oligomers and for toxicity (Hoop 2014, Lyubchenko 2012).

## Parkinson's disease

With a prevalence of 1% at age 65 and 5% at age 85, Parkinson's disease (PD) is the second most common neurodegenerative disorder. Symptoms of Parkinson's disease are typically chronic and slowly progressive with a mean duration of 15 years from diagnosis to death. Patients suffer from muscle tremor, rigidity, postural instability, sleep disorder, and dementia (Shulman 2011).

Pathologically, PD is defined by neurodegeneration of dopaminergic cells within the Substantia nigra. Here,  $\alpha$ -synuclein forms the core and major component of cytoplasmic protein-rich inclusions termed Lewy Bodies (described by the neurologist Friedrich Lewy in 1912). With 60% of neuronal death within the Substantia nigra, losses are substantial when symptoms appear. Lewy Bodies were found throughout the central nervous system and the neuronal periphery. Symptoms of PD can also accompany other neurodegenerative disease, summarized by the "syndromes of parkinsonism". These interrelations demonstrate obvious difficulties in defining and differentiating between related neurodegenerative diseases. On the other hand, findings of Lewy Body pathology might appear without apparent clinical manifestations (Shulman 2011).

PD has been considered as a sporadic disorder influenced by environmental triggers, such as pesticides (Priyadarshi 2000). Meanwhile, a number of associated genetic variants were identified. Mutations in the SNCA gene (encoding  $\alpha$ -synuclein; A53T, A30P, or E46K) or gene duplications leading to increased  $\alpha$ -synuclein levels were associated with early-onset and rapid disease progression (Shulman 2011).  $\alpha$ -synuclein associates with presynaptic vesicles and consists of an amphipathic N-terminus, a hydrophobic core, and a negatively charged, unstructured C-terminus (Ulmer 2005).

Interestingly,  $\alpha$ -synuclein was found to be degraded by chaperone-mediated autophagy (CMA). Due to its CMA specific recognition motif (V<sub>95</sub>KKDQ<sub>99</sub>),  $\alpha$ -synuclein is selectively translocated into lysosomes for degradation. Moreover, the pathogenic A53T and A30P mutants bound lysosomes more strongly, but inhibited translocation and degradation, causing an arrest of cellular CMA functions. The pathogenic mutants inhibited not only their own degradation, but also that of long-lived and misfolded sequences (Cuervo 2005). Such gain-of-functions might ultimately develop into significant proteostasis challenges, especially since  $\alpha$ -synuclein assembles into oligomeric and fibrillary  $\beta$ -sheet structures on its own.

A set of genes has been especially related to autosomal recessive juvenile forms of PD: Parkin, PINK1, and DJ-1, whereby loss- and gain-of-function seem to be especially interrelated. Under cell stress, Parkin is acting most likely downstream of the mitochondrial kinase PINK1 (PTEN-induced kinase) towards pro-survival signaling (Winklhofer 2008, Lo Bianco 2004). Parkin and PINK1 have been implicated in induction of mitophagy by polyubiquitination of VDAC1 (Geisler 2010), which may cause mitochondrial apoptosis (still controversial; Kroemer 2007, Alavian 2014). On the other hand, mutations in both of the proteins, Parkin and PINK1, mutually affect their stability and aggregation (Um 2009, Um 2010), and Parkin itself was found as an enriched component in Lewy Bodies (Chung 2001). Also, short C-terminal truncations of Parkin result in cytoplasmic aggregation of the proteins (Winklhofer 2003). Neuroprotection under mild stress may therefore transform into misfolding and aggregation, when the cellular stress overwhelms Parkin's own folding equilibrium.

Although currently available therapies delay disability and prolong life expectancy, none was able to interfere considerably with the neurodegenerative process. New therapeutic avenues include viral vectors intervening in the dopamine equilibrium and transplantation of fetal nigral cells into the striatum. Interestingly, the fetal cells developed Lewy Bodies only a few years after transplantation despite their own "young age", suggesting a strong influence of the local environment (Shulman 2011, Obeso 2010).

## Nucleo-cytoplasmic transport of proteins and RNAs

### Subcellular compartmentalization and proteostasis

Cells are subdivided into several compartments to allow different chemistry taking place and to separate cellular functions. Major compartments comprise the cytoplasm, nucleus, endoplasmic reticulum (ER), Golgi network, mitochondria, and cell membranes. There are further sub-compartments with specific activities exist, such as the nucleoli (ribosome assembly), euchromatin (active genes), heterochromatin (inactive genes), Hsf1 foci (active during proteome stress), various snRNPs (small nuclear ribonucleoprotein particles for RNA processing) in the nucleus (Matera 2009, Francastel 2000).

Although some cellular subcompartments can be completely created by self-assembly, many require the incorporation of additional molecules (proteins, lipids) into preexisting structures to grow and proliferate (Noda 2002). Thousands of proteins are actively targeted into cellular locations, addressed via specific targeting sequences that are incorporated into the polypeptide chains (Sabatini 1971, Akopian 2013). Different subcellular biochemistries bear specific challenges for proteostasis, promoting cellular functions such as protein synthesis and folding in the cytoplasm, energy metabolism in mitochondria, preservation of genetic material in the nucleus, or an oxidizing milieu in the ER. Every compartment possesses its distinct proteostasis machinery corresponding to the prevalent conditions.

### Nuclear envelope and nuclear pores

Recently, the cellular interactors of amyloid-like aggregates were identified in human cells. Toxicity may originate from an impairment of cellular pathways related to these interactors, which also included several factors involved in molecular nucleo-cytoplasmic transport (Olzscha 2011). During the course of this study, we furthermore observed a disturbed morphology of the nuclear envelope and a speckled chromatin structure in cells with protein aggregates.

In neurons of *C. elegans*, glutamate triggered excitotoxicity leading to neurodegeneration was found to increase the permeability of nuclear pores via elevated calcium levels. The nuclear barrier and transport machinery appeared to be compromised, finally supporting cell death by apoptosis (Bano 2010 Cell Death Diff/Nucleus). Nuclear irregularity has furthermore been observed in hippocampal and neocortical biopsies of Alzheimer's disease patients, often in association with neurofibrillary tangles (Sheffield 2006).

All these indications made us interested in studying the efficiency of nucleo-cytoplasmic transport in cells affected by protein aggregation. Subcellular and nucleo-cytoplasmic transport is essential for many cellular functions, especially for stress signaling, inducing cellular responses to cope with e.g. increased amounts of misfolded structures or reactive oxygen species. Very recently, morphological abnormalities of nuclear were described in cells expressing mutant Huntingtin (Liu 2015). Studies on the C9orf72 repeat expansion related to ALS/FTD documented a compromised nucleo-cytoplasmic transport in different model systems (Freibaum 2015, Jovicic 2015, Zhang 2015).

The nuclear envelope separates the nuclear matrix from the cytoplasm. The envelope is composed of two lipid membranes contiguous with the ER. Membranes of the nuclear envelope are underlaid by a fibrous sheet of proteins. This lamina consists mostly of  $\alpha$ -helical intermediary filaments of type V

(lamins) that associate to integral or peripheral membrane proteins, which furthermore connect to chromatin-associated proteins. Lamins dissociate upon phosphorylation early during mitosis, although their degree of disassembly remains uncertain (Guettinger 2009).

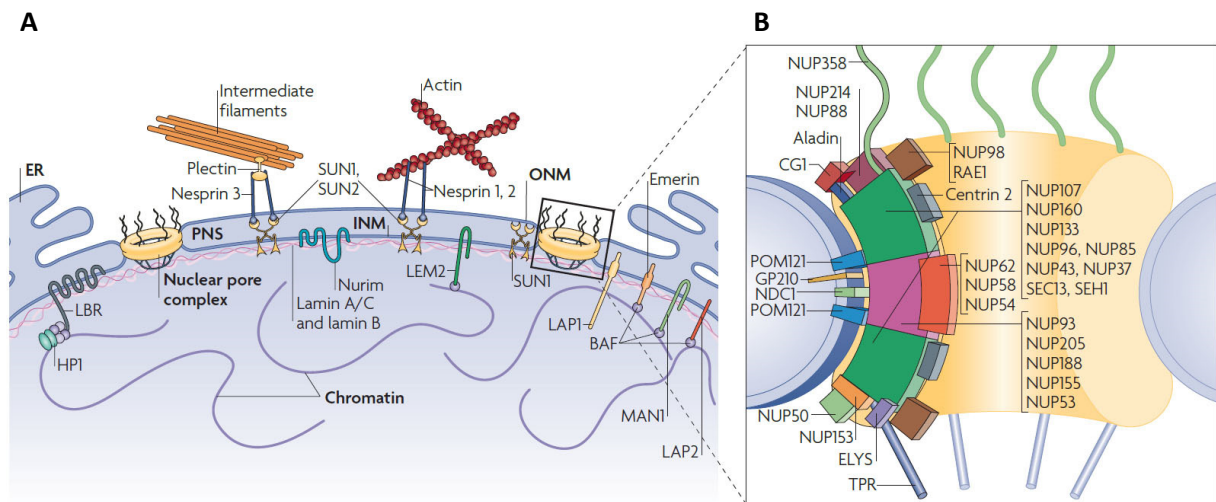


**Figure 18 | The main structural features of the nuclear envelope and nuclear pore complexes.** **A** Inner and outer nuclear membranes (INM/ONM) are separated from the perinuclear space (PNS), contiguous with the ER lumen. INM proteins link the nuclear envelope membrane to the underlying lamina and to chromatin, whereas ONM proteins connect to the cytoskeleton. The lamin B receptor, for example, connects to B-type lamins and to chromatin-associated heterochromatin protein 1 (HP1). Other proteins are linked to DNA replication, nuclear envelope assembly, and gene regulation. **B** Nuclear pore complexes (NPCs) are large macromolecular assemblies of up to 120 MDa with eight-fold rotational symmetry. They are built from around 30 different nucleoporins (Nups), assembled from subcomplexes forming building blocks. The central channel of the NPC is filled with FG-repeat proteins, providing interaction sites for transport receptors (figure from Güttinger 2009).

The only (known) passages through the nuclear envelope are the nuclear pores. They are dynamic and selective tunnels formed by large protein assemblies, the nuclear pore complexes (NPCs). Molecules up to a size of around 30 kDa can freely pass through these molecular sieves, larger proteins need to be actively transferred. In addition, many smaller biomolecules (proteins, RNA) are actively sorted between the two compartments. Their location and gradients between cytoplasm and nucleus are essential for their cellular function and for maintaining homeostasis.

Active nucleocytoplasmic transport is mediated by transport complexes that recognize specific targeting signals on their cargos. Substrate binding, low-affinity interactions with nucleoporins (NPC proteins) during translocation, and substrate release are the major steps in this process. Many transport proteins that mediate nucleocytoplasmic transport belong to the family of karyopherin  $\beta$  proteins. They are a family of at least 20 relatively large proteins of around 100 kDa and a weak sequence homology (identities of typically 15-20%). Known structures comprise  $\sim 20$  HEAT repeat domains of  $\sim 40$  amino acids length. HEAT repeat domains fold into pairs of  $\alpha$ -helices stacked together in a slightly twisted parallel fashion. This “superhelical” architecture leads to an inner concave and an outer convex surface, whereby N- and C-terminal arches can often be distinguished (Cook 2007).

## Nucleo-cytoplasmic targeting of proteins

Proteins intended for active cellular localization contain specific targeting sequences that are recognized by transport receptors or adaptor proteins (first suggested for ER proteins by Günter Blobel; Sabatini 1971). Classical nuclear localization signals (NLS) can be monopartite, consisting of a cluster of 3-5 positively charged residues, or bipartite with a second cluster of lysine or arginine residues following a 10-12 residue long linker (Kalderon 1984). Nuclear export sequences (NES) on proteins for cytoplasmic localization are leucine-rich sequences. They are harder to predict as they show a higher variation and can be similar to regions hidden in hydrophobic cores of folded proteins (la Cour 2004).

### Nuclear import

Classical NLSs are recognized by importin  $\alpha$  proteins with two clusters of lysine-binding pockets, which recognize the two stretches of a bipartite sequence. A series of tryptophans engages in hydrophobic interactions with the aliphatic tails of the lysine residues, while the positively charged amino groups find their negatively charged counterparts in nearby acidic residues.

Importin  $\alpha$  proteins are adaptor proteins with an importin  $\beta$ -binding domain (IBB). Although most karyopherin  $\beta$  proteins bind their cargo directly at the inner concave surface, NLS cargoes seem to be an exception to that rule. Once a ternary complex of NLS-cargo:importin  $\alpha$ :importin  $\beta$  is formed, it translocates through the nuclear pores into the nucleus. Here the complex encounters Ran, a 24 kDa GTPase. RanGTP binding causes the dissociation of karyopherin  $\beta$  complexes and a release of the cargo. The release is triggered by direct steric interference with the cargo binding sites, and allosterically through conformational changes. Thereby, the IBB domain of importin  $\alpha$  is expelled from importin  $\beta$ . The IBB domain appears largely disordered, but likely folds back on the NLS binding sites, leading to an autoinhibited state. Another karyopherin  $\beta$  is transportin 1, recognizing M9 NLSs of many mRNA binding proteins involved in RNA processing and nuclear export (Cook 2007).

### Nuclear export

Importin  $\alpha$  needs to be returned to the cytoplasm, which is mediated by its specific exporter CAS. Only the auto-inhibited conformation of importin  $\alpha$  is recognized by CAS in the presence of RanGTP, and the complex dissociates upon entry in the cytoplasm. Nuclear export of a broad variety of cytoplasmic cargo proteins is mediated by the exportin Crm1, which binds NES generally with lower affinities. Crm1-dependent transport can be inhibited by the small molecule drug Leptomycin B (LMB) that covalently attaches to a cysteine residue on Crm1 and thereby interferes with cargo binding (Fornerod 1997, Cook 2010).

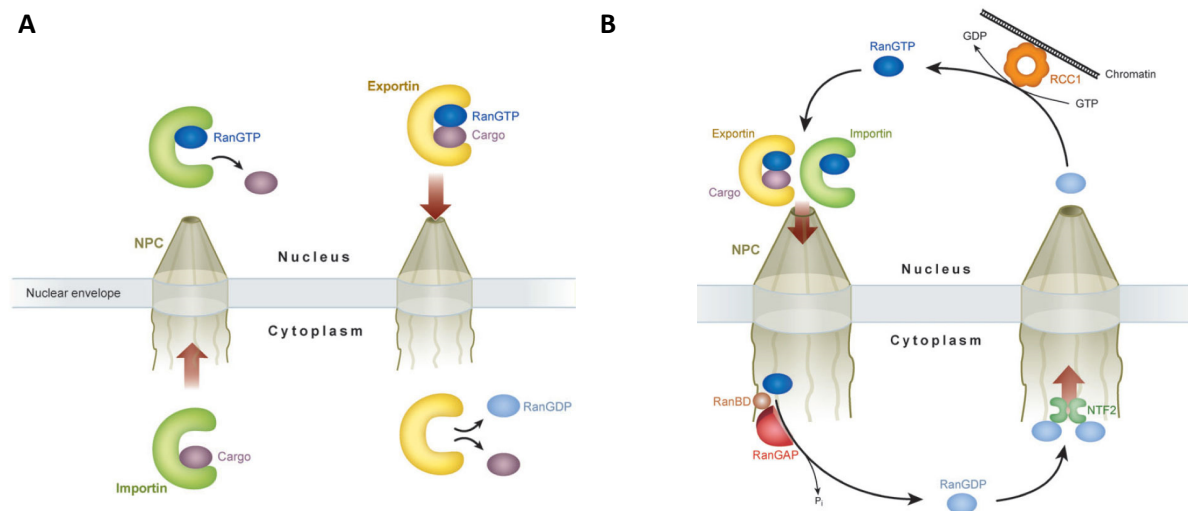


**Figure 19 | Karyopherin  $\beta$  proteins (also known as importins or exportins) mediate nuclear import and export, driven by the Ran cycle. (A)** Importins recognize cargo in the cytoplasm at specific binding sites, which partially overlap with RanGTP binding sites after translocation through the nuclear pore complex (NPC) into the nucleus. Exportins bind cargo and RanGTP in the nucleus and translocate to the cytoplasm, where GTP hydrolysis triggers the release of both factors. **(B)** RanGAP (GTPase-activating protein) maintains a high concentration of RanGDP in the cytoplasm. NTF2 transports RanGDP back into the nucleus, where RCC1 restores RanGTP to maintain the gradient (figures from Cook 2007).

### The Ran cycle

The dissociation of export complexes is triggered by the hydrolysis of RanGTP to RanGDP in the cytoplasm. Already at the NPC, Ran binding proteins (RanBP1, RanBP2) promote the dissociation of RanGTP from karyopherins and stimulate RanGAP1-mediated (GTPase activating protein) hydrolysis. RanGDP has only a very low affinity for karyopherins. Sumoylation localizes RanGAP to the cytoplasmic face of NPCs through interactions with RanBP2.

RanGDP is recycled back into the nucleus by its specific importer NTF2. Back in the nucleus, the chromatin associated RCC1 (with a seven-bladed  $\beta$ -propeller structure) functions as a RanGEF (guanidine exchange factor) and mediates nucleotide exchange (Cook 2007). Restoring nuclear RanGTP ultimately gives directionality to the whole nucleo-cytoplasmic transport process.

### Messenger RNA processing and nuclear export

Transcription, processing, and nuclear export of messenger RNAs (mRNAs) are tightly coupled in the eukaryotic cell. Large RNA-protein complexes form and proceed in a dynamic manner in functional small nuclear ribonucleoprotein particles (snRNPs, or “snurps”). snRNPs are distinct from other nuclear subcompartments, such as nucleoli or Hsf1 related stress granules (Metz 2004, Biamonti 2010).

The THO complex is one of the key factors of this process. THO is conserved from yeast to human. The complex associates during snRNP biogenesis, prevents base pairing between nascent RNA and its DNA template, and recruits processing factors. THO finally mediates nuclear export only of fully processed mRNA. Several THO proteins (human: Thoc1-7) are part of the human TREX (transcriptional export) complex in conjunction with additional factors that are dynamically integrated and released (Jimeno 2010). Thoc4 (Aly/Ref) directly interacts with Thoc2 and Thoc5 linking a TREX core protein, UAP56, to the cap-binding protein CBP80 (Chi 2013). CBP80 itself is part

of the cap-binding complex (CBC), which binds cotranscriptionally to the 5'-cap of pre-mRNA and is involved in splicing by the spliceosome and in transcriptional regulation. UAP56 is an RNA helicase and a core component of TREX. The complex furthermore interacts with the exon-junction complex (EJC) that marks splicing sites (Chi 2013, Erkmann 2004).

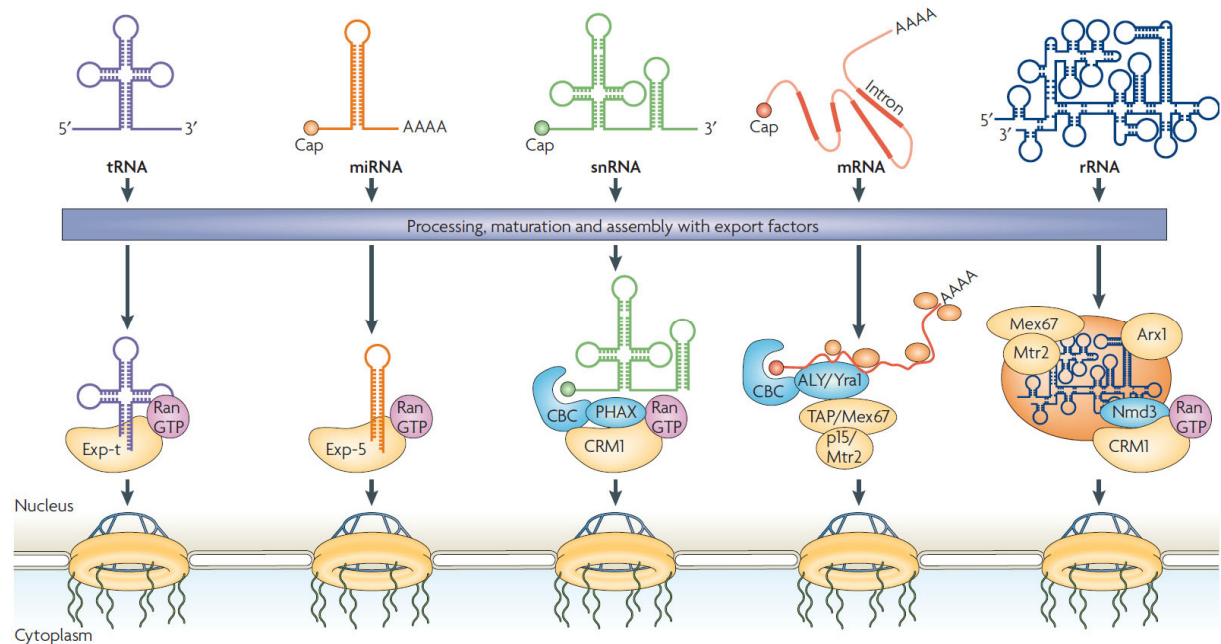


**Figure 20 | Different classes of RNAs and their nuclear export pathways.** Biogenesis, processing, and nuclear export of RNAs are usually highly coupled and regulated processes. Different classes of RNAs employ different nuclear export systems. Besides mRNA, all other RNA classes are exported by exporters of the karyopherin  $\beta$  family (tRNA by exportin-t, miRNA by exportin-5, snRNA and rRNA by Crm1), driven by the RanGTP/RanGDP cycle. The majority of mRNA transport is conducted Crm1/Ran-independently. Processing and transport include several huge protein complexes and associated factors, such as the exon-junction-complex (EJC) and the transcriptional export complex (TREX) comprising the THO proteins. The heterodimer Tap:p15, the RNA adaptor Aly/Ref, and the ATP-dependent helicase Dbp5 are directly involved in the nuclear mRNA export at the nuclear pore complex, which is under debate for proteins of the EJC and TREX complex (figure from Köhler 2007).

The majority of mRNA export occurs independently of karyopherin  $\beta$  proteins or Ran. The heterodimeric complex Tap:p15 directly interacts with nucleoporins. p15 shows significant sequence homology with NTF2 (recycling RanGDP). Tap (or Nxf1) is a multi-domain protein with an RNA binding domain (RBD) and a nucleoporin binding site. Tap:p15 works in conjunction with the TREX complex, the exon-junction complex (EJC), Aly/Ref (Thoc4), which additionally bind RNA as an adaptor complex, and Dbp5, an ATP-dependent helicase (Cook 2007). Nxf1 has been demonstrated to change into an open, mRNA-binding conformation once it made contact to Thoc4/5 binding sites on the TREX complex, indicating “that TREX provides a license for mRNA export by driving Nxf1 into a conformation capable of binding mRNA” (Viphakone 2012, Müller-McNicoll 2013).

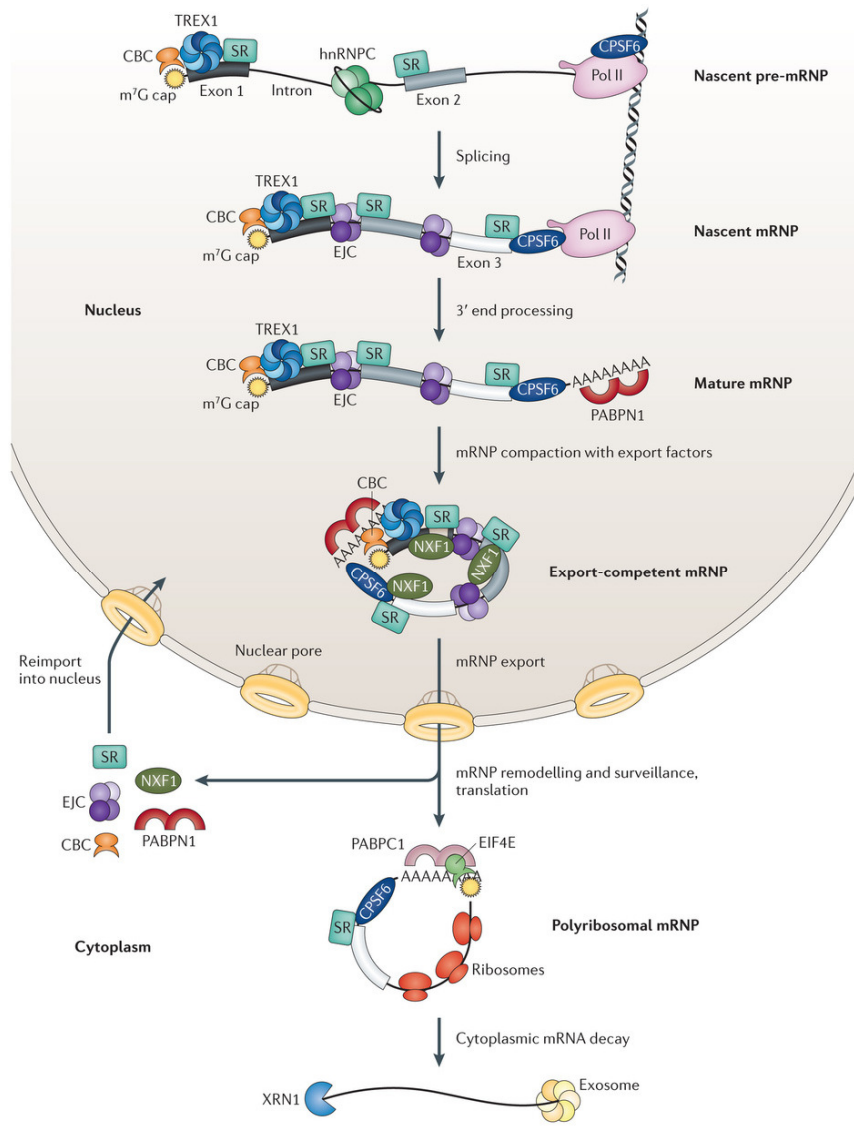


**Figure 21 | Current view of co-transcriptional mRNA processing and export to the cytoplasm. Processing includes the assembly of messenger ribonucleic acid particles (mRNPs), mRNA capping, splicing, polyadenylation, and quality control.** The TREX complex including THOC proteins bind early during mRNA synthesis and ensure a full maturation, before the mRNA can be exported to the cytoplasm. The mRNA quality control factors, such as the cap-binding complex (CBC) or the cleavage and polyadenylation specificity factor 6 (CPSF6), become included into the mRNP complexes after individual maturation steps. After full processing, Thoc4 together with Thoc5 promote the binding of Nxf1 (Tap:p15), which reveals its interaction sites for mRNA and the nuclear pores, initiating the export of mature mRNA to the cytoplasm. Here, most mRNA bound proteins are replaced by actively translating ribosomes, and the mRNA maturation factors are reimported into the nucleus (figure from Müller-McNicoll 2013).

Ultimately, various factors of the TREX complex ensure that only fully processed mRNA (5' capping, splicing, polyadenylation) is being exported to the cytoplasm, or otherwise being degraded (Masuda 2005, Erkmann 2004). The export occurs via direct transient interactions with factors of the nuclear pore complex (Braun 2002).

In analogy to cellular protein folding, the maturation of mRNA is under such a precise quality control and regulation by its processing machinery, that these factors may be described as “mRNA chaperones”. They guard mRNAs on the way from nuclear processing to ribosomal translation, and at the same time protect them against detrimental interactions (premature export, degradation). The chronological dynamics, structure, and functions of most proteins involved in this highly coupled, complex process are still under intense investigation.



## Designed $\beta$ proteins as experimental model to investigate molecular mechanisms behind neurodegenerative diseases

Amyloid fibrils were discovered as the hallmarks of dementia and other protein misfolding diseases (Alzheimer 1907). Amyloid-like aggregates assemble from diverse, disease-dependent proteins that misfolded from their native state into planar cross- $\beta$ -sheet structures (Astbury 1959). Protein misfolding is accompanied by a functional loss of the respective protein, and potentially by a destructive functional gain originating from the misfolded structures that influence their cellular environment (Winklhofer 2008). Thus, a complex combination of multiple malfunctions may occur in cells, which complicates scientific analyses and hampers efforts in understanding dementia-related diseases.

For focusing on the toxic gain-of-function, we utilized artificially designed proteins folding into fibrillary cross- $\beta$ -sheet structures, comparable to amyloids appearing in neurodegenerative diseases. This allowed us to observe the toxic impact of amyloid-like structures on living cells without interference from loss-of-function effects that accompany the misfolding of every natural disease-associated human protein.

It is still a major challenge to design novel proteins with any desired, e.g. enzymatic function. However, utilizing knowledge about the geometry of secondary structures and the hydrophobic effect allows engineering certain protein conformations. Artificial proteins with  $\alpha$ -helical or  $\beta$ -sheet structures have been achieved by positioning hydrophobic amino acids in such a way that they become buried upon folding. On the protein surface, mainly polar and charged residues remain.

Libraries of such proteins were pioneered by Prof. Michael Hecht and his colleagues. Artificial  $\beta$ -sheet proteins were designed by alternating hydrophilic and hydrophobic side chains in a binary pattern (...①②③④⑤⑥⑦...), since side chains in  $\beta$ -sheet structures are directed up and down in an alternating pattern. Serial strings of such  $\beta$ -strand building blocks were connected by flexible and typical strand breaking residues, such as glycine, serine, or proline. Connecting several  $\beta$ -sheets of identical length by short turns resulted in the formation of stable, artificial  $\beta$ -sheet proteins (here: 7 residues long  $\beta$ -strands, 4 residues long turns; 6  $\beta$ -strands in series). However, proteins produced by this technique not only formed  $\beta$ -sheet structures, but independently of the exact sequence resembled amyloid cross- $\beta$ -sheet fibrils comparable to those occurring in neurodegenerative disorders (West 1999). Nature actually strongly disfavors such binary patterns in native sequences, which already indicates potential difficulties of inherently amyloidogenic structures that appear in cells (Broome 2000).

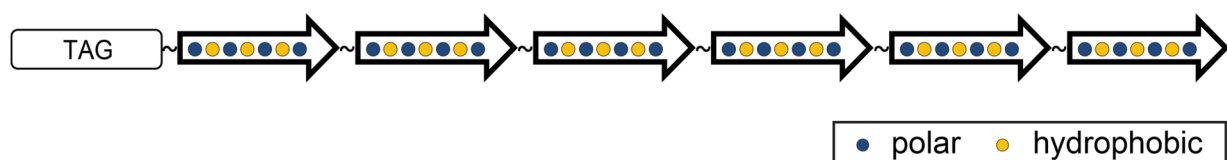


**Figure 22 | Sequence design of artificial  $\beta$  proteins utilized for folding into amyloid-like structures. We utilized such  $\beta$  proteins to model the effects of protein misfolding, as it occurs in different forms of dementia.** Short polypeptide stretches constructed by alternating patterns of polar (blue) and hydrophobic (yellow) side chains were connected by short linker sequences. These consist of strand breaking side chains, allowing  $\beta$ -turns ( $\sim$ ) to form in between two  $\beta$ -sheets (arrows). The resulting  $\beta$  proteins comprising six potential  $\beta$ -sheets were fused to N-terminal tags. Tags facilitated detection (c-Myc) or targeted the proteins into cellular compartments, such as nucleus, cytoplasm, or mitochondria (adapted from West 1999).

The polar-hydrophobic pattern is primarily important for the formation of secondary structures in such designed proteins. Individual residues therefore can be varied in compliance with the polar-hydrophobic pattern, allowing the creation of a large variety of sequences (West 1999). Sequence dependently, variations from the idealized  $\beta$ -sheet structure may certainly occur.

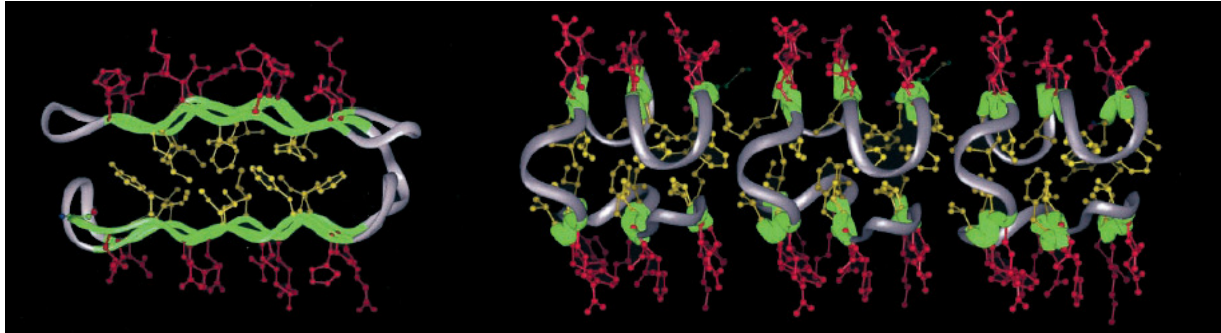


**Figure 23 | Structural model of designed  $\beta$ -sheet proteins (left, monomer) and amyloid-like fibrils (right, fibril section with 3 monomers, assembling via open hydrophobic surfaces).** The protein backbone (green) folds into planar  $\beta$ -strands of 7 amino acids in length, interrupted by 4 amino acid turns (gray). Turns connect six antiparallel  $\beta$ -sheets within a monomer. Side chains project alternately up (polar residues, red) or down (hydrophobic residues, yellow). Interactions between open hydrophobic surfaces lead to the polymerization of  $\beta$  protein monomers into cross- $\beta$ -sheet fibrils (amyloids), whereby the  $\beta$ -sheets run orthogonal to the fibril axis (from left to right; figure adapted from Wang 2002). While in native proteins  $\beta$ -sheet structures are rather twisted (Chothia 1981, Zandomenighi 2004), short  $\beta$ -strands can be forced into planar conformations, allowing the assembly of long repetitive amyloid fibrils.

Artificial  $\alpha$ -helical proteins can be designed by a different distribution of polar and hydrophobic side chains (such as  $\circ\bullet\circ\circ\bullet\bullet\circ\circ\bullet\circ\bullet\circ$ ). Following  $\alpha$ -helical geometry in a polypeptide sequence, polar and hydrophobic surface regions can be created. Several helices can then assemble to e.g. a four-helix-bundle, stabilizing the whole structure by orienting hydrophobic residues to the inside (Kamtekar 1993, Hecht 2004). In contrast to the  $\beta$ -sheet proteins, such designed soluble  $\alpha$ -helical structures should be devoid of amyloid-like nature or tendencies to assemble into higher-molecular-weight polymers. Therefore,  $\alpha$ -helical proteins served us to control effects of expressing any artificial structures in cells.

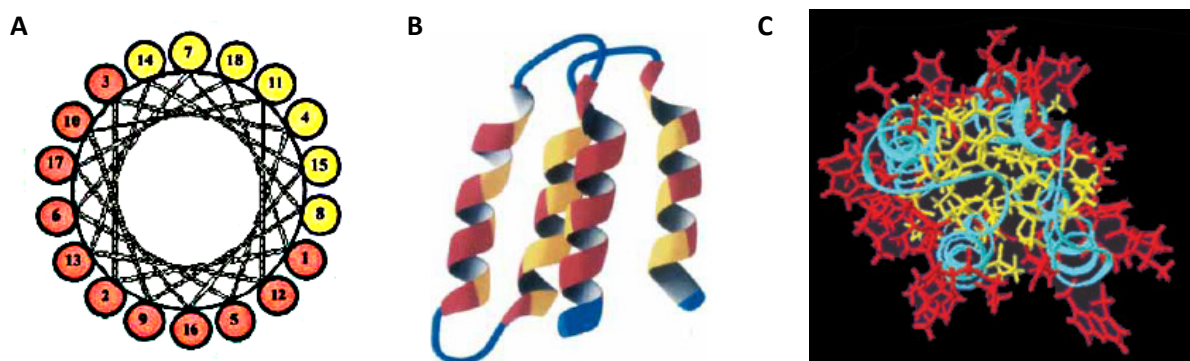


**Figure 24 | Geometry and design principle of an artificial  $\alpha$ -helical four-helix-bundle protein, and solution structure of  $\alpha$ S824, an artificial  $\alpha$ -helical protein.** (A) Helix wheel representing the geometry and periodicity of an amphiphilic  $\alpha$ -helix with hydrophobic (yellow side chains) and polar (red side chains) surface regions (figure adapted from Kamtekar 1993). (B) Structural model of a four-helix-bundle, burying its hydrophobic regions in the inner core of the bundle (figure adapted from Kamtekar 1993, Hecht 2004). (C) Solution structure of  $\alpha$ S824, an artificial  $\alpha$ -helical protein (figure adapted from Wei 2003).

## Aims of this study

Fibrillar plaques and intracellular tangles were first described by Alois Alzheimer in a brain autopsy of his famous patient Auguste Deter (Alzheimer 1907/1995). Since then, proteinaceous aggregates became the hallmark not only of Alzheimer's, but a wide range of neurodegenerative diseases, many of them comprising related symptoms and pathology.

The proteins held responsible for initiating the process of aggregation in cells are usually not toxic per se, but perform specific biological functions in their native states. Nevertheless, proteins may turn harmful e.g. through conformational transitions, proteolytic fragmentations, or sequence mutations. Conformational transitions can also be influenced by "environmental" factors in the cell, including alterations in the proteostasis network as they may occur during aging processes. Certain non-native protein conformations may then accumulate, over long times or because they cannot be removed. If they are able to assemble into higher-molecular-weight structures and to interact with other cellular factors, they may gain toxic functions on cells. In this study, we aimed to focus on such emanating toxic functions that protein structures may acquire by misfolding, in contrast to the functional loss of individual misfolded proteins. Therefore, we utilized a set of artificial  $\beta$  proteins that were designed to adopt directly amyloid-like oligomeric and fibrillary structures, without the background of evolutionary selection regarding their structure or biological function. Thus, with the designed  $\beta$  proteins we aimed to investigate the general toxic potential of misfolded amyloid-like protein conformations in cells.

In the first part of this study, we tried to increase our knowledge about the structural origins of amyloid-related toxicity. We therefore purified different  $\beta$  proteins and reconstituted their aggregation *in vitro* under physiological conditions. After demonstrating their amyloid-like nature, we analyzed their physicochemical properties to set them in correlation to their toxicity. Oligomerization and fibril formation was observed by electron microscopy and various spectroscopic and biochemical methods. Toxicity of the amyloid-like  $\beta$  proteins was assessed in different cellular systems to understand the fundamental biology behind the known neuronal vulnerability. In conjunction with properties of the cellular interactors of the  $\beta$  proteins, we hoped to gain a better understanding of the structural determinants of amyloid-related toxicity in cells.

Numerous cellular malfunctions and defects were observed in model systems and patient's tissues associated to protein aggregation and neurodegenerative diseases. Toxicity appears to spread in a complex manner through cells, its origins still remaining unclear. Protein aggregates and distributed oligomeric material occur dependent on the specific disease often simultaneously in different cellular compartments. To describe cellular mechanisms of toxicity we decided to direct the aggregation into individual compartments to observe arising localized toxicities, corresponding cellular malfunctions, as well as strengths and weaknesses of subcellular proteostasis networks. Cellular interactors should direct us towards affected cellular pathways with a special focus on the early events during the aggregation process. This strategy should help us to resolve the multifactorial nature of neurodegenerative disease mechanisms and to reveal previously unknown compartment-specific proteostasis functions and factors. Our observations on the  $\beta$  proteins as general misfolding model sequences should then be compared to human disease associated proteins and related animal models to evaluate the significance and disease relevance of our findings.

# Results

## Designed $\beta$ proteins

The three  $\beta$  proteins utilized in our studies,  $\beta$ 4,  $\beta$ 17, and  $\beta$ 23, were constructed using the same alternating polar-hydrophilic amino acid pattern.  $\beta$ 4,  $\beta$ 17, and  $\beta$ 23 contain the same number of amino acids and proposed  $\beta$ -strands (6 strands of 7 amino acids length, connected by 4 amino acid long turns). They vary, however, in their individual amino acid sequence.

Among the  $\beta$  proteins,  $\beta$ 23 has the most negative net charge, the highest hydrophobic volume (volume occupied by aliphatic side chains), and the highest  $\beta$ -sheet propensity. The increased hydrophobic volume and  $\beta$ -sheet propensity of  $\beta$ 23 were ascribed to its high isoleucine content (Tartaglia 2008).

	Amino acids	Molecular weight (kDa)	Net charge at pH7	Rel. hydrophobic Volume (a.u.)	Isoleucine residues	Hydrophobic aromatic side chains
<b><math>\beta</math>4</b>	80	8.94	-8.1	75	4	3xF, 1xY, 0xW
<b><math>\beta</math>17</b>	80	8.87	-8.6	75	5	3xF, 1xY, 0xW
<b><math>\beta</math>23</b>	80	9.05	* -11.6 *	* 80 *	* 11 *	3xF, 1xY, 0xW

**Table 1 | Sequence analysis summarizing basic physicochemical properties of the c-Myc tagged  $\beta$  proteins.** The most toxic  $\beta$ 23 (see below) stands out due to its high negative net charge and its increased hydrophobicity and isoleucine content (replacing alanines or valines in  $\beta$ 4 and  $\beta$ 17). The number of hydrophobic aromatic side chains was equal for the 3 sequences (F, phenylalanine; Y, tyrosine; W, tryptophan). Properties calculated by ProtParam (Gasteiger 2005).

To ascribe properties of the designed  $\beta$  proteins to their amyloid character and to distinguish them from features of non-amyloidogenic sequences, we made use of an artificial soluble  $\alpha$ -helical protein ( $\alpha$ S824). Overall,  $\alpha$ S824 comprises a similar amino acid composition as the  $\beta$  proteins. A different order of the residues within the sequence causes  $\alpha$ S824 to fold into a soluble 4-helix bundle with an inner hydrophobic core, as demonstrated by NMR (Wei 2003).

## Artificial $\beta$ proteins are cytotoxic in *E. coli*

The  $\beta$  proteins were shown to form amyloid-like fibrils *in vitro* (West 1999). Since amyloidogenic aggregation is observed with many proteins associated to neurodegenerative disease, we were wondering whether a general proteotoxic effect emanating from amyloid structures could be caused by the artificial  $\beta$  proteins in the different kingdoms of life.

For analyzing potential toxicity in bacteria, *E. coli* cells (BL21) were transformed with inducible plasmids (trc promoter containing the lacO operator and the lacIq repressor) encoding the  $\beta$  proteins and grown overnight on selective LB agar. A single colony was picked and grown in liquid selective LB medium. On the next day, cultures were diluted to an equal cellular density ( $OD_{600nm}$  of 0.15). When *E. coli* cultures initiated exponential growth after 90 min, protein expression was induced by addition of 0.5 mM IPTG.

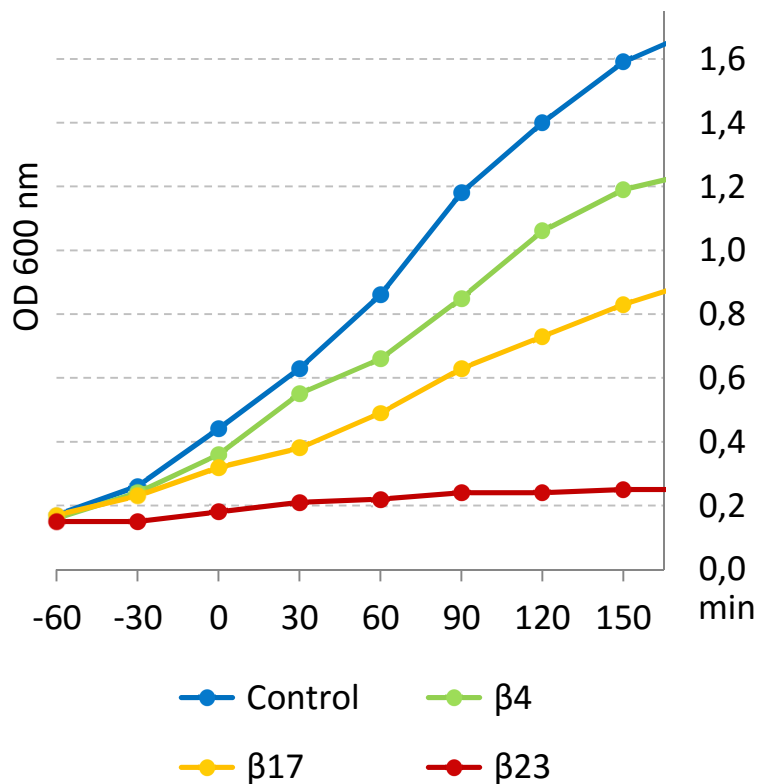


**Figure 25 | Growth curves of *E. coli* cells expressing  $\beta$  proteins in comparison to wildtype cultures (transformed with empty vectors).** *E. coli* cells expressing  $\beta$  proteins exhibit a sequence dependent growth defect, varying from slightly delayed division rates in case of  $\beta 4$  to virtually no growth in case of  $\beta 23$ . Representative growth curves of 3 independent experiments.

*E. coli* cultures carrying an empty plasmid backbone (control) grew exponentially for around 3 hours before growth saturated into stationary phase. *E. coli* cells carrying plasmids encoding  $\beta 4$  and  $\beta 17$  showed a similar exponential growth behavior, however, their division rates were significantly slowed down, and growth stopped at lower cell densities compared to wildtype *E. coli* cultures. Virtually no growth could be observed for cells expressing  $\beta 23$ , entirely preventing cell division. Accurately, growth was inhibited even before chemical induction of  $\beta 23$  expression, most likely due to leaky expression within the pre-culture (low levels of  $\beta$  proteins were observed by immunoblotting of non-induced cells).  $\beta 23$  therefore proved to be highly toxic in *E. coli* cells even at low cellular levels.

### Structural modifications affect toxicity

To analyze effects of structural alterations on cellular toxicity, the  $\beta$  proteins were modified. In one set, two positively charged lysine residues were introduced at the predicted hydrophobic interaction surfaces between  $\beta$  protein monomers (in the middle of the first and the last  $\beta$  strand, respectively). By weakening these hydrophobic contacts, aggregation into oligomers and fibrils should become less favorable. *In vitro*,  $\beta$  proteins carrying these two lysine mutations have been shown to be soluble and monomeric (Wang 2002).

*E. coli* cultures expressing such “ $\beta 17$  Lys” or “ $\beta 23$  Lys” mutants grew considerably faster than their non-mutated counterparts. “ $\beta 17$  Lys” grew as fast as  $\beta 4$ . This suggests that indeed amyloid-like oligomers and fibrils are responsible for the observed growth impairment, and a destabilization of such structures positively affects cellular survival. Beyond polymerization prevention, the exchange of hydrophobic surface residues for charged amino acids might also reduce unspecific interactions with cellular factors.

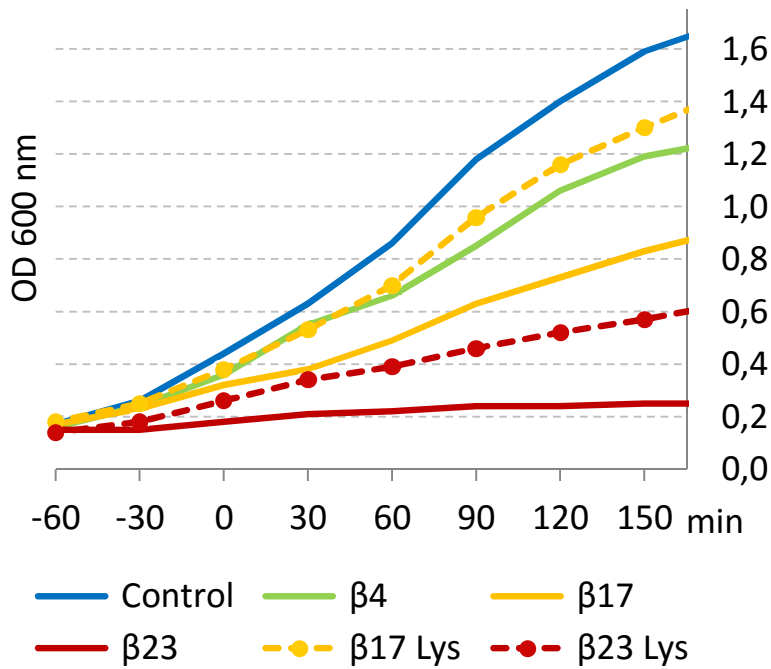


**Figure 26 | Growth curves of *E. coli* cells expressing  $\beta$  protein mutants with inhibited fibril assembly (continuous lines).** The expressed mutants carry charged lysine residues on their polymerization surfaces, weakening the hydrophobic contacts that are necessary for fibril growth. *E. coli* cells expressing these  $\beta$  proteins mutants markedly increased their growth rates, compared to the respective original sequences. Representative growth curves of 3 independent experiments.

In an opposing way, unpaired  $\beta$  strands could act as additional interaction surfaces, and increase interactions to cellular factors. To analyze effects on toxicity, a single  $\beta$ -strand either was added to ( $\beta 17+4$ ,  $\beta 17+23$ ) or was removed from ( $\beta 23$ short) the standard  $\beta$  protein sequences. As expected, growth for the extended  $\beta$  proteins with seven  $\beta$  strands was furthermore decreased in comparison to  $\beta 17$  alone.  $\beta 23$ short with only 5  $\beta$  strands grew similar to the anyways highly toxic  $\beta 23$ .

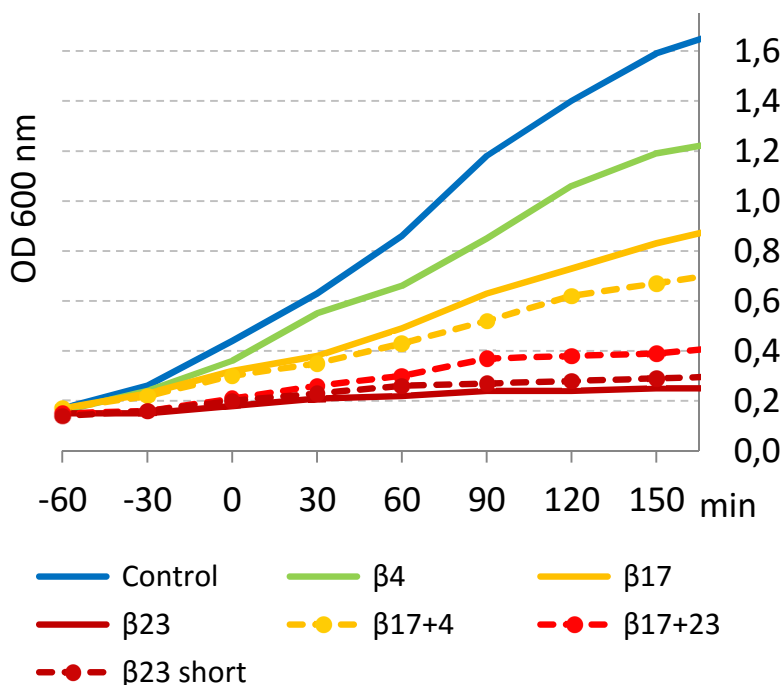


**Figure 27 | Growth curves of *E. coli* cells expressing  $\beta$  protein mutants with an odd number of  $\beta$ -sheets, potentially increasing interaction surfaces towards other cellular factors (continuous lines).** *E. coli* cells expressing these  $\beta$  protein mutants further slowed down in growth, demonstrating their increased toxicity compared to the respective original sequences.  $\beta 17+23$  differed from  $\beta 17+4$  only by an isoleucine and a leucine side chain (replacing valine and phenylalanine). The residual sequences were identical. Already  $\beta 23$  stood out by its high frequency of isoleucine. Representative growth curves of 3 independent experiments.

In conclusion, when expressed in *E. coli* cells, the  $\beta$  proteins exhibited a sequence specific effect on growth.  $\beta$  proteins with an odd number of  $\beta$  strands exhibited an increased toxicity, whereas variants with diminished aggregation and hydrophobic surfaces proved to be less detrimental. The  $\beta$  proteins could therefore be modified in a rational manner, and they caused toxicity in an alleageable way.

## $\beta$ proteins are purified from *E. coli* inclusion bodies

The  $\beta$  proteins were expressed under the control of an IPTG inducible lac-promoter in *E. coli* cells, where they formed insoluble inclusion bodies. The c-Myc tagged proteins were isolated from inclusion bodies by denaturation in urea, followed by ion exchange and size exclusion chromatography (West 1999). However, since other cellular factors were apparently entrapped into the inclusion bodies, their color turned from typically white to yellowish-brown. To guarantee a high purity of the final isolate, additional purification steps (a denatured size exclusion chromatography) were included.

$\alpha$ S824 was expressed as soluble hexa-histidine tagged protein and purified by Ni-NTA chromatography. After TEV cleavage of the His-tag, highly pure c-Myc tagged  $\alpha$ S824 protein was obtained.

The purity of the  $\beta$  proteins was confirmed by Coomassie Brilliant Blue stained SDS-PAGE, immunoblotting, UV/VIS spectroscopy, and amino acid analysis. The Coomassie Brilliant Blue stained SDS-PAGE showed monomeric  $\beta$  proteins and  $\alpha$ S824. Due to their hydrophobic nature and their small size, the  $\beta$  proteins bound Coomassie Brilliant Blue rather weakly. Immunoblotting with an anti-c-Myc antibody confirmed the identity of the proteins.

The purified  $\beta$  proteins appear at an apparent size between 10-15 kDa, despite their arithmetical molar masses of close to 9 kDa. Reasons for their gradually decreased mobility might be a differentially preserved residual structure during PAGE, or a different affinity towards SDS molecules. The partial loss of this effect under denaturing conditions (4M Urea SDS-PAGE) supports this hypothesis. The differential mobility appears for the purified proteins as well as for whole cell lysates independently from organism (human or bacterial cells), lysis, or purification methods.  $\alpha$ S824 appeared as pure, monomeric protein at around 15 kDa (arithmetical mass of 13 kDa) on Coomassie Brilliant Blue stained SDS PAGE and immunoblots.

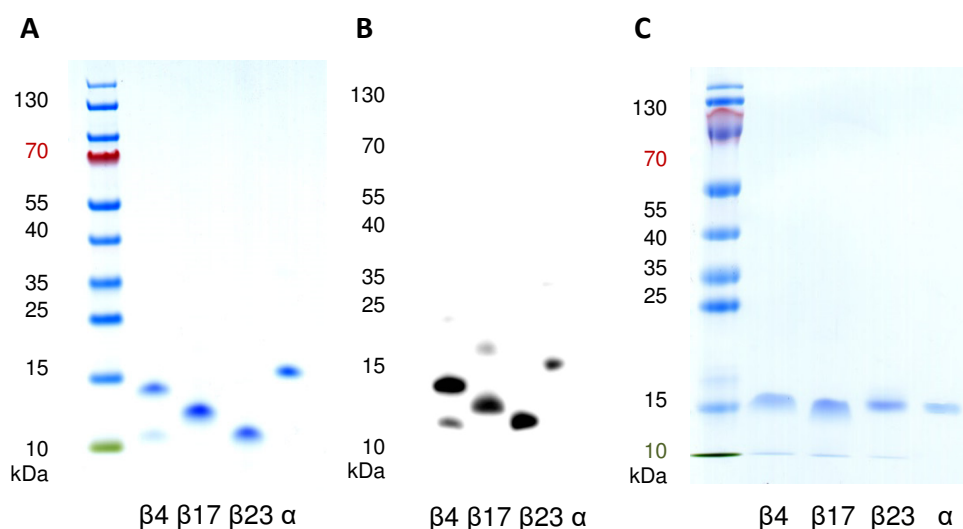


**Figure 28 | Purified  $\beta$  proteins and  $\alpha$ S824 on (A) SDS-PAGE, (B) corresponding anti-c-Myc immunoblot, and (C) 4 M urea SDS-PAGE. SDS-PAGEs were stained by Coomassie Brilliant Blue.**

## Concentration and purity of the $\beta$ proteins

Near and far UV spectroscopy can be applied to gain information about concentration and purity of protein solutions (Aitken 1996). Among the aromatic amino acids, especially tryptophan absorbs radiation around 280 nm, tyrosine and phenylalanine only to a much weaker extend (~20% and ~5% of tryptophan, respectively). The  $\beta$  proteins do not contain any tryptophan in their sequence, only a single tyrosine, each.  $\alpha$ S824 contains one tryptophan and one tyrosine.

The absorption spectra of the  $\beta$  proteins reflect this situation. All purified  $\beta$  proteins show a very low absorbance at 280 nm, indicating their high purity and the absence of other (tryptophan containing) proteins.  $\alpha$ S824 in contrast shows a classical tryptophan peak with a maximum around 280 nm.

Concentrations of proteins in solution are commonly determined by their absorbance at 280 nm. The absence of tryptophan residues in the  $\beta$  proteins required a different method for quantification. Peptide bonds absorb strongly in the far UV. Here, the absorption coefficient depends linearly on the length (number of peptide bonds) of a protein. Therefore, the protein concentrations of the  $\beta$  proteins were determined at 210 nm with an absorption coefficient of 20 for 1 mg/mL of protein (Aitken 1996).

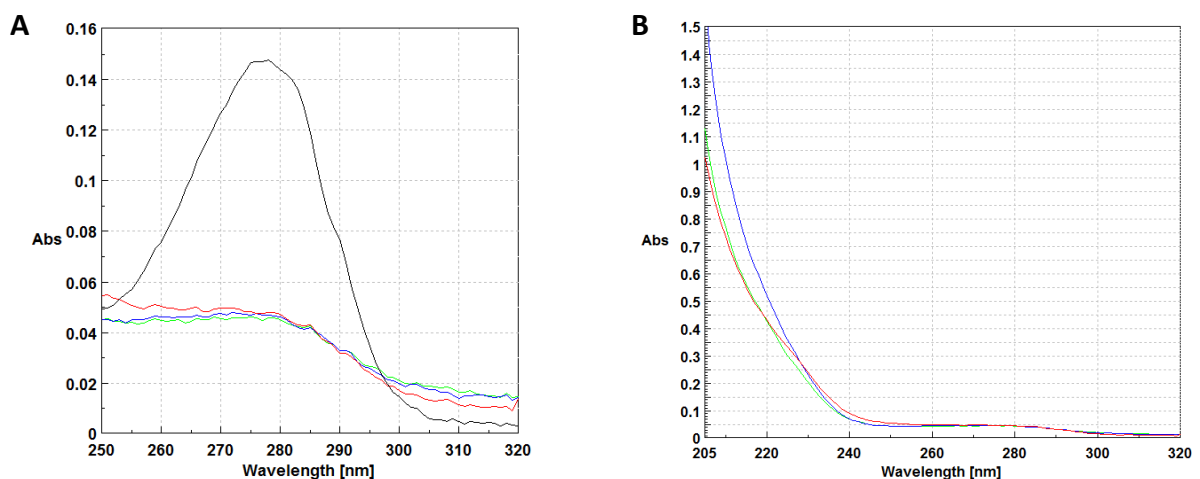


**Figure 29 | Absorption spectra of purified  $\beta$  proteins and  $\alpha$ S824.** (A) Tryptophan absorption around 280 nm only occurred for  $\alpha$ S824 (black), not for the  $\beta$  proteins (colored). (B) The peptide bonds of the purified  $\beta$  proteins absorb in the far UV ( $\beta$ 4 in green,  $\beta$ 17 in blue,  $\beta$ 23 in red).



## Structural properties of the $\beta$ proteins

### Amyloid-like oligomers and fibrils revealed by transmission electron microscopy

Purified  $\beta$  proteins in a physiological solution (150 mM KCl, 0.5 mM  $MgCl_2$ , 25 mM HEPES, pH 7.5) were negatively stained on metal grids for transmission electron microscopy. The  $\beta$  proteins formed thin filaments with diameters of  $\sim 3$  nm and lengths of 100-500 nm. The fibril diameters suggested a linear assembly of monomeric  $\beta$  proteins into fibrils, consisting of up to several hundred monomers (expected diameter of a  $\beta$ -sheet containing seven residues including terminal turns is  $\sim 2.7$  nm).

In addition, globular oligomers were found, particularly in case of  $\beta 23$ . The diameter of the spherical oligomers ranged from 10-30 nm. The size variation indicated oligomers comprising a variable number of monomers in the population, not limited to a unique defined species. Globular oligomers made up a large fraction of the  $\beta 23$  species (up to 50% in physiological buffer). On the other hand, they were mostly absent in samples of  $\beta 4$  and  $\beta 17$ , which were predominantly assembling into fibrils.

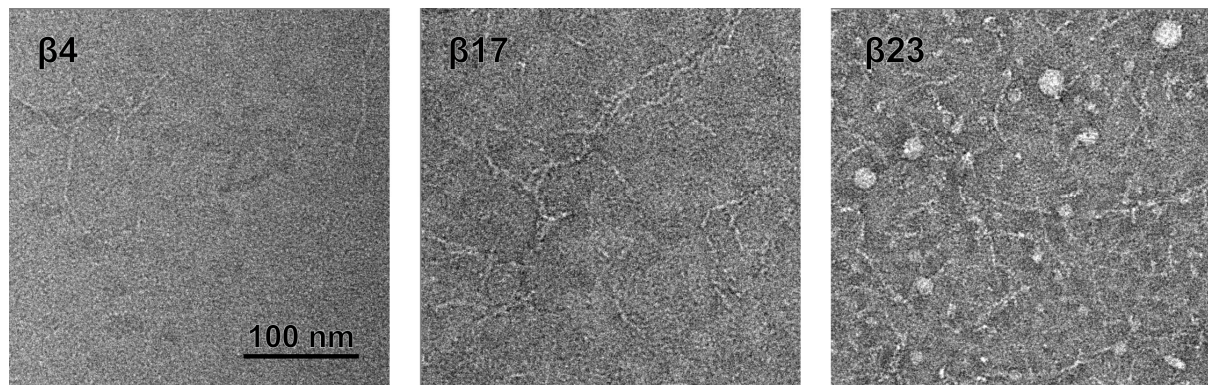


**Figure 30 | Transmission electron microscopy of aggregates formed by purified  $\beta$  proteins refolded in physiological buffer at pH 7.5.** Proteins were negatively stained and observed at a magnification of 55,000 x.

Length and thickness of the fibrils increased on lowering the pH from 7.5 to 6. This observation seems rational, considering the high charge density of the  $\beta$  proteins (80 residues, net charges of -9 to -13 at neutral pH). Negative net charges decrease due to protonation of acidic residues, lowering intra- and extramolecular repulsion. Longer fibrils of several hundred nanometers up to micrometers were found in 10 mM potassium phosphate at pH 6. The fibrils started to entangle each other, forming higher order fibrils (with diameters up to 10-12 nm under these conditions).

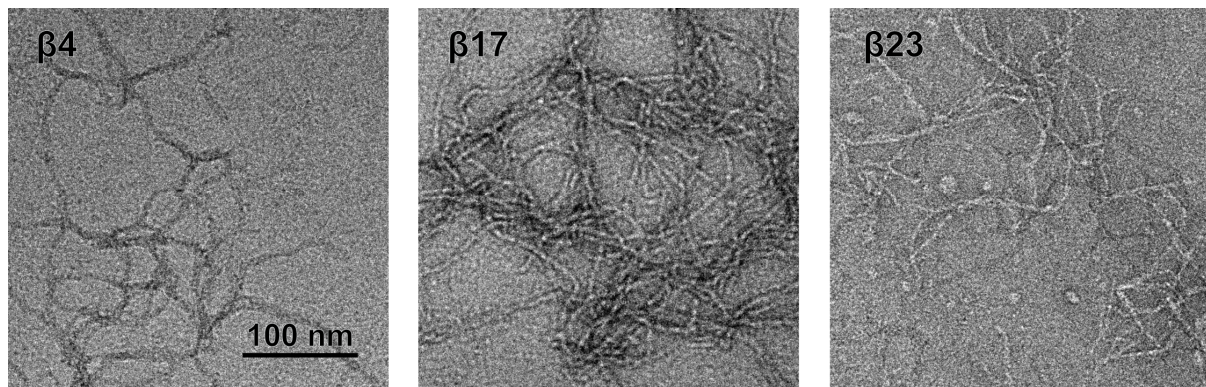


**Figure 31 | Transmission electron microscopy of aggregates formed by purified  $\beta$  proteins refolded at pH 6 for 24 h.** Proteins were negatively stained and observed at a magnification of 55,000 x.

Fibrils were forming in a time-dependent manner after dilution from denaturant (8 M guanidinium hydrochloride). Already after 5 min of refolding in physiological buffer, short fibrils of 10-30 nm became visible in case of  $\beta 17$  and  $\beta 23$ . In addition, first globular  $\beta 23$  oligomers were present after 5 min. During the next two hours, fibrils grew in size, reaching not yet the lengths present after 24 h. The kinetic electron microscopy data indicates, in consistency with the fluorescent amyloid stains (Thioflavin T, NIAD-4, see below), that the  $\beta$  proteins refold very rapidly into their fibrillary conformation. Fibril assembly initiates immediately without a (by the applied methods) detectable nucleation phase, but develops over hours to reach equilibrium conditions *in vitro* in a physiological buffer.

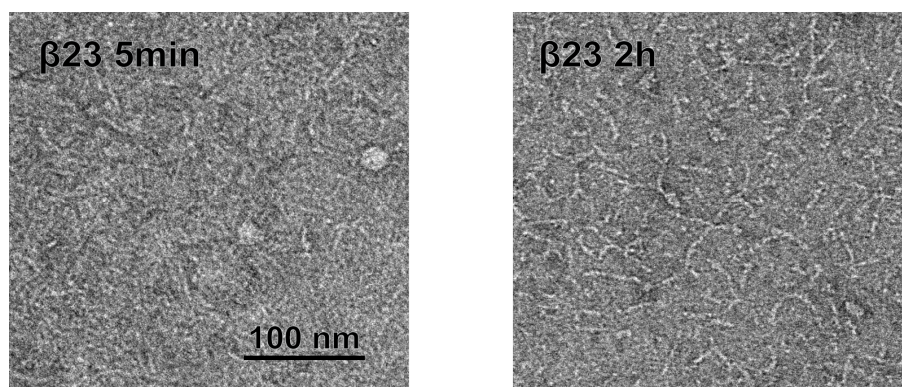


**Figure 32 | Transmission electron microscopy of aggregates formed by denatured  $\beta$  proteins refolded for 5 min or 2 h in physiological buffer at pH 7.5.** Proteins were negatively stained and observed at a magnification of 55,000 x.

## CD spectroscopy demonstrates $\beta$ -sheet secondary structure

To determine secondary structures of the  $\beta$  proteins, circular dichroism (CD) spectroscopy was applied after refolding the proteins *in-vitro* in a physiological buffer solution (150 mM KCl, 0.5 mM  $\text{MgCl}_2$ , 25 mM HEPES, pH 7.5). To allow measurements in the far UV, the aggregated  $\beta$  proteins were diluted into a low salt buffer before the measurement (25 mM KCl, 6 mM HEPES, pH 7.5), assuming the aggregates and their secondary structures were mainly preserved. Measurements were performed at a protein concentration of 0.1 mg/mL.  $\beta$  protein fibrils and oligomers forming at this concentration stayed in solution and did not precipitate or sediment during the measurement.

The CD spectra of  $\beta 4$ ,  $\beta 17$ , and  $\beta 23$  resemble classical  $\beta$ -sheet protein spectra with a global minimum at 216 nm. Minor deviations occurred for  $\beta 4$ . The spectrum of  $\alpha 824$  contains two minima at 208 and 222 nm, characteristic for an  $\alpha$ -helical protein.

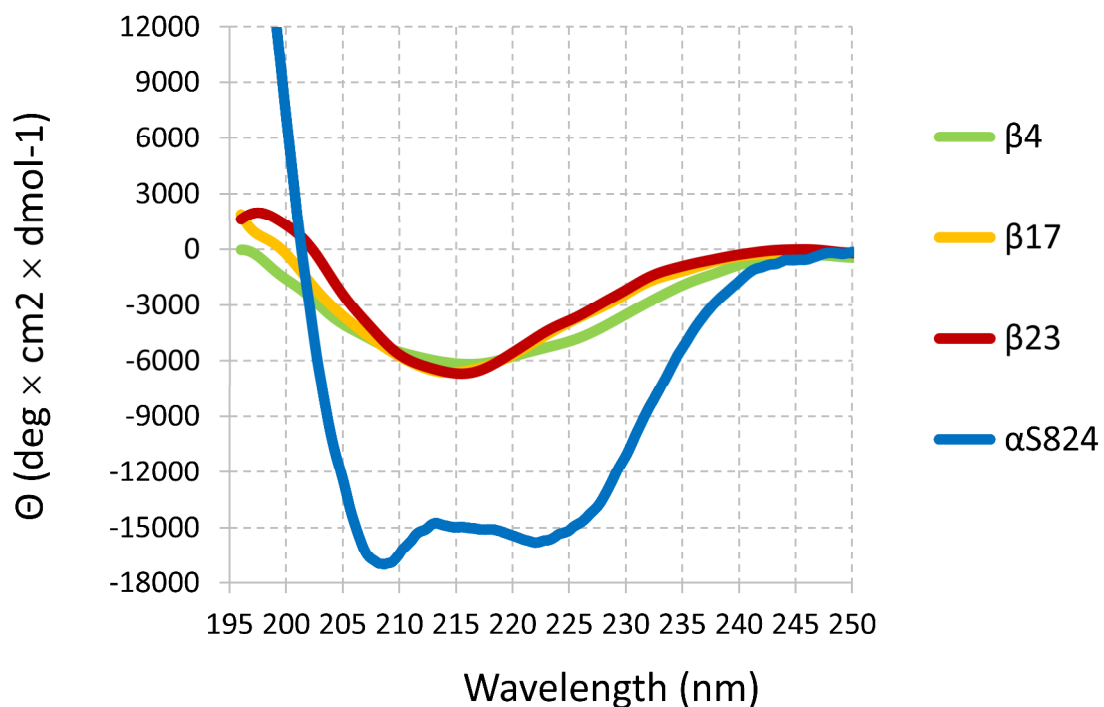


**Figure 33 | CD spectra of purified and refolded  $\beta$  proteins and  $\alpha 824$ .** The  $\beta$  proteins were refolded in physiological buffer and show typical spectra of  $\beta$ -sheet rich proteins.  $\alpha 824$  shows two minima and a stronger negative signal, as typical for  $\alpha$ -helical proteins.

Relative contributions of different secondary structure elements were calculated by the CDSSTR algorithm (Johnson 1999, Sreerama 2000). This analysis considers a CD spectrum as a linear combination of spectra of individual secondary structure elements, and calculates the composition mathematically via singular value decomposition.

The analysis confirms that all three  $\beta$  proteins consist mainly of  $\beta$ -sheets as the main structural component (62-63%). However, a significant fraction of the polypeptide chains seems to contain unstructured regions (~32%) each. Such deviations from perfect  $\beta$ -sheet structures may be expected for artificially designed proteins. Moreover, these deviations may be crucial for the properties and interactions of the  $\beta$  proteins in cells. The residual 5-6% of  $\alpha$ -helical content may be ascribed to the 10 amino acid long N-terminal c-Myc sequence (EQKLISEEDL), which stems from an  $\alpha$ -helical part of the c-Myc protein (Nair 2003).

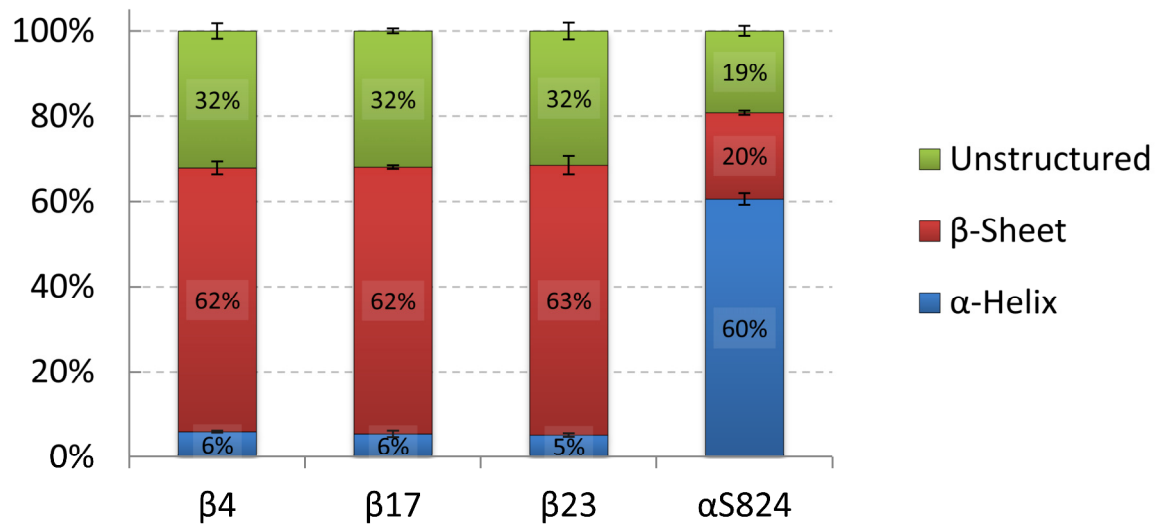


**Figure 34 | Estimation of secondary structure content by singular value decomposition (CDSSTR) of the CD spectra of the  $\beta$  proteins and  $\alpha$ S824.** Analyses revealed mainly  $\beta$ -sheet structure and some unstructured regions for the  $\beta$  proteins, whereas  $\alpha$ S824 was found to be mainly  $\alpha$ -helical.

Noticeable is the high consensus between the secondary structures of the three  $\beta$  proteins. Conclusively, the differential toxicity cannot be explained by general differences in the secondary structural composition here. However, the three-dimensional arrangement within the  $\beta$  proteins may vary considerably. Especially the unstructured regions may significantly contribute to structural variation, with potentially crucial consequences for cellular toxicity.

## FTIR spectroscopy confirms amyloid-like nature

Amyloid fibrils consist of cross  $\beta$ -sheet structures. These secondary structures differ generally from  $\beta$ -sheet folds of native proteins regarding their distribution of  $\phi/\psi$  dihedral angles (Ramachandran plot), their number of strands per sheet, and their  $\beta$ -sheet twist (Zandomenighi 2004). These differences are reflected in the amide I region of infrared spectra of proteins. Infrared signals originate primarily from stretching vibrations of main-chain carbonyl groups, which can be observed in the wavenumber range of 1600-1700  $\text{cm}^{-1}$ .

As observed by Zandomenighi et al., the maximum of the Amide I band of native globular  $\beta$ -sheet proteins occurs between 1630-1645  $\text{cm}^{-1}$ . Contrary, a multitude of amyloid fibers populates in the range of 1610-1630  $\text{cm}^{-1}$ , for example  $\text{A}\beta_{1-40}$  at 1625  $\text{cm}^{-1}$ . This observation demonstrates that native, slightly twisted  $\beta$ -sheets differ in structural details from flat, cross- $\beta$ -sheet conformations of amyloids (despite the exception of functional amyloids).

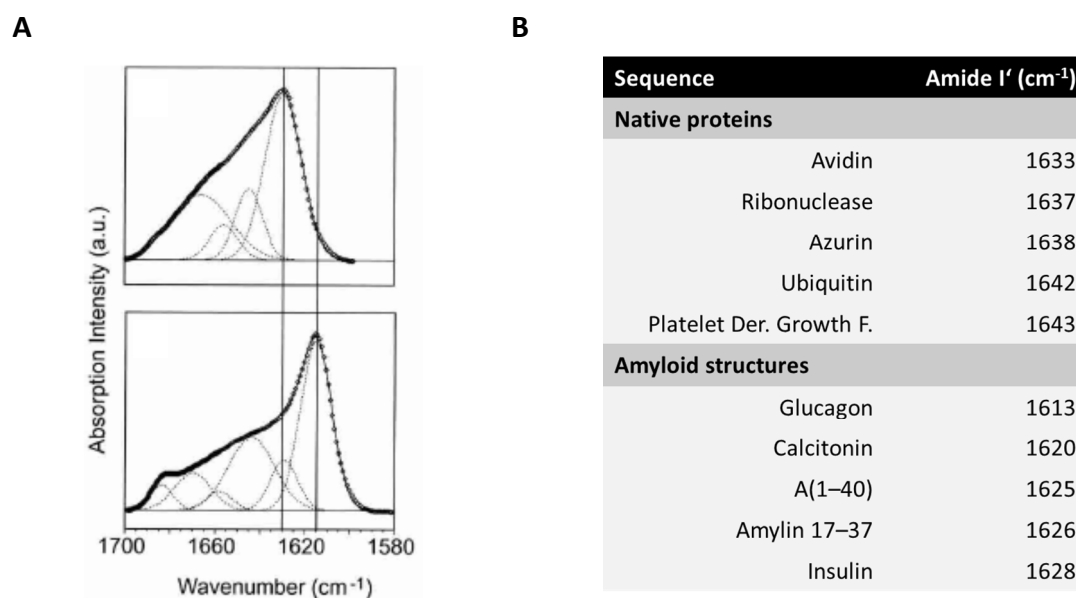


**Figure 35 | Structural differences between native, slightly twisted  $\beta$ -sheet structures and flat cross- $\beta$ -sheet conformations within amyloid fibrils can be observed by FTIR spectroscopy. (A)** Transmission mode FTIR spectra of native transthyretin (TTR, above) and misfolded TTR in form of amyloid fibrils (below) in  $\text{D}_2\text{O}$ . The global maximum of the Amide I band, originating from  $\beta$ -sheet secondary structures, prominently shifts from 1630  $\text{cm}^{-1}$  (native TTR) to 1615  $\text{cm}^{-1}$  (fibrillary TTR; Zandomenighi 2004). **(B)** A literature survey revealed that native  $\beta$ -sheet proteins and amyloid fibrils absorb generally in distinct spectral regions of the Amide I band. Higher wave numbers in this region correspond to different dihedral angles ( $\phi/\psi$ ), reflected in larger twist angles of most native  $\beta$ -sheet proteins compared to flat, cross  $\beta$ -sheet amyloid fibrils (Zandomenighi 2004).

The  $\beta$  proteins were dried under  $\text{N}_2$  as a thin film on a Germanium crystal, where H-D exchange was performed by flushing through  $\text{D}_2\text{O}$ -saturated  $\text{N}_2$ . The spectral region of the Amide I band (1705 to 1595  $\text{cm}^{-1}$ ) was extracted, corrected for the base line, and scaled such to obtain a constant integral value. Peak positions of spectral components were analyzed using Fourier-self deconvolution and the second derivative of the spectra.

All three  $\beta$  proteins displayed a global maximum at exactly  $1624\text{ cm}^{-1}$ . This verifies not only the amyloid nature of the  $\beta$  proteins, but also points towards their mutual similarity regarding their  $\beta$ -sheet structure (similarly flat  $\beta$ -sheets). Furthermore, all three  $\beta$  proteins show a small peak around  $1690\text{ cm}^{-1}$ , which indicates an antiparallel orientation of the  $\beta$ -sheets.

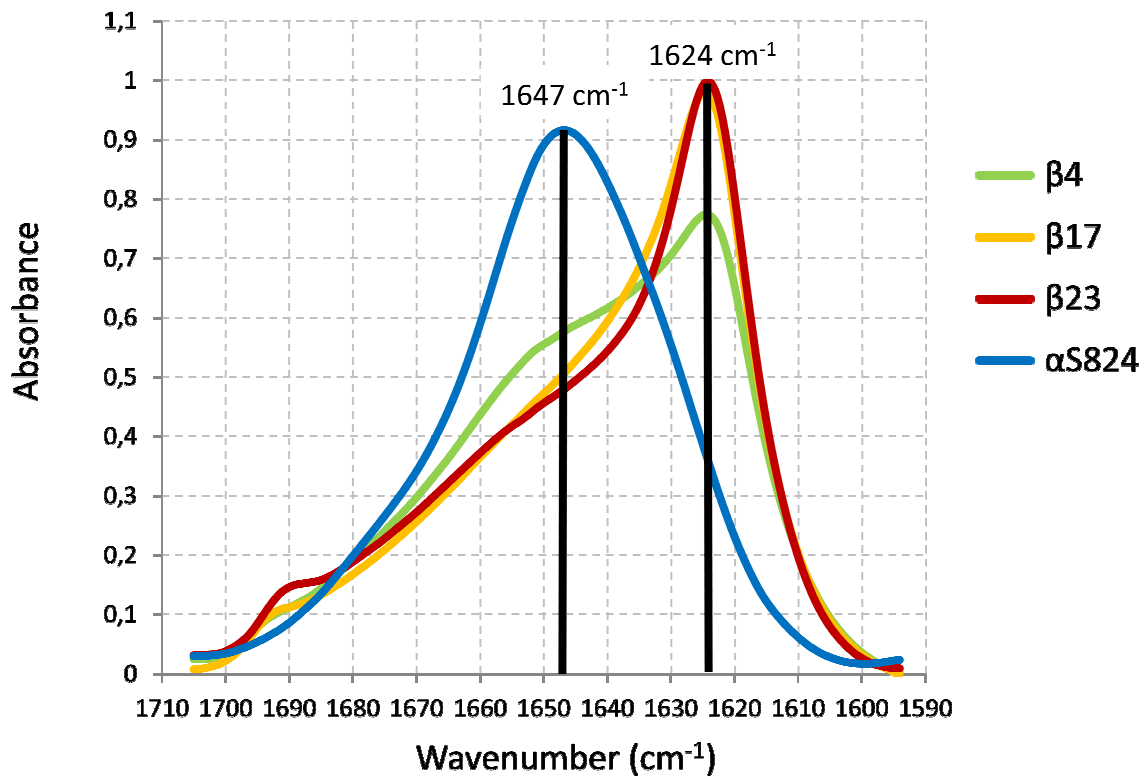


**Figure 36 | FTIR spectra of purified, refolded  $\beta$  proteins and  $\alpha$ S824.** The absorption at  $1624\text{ cm}^{-1}$  is very characteristic for fibrillary  $\beta$ -sheet structures. The small peaks around  $1690\text{ cm}^{-1}$  point toward an antiparallel orientation of the  $\beta$ -sheets.  $\alpha$ S824 showed a very symmetrical peak and a prominent maximum of  $1647\text{ cm}^{-1}$ , confirming its  $\alpha$ -helical structure.

$\beta$ 4 shows a slightly decreased intensity at  $1624\text{ cm}^{-1}$ . Therefore a small peak around  $1650\text{ cm}^{-1}$  appeared, a characteristic region for  $\alpha$ -helices. Since the spectra were normalized by the surface beneath their curves, it can be estimated from these measurements that  $\beta$ 4 contains around 5% more  $\alpha$ -helical structure than  $\beta$ 17 and  $\beta$ 23. Slightly increased  $\alpha$ -helical content is in agreement with the CD analysis of  $\beta$ 4, although the CDSSTR algorithm did only find a minor increase of  $\sim 1\%$   $\alpha$ -helical structure. However, this minor difference seems rather unlikely to reveal a major causal explanation of the significantly lower toxicity of  $\beta$ 4 in comparison to  $\beta$ 17 and  $\beta$ 23 *in vivo*.

The FTIR spectrum of  $\alpha$ S824 showed a very symmetrical prominent peak with a global maximum at  $1647\text{ cm}^{-1}$ , confirming its overall  $\alpha$ -helical structure.

## Amyloid properties and aggregation kinetics

### $\beta$ proteins bind classical and novel amyloid sensors – in correlation with toxicity

Thioflavin T and Congo Red are dyes that have traditionally been used as amyloid sensors due to changes of their absorbance and fluorescence properties upon amyloid binding.

Congo Red displays a green birefringence under polarized light when bound to amyloid fibrils. Its absorbance slightly increases in intensity, and a small redshift occurs (Eisert 2006). Thioflavin T was introduced 1959 by Vassar and Culling as a “fluorescent stain with special reference to amyloid and connective tissues” (Vassar 1959). Thioflavin T, an amphiphatic, positively charged small molecule, was found to form micelles at concentrations used in amyloid binding assays (10-20  $\mu$ M) of 3 nm diameter (Khurana 2005) that bound along surface side-chain grooves running parallel to the long axis of  $\beta$ -sheet fibrils (Biancalana 2010). Upon amyloid binding, a new excitation peak at 450 nm appears, leading to an enhanced fluorescence emission at 482 nm (Khurana 2005). By this, the presence of amyloid fibrils as well as their kinetics of formation can be monitored.

NIAD-4 is a recently discovered amyloid binding fluorophore with the ability to cross the blood-brain barrier. The dye is only weakly fluorescent in aqueous buffer, but its emission intensity greatly increases upon binding to A $\beta$  or other amyloid fibrils (Nesterov 2005, Brandenburg 2012).

Purified  $\beta$  protein fibrils bound all three tested amyloid sensors: Thioflavin T, NIAD-4, and Congo Red.

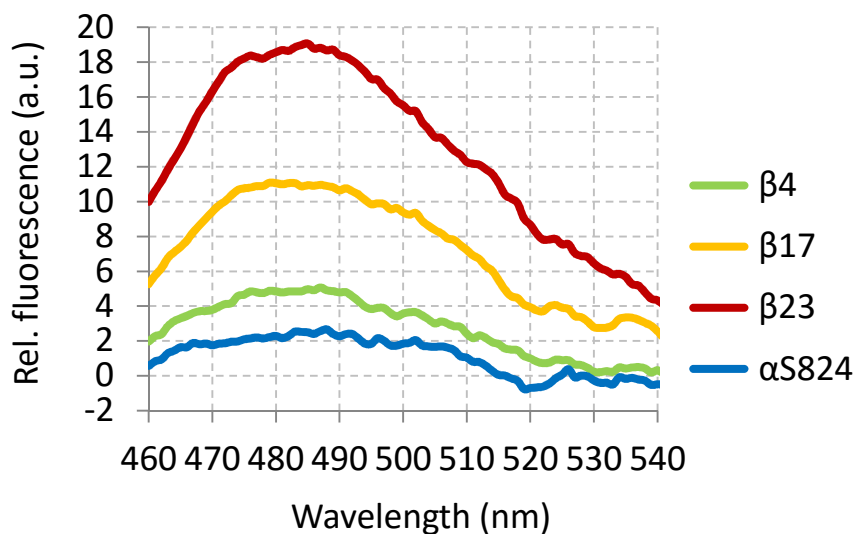


**Figure 37 | Thioflavin T fluorescence upon binding to  $\beta$  proteins or  $\alpha$ S824.** The fluorescence intensity significantly increases in presence of preformed  $\beta$  protein fibrils (refolded from guanidine), correlating to the toxicity of the  $\beta$  proteins. 3  $\mu$ M of monomeric protein were diluted in physiological buffer with 20  $\mu$ M Thioflavin T. Representative spectra of at least 4 experiments are shown. Thioflavin T background fluorescence was subtracted.

$\beta$  protein fibrils assembled after dilution from denaturant into physiological buffer (150 mM KCl, 0.5 mM MgCl<sub>2</sub>, 25 mM HEPES, pH 7.5) for 24 h showed an increase in Thioflavin T fluorescence. The intensities of Thioflavin T fluorescence correlated to the cellular toxicity of the  $\beta$  proteins:  $\beta$ 23 showed the highest toxicity and Thioflavin T fluorescence, followed by  $\beta$ 17 and  $\beta$ 4.

Under equal conditions, NIAD-4 bound to fibrils of the three  $\beta$  proteins, resulting in a similar increase in fluorescence from  $\beta$ 4 over  $\beta$ 17 to  $\beta$ 23. Both fluorescent dyes bound the  $\beta$  proteins in a gradual manner, reflecting their toxic impact on living cells.

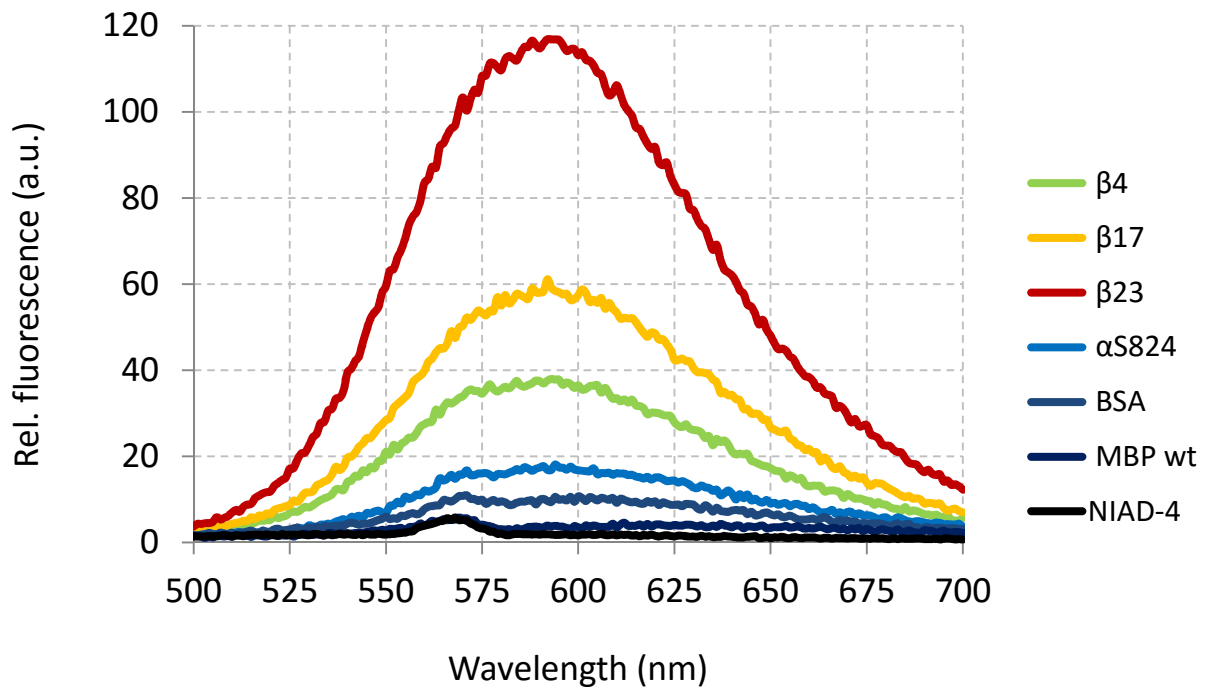


**Figure 38 | NIAD-4 fluorescence upon binding to  $\beta$  proteins,  $\alpha$ S824, BSA, or MBP.** The NIAD-4 fluorescence increases strongly in presence of preformed  $\beta$  protein fibrils (refolded from guanidine), correlating to their toxicity. 3  $\mu$ M of monomeric protein with 1  $\mu$ M NIAD-4 were diluted in physiological buffer (25 mM HEPES, 150 mM KCl, 0.5 mM  $MgCl_2$ , pH7.5). Representative spectra of at least 4 experiments are shown.

The  $\alpha$ -helical protein  $\alpha$ S824 showed only a marginal increase in Thioflavin T and NIAD-4 fluorescence, most likely due to unspecific low-level binding. In addition, equal mass concentrations of BSA and Maltose binding protein (MBP) were tested for their NIAD-4 binding. They showed an even lower fluorescence than  $\alpha$ S824.

Congo Red was also bound by the three  $\beta$  proteins. The binding leads to an increased absorbance at 535 nm and to a small redshift of the absorbance maximum from 490 nm towards  $\sim$ 500 nm in comparison to Congo Red in physiological buffer solution. This behavior is characteristic for Congo Red binding to amyloid fibrils, as shown for e.g. lysozyme fibrils (Krebs 2000). Differences between the three  $\beta$  proteins were hardly visible.  $\alpha$ S824 displayed no redshift and no increase in absorbance. Its absorbance at the 490 nm maximum was even a bit lowered.

The amyloid-like structures of the  $\beta$  proteins were specifically recognized by the amyloid sensors Congo Red, Thioflavin T, and NIAD-4. Amyloid sensor binding correlated very well with the cellular toxicity of the  $\beta$  proteins. More knowledge about structural details of the dye binding sites may promise clearer insights into the hazardous potential of distinct amyloid conformations.



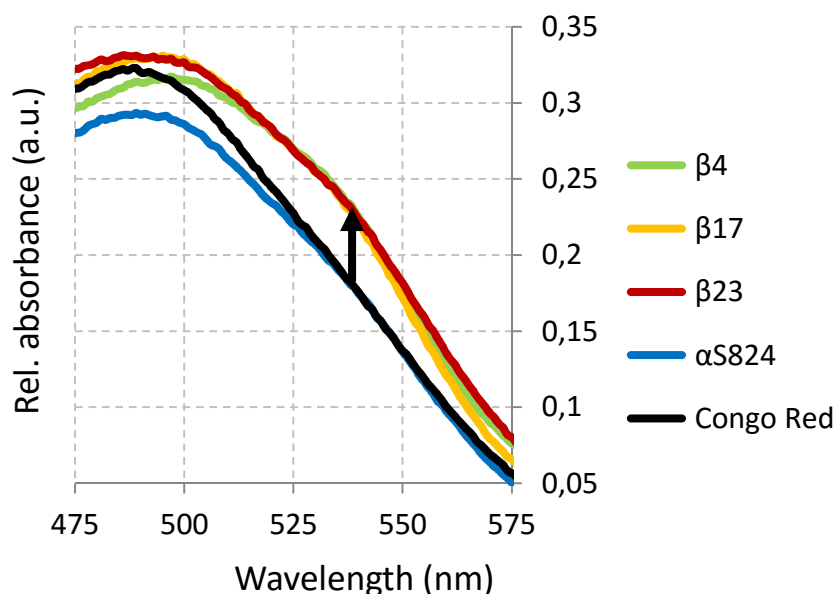


**Figure 39 | Congo Red absorption in presence of  $\beta$  proteins and  $\alpha S824$ .** 10  $\mu M$  of  $\beta$  proteins were refolded from 8 M guanidine into physiological buffer with 7  $\mu M$  Congo Red. Binding of Congo Red to the  $\beta$  protein fibrils can be recognized by an increased absorbance around 535 nm (arrow). Representative spectra of 3 experiments are shown.

### **$\beta$ proteins contain hydrophobic surface patches – in correlation with toxicity**

ANS (8-Anilino-1-naphthalenesulfonic acid) is a fluorescent dye that was originally found to bind to non-polar environments on apomyoglobin (but not to myoglobin or hemoglobin), giving rise to a huge fluorescence blueshift in comparison to the dye in a polar or aqueous surrounding (Stryer 1965). Since then, ANS was used in protein folding studies to characterize individual steps of protein folding, leading in general to an initial rise followed by rapid decline of ANS fluorescence. Rise and decline correspond to the formation of hydrophobic patches on molten globule states and the later burial of such hydrophobic patches in the core of a protein. Proteins with hydrophobic patches on their folded structure, as they are characteristic for interaction surfaces, retain their ability to bind ANS to some degree.

The  $\beta$  proteins were tested for their ability to bind ANS after refolding from denaturant in a physiological buffer in equilibrium. All three  $\beta$  proteins show a significantly higher ANS fluorescence than control proteins, such as  $\alpha S824$ , or maltose-binding protein (MBP wildtype).

ANS binding correlated with the cytotoxicity of the  $\beta$  proteins. Similarly, the ANS fluorescence maximum exhibited a stronger blueshift for the more toxic  $\beta$  sequences, indicating an environment of higher hydrophobicity. The fluorescence maxima of  $\alpha S824$  and MBP of around 525 nm correspond approximately to the fluorescence maximum of ANS in water, demonstrating that these proteins are fully folded exposing a polar surface. The fluorescence maximum of ANS in presence of the  $\beta$  proteins is strongly blueshifted. The fluorescence maximum at 472 nm for  $\beta 23$  is comparable to an ANS spectrum in an organic solvent, such as DMSO (Hawe 2008), or ANS bound to misfolded protein structures.

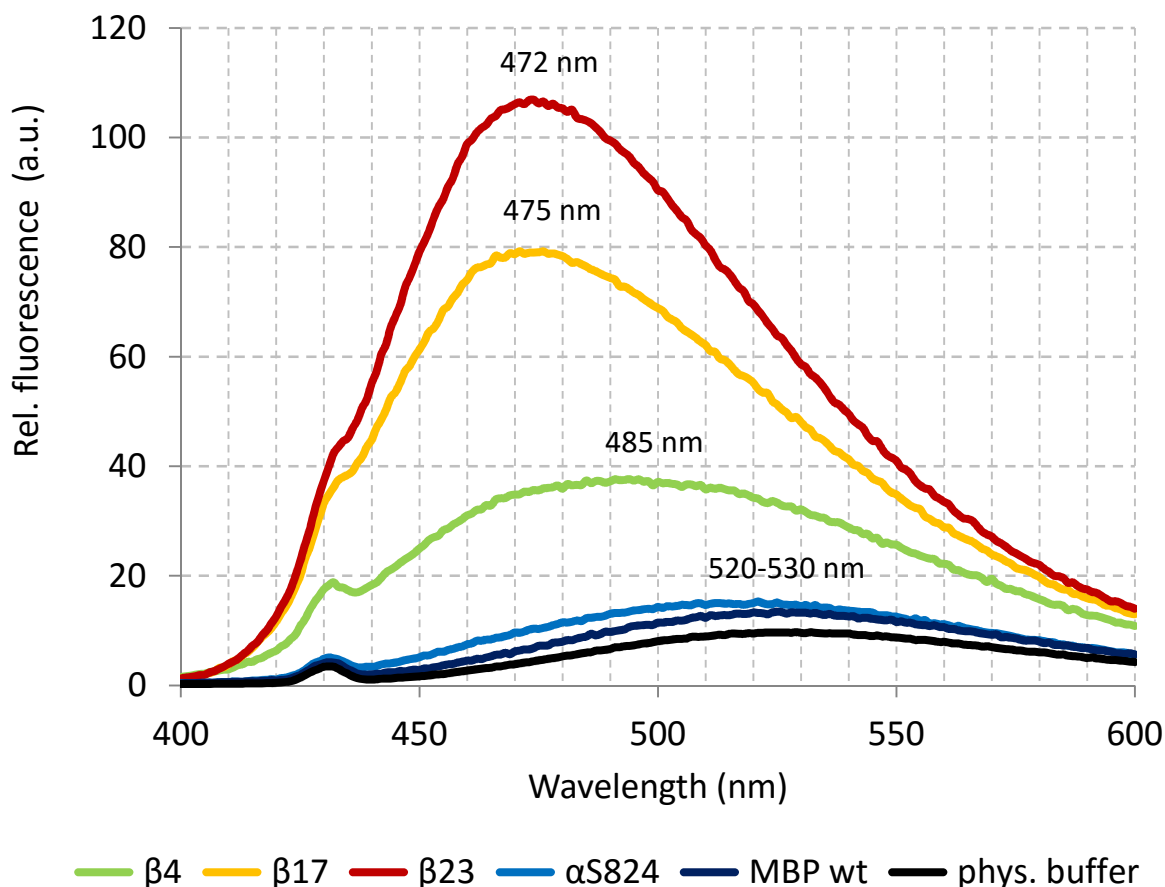


**Figure 40 | ANS fluorescence upon binding to  $\beta$  proteins,  $\alpha$ S824, MBP wildtype, or in physiological buffer.** The fluorescence intensity significantly increased in presence of preformed  $\beta$  protein fibrils (refolded from guanidine), and the fluorescence maximum shifts towards shorter wavelength. In presence of  $\alpha$ S824 or MBP, the ANS fluorescence changes only marginally. 3  $\mu$ M of monomeric proteins were diluted in physiological buffer (25 mM HEPES, 150 mM KCl, 0.5 mM  $MgCl_2$ , pH7.5) containing 20  $\mu$ M ANS. Representative spectra of at least 4 experiments are shown.

Electrostatic attractions of ANS to the  $\beta$  proteins are not expected, since ANS and the three  $\beta$  proteins are negatively charged,  $\beta$ 23 containing the highest negative net charge of -13. Beyond amyloid sensor binding (Thioflavin T, NIAD-4), the steadily accessible hydrophobic surfaces on the refolded  $\beta$  protein aggregates correlate to their toxicity and may constitute one of its major sources.

### **$\beta$ proteins refold rapidly and spontaneously – with highly similar kinetics**

ANS and Thioflavin T can be used to follow the kinetics of refolding and aggregation of the  $\beta$  proteins after dilution from the unfolded state in denaturant into a physiological buffer. The fluorescent sensors bind the assembling structures during the formation of accessible hydrophobic patches or the creation of amyloid binding sites.

The three  $\beta$  proteins aggregated very rapidly. The Thioflavin T fluorescence rose instantly upon dilution of the  $\beta$  proteins from denaturant (8 M guanidinium). The kinetics of Thioflavin T binding were highly comparable among all three  $\beta$  proteins. Already after two minutes of refolding, the Thioflavin T signal reached 90% of its final intensity. Initial lag phases could not be observed.

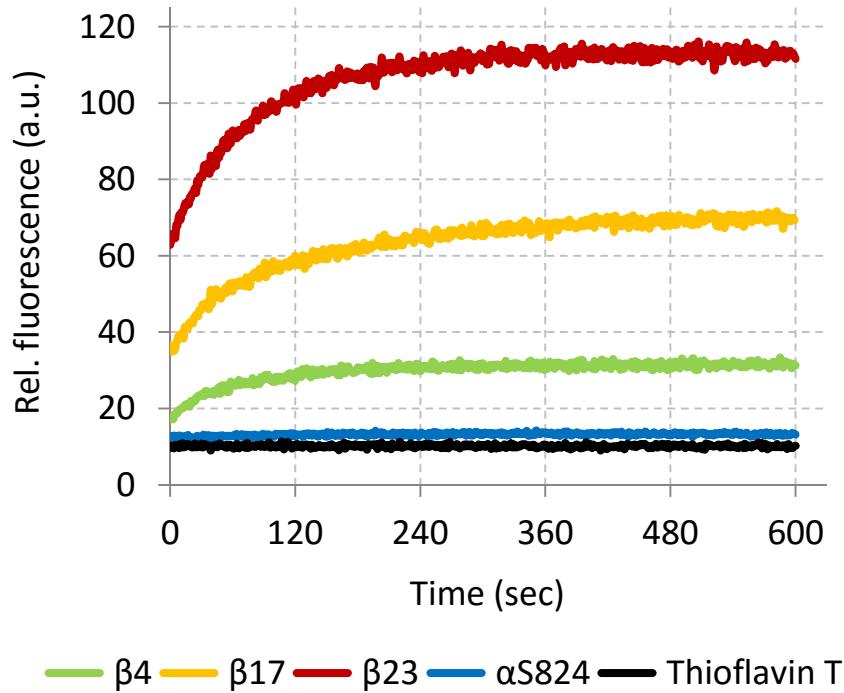


**Figure 41 | Thioflavin T binding kinetics of  $\beta$  proteins refolding from guanidine assemble within minutes into amyloid-like fibrils.** 20  $\mu$ M of  $\beta$  proteins were diluted from 8 M guanidine into physiological buffer (150 mM KCl, 0.5 mM  $MgCl_2$ , 25 mM HEPES, pH 7.5). For comparison,  $\alpha$ S824 is shown (diluted from folded state). Representative kinetics of at least 4 experiments are shown.

However, the relative intensity of Thioflavin T binding varied in correlation with cytotoxicity, as described above.  $\alpha$ S824 did not show any changes in fluorescence over time.

Kinetics of refolding and aggregation of the  $\beta$  proteins were furthermore monitored by ANS fluorescence. The formation of surface accessible hydrophobic patches rose exponentially within the first seconds of refolding. ANS fluorescence appeared even slightly faster than Thioflavin T binding. Most likely, ANS bound already to monomers or small oligomers during or after refolding.

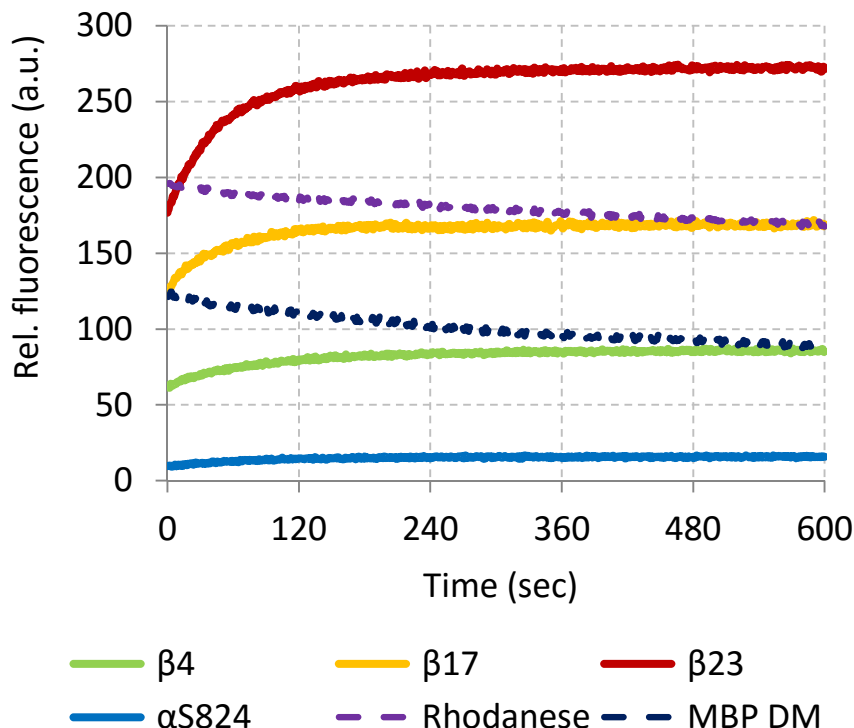


**Figure 42 | ANS binding kinetics of  $\beta$  proteins, rhodanese, and MBP double mutant refolding from guanidine.** 20  $\mu$ M of  $\beta$  proteins or equal amounts (w/w) of rhodanese or MBP double mutant were diluted from 8 M guanidine into 10 mM potassium phosphate, pH 6.0 (same conditions as for electron microscopy, second condition). The ANS fluorescence of the slowly folding MBP double mutant decreased further to lower values over time. All other proteins almost reached their equilibrium. For comparison,  $\alpha$ S824 is shown (diluted from folded state). Representative kinetics of at least 3 repetitions are shown.

Unlike for most native cellular proteins, the ANS fluorescence did not decrease during refolding after an initial burst, but remained persistently high in steady state. Hydrophobic patches therefore appeared during refolding and fibril assembly of the  $\beta$  proteins. The hydrophobicity did not fully become buried inside of the structures, but remained exposed on the surface of the assembled fibrils (Lindgren 2005). Hydrophobic exposure has been shown to be a characteristic determinant of toxicity on protein oligomers, especially in combination with structural flexibility (HypF-N oligomers; Campioni 2010).

A very slowly refolding double mutant of the maltose binding protein (MBP DM) and the GroEL dependent rhodanese were diluted from 8 M guanidine into physiological buffer in absence of chaperonins (required for rapid native refolding of these proteins). ANS fluorescence of these “misfolded conformations” of natural proteins was similar to  $\beta$ 4 and  $\beta$ 17, clearly exceeded by the ANS fluorescence of  $\beta$ 23. Equal masses of proteins were applied for these experiments. High fluorescence intensities and strong fluorescence blueshift, both properties demonstrate the high surface hydrophobicity of the  $\beta$  proteins (Figure 42).

Most aggregation prone proteins show an initial lag phase (nucleation) before they start to aggregate exponentially. During nucleation, a protein refolds from its native into a misfolded structure, which can happen either spontaneously or through interactions with e.g. other misfolded monomers. If this conformation is stable enough to persist, it may recruit more molecules into the thereby growing fibrils (Hortschansky 2005). Overall, sigmoidal aggregation kinetics finally become stationary, when the growth of fibrils saturates.

This nucleation time appears to be absent for the  $\beta$  proteins, which likely assemble directly from their unfolded state into rapidly growing fibrils. Such a behavior seems plausible, since the artificial  $\beta$  proteins were not designed to fold into any native structure distinct from the  $\beta$ -sheet conformation. Moreover, they are of very small size, and thus rapidly fold into an amyloid-like  $\beta$ -sheet conformation. This creates a high concentration of “monomeric building blocks” that can immediately assemble into fibrils. A distinct “native state” as a form of kinetic trap, delaying the way to aggregation, does not exist (see discussion).

Transmission electron micrographs of  $\beta$ 17 and  $\beta$ 23 were taken to achieve a better insight into fibril structures forming shortly after refolding from denaturant. Already after 5 min, short fibrils were visible. They continued to grow over the hours. In case of  $\beta$ 23, small oligomers were visible after 5 min, and they remained present in equilibrium with the growing fibrils (Figure 32).

## **ANS, Thioflavin T, and NIAD-4 differentiate between monomers, oligomers, and fibrils**

Formation of hydrophobic surface patches occurred even more rapidly than fibril formation (ANS vs. NIAD-4 or Thioflavin T kinetics), saturating in a multi-sigmoidal curve after 120 sec of refolding. ANS fluorescence kinetic curves were composed of two or more sigmoidal processes (Figure 43). The underlying reactions started together with the dilution of the  $\beta$  proteins from denaturant, but processed with different rates. Initial hydrophobic patches were presumably already forming on transient monomeric folding intermediates, giving rise to the first burst of ANS fluorescence (phase 1, refolding monomers, very fast rate, and early saturation). Conformational rearrangements caused a partial coverage of hydrophobic surfaces on the oligomerization sites, which is reflected in a slower second (and potentially third?) phase of ANS fluorescence (phase2, oligomerization and/or fibril growth, slower rate, later saturation; see bi-logistic growth, Meyer 1994).

Similar to ANS, Thioflavin T fluorescence kinetics of refolding  $\beta$ 23 deviated from a single logarithmic fit. The kinetics initially rose faster than expected, but saturated within 5 min. Thioflavin T is most likely not completely specific for amyloid fibrils, but also binds to intermediate oligomeric species or short protofibrils of high  $\beta$ -sheet content. These structures subsequently mainly fuse to form longer, mature fibrils, which is then not reflected in a fluorescent change any more (saturated signal).

The NIAD-4 fluorescence is contrarily very well described by a single logarithmic function. There was no initial signal “overshoot”, and the fluorescence did never completely saturate, but continued to increase. This behavior indicates that NIAD-4 may be the most specific amyloid fibril sensor here, binding neither to monomers nor to early oligomerization intermediates. NIAD-4 fluorescence therefore increased with the maturation of fibrils over hours.

The  $\beta$  proteins therefore behaved overall very similar to native proteins in the process of amyloid-like misfolding and aggregation. A very rapid nucleation phase, originating from a direct folding into the building blocks of oligomerization, is followed by exponential fibril growth. Eventually, fibril maturation processes over hours and days by growth and association of preformed (proto-)fibrils, which results in precipitating high-molecular-weight fibers (Dobson 2003).

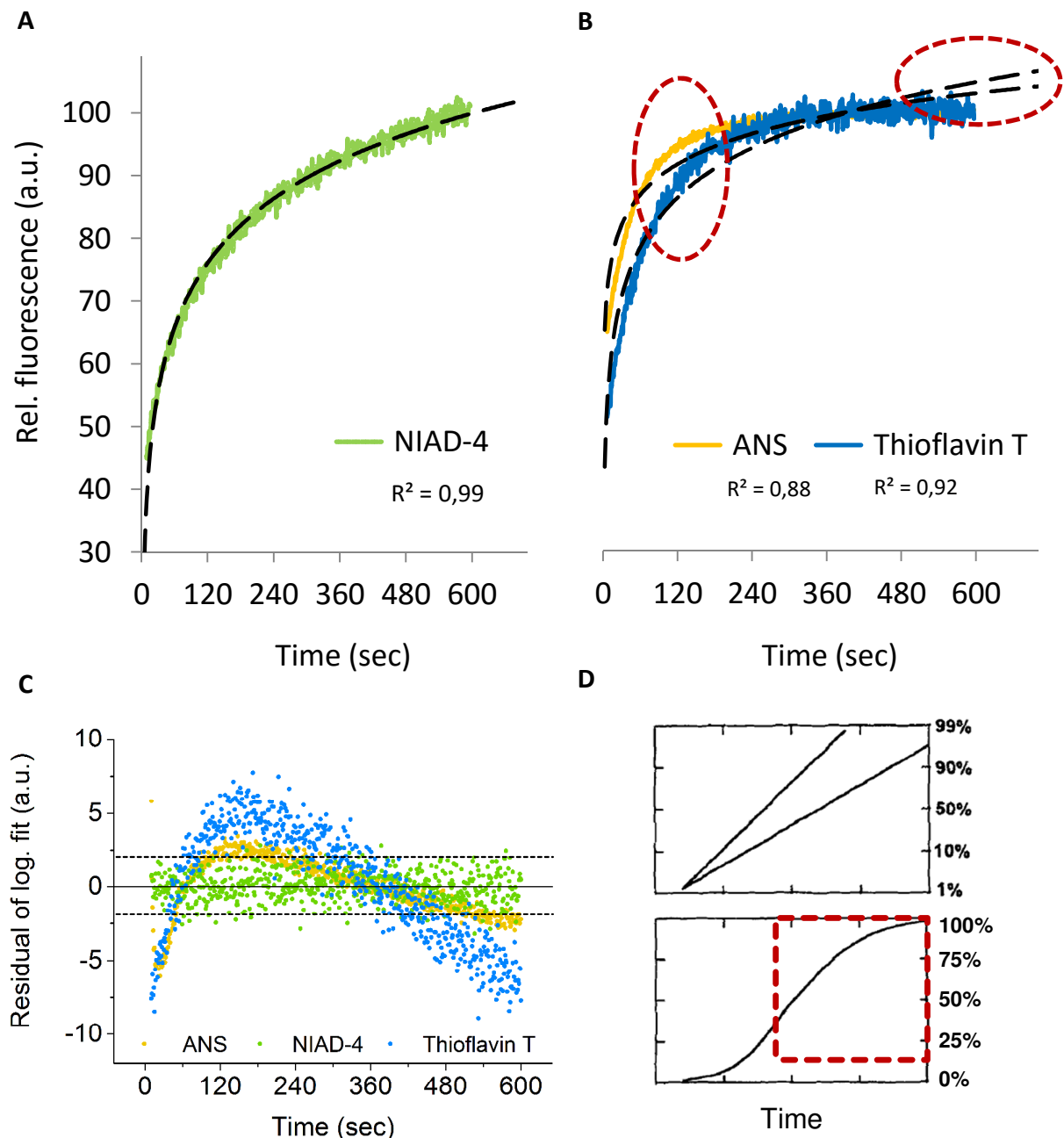


**Figure 43 | Refolding and aggregation kinetics of  $\beta$ 23 diluted from denaturant (8M guanidine), observed by ANS, NIAD-4, and Thioflavin T binding.** (A) Single logarithmic fit (black dashed curve) on the fluorescence of NIAD-4, binding to refolding  $\beta$ 23. (B) Single logarithmic fits (black dashed curves) on the fluorescence of ANS and Thioflavin T, binding to refolding  $\beta$ 23. In contrast to NIAD-4, the fluorescence of ANS and Thioflavin T initially rose faster than a single logarithm, but then remained constant (deviations within red dashed areas). (C) Residuals describing the deviation of the single logarithmic fits from the experimental fluorescence data. Whereas NIAD-4 residuals distribute evenly around zero (green, like noise), ANS and Thioflavin T residuals initially rose for  $\sim 2$  min and then declined continually. Supposedly, the two dyes bound to refolding intermediates (monomers, oligomers), whereas NIAD-4 only recognized the  $\beta$  protein fibrils. (D) Theoretical “diverting bi-sigmoidal curve”, describing two sigmoidal processes beginning at the same time, but growing with different rates (such as refolding and fibrilization; top graph). “It is noteworthy that [diverting bi-sigmoidal curves] are S-shaped but asymmetric. They do not ‘look logistic’” (figure adapted from Meyer 1994). Since nucleation happened very fast for refolding  $\beta$  proteins, only the second part of the curve (dashed square in bottom graph) could be observed in (A) and (B).

## $\beta$ proteins bind anti-amyloid oligomer (A11) antibody

The A11 anti-oligomer antibody was raised against a molecular mimic of soluble A $\beta$  oligomers. Moreover, A11 recognizes oligomeric species from different neurodegenerative disease proteins, most likely forming a common epitope independent of specific sequences (Kayed 2003, Kayed 2006).

In an earlier attempt, cell extracts prepared from HEK293T cells expressing  $\beta$  proteins were separated by gel filtration. The individual fractions showed an A11 reactivity overlapping with the anti-c-Myc recognition of the  $\beta$  proteins (Olzscha 2011). Here, equal amounts of purified  $\beta$  proteins were refolded in a physiological solution, directly blotted on a nitrocellulose membrane, and tested for their A11 reactivity. A11 recognized all three  $\beta$  proteins, as in case of the cellular lysates. Quantitatively there was no significant difference.  $\alpha$ S824 showed minor A11 binding, which was not visible for MBP or BSA.

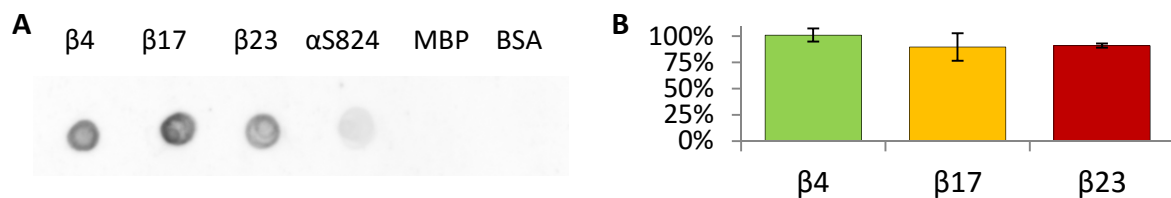


**Figure 44 | A11 anti-oligomer antibody reactivity of  $\beta$  proteins, purified  $\alpha$ S824, MBP or BSA *in vitro*.** (A) Native dot blot of  $\beta$  proteins (purified and refolded in physiological buffer),  $\alpha$ S824, MBP and BSA. The proteins were directly blotted on nitrocellulose membranes tested for A11 reactivity. All three  $\beta$  proteins were recognized by A11.  $\alpha$ S824 showed some minor, MBP and BSA did not show any A11 reactivity. (B) Quantification of A11 reactivity for the  $\beta$  proteins, normalized to the amount of protein blotted, as determined by the c-Myc antibody signal intensity (not shown here, equal amounts were blotted). There was no significant difference in A11 reactivity between the three  $\beta$  proteins *in vitro*.

Purified and refolded  $\beta$  proteins formed oligomeric species that are recognized by A11 *in vitro*. However, the equilibrium amount of different oligomeric species (monomers, small oligomers, aggregates) assembling *in vivo* and from purified protein *in vitro* may differ to some degree, as *in vivo* cellular factors likely influence or participate in oligomer formation. A11 indicated the presence of epitopes common to oligomeric forms of neurodegenerative disease proteins on all three  $\beta$  proteins, despite the absence of visible spherical oligomers on the electron microscopic recordings. However, A11 epitopes might also be present on the surface or the termini of shorter (proto-)fibrils.

## **$\beta$ proteins interact directly with Hsp110 – quantitatively correlating with toxicity**

Hsp110, a heat shock protein structural related to and collaborating with Hsp70 (Polier 2008), was found to interact and to colocalize with all three  $\beta$  proteins in cells (Olzscha 2011). Overexpression of Hsp110 partially rescued the toxicity of  $\beta$  proteins in HEK293T cells (Olzscha 2011). A direct molecular interaction of Hsp110 and the  $\beta$  proteins was not shown so far.

Equal amounts of purified  $\beta$  proteins and  $\alpha$ S824 were incubated with anti-c-Myc antibodies coupled to magnetic beads in a physiological buffer including 0.5% BSA, blocking unspecific interactions. After washing away unbound  $\beta$  proteins, the beads were incubated with equal amounts of purified Hsp110, followed by intense washing. Bound proteins were eluted under denaturing conditions (SDS) and analyzed by SDS-PAGE and immunoblotting.

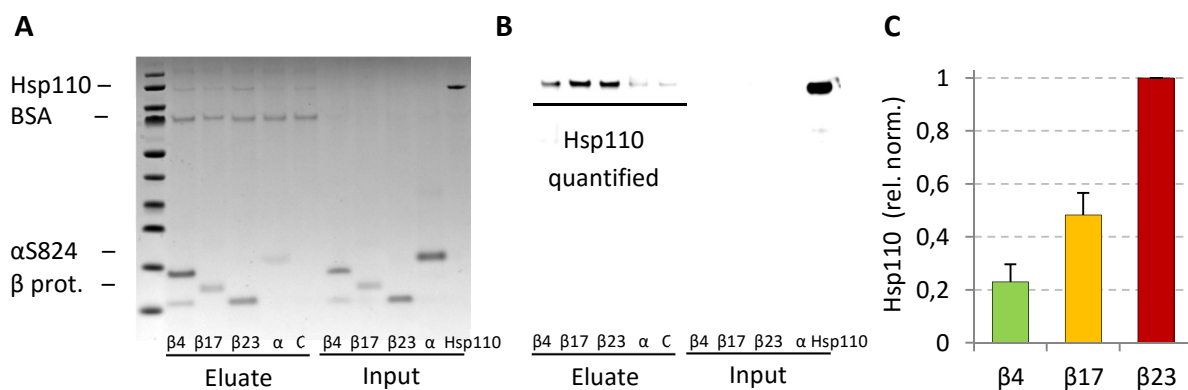


**Figure 45 | Analytical affinity chromatography of Hsp110 by  $\beta$  proteins bound to anti-c-Myc antibodies coupled to magnetic beads.** (A) Purified  $\beta$  proteins or  $\alpha$ S824 (input) binding to magnetic anti-c-Myc beads were incubated with Hsp110 (input). Proteins eluted from the beads were separated (eluat) by gradient SDS PAGE stained with Coomassie Brilliant Blue. (B) For quantification, input and eluat were immunoblotted and labeled with anti-Hsp110 antibodies. (C) Quantification of Hsp110 binding to the  $\beta$  proteins from (B). Result from three independent experiments. Background binding (control) was subtracted, Hsp110 binding was normalized to the amount of  $\beta$  protein in the eluat (anti-c-Myc signal).

A quantitative analysis of the eluate revealed that Hsp110 bound to  $\beta$  proteins *in vitro* in correlation to their toxicity.  $\beta$ 23 bound 5 times more Hsp110 than equal amounts of  $\beta$ 4, and 2 times more Hsp110 than equal amounts of  $\beta$ 17. The data indicates a potential direct interaction between the  $\beta$  proteins and Hsp110 alone. Possibly, additional cellular factors (such as Hsp70 or other cochaperones) may further increase the interaction or render it functional towards a structural modification or disaggregation, which could not be observed under the applied *in vitro* conditions here.

Meanwhile, Hsp110 was found to engage in disaggregation of misfolded substrates (luciferase and GFP), together with Hsp70/Hsp40, and independent of the AAA+ ATPase p97. Hsp110 was found to hydrolyze ATP, and to promote nucleotide exchange on Hsp70 for promoting disaggregation of disordered aggregates, though failing in case of amyloid forms of  $\alpha$ -synuclein or the yeast prion protein Sup35 (Shorter 2011). Furthermore, human cytoplasmic Hsp110 ATP-dependently refolded misfolded luciferase *in vitro* in the absence of Hsp70, but together with Hsp40, demonstrating an own ATP-dependent chaperone function of Hsp110 (Mattoo 2013). Cofactors such as Hsp40s and Hsp70s might still enhance a disaggregation function of Hsp110 in cells.



## Purified $\beta$ proteins are cytotoxic on addition to human cells

Similar to prion proteins, misfolded protein structures might be released e.g. through exocytosis or during cell death and be distributed locally, over organs or the human body. Misfolded structures may damage cells from the extracellular site, or they may become internalized again, with the potential of propagating their detrimental effects. Large A $\beta$  deposits accumulate mainly in the extraneuronal space, but their role in the pathogenesis of Alzheimer's disease remains still unclear.

To analyze these phenomena, purified  $\beta$  proteins were added into the culture medium of HEK293T cells to study their toxicity on cells from the extracellular side.  $\beta$  proteins were refolded from guanidine and assembled into oligomers and fibrils (non-precipitating at these concentrations). Added to the culture medium, the  $\beta$  proteins did not show any detrimental impact on cell survival (tested in different concentrations, with or without fetal bovine serum in the culture medium).

Interestingly, toxicity appeared after sonication of the refolded  $\beta$  protein oligomers. The samples were sonicated in a physiological buffer solution for a few seconds with a tip sonicator. Directly afterwards, the  $\beta$  proteins were diluted into culture medium, which was then added to HEK293T cells. Here, the  $\beta$  proteins had a concentration dependent toxic impact, as determined by MTT assay (see below). Toxicity was even observed at very low concentrations ( $\beta$ 23 at 20 nM).

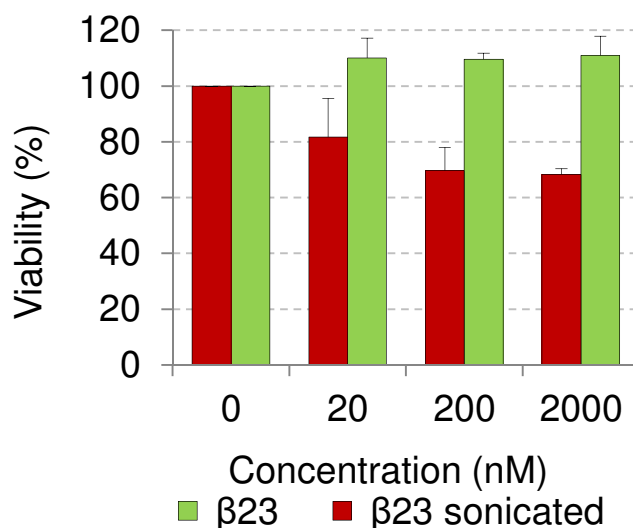


**Figure 46 | Viability of HEK293T cells treated with purified and *in vitro* refolded  $\beta$  proteins.** The viability of HEK293T cells after treatment with different concentrations of  $\beta$ 23 for 24 h was determined based on MTT reduction. In one set (red), the  $\beta$  proteins were treated for 5 sec with a tip sonicator in physiological buffer, before diluting them into culture medium that was added to the cells. Averages and SD from 3 experiments.

Sonication most likely breaks down aggregates into smaller particles and exposes previously buried hydrophobicity to the surface. As we see below, the  $\beta$  proteins indeed converted into conformations with increased surface hydrophobicity.

## Sonicated $\beta$ proteins are more hydrophobic

To examine structural changes before and after sonication, equal concentrations of purified  $\beta$  proteins, refolded from guanidine, were compared regarding their ability to bind ANS. For all three  $\beta$  proteins, the intensity of ANS fluorescence doubled after sonication, indicating that their exposed hydrophobic surfaces increased strongly. Increased surface hydrophobicity likely appeared due to a fragmentation of particles into smaller oligomers. Additionally, conformational changes may expose hydrophobic residues previously buried within preformed aggregate structures in equilibrium.

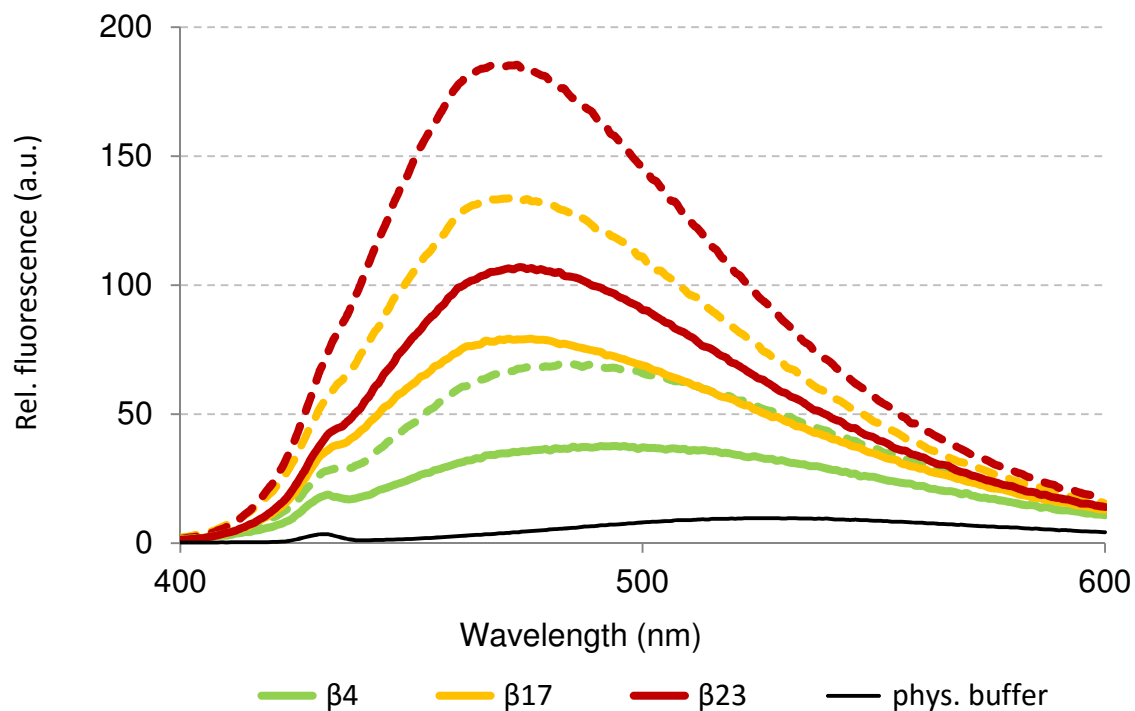


**Figure 47 | Hydrophobic surface patches of  $\beta$  protein aggregates increase after sonication.** ANS spectra of purified and refolded  $\beta$  proteins, before (continuous spectra) and after (dashed spectra) sonication with a tip sonicator in physiological buffer solution.

The purified  $\beta$  proteins shown to be toxic in the medium on HEK293T cells exposed an increased hydrophobicity on their surface and presumably decreased in average molecular weight. Such conformations might be more reactive on cells, coming into contact with membrane proteins or the lipid bilayer. Whether the  $\beta$  proteins were able to cross the bilayer directly or by endocytosis and to reach the cellular interior is an interesting question worthwhile to study. However, HEK293T cells were rather resistant towards preassembled (non-sonicated)  $\beta$  protein aggregates, which did not to cause immediate toxicity on cultures.

## Extracellular $\beta$ proteins induce neurotoxic signaling by the cellular prion protein

In a different attempt, cells became sensitized towards extracellular  $\beta$  proteins and other amyloid structures (such as A $\beta$  and the infectious prion proteins PrP<sup>Sc</sup> and Sup35) by overexpression of the cellular prion protein (PrP<sup>C</sup>). As an integral membrane receptor, PrP<sup>C</sup> might be a critical cellular target of extracellular misfolding and aggregation and an important signaling factor initiating cellular responses.

The experiments with extracellular oligomeric and fibrillary  $\beta$  proteins on cells overexpressing membrane anchored PrP<sup>C</sup> were mainly planned and accomplished by Dr. Ulrike K. Resenberger and Prof. Dr. Jörg Tatzelt (at the Adolf-Butenandt-Institute, Ludwig-Maximilians-University Munich, Germany, now Ruhr-Universität Bochum, Germany).

SH-SY5Y cells expressing GPI anchored PrP<sup>C</sup> were treated with 200 nM  $\beta$  proteins ( $\beta$ 17) or  $\alpha$ S824 in the medium for 12 h. Only the (here non-sonicated)  $\beta$  proteins caused an increase in cell death.

Beyond the  $\beta$  proteins, PrP<sup>C</sup> mediated toxic signaling of homologous and heterologous PrP<sup>Sc</sup>, oligomeric but not high-molecular-weight forms of A $\beta$  (secreted from co-cultured CHO-7PA2 cells stably expressing A $\beta$  V717F), as well as  $\beta$ -sheet rich conformers of the yeast prion protein Sup35 (prepared as  $\beta$ -sheet rich low-molecular-weight oligomers formed by the middle and N-terminal region; Resenberger 2011). PrP<sup>C</sup> therefore recognized and responded to very different amyloid and prion proteins, suggesting common structural features determine a binding site on PrP<sup>C</sup> for activation (Resenberger 2011). For mediating toxic effects, both the intrinsically disordered N-terminal domain and the C-terminal GPI anchor of PrP<sup>C</sup> were required (Resenberger 2011).

The toxic signaling by the cellular prion protein was inhibited by expressing a secreted soluble version of the intrinsically disordered N-terminal domain of PrP devoid of the GPI anchor. Co-immunoprecipitation demonstrated an efficient capturing of extracellular  $\beta$  proteins by secreted N-terminal PrP domains (fused to Fc portions of human IgG<sub>1</sub> allowed expression and secretion of the construct in SH-SY5Y cells). Expression and secretion of these soluble PrP constructs reduced toxic signaling of extracellular  $\beta$  proteins (50 nM) or A $\beta$  (Resenberger 2011).

In primary cortical neurons, the purified  $\beta$  proteins only caused toxicity in cultures isolated from PrP<sup>+/+</sup>, not from knockout mice (PrP<sup>0/0</sup>). The  $\beta$  proteins were added on day 4 and 5 at 2 or 5  $\mu$ M, and the neurons were fixed at day 6. Cellular growth and morphology was examined by immunofluorescence using an anti- $\beta$ 3 tubulin antibody. The  $\beta$  proteins caused significant dendritic damage and neuronal loss in PrP<sup>+/+</sup> neurons, while no toxicity occurred in neuronal cultures from PrP<sup>0/0</sup> mice (Resenberger 2011).

Toxic signaling of the  $\beta$  proteins or A $\beta$  could moreover be reduced by the A11 antibody, recognizing and binding toxic oligomers in the medium of SH-SY5Y cells. Furthermore, pre-treatment of cells with the NMDA receptor antagonist memantine reduced the toxic signaling, as NMDA receptor and PrP<sup>C</sup> signaling interfere with each other regarding excitotoxicity and neurotoxic signaling (Khosravani 2008, Ondrejcek 2010, Resenberger 2011). These experiments revealed that the  $\beta$  proteins – in an equivalent way to natural amyloid and prion proteins – were able to induce a cellular response in form of neurotoxic PrP signaling. PrP<sup>C</sup> sensitized cells toward neurotoxic signaling independently from its own misfolding and prion replication (Resenberger 2011). Neurotoxic PrP signaling initiated by extracellular protein aggregation demonstrated that the presence of signaling pathways enables

cells to respond to local misfolding e.g. by apoptosis. Induced cell death may prevent further “infection” and distribution of misfolded proteins in an attempt of local restriction of aggregate burdens.

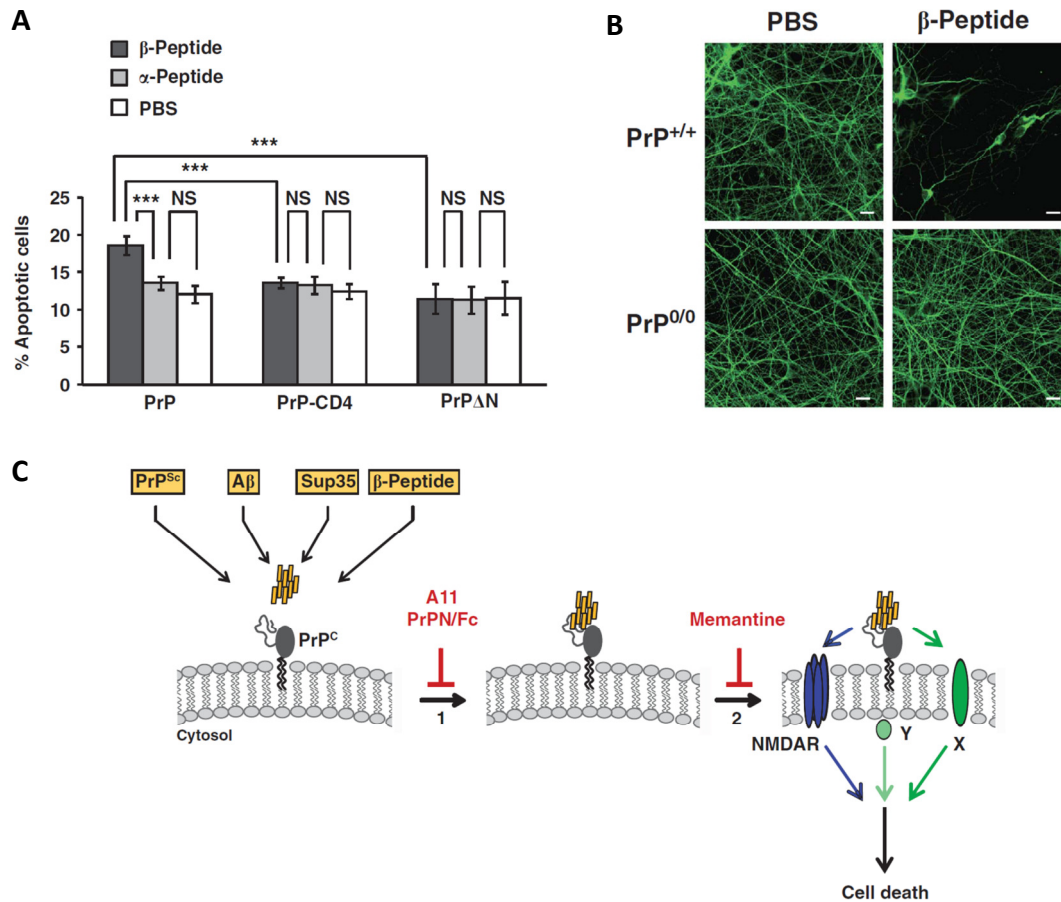


**Figure 48 | The cellular prion protein (PrP<sup>C</sup>) mediates neurotoxic signaling induced by β proteins, amyloid beta (Aβ), and prion proteins.** (A) Extracellular β proteins (here named β-peptides, 200 nM) cause neurotoxic signaling and induce apoptosis, but only in cells expressing the membrane bound cellular prion protein PrP<sup>C</sup> (full length). Deleting the intrinsically disordered N-terminal domain or the C-terminal GPI anchor abolished apoptosis induction. (B) β proteins caused neuronal toxicity and cell death only in PrP<sup>+/+</sup> neurons, whereas PrP<sup>0/0</sup> neurons were resistant. (C) Putative model of neurotoxic signaling induced by oligomeric amyloid structures via PrP<sup>C</sup>. β-sheet rich structures of misfolded proteins bind to PrP<sup>C</sup> sitting in the plasma membrane. Neurotoxic signaling can be inhibited by trapping misfolded structures by e.g. A11 antibodies or soluble PrP domains in the extracellular environment, or by signaling of the NMDA receptor antagonist memantine. Different intracellular factors might be involved in transmitting neurotoxic signals inside of cells, finally influencing apoptotic pathways (Resenberger 2011).

## **$\beta$ proteins are highly toxic in the human cytoplasm**

The c-Myc labeled  $\beta$  proteins were expressed in HEK293T cells for three days, where they exhibit a gradual toxicity (Olzscha 2010, Olzscha 2011).

MTT (3-(4,5-dimethylthiazol-2-yl)-2,5-diphenyltetrazolium bromide) is a water soluble dye that readily enters the cells across the membranes and becomes reduced by cellular enzymes. Thereby MTT changes its color and fluorescence properties (Mosmann 1983, Shearman 1995). Reduced MTT in a colorimetric cell survival assay reflects the redox state of a cell population. It depends on the cellular reduction potential (NADH content and cellular oxidoreductases), including the number of cells in a population.

Viability was increasingly reduced for HEK293T cells expressing  $\beta_4$ ,  $\beta_{17}$ , or  $\beta_{23}$ ; the soluble  $\alpha S824$  protein was not toxic (Olzscha 2011). The relative cytotoxicity of the three  $\beta$  proteins is equal to that observed in *E. coli* cells (growth inhibition). The sequence-dependent proteotoxicity of the  $\beta$  proteins was therefore independent from the species being affected.

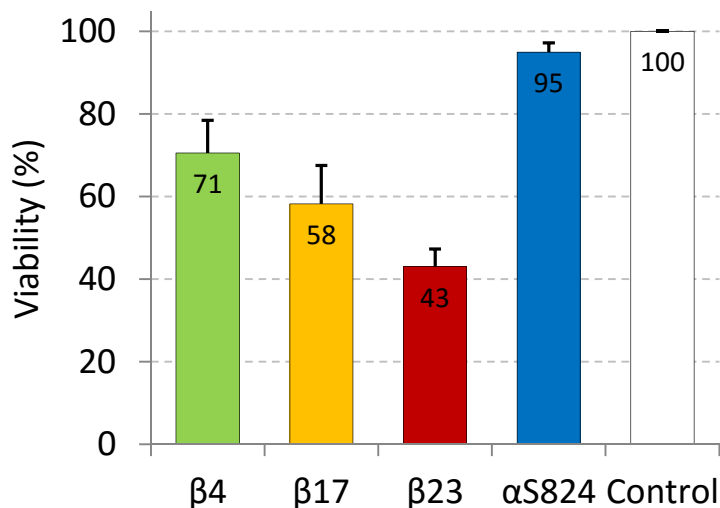


**Figure 49 | Viability of HEK293T cells expressing  $\beta$  proteins or  $\alpha S824$ , compared to cells transfected with empty plasmid backbones.** The  $\beta$  proteins affect the cellular viability in a sequence dependent manner. Cytotoxicity rose from weak ( $\beta_4$ ) over intermediate ( $\beta_{17}$ ) to strong ( $\beta_{23}$ ). Cells expressing the soluble  $\alpha S824$  showed no toxicity. Cellular viability was determined by the cellular capability of reducing MTT. Averages and SD from at least 5 independent experiments (compare to Olzscha 2011).

## **$\beta$ proteins are highly toxic in the cytoplasm, and less toxic in the nucleus**

Mammalian cytoplasm and nucleus strongly differ in their basic proteostasis machineries, including their chaperone content and degradation systems (Nielsen 2014). During cellular stress, many components of the proteostasis machineries are specifically expressed and become localized to distinct cellular sites. For example, chaperones are increasingly imported into the mammalian nucleus (Miyamoto 2014, Kose 2012, Park SH 2013). Many human neurodegenerative disease proteins form insoluble inclusions in the cytoplasm (tau, TDP-43,  $\alpha$ -synuclein), whereas especially fragments of polyglutamine repeat proteins accumulate in the nucleus, or spread between both compartments (huntingtin, ataxin; Soto 2003, Woulfe 2007, Miller 2011).

To examine how different compartments handle misfolded protein structures and to reveal compartment-specific vulnerabilities towards protein aggregation, we fused  $\beta$  proteins to nuclear export signals (NES) and nuclear localization sequences (NLS). We expressed these constructs in

HEK293T cells, utilizing cellular transport systems to direct the  $\beta$  proteins to cytoplasm or nucleus, respectively. Toxicities of cells expressing these  $\beta$  proteins for 3 days were determined by MTT assays. Expressing the  $\beta$  proteins targeted to the cytoplasm resulted in toxicities comparable to  $\beta$  proteins carrying no localization sequence, which were distributed over cytoplasm and nucleus. Surprisingly, all  $\beta$  proteins directed to the nucleus showed a significantly lowered cytotoxicity. The relative, sequence-dependent toxicities among the  $\beta$  proteins were maintained for the constructs targeted to distinct compartments ( $\beta_4 < \beta_{17} < \beta_{23}$ ).

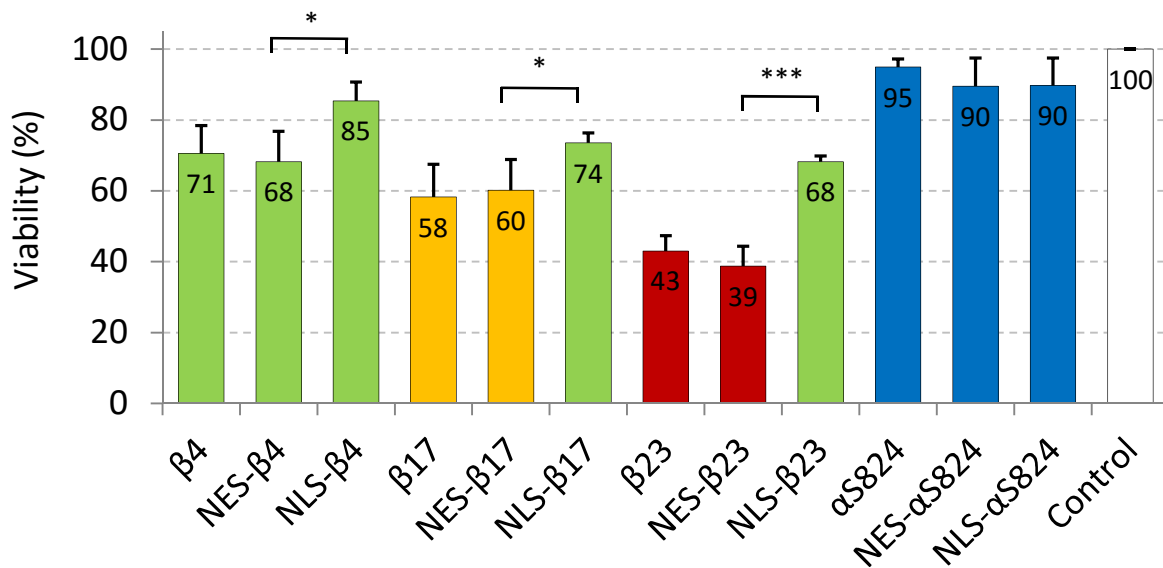


**Figure 50 | Viability of HEK293T cells expressing  $\beta$  proteins directed to cytoplasm (NES) or nucleus (NLS) in comparison to cells transfected with the non-targeted  $\beta$  proteins (c-Myc tag only), different versions of  $\alpha$ S824, or empty plasmid backbones (control).** Surprisingly, the detrimental impact of the  $\beta$  proteins as misfolding model proteins was strongly decreased for all  $\beta$  proteins targeted to the nucleus. The toxicity of cytoplasmic  $\beta$  proteins remained at a high level similar to the original, non-targeted  $\beta$  proteins distributing over cytoplasm and nucleus. Cells expressing different versions of  $\alpha$ S824 showed no significant toxicity. Cellular viability was determined by the cellular capability of reducing MTT. Averages and SD from at least 4 independent experiments. Significances according to Students T-test.

Cellular targeting sequences fused to the  $\beta$  proteins might alter their biophysical properties, and thereby influence their conformations and behavior in cells. Therefore, we introduced a point mutation within the nuclear targeting signal. NLS- $\beta_{23}$ (K7T, K15T) carries two single K to T mutation within the NLS repeat (DPK**K**KR**K**V mutated to DPK**T**KR**K**V), which renders nuclear localization inefficient (Kalderon 1984, Makkerh 1996, Hodel 2001). Thus, aggregates of NLS- $\beta_{23}$ (K7T, K15T) were distributed over cytoplasm and nucleus, similar to  $\beta_{23}$ , despite of the additional N-terminal tag. The toxicity rose again to levels comparable to non-targeted or cytoplasmic  $\beta$  proteins. It seems therefore unlikely that the addition of the NLS itself was mainly responsible for the observed decrease in toxicity.

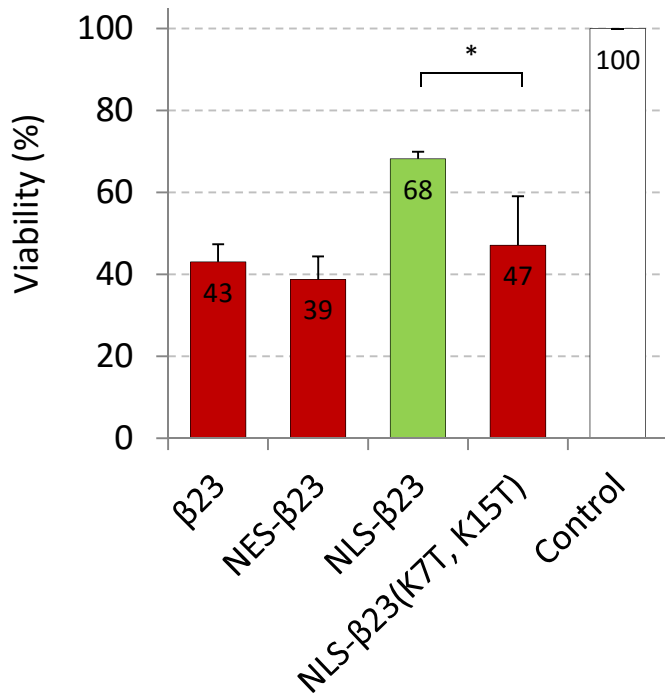


**Figure 51 | Viability of NLS-β23(K7T, K15T), carrying an inefficient NLS, in comparison to different β23 variants.** NLS-β23(K7T, K15T) carries a point mutation in each of its two SV40 derived NLS repeats. The protein aggregates in cytoplasm and nucleus simultaneously. Toxicity was found to be comparable to β23 and NES-β23 (MTT assay). Averages and SD from at least 3 independent experiments.

### β protein-EGFP fusions remain toxic

The β proteins were fused via a flexible 16 amino acids long linker sequence (TSGSAASAAGAGEAAA; Chang 2005) N-terminal to EGFP, enabling e.g. fluorescent live-cell imaging applications. MTT assays demonstrated toxicities comparable to constructs lacking EGFP, indicating that the toxic function of the β proteins was essentially retained after fusion to the soluble fluorescent protein.

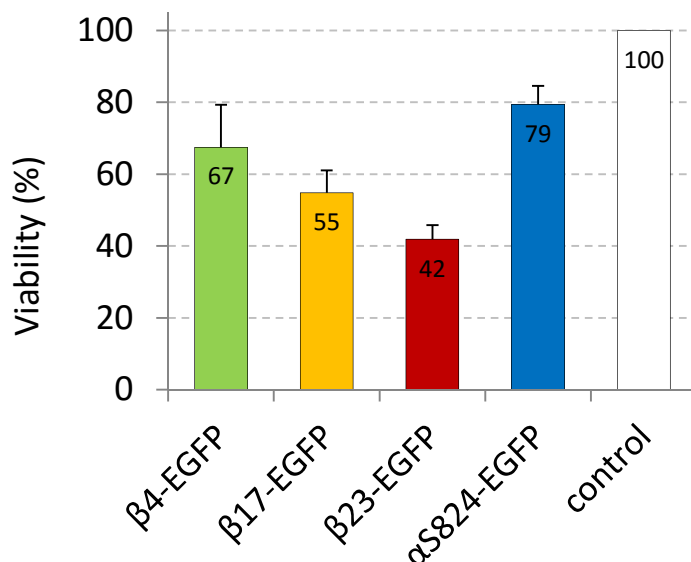


**Figure 52 | Viability of HEK293T cells expressing c-Myc tagged β protein-EGFP fusions in comparison to cells transfected with αS824-EGFP or empty plasmid backbones.** Toxicities are highly comparable to the β proteins lacking EGFP, indicating a dominant effect of the β sequences regarding their toxic functions. Cellular viability was determined by the cellular capability of reducing MTT. Averages and SD from 3 independent experiments. Significances according to Student's T-test.

## Nuclear $\beta$ protein levels are slightly higher than cytoplasmic

Toxicity occurs usually in a concentration dependent manner. Expression levels of the cytoplasmic and nuclear  $\beta$  proteins were detected by immunoblotting against the N-terminal c-Myc epitope. Cell lysates were separated by SDS-PAGE and blotted on Nitrocellulose or PVDF membranes. The two types of membrane non-covalently bind proteins due to different physical properties (electrostatic and hydrophobic interactions, respectively) and show different binding capacities. Binding affinities can therefore vary for the different  $\beta$  protein sequences.

The cellular levels of the  $\beta$  proteins targeted to the cytoplasm were slightly highly comparable to the non-targeted  $\beta$  proteins and showed in general an inverse correlation to cytotoxicity – with lowest protein levels for  $\beta$ 23 and NES- $\beta$ 23.

Nuclear  $\beta$  proteins, however, were expressed at higher cellular levels. Thus, the decreased toxicity of nuclear  $\beta$  proteins was not caused by decreased  $\beta$  proteins levels. Under equal  $\beta$  protein concentrations, the toxic impact of cytoplasmic  $\beta$  proteins may even be higher than observed under the given conditions.

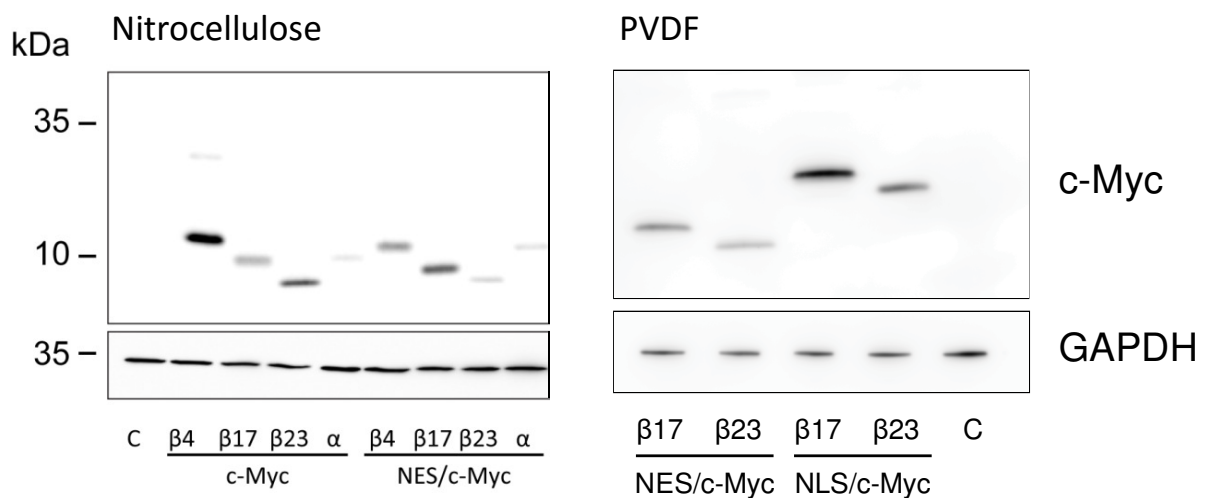


**Figure 53 |  $\beta$  protein levels detected by immunoblotting with anti-c-Myc antibodies.** Levels of non-targeted  $\beta$  proteins (only c-Myc tagged) and  $\beta$  proteins targeted to the cytoplasm (NES/c-Myc) showed comparable protein levels. The  $\beta$  proteins reached slightly higher levels in the nucleus (NLS/c-Myc), as observed on nitrocellulose and PVDF membranes.



## Diverse cytoplasmic aggregates distort the nuclear pore complex

In HEK293T cells,  $\beta$  proteins targeted to the cytoplasm or nucleus were expressed for 24 h. Cells were fixed and stained for the  $\beta$  proteins by anti-c-Myc antibodies. To discriminate the localization and aggregation behavior of the  $\beta$  proteins, cells were additionally stained for nuclear pore complex (NPC) proteins. Therefore, an antibody recognizing FG-repeat domains in nucleoporins (such as Nup62, Nup152, or Nup90) residing within the nuclear envelope was applied. The nuclear DNA was stained by DAPI (4',6-diamidino-2-phenylindole). Cells expressing NES- $\beta$  proteins directed to the cytoplasm formed large perinuclear inclusions, mostly of spherical shape, which were accompanied by  $\beta$  proteins distributed over the whole cytoplasm. NLS- $\beta$  proteins targeted to the nucleus formed several intranuclear inclusions of rather asymmetric shapes. In addition, tiny punctuated aggregates were visible around the inner side of the nuclear envelope.

To assess our analyses on the designed  $\beta$  proteins, we utilized several human proteins associated to neurodegenerative diseases for comparison: c-Myc tagged, polyglutamine expanded Huntingtin exon 1 (Htt96Q), forming mostly cytoplasmic, aggresome-like inclusions (Schaffar 2004); TDP-43 fragment 4 EGFP (TDP-F4), driving the coaggregation of endogenous full-length TDP-43 into cytoplasmic aggregates similar to the disease case in ALS/FTLD patients (Pesiridis 2009, Yang 2014); and a Parkin mutant lacking Parkins last 13 amino acids, causing the mutant to aggregate in the cytoplasm (Winklhofer 2003). The specified aggregate locations reflect the situation in neurons of human patients. Fragments of polyglutamine-expanded huntingtin, however, accumulates in nuclear inclusions in co-occurrence with cytoplasmic aggregates. The relative distribution depends on cell types, polyglutamine extension length, organism, and age (Hackam 1999 1/2, DiFiglia 1997, Woulfe 2007, Miller 2011, and others).

The large perinuclear  $\beta$  protein aggregates in the cytoplasm were co-stained by the antibodies against nuclear pore proteins. Thus, FG-repeat proteins that usually reside at the nuclear pores were recruited into the cytoplasmic  $\beta$  protein aggregates. At the same time, the fluorescence intensity around the nuclear envelope decreased, indicating a real local loss of NPC proteins. The shape of the nucleus was often irregular, and the chromatin structure appeared rather disturbed (inhomogeneous, speckled DAPI staining).  $\beta$  proteins aggregates were not found at the nuclear pores, where they likewise could interact with FG-repeat proteins (e.g. due to their similar polar-hydrophobic side-chain pattern) or become stuck during transport in or out of the nucleus.

Strikingly, also the human disease related proteins distorted NPCs, especially Htt96Q and TDP-F4 (see also Liu 2015). NPC protein aggregates appeared in the cytoplasm often separated from the transgenic proteins (in contrast to the coaggregation with cytoplasmic  $\beta$  proteins). Again, the fluorescence intensity around the nuclear envelope decreased in cells expressing cytoplasmic, disease-associated proteins.

Contrary to proteins aggregating in the cytoplasm,  $\beta$  proteins directed to the nucleus did neither interfere with NPC structures, nor disturb the distribution of nuclear DNA (DAPI staining). Cellular and nuclear morphology were well preserved. The DNA was distributed homogeneously within the nuclear matrix (surrounding nucleoli and  $\beta$  protein aggregates), apparently highly similar to wildtype cells. Low toxicity was accompanied by a healthy morphology in absence of any NPC protein coaggregation.

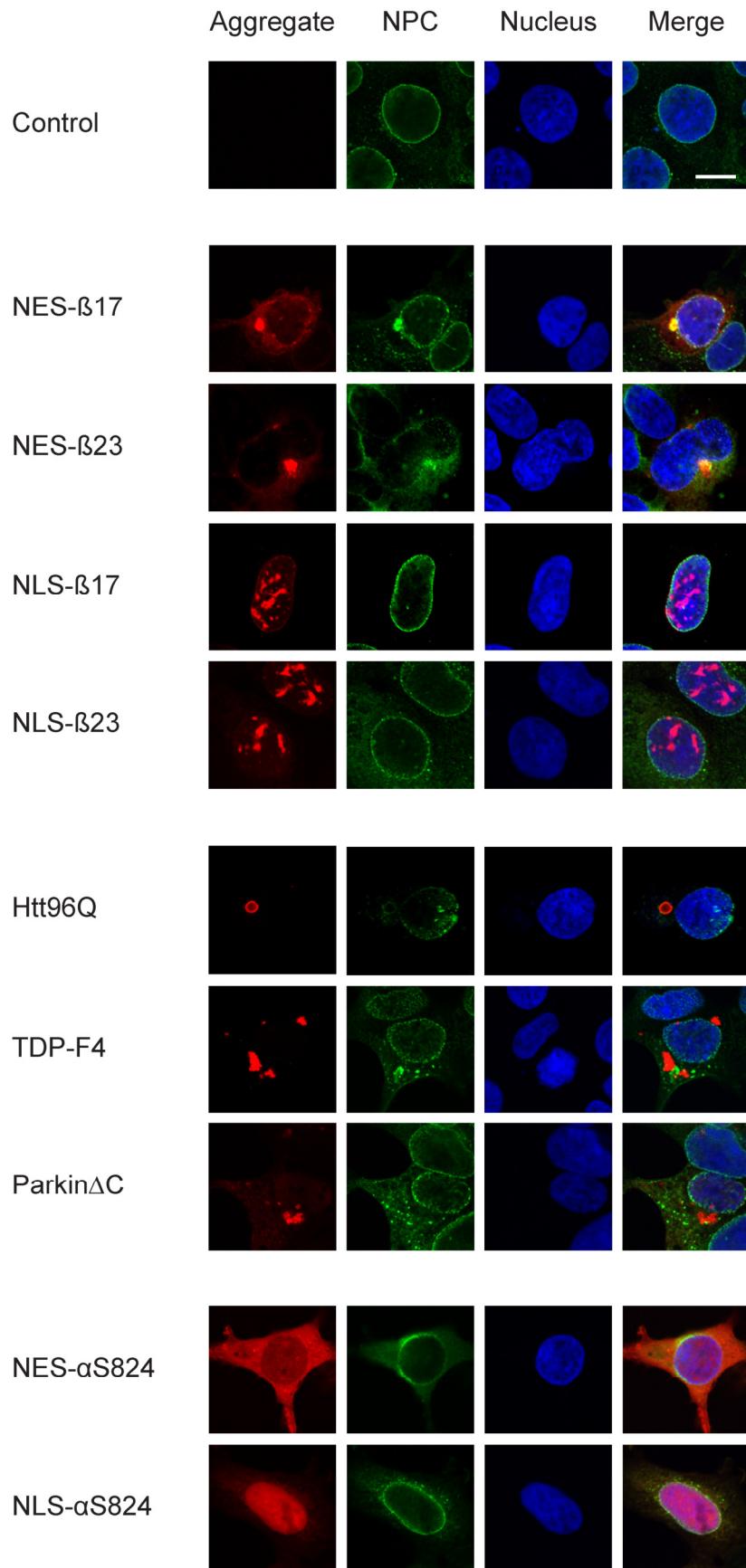


**Figure 54 | HEK293T cells expressing  $\beta$  proteins or  $\alpha$ S824 targeted to cytoplasm or nucleus, Htt96Q, TDP-F4, or Parkin $\Delta$ C (red) were immunolabeled with antibodies recognizing FG-repeat proteins of the NPC (green) 24 h after transfection. In control cells transfected with empty vectors, the signal of the nuclear pore proteins encircles the nuclear envelope, indicating the border between cytoplasm and nucleus. DAPI binds nuclear DNA and stains the nuclear matrix, surrounding the protein-dense nucleoli (blue). Cells transiently transfected with  $\beta$  proteins targeted to the cytoplasm (NES) formed  $\beta$  protein aggregates outside of the nucleus. Perinuclear aggregates occasionally appeared to penetrate the nuclear envelope from the cytoplasmic side, but remained cytoplasmic. Nuclear pore proteins became recruited into cytoplasmic  $\beta$  protein aggregates. Nuclei were often shaped irregularly, and the intranuclear distribution of DNA was rather inhomogeneous (DAPI). Cells expressing  $\beta$  proteins directed to the nucleus formed several larger aggregates within the nuclear matrix. Here, no distortion of the nuclear membrane was observed. Cells had a wildtype-like morphology. In cells expressing Htt96Q, TDP-F4, or Parkin $\Delta$ C, however, a fraction of nuclear pore proteins was found to sequester in cytoplasmic inclusions, distinct from the transgenic proteins. As in cells expressing cytoplasmic  $\beta$  proteins, the fluorescence around the nuclear envelope was regularly reduced, indicating a loss of functional proteins at the nuclear pores. The soluble, distributed  $\alpha$ S824 did not cause any irregularities, neither in the cytoplasm, nor in the nucleus. Representative images of 3 independent experiments are shown. Scale bar length 10  $\mu$ M.**

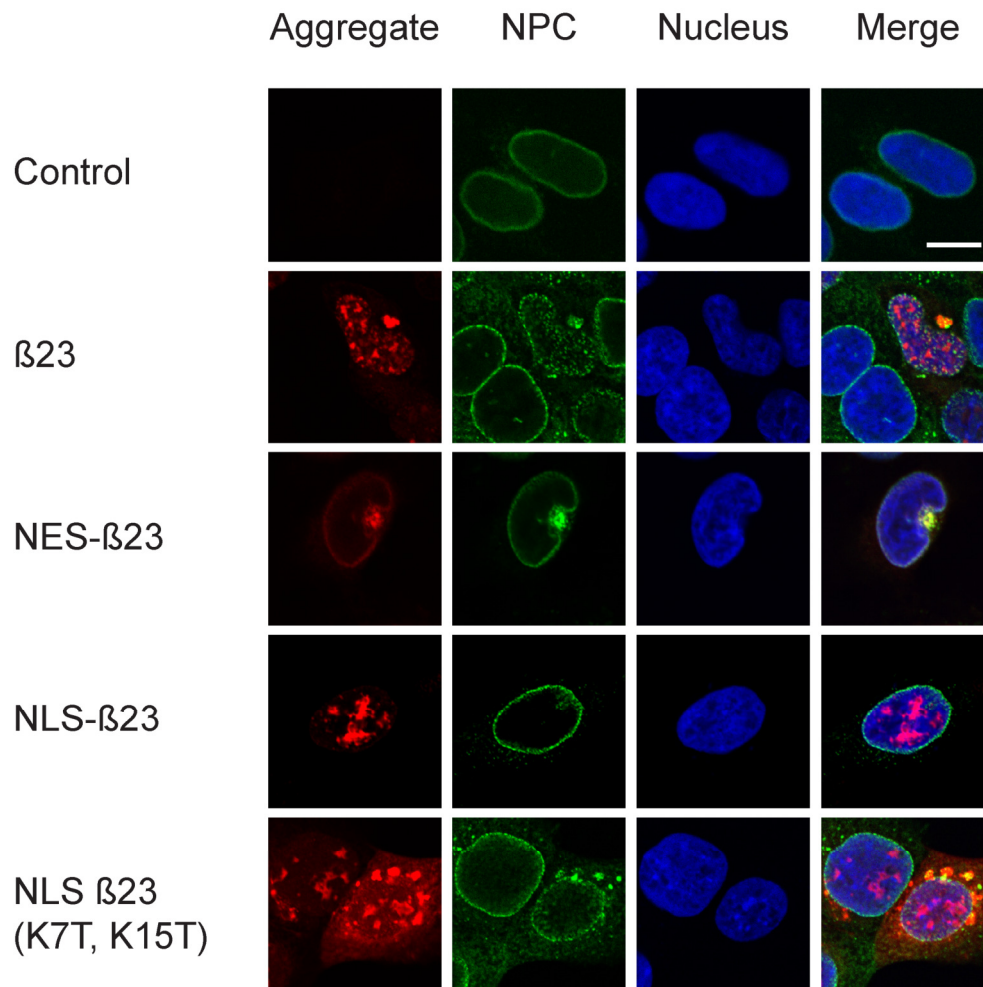


**Figure 55 | Distribution of  $\beta$ 23 proteins with different cellular targeting sequences in HEK293T cells 24 h after transfection.** Non-targeted  $\beta$ 23 proteins form aggregates in cytoplasm and nucleus.  $\beta$ 23 can also be specifically directed to the cytoplasm by a nuclear export signal (NES), or to the nucleus by a nuclear localization sequence (NLS). A mutation of a single lysine residue in the (2 repeats long) NLS to threonine rendered the nuclear targeting of the  $\beta$  proteins inefficient, keeping the rest of the positively charged NLS unchanged. The mutation resulted in a distribution of NLS- $\beta$ 23(K7T, K15T) aggregates over cytoplasm and nucleus again. Representative images of 3 independent experiments are shown. Scale bar length 10  $\mu$ M.

Cells transfected with non-targeted, c-Myc tagged  $\beta$  proteins showed all detrimental features described for cells expressing  $\beta$  proteins directed to the cytoplasm, and they caused a similar toxicity (MTT assay). Apparently,  $\beta$  proteins in the cytoplasm exhibited strong dominant effects over nuclear  $\beta$  proteins on cells and their phenotypes.

In cells expressing NLS- $\beta$ 23(K7T, K15T) with inefficient nuclear targeting, nuclear pore proteins were only trapped into the cytoplasmic aggregates, but were absent from the nuclear ones. This observation demonstrates that it very unlikely were solely the compartmental targeting signals, but rather the cellular localization of the  $\beta$  proteins that mainly caused the distinct phenomena (toxicity, coaggregation, and cellular morphology).

The observed interactions with nuclear pore proteins and the distorted nuclear envelopes made us interested in the efficiency of nucleo-cytoplasmic transport processes in cells harboring protein aggregates in these two compartments. Furthermore, compartment-specific differences regarding cellular interactions of such misfolding structures and their handling by the compartment specific proteostasis machinery may explain our observations.

## Nuclear $\beta$ proteins associate with nucleoli and scatter around the nuclear envelope

For cells expressing  $\beta$  proteins directed to the nucleus, the morphology of the nucleus and of the nuclear envelope were highly preserved in comparison to wildtype cells. Immunofluorescence microscopy brought no indications for any interactions between the nuclear  $\beta$  proteins and chromatin (DNA, DAPI staining). Nuclear  $\beta$  proteins formed several distinct bodies in the nuclear matrix, from which macro-fibrillary structures appeared to grow out. In addition, very small particles encompassed the nuclear envelope. As the nuclear  $\beta$  proteins seemed to be separated from the DNA in the nuclear matrix, we wondered whether they were localizing at the nucleoli.

Nucleoli are sub-compartments in the nuclear matrix forming around ribosomal gene clusters. They are responsible for transcription and local pre-assembly of ribosomal subunits and other ribonucleoprotein particles. Beyond that, nucleoli are involved in cell-cycle progression and in many forms of stress response. Additional functions are still being uncovered (Boisvert 2007, Boulon 2010).

NPM-1 (nucleophosmin, or B23) is a nucleolar protein involved in diverse cellular processes, such as ribosome biogenesis and tumor suppressor regulation (through p53 and ARF). NPM-1 interacts with rRNAs and directs the nuclear export of the 40S and 60S subunits (Maggi 2008). NPM-1 contains several NESs and NLSs and is capable of shuttling between cytoplasm and nucleus. *In vitro*, NPM-1 was shown to prevent the aggregation of several denatured proteins (Szebeni 1999). The phosphoprotein of 294 amino acids is charged highly negatively (net charge of -24, which is increased by multiple posttranslational phosphorylations). The C-terminal half of NPM-1 contains mainly low-complexity regions predicted to be disordered (by IUPRed; Meszaros 2009).

HEK293T cells expressing nuclear  $\beta$  proteins for 24 h were co-labeled for NPM-1 as a nucleolar marker. NPM-1 closely associated to the  $\beta$  protein inclusions in the nuclear matrix. Thereby, NPM-1 mainly surrounded the nuclear  $\beta$  protein aggregates, rather than to overlap with them completely. Moreover, the nucleolar (but not the nuclear) morphology appeared slightly disturbed in presence of nuclear  $\beta$  proteins. The typical smooth and spherical bodies observed in wildtype cells were transformed into rather irregular, angular structures.

NPM-1 furthermore colocalized to the small  $\beta$  protein aggregates locating at the inner side of the nuclear membrane, demonstrating an interaction beyond the nucleoli itself. However, these small inclusions were too small to distinguish between a direct overlapping and a neighboring association of the  $\beta$  proteins and NPM-1, so that mutual interferences could be of a different nature here.

Observations of nucleoli and the nuclear envelope demonstrated that the nuclear  $\beta$  proteins do interact with cellular structures, and the  $\beta$  proteins are able to disturb the wildtype morphology in the nucleus (nucleoli). Whether the packing of  $\beta$  proteins into nucleolar structures has primarily protective functions, such as shielding the aggregates from more harmful cellular interactions, or whether this nucleolar clustering is accompanied by detrimental effects, such as on nucleolar dysfunctions, remains to be elucidated.

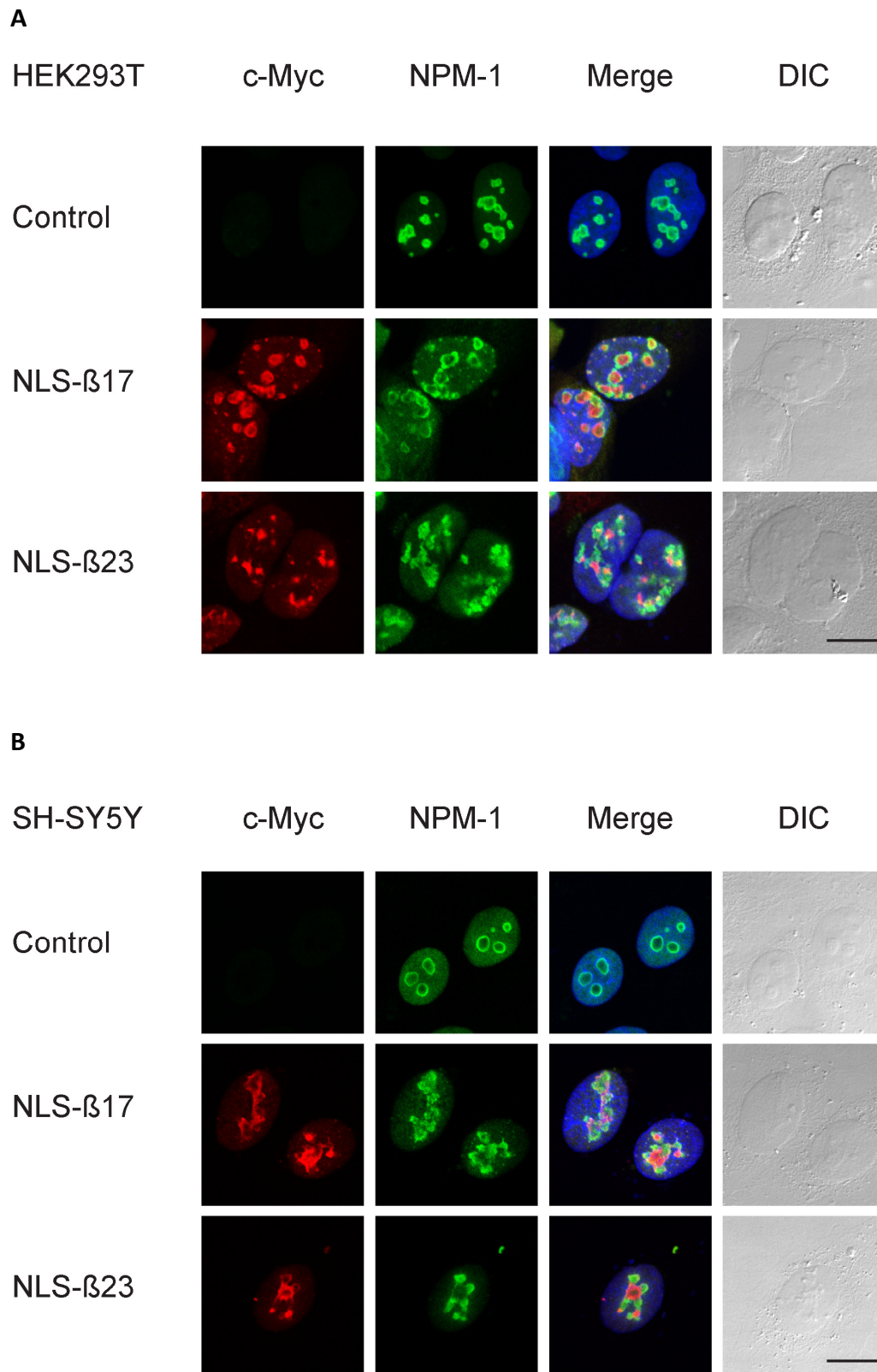


**Figure 56 | Nucleolar association of  $\beta$  protein aggregates in the nucleus, as visualized by Nucleophosmin staining (NPM-1).** HEK293T (**A**) or SH-SY5Y cells (**B**) were transfected with  $\beta$  proteins (red) and, after 24 h, stained for endogenous Nucleophosmin (by antibodies, green), a nucleolar protein and chaperon. Nuclear DNA was stained by DAPI (blue). Nucleophosmin surrounded the nucleolar structures, which, upon expression of nuclear  $\beta$  proteins, seemed to break up and cluster the  $\beta$  protein aggregates at their center. Representative images of 3 independent experiments are shown. Scale bar length 10  $\mu$ M.

However, no decline of protein biosynthesis could be observed (see below), as it might be expected in case of a dysfunctional nucleolar ribosome biogenesis.

Although nuclear DNAs and RNAs are strongly covered in proteins, which additionally are often rich in extended disordered regions, interactions with the nuclear  $\beta$  proteins were not apparent by confocal microscopy. Detrimental interactions therefore seem to be markedly limited in the nucleus, especially in comparison to the influence of cytoplasmic  $\beta$  proteins on nuclear morphology.

### **Nuclear $\beta$ protein aggregates remain intact during cell division**

In higher eukaryotic cells, the nuclear envelope almost completely disassembles during initial cell division (“open mitosis”; Güttinger 2009). Likewise, nucleolar structures fall apart. While certain nucleolar factors become distributed over the surrounding cytoplasm (such as phosphorylated NPM-1), a distinct machinery remains in an inactivated nucleolar complex (transcription and RNP processing factors), which is distributed among the separating cells for new nucleolar assembly (Hernandez-Verdun 2011).

Most cerebral neurons are highly differentiated and do not enter into mitosis any more. Neuronal progenitors and other somatic cells however may divide in the presence of nucleolar associated protein aggregates. Thereby, either the aggregates may stay associated with nucleolar core particles that remain localized within the nuclei, or the aggregates may distribute over the whole cell in form of aggregated or dissociated structures. Moreover, they may keep their nuclear properties (regarding structure, reactivity, and toxicity), or they may transform into aggregates with cytoplasmic or mixed properties with harmful consequences for the cells.

To elucidate the fate of nucleolar aggregates during mitosis, we searched for mitotic cells that were expressing  $\beta$  proteins. Mitotic cells were identified by their condensation and appearance of chromosomes (DAPI staining), as they are characteristic for the different states during nuclear and cell division. Thereby it became obvious that the nucleolar localized  $\beta$  protein aggregates remained at the center of the cells in close proximity to the condensed chromosomes during the whole process. At later states of mitosis, the “nuclear aggregates” were segregated with the chromatids, whereby they were distributed between the two separated cells. Also here they remained nuclear, after the nuclear envelope reassembled.

In control cells, the nucleolar NPM-1 was distributed over the whole cytoplasm and excluded from the chromosomal DNA. In contrast to that, a fraction of NPM-1 remained colocalizing with the  $\beta$  protein aggregates and most likely other nucleolar factors. Residual nucleolar particles are actively separated during chromosomal segregation and responsible for an equal distribution among the separating cells (Hernandez-Verdun 2011). In some cells, low amounts of residual “non-aggregated” NLS- $\beta$ 17 was distributed over the cell during mitosis. Similar to NPM-1 and other nuclear proteins, it can most likely be reimported into the nucleus, once the nuclear envelope is reassembled. However, this does not exclude that damage may be caused by distributed oligomers or aggregates that may be seeded in the cytoplasm during cell division. Overall, the nucleolar aggregates remained secluded during mitosis.

Mitotic-like cells harboring cytoplasmic aggregates of NES- $\beta$ 17 were extremely rare. The high toxicity of cytoplasmic  $\beta$  proteins prevented further cell divisions. Missing growth was also observed for the untargeted  $\beta$  proteins (see Olzscha 2010).

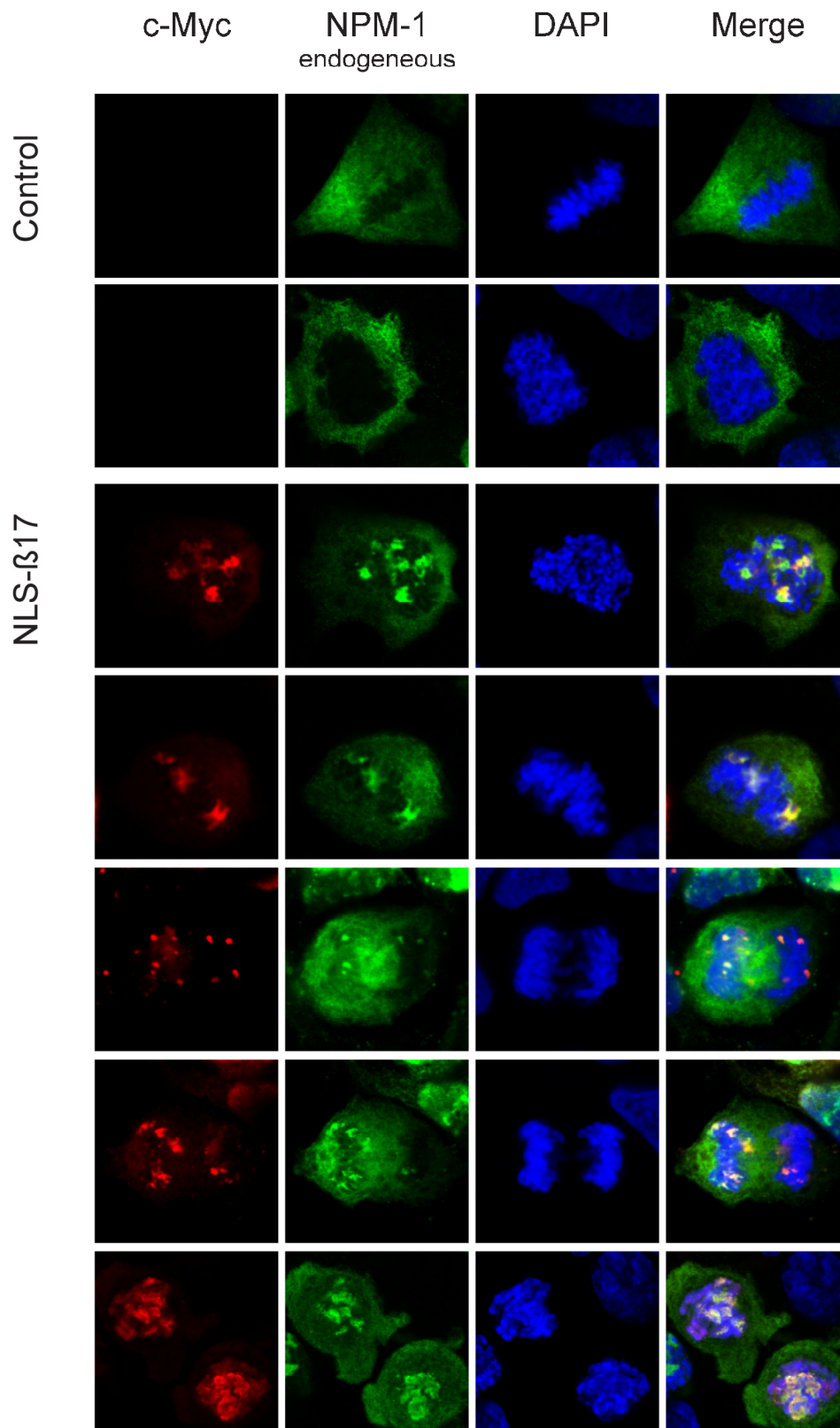


**Figure 57 | Nuclear  $\beta$  protein aggregates remain nuclear during and after cell division.** HEK293T cells transfected with NLS- $\beta$ 17 at different states of mitosis and cytokinesis demonstrated a continuance of nucleolar deposition. The aggregates were distributed between the two newly forming cells. A fraction of the cellular NPM-1 remained bound to the aggregates during the whole process, while residual NPM-1 was distributed over the cytoplasm, similar to control cells. Representative images of 3 independent experiments are shown.

## Increased solubility of $\beta$ proteins in the cytoplasm

Labeling the  $\beta$  proteins in HEK293T or SH-SY5Y cells with fluorescent antibodies, a visual analysis of fluorescence microscopy images already suggested a stronger distribution of lower-molecular-weight species over the cytoplasm. Contrary in the nucleus,  $\beta$  protein aggregates formed very compact nucleolar structures, fairly confined from their surroundings.

The solubility of  $\beta$  protein aggregates in cytoplasm and nucleus was analyzed by sedimentation. To promote an efficient lysis of cell membranes and nuclear envelopes, cells were lysed in phosphate buffer supplemented with 1% Triton X-100, 420 mM NaCl, 10 mM MgCl<sub>2</sub>, protease inhibitors, and benzonase (nuclease). 24 h after transfection, HEK293T cells were lysed at 4 °C, and aggregates were sedimented at 20,000 x g for 5 min. The supernatant was separated, the pellet was resuspended in an equal amount of lysis buffer, and both samples were denatured in SDS loading buffer. Beforehand, a fraction was kept without centrifugation (total lysate). Samples were run on SDS PAGE and immunoblotted against c-Myc, GAPDH, and nuclear Histone-H3.

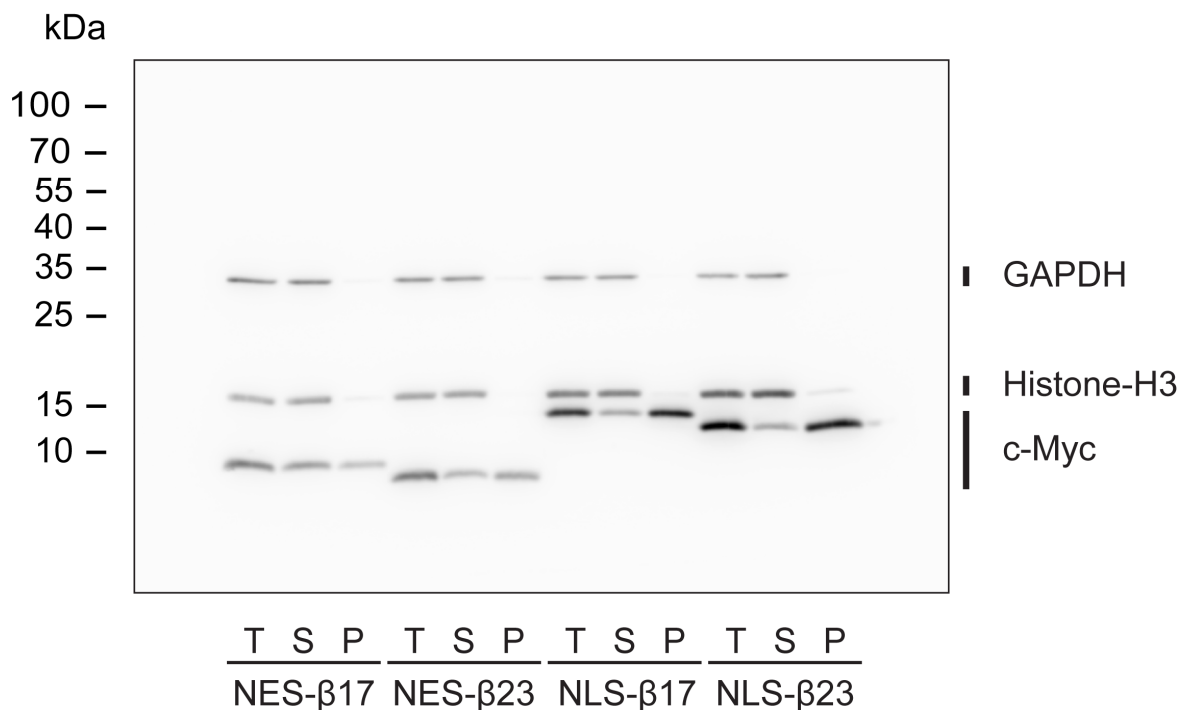


**Figure 58 | Immunoblot of a solubility analysis of  $\beta$  proteins directed to cytoplasm and nucleus.** HEK293T cells transfected with  $\beta$  proteins were lysed after 24 h, and insoluble aggregates were sedimented by centrifugation (20,000 x g for 10 min). Total (T), supernatant (S), and pellet (P) fractions were separated by SDS-PAGE and blotted on PVDF membranes. These were immunostained to quantify  $\beta$  protein levels (c-Myc signals). Histone-H3 levels demonstrated an efficient lysis of the nuclear envelope and, together with GAPDH levels, an equal loading of lysates. A representative immunoblot of more than 3 experiments is shown.



All three nuclear  $\beta$  proteins were efficiently sedimented to a degree of 65-78%, corresponding to soluble fractions of 22-35%, demonstrating low solubility and high compactness. In contrast, a significantly higher fraction of cytoplasmic  $\beta$  proteins were found not to sediment at 20,000 x g, especially in case of  $\beta 4$  and  $\beta 17$  (soluble fractions of 47% and 63%). As indicated by immunofluorescence microscopy, cytoplasmic  $\beta$  proteins seem to form increased amounts of lower-molecular-weight assemblies, such as oligomers and smaller aggregates, which distribute over the whole cytoplasm. Similarly,  $\beta 23$  showed a significant higher solubility in the cytoplasm, although the difference was less pronounced (45% in cytoplasm versus 35% in nucleus).

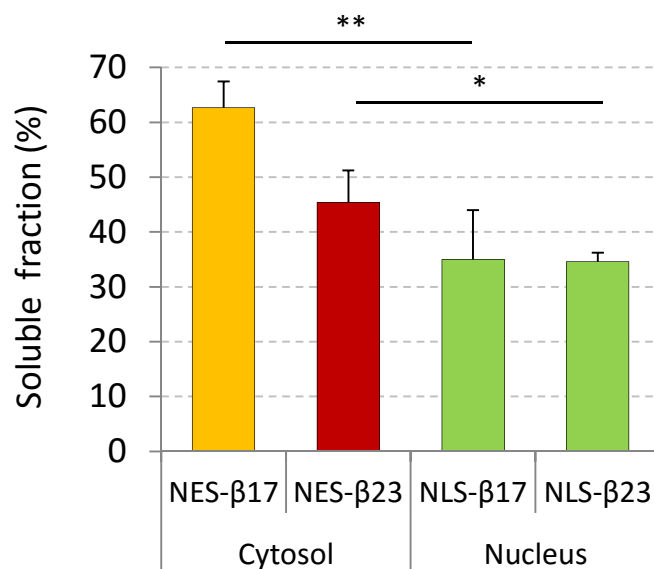


**Figure 59 | Quantification of soluble fractions of cell lysates with  $\beta$  proteins in cytoplasm and nucleus.** Averages and standard deviations from 3 independent experiments are shown. Significance levels as determined by unpaired Student's t-test.

Compared to physiological conditions, an increased amount of sodium chloride (420 mM NaCl) in the lysis buffer was necessary to enable an efficient nuclear lysis, which does not occur in PBS with 1% TritonX-100 and 137 mM NaCl (standard concentration). However, the higher salt content might influence the stability of the  $\beta$  protein aggregates, especially by weakening protein-protein interactions. This may increase the soluble fractions and thereby diminish the real differences. Nevertheless, the analysis allows concluding about the relative soluble material within the two compartments.

## Oligomers of intermediate-molecular-weight in the cytoplasm

Lysates of HEK293T cells expressing NES- $\beta$ 17 or NLS- $\beta$ 17 for 24 h were subjected to size-exclusion chromatography to analyze the presence and size-distribution of oligomeric  $\beta$  protein species in the two compartments.

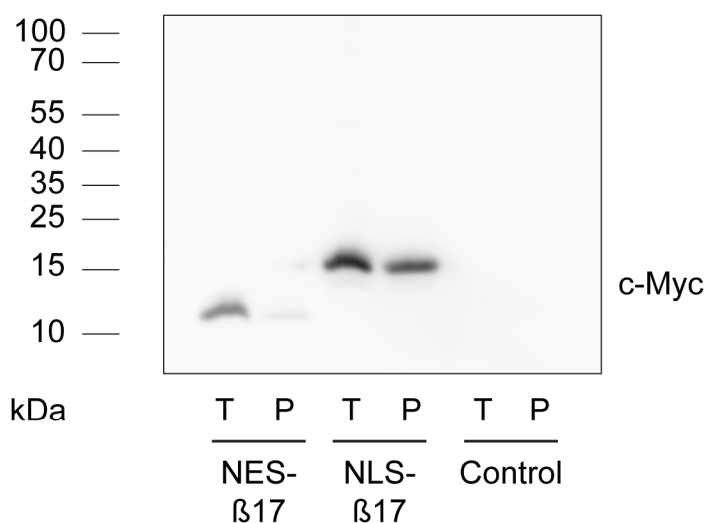
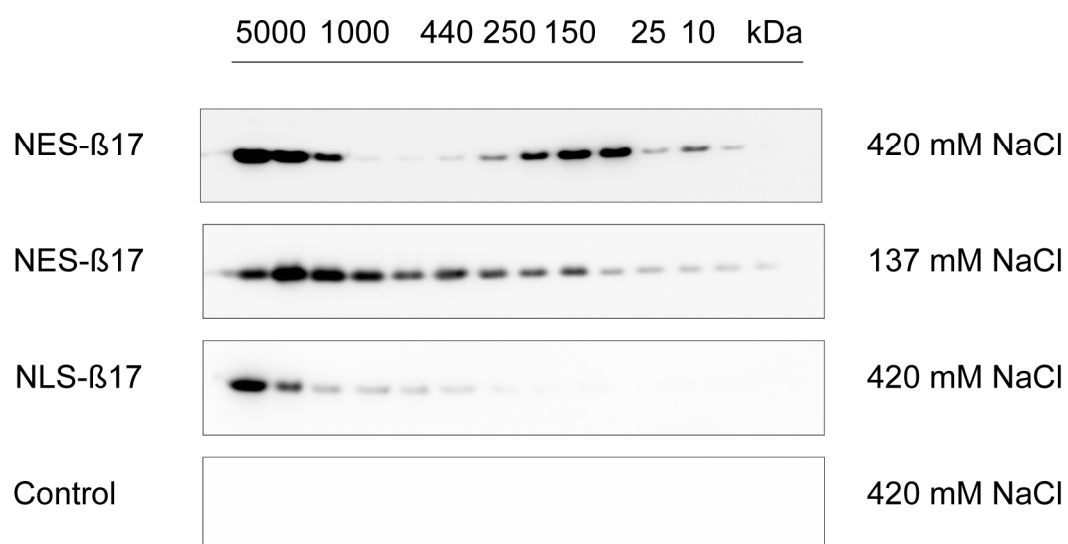
To do so, HEK293T cells were lysed in a nuclear extraction buffer (PBS including 420 mM NaCl, 1% TritonX-100, Complete Protease Inhibitor Cocktail (Roche), and benzonase). This procedure ensured nuclear lysis and digestion of cellular DNA (short vortexing followed by slow shaking at 4 °C for 20 min). Lysates were centrifuged at 2,000 x g to remove large insoluble debris. The supernatants were applied to a Superose 6 size exclusion column (30 mL column volume) in PBS at 4 °C. 14 fractions over a size range from 5 MDa to 5 kDa were collected. Fractions, pellets, and supernatants were analyzed for their  $\beta$  protein content.

While the cytoplasmic  $\beta$  proteins of NES- $\beta$ 17 could mainly be applied to the Superose 6 column, a significant part of the nuclear NLS- $\beta$ 17 was already removed by centrifugation at 2,000 x g. The solubility analysis (above) already indicated a greater insoluble content for the nuclear aggregates. As expected, condensed accumulations of  $\beta$  proteins associated to nucleoli sedimented at such centrifugation speeds.

Running a size exclusion chromatography, both, the cytoplasmic and nuclear  $\beta$  proteins started eluting at maximal particle sizes of several megadaltons (up to 5 MDa). While the signal of the nuclear  $\beta$  proteins quickly declined in fractions below megadalton sizes, oligomers formed by the cytoplasmic  $\beta$  proteins appeared in the range of 200-50 kDa. A small signal was observed around the potentially monomeric form of the  $\beta$  proteins (~10 kDa). Similar to the solubility analysis by centrifugation at 20,000 x g, this results suggested that the vast majority of the  $\beta$  proteins aggregate into very high-molecular-weight forms in the nucleus.

A hyperphysiological salt concentration was only necessary for nuclear lysis, but not for sole lysis of the cell membrane surrounding the cytoplasm. Therefore, a sample of NES- $\beta$ 17 expressing cells was subjected to rather physiological salt conditions in the lysis solution (137 mM NaCl) followed by size exclusion. The NES- $\beta$ 17 signal now spread over an even larger size range from above 1 MDa to 100 kDa. Apparently, the increased ionic strength caused a partial disintegration of oligomeric structures of several 100 kDa, suggesting that under more physiological conditions a heterogeneous population of oligomeric species formed in the cytoplasm. Thus with a size of around 10 kDa per monomer, cytoplasmic oligomers may include variable assemblies comprising 10-100  $\beta$  protein molecules. Assemblies of the purified  $\beta$  proteins as observed by electron microscopy may correspond to such size ranges (spherical and fibrillary oligomers of 10-100 molecules).

However, the size exclusion chromatography was performed from *in vivo* lysates, so that the  $\beta$  protein oligomers presumable bound various cellular factors of different sizes. As long as they remain bound, these interactors contribute to the overall mass and running behavior observed here. Thus, a range of small- to intermediate-size oligomers appeared *in vivo*. Since they were formed by unspecific, non-natural interactions, such oligomers easily fell apart at higher ionic strength.

**A****B**

**Figure 60 | Size exclusion chromatography of HEK293T lysates. (A)** Centrifugation of the lysates at 2,000 x g removed the cellular debris and a substantial fraction of the nuclear aggregates, which were too large to be analyzed on a Superpose 6 column. The cytoplasmic aggregates remained almost completely in the supernatant, which was subjected directly to size exclusion chromatography. **(B)** Analysis of the fractions revealed huge megadalton-sized structures formed by the  $\beta$  proteins in cytoplasm and nucleus. These large aggregates were accompanied by molecular assemblies of several hundred kilodaltons of size in the cytoplasm. They may also contain cellular interactors of the  $\beta$  proteins contributing to their final mass. Assemblies below 1 MDa were almost absent in the nucleus. Representative anti-c-Myc immunoblots from 2-3 independent experiments.

## Major aggregates are stable and immobile in cytoplasm and nucleus (FRAP)

Fluorescence recovery after photo bleaching (FRAP) was applied to determine the structural dynamics of the major aggregates of cells transfected with NES- $\beta$ 17-EGFP or NLS- $\beta$ 17-EGFP. FRAP allows to bleach a region of interest (ROI) of a fluorescent protein within a living cell, and to follow the fluorescence recovery within that region over time. The faster the fluorescence recovers, the higher the mobility and the exchange of particles between a bleached region and its surrounding. The recovery depends on the size of the fluorescent particles, e.g. due to binding to cellular structures such as cytoskeleton, membranes, or nucleic acids, and on the aggregates internal dynamics (mobility of molecules within).

HEK293T cells expressing NES- $\beta$ 17-EGFP, NLS- $\beta$ 17-EGFP, or EGFP alone for 24 hours were subjected to FRAP measurements at 37 °C. A ROI was bleached by laser light at 405 and 480 nm for ~1 sec, and fluorescence recovery was followed over 120 sec.

The bleached regions only marginally recovered in fluorescence over almost 2 min, and the bleached spots could still be identified over 1 h after bleaching (not shown). Both, the aggregates of cytoplasmic and nuclear  $\beta$  proteins fused to EGFP were highly immobile and did not exchange with surrounding fluorescent  $\beta$  protein molecules. A difference in mobility between the two compartments could not be observed. Soluble EGFP, in contrast, was highly mobile and immediately returned to equilibrium.

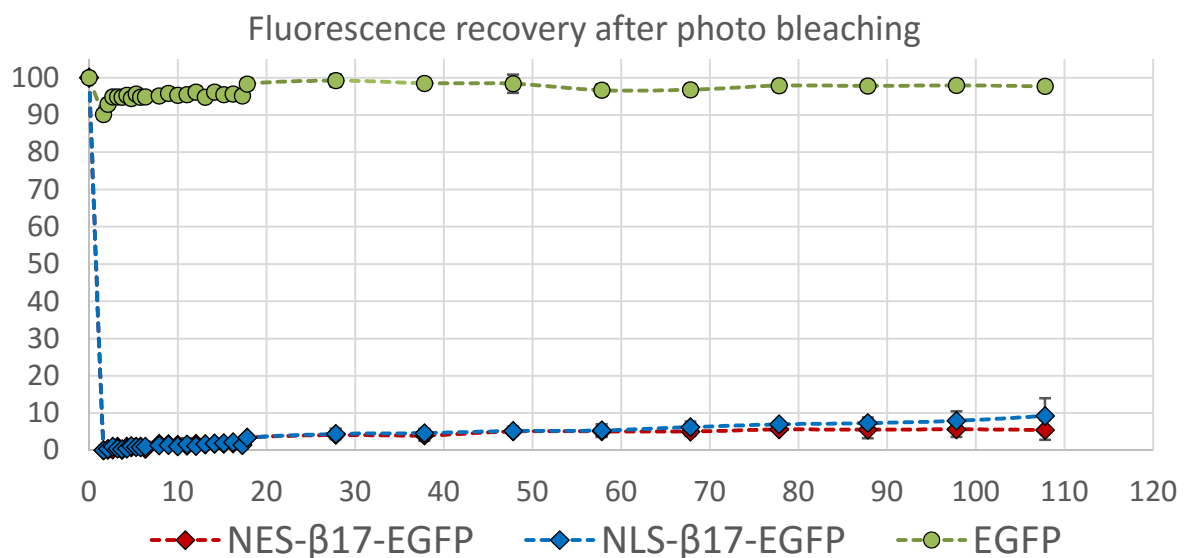


**Figure 61 | The major aggregates in cytoplasm and nucleus are highly immobile and do not exchange molecules within their structures**, as they show no fluorescence recovery after bleaching a small spot within their boundaries. Recovery curves are averages of 3 independent experiments; standard deviations are shown.

However, a difference in mobility may be found in the rather distributed, oligomeric particles (see solubility analysis, size exclusion chromatography). However, as the  $\beta$  proteins-EGFP fusions not fully represent the properties of the c-Myc tagged  $\beta$  proteins, the analyses were restricted here to the major inclusions forming in the two compartments. The  $\beta$  protein-EGFP fusions may display an altered solubility as they expressed at higher levels, formed extended aggregates with often rather amorphous-like morphology, and showed no NIAD-4 binding (see below).

## Structural differences of $\beta$ protein assemblies forming in cytoplasm or nucleus

Targeting  $\beta$  proteins to the cytoplasm or the nucleus resulted in striking differences regarding their toxicity and their structural properties. Distinct  $\beta$  protein conformations may also be differentially recognized by fluorescent amyloid sensors *in vivo*. NIAD-4 is a fluorescent sensor developed for specifically binding to A $\beta$  fibrils and other amyloid structures (Nesterov 2005, Brandenburg 2012). Its chemical structure (aromatic rings, aliphatic hydrocarbons) and its ability to cross the blood-brain barrier suggests that hydrophobic interactions may also influence binding and fluorescence properties of NIAD-4, beyond its general selectivity for amyloid structures (see *in vitro* binding of NIAD-4 and ANS, Figure 38 and following).

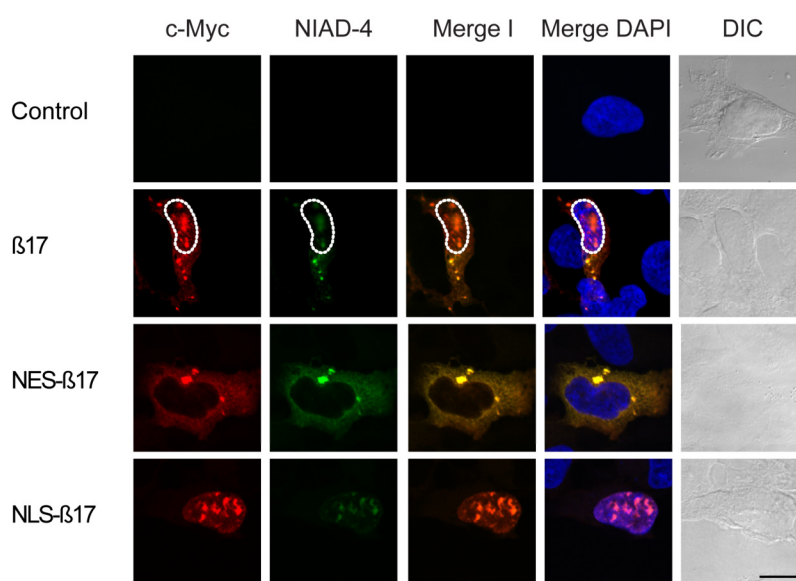


**Figure 62 | Structural differences of  $\beta$  protein aggregates in cytoplasm and nucleus.** The  $\beta$  proteins were expressed in HEK293T cells and stained by anti-c-Myc-antibodies (red) and the amyloid sensor NIAD-4 (green). A white dashed line labels the nuclear envelope in case of  $\beta$ 17. Merge I is a superposition of anti-c-Myc antibody and NIAD-4 staining; here, red indicates a low NIAD-4 fluorescence, but high c-Myc signal, while yellow indicates high antibody and high NIAD-4 staining. In the cytoplasm, anti-c-Myc and NIAD-4 staining were distributed and localized to spherical inclusions. The  $\beta$  proteins in the nucleus formed irregular, compact structures. In “Merge DAPI”, nuclear DNA staining was included (blue). Representative images of 3 independent experiments. Scale bar length 10  $\mu$ M.

Probing structural properties of the  $\beta$  proteins in cytoplasm and nucleus with NIAD-4, the nuclear aggregates bound the amyloid sensor only weakly, compared to the large juxtannuclear inclusions in the cytoplasm. This differential binding of NIAD-4 suggests conformational alterations or a different molecular shielding of the  $\beta$  proteins in the two compartments. Differences may originate from a different degree of order of the  $\beta$ -sheets within the amyloid core, or different amounts of hydrophobicity being exposed to the surface of the fibrils. The surface of cytoplasmic  $\beta$  proteins amyloids presented more structurally complementary “epitopes” for NIAD-4 binding. Additionally, cytoplasmic aggregates might expose a higher surface hydrophobicity. Molecular shielding through nuclear factors such as NPM-1 (nucleophosmin, see above) might further influence the oligomerization and aggregation process, or cover the NIAD-4 binding sites of the nucleolar amyloids. Such a molecular shielding might prevent many other cellular interactions, too.

NIAD-4 staining, together with the size and solubility analyses, indicates significant structural differences between oligomers and aggregates forming in cytoplasm or nucleus.

## Cytoplasmic $\beta$ proteins suppress induction of the cytosolic stress response – nuclear $\beta$ proteins (partially) induce a response

$\beta$  proteins (without cellular targeting sequences) were shown to inhibit cellular stress response pathways (Olzscha 2011) that react upon misfolding, chemical, or heat stress. A functional heat shock response reacts e.g. with increasing cellular chaperone levels, such as Hsp27, Hsp70, or Hsp90.

One reason for a decreased cytotoxicity of nuclear  $\beta$  proteins might be an improved cellular response towards internal or external stresses. Therefore, a luciferase reporter protein under the control of the Hsp70 promoter was coexpressed in HEK293T cells with the compartmentally targeted  $\beta$  proteins. As readout of Hsp70 promoter activation, the luciferase activity was detected and compared between cells expressing different  $\beta$  proteins.

Without external stress, cells expressing non-targeted or cytoplasmic  $\beta$  proteins showed an activity similar to wildtype cells (blue bars, Figure 63). Quite surprisingly, expression of  $\beta$  proteins targeted to the nucleus caused an increase of luciferase activity, even in the absence of additional stress (such as heat shock). This Hsp70 promoter induction of the  $\beta$  proteins was inversely correlated to their toxicity: NLS- $\beta$ 4 caused a 5-fold and NLS- $\beta$ 17 a 2.5-fold induction of luciferase activity, compared to wildtype cells.

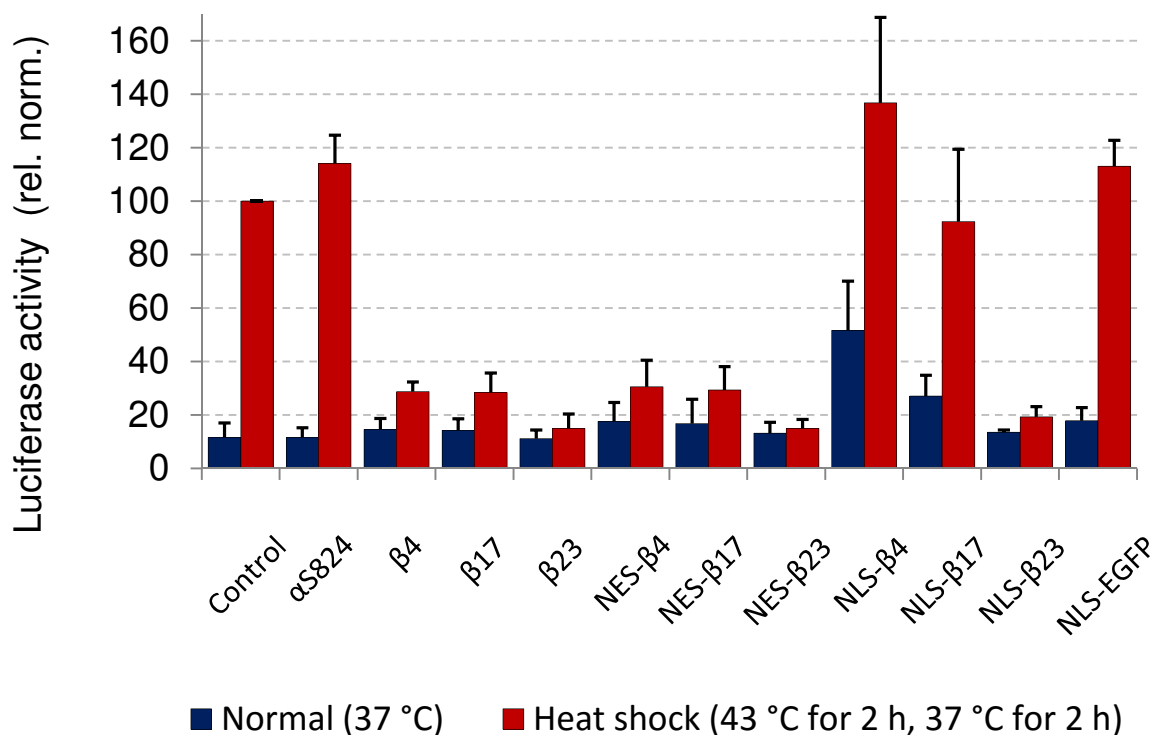


**Figure 63 | Induction of the Hsp70 promoter controlling luciferase expression in HEK293T cells with or without additional heat shock. Cells were cotransfected with  $\beta$  proteins,  $\alpha$ S824, nuclear EGFP, or empty vectors. Averages and standard deviations from 3 independent experiments are shown. Values of individual experiments were normalized to control cells after heat shock, which were set to 100.**

Cells were now tested for their stress reaction upon heat shock at 43 °C for 2 h, followed by a recovery period at 37 °C for 2 h. Afterwards, the luciferase activity was determined. The heat stress led to a strong (10-fold) induction of the Hsp70 promoter in control cells, as in cells expressing  $\alpha$ S824. Luciferase levels of cells expressing non-targeted or cytoplasmic  $\beta$  proteins only rose marginally, indicating a defective stress response in these cells.

Cells with nuclear  $\beta$  proteins, in contrast, showed a clear induction of the Hsp70 promoter. Luciferase activity was increased more than 10-fold in case of  $\beta$ 4 and 8-fold in case of  $\beta$ 17, compared to untreated wildtype cells. Solely cells expressing NLS- $\beta$ 23 did respond neither to protein aggregation, nor to heat shock.

This observation may have different origins, since  $\beta$ 23 is in general the most toxic sequence among the  $\beta$  proteins. Also in the nucleus,  $\beta$ 23 caused a distinct toxicity, even if it was significantly lower than in the cytoplasm (MTT viability of 68% for NLS- $\beta$ 23 vs. 39% for NES- $\beta$ 23). Malfunctions of cellular responsiveness towards stress might either arise due to a disturbance of typical nuclear processes (transcription factor signaling, transcription, RNA processing) specifically by NLS- $\beta$ 23, or of luciferase synthesis and folding. A quantification of luciferase mRNA and protein levels might be helpful here. Otherwise, minor levels of NLS- $\beta$ 23 mislocalized to the cytoplasm might already be enough to cause a stress response deactivation. As we observed later, neither the general protein synthesis, nor the cytoplasmic-nuclear transport of proteins and RNA were significantly inhibited by NLS- $\beta$ 23. Thus, the inhibition of the Hsp70 promoter induction appears to represent a specific defect caused by  $\beta$ 23 in the nucleus.

In summary,  $\beta$  proteins in cytoplasm caused a strong suppression of the cellular response to misfolding or heat shock. On the contrary, cells expressing the less toxic nuclear  $\beta$  proteins were capable of sensing misfolding and heat shock stresses. However, also nuclear  $\beta$  proteins partially suppressed the stress response induction. Especially NLS- $\beta$ 23 did not show any reaction to the Hsp70 promoter controlled luciferase.

## Interactions between proteostasis sensors and $\beta$ proteins in the cytoplasm, molecular exclusion in the nucleus

The  $\beta$  proteins and many other misfolded structures engage in a variety of aberrant cellular interactions (Olzscha 2011). It is still a major question, however, how many and which of those interactions are ultimately harmful for cells, putting their survival at risk.

Misfolded structures might directly interact with individual cellular proteins and deactivate them through recruitment into aggregates. However, misfolded structures might also promote further misfolding and aggregation through a disturbance of the protein folding homeostasis (proteostasis). An excessive occupancy of molecular chaperones might lower the cellular folding capacity, so that newly synthesized or structurally unstable proteins start to aggregate. Degradation pathways might become overloaded, disturbed, or confronted with non-degradable substrates. Misfolded structures may then accumulate and themselves take part in aberrant interactions. Reaching a certain threshold in the disturbance of cellular proteostasis might thus cause the final cellular collapse.

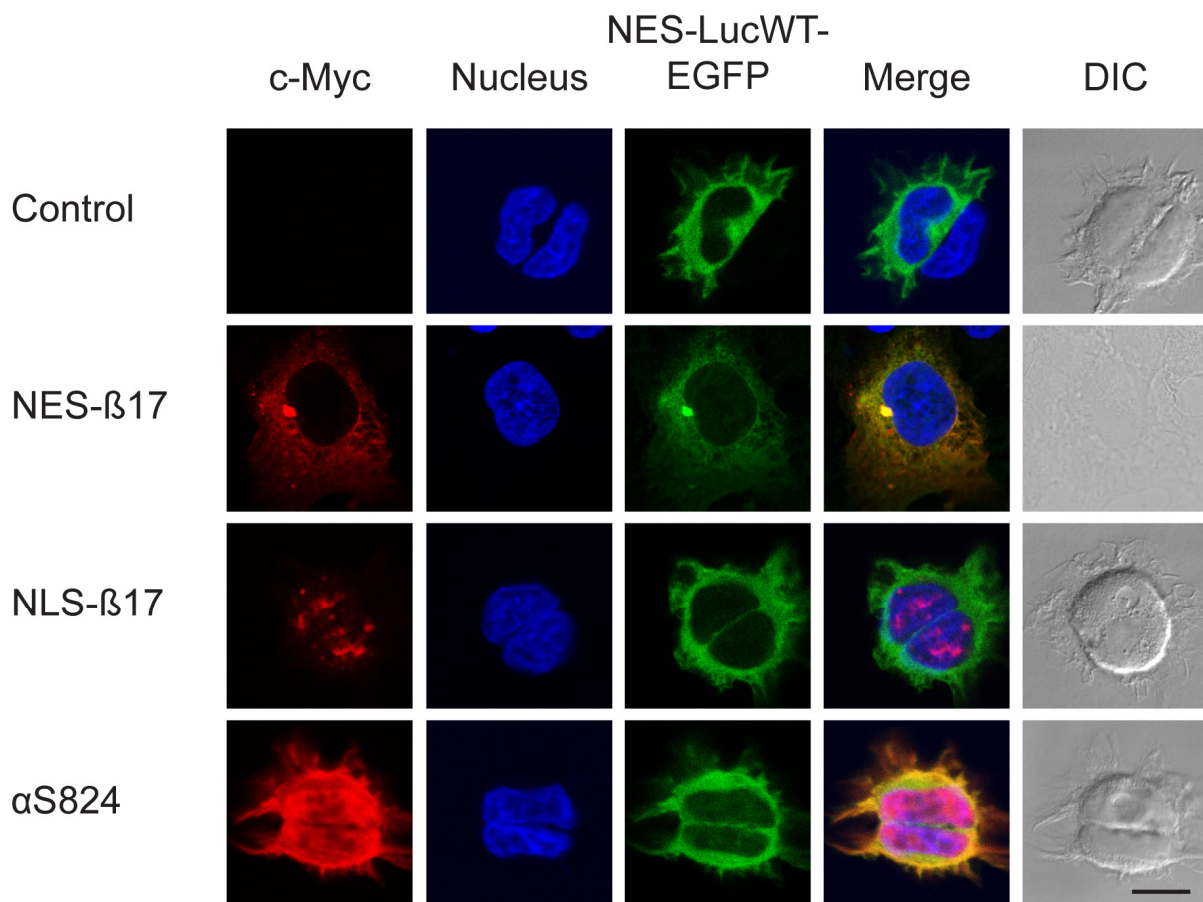


**Figure 64 | Cytoplasmic luciferase-EGFP proteostasis sensors coexpressed with  $\beta$  proteins targeted to cytoplasm or nucleus.** HEK293T cells were cotransfected with NES-LucWT-EGFP (green) and empty control vectors,  $\beta$  proteins, or  $\alpha$ S824. Cells were fixed 24 h after transfection and labeled with anti-c-Myc antibodies (red) and for nuclear DNA (DAPI, blue). Representative images of 3 independent experiments are shown. Scale bar length 10  $\mu$ M.



To evaluate compartment-specific attributes of proteostasis,  $\beta$  proteins were coexpressed with proteins designed for sensing proteostasis stress. Firefly luciferase, a protein strongly dependent on molecular chaperones for folding and refolding, was fused to EGFP (Rajat Gupta 2011). In addition, similar targeting sequences that directed the  $\beta$  proteins to cytoplasm and nucleus (NES, NLS, now without a c-Myc tag) were added. With these localized proteostasis sensors we intended to monitor compartmental proteostasis states as well as aberrant interactions in the presence of  $\beta$  proteins.

Wildtype (WT) and a destabilized double mutant (DM) of luciferase-EGFP (Rajat Gupta 2011) were directed to cytoplasm or nucleus (NES/NLS-LucWT/DM-EGFP). The sensor proteins were in general soluble and homogeneously distributed over the respective compartment. Expressed at higher levels (transfection of the 5-fold amount of DNA), the double mutants started to form inclusion on their own in cytoplasm or nucleus, demonstrating they were at risk of aggregation and have the potential to sense increased stress levels.

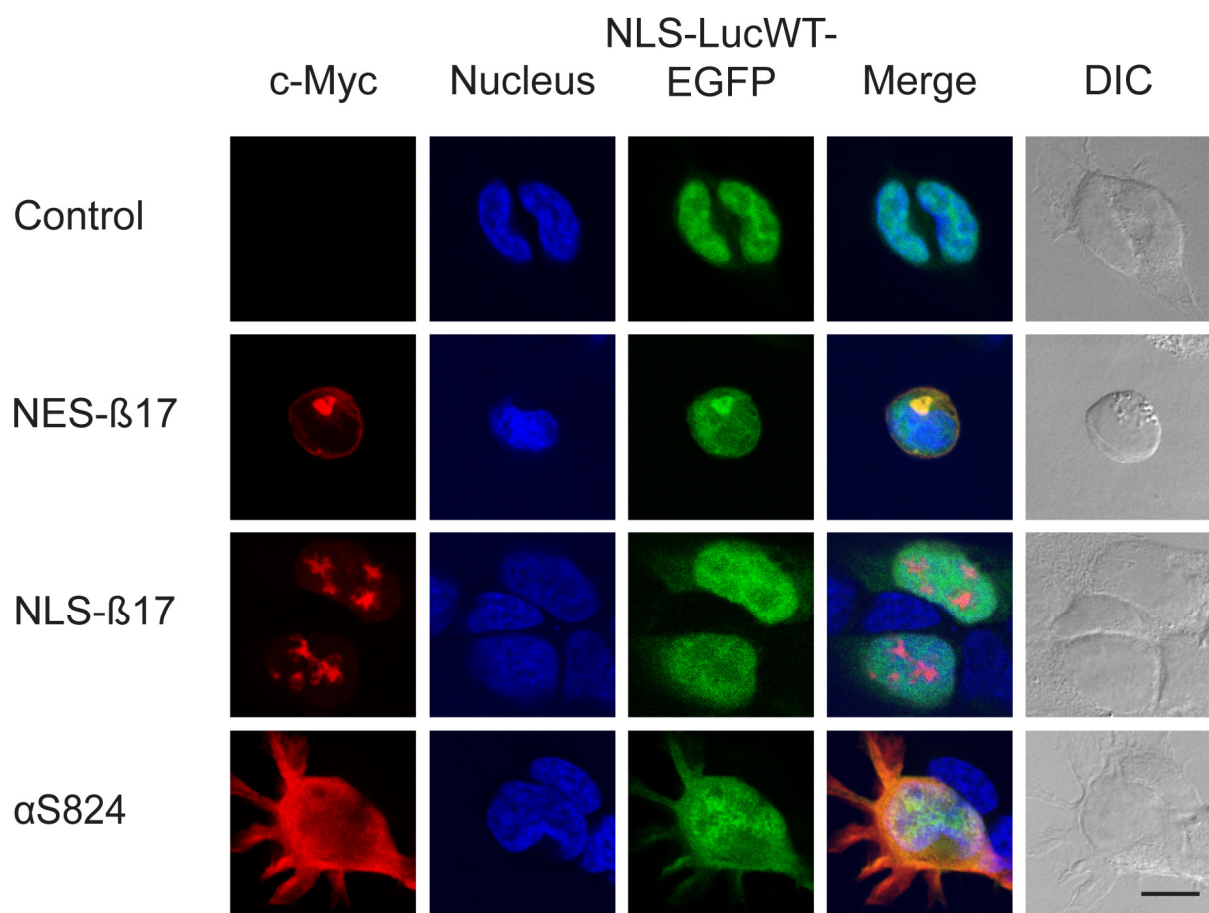


**Figure 65 | Nuclear luciferase-EGFP proteostasis sensors coexpressed with  $\beta$  proteins targeted to cytoplasm or nucleus.** HEK293T cells were cotransfected with NLS-LucWT-EGFP (green) and empty control vectors,  $\beta$  proteins, or  $\alpha$ S824. Cells were fixed 24 h after transfection and labeled with anti-c-Myc antibodies (red) and for nuclear DNA (DAPI, blue). Representative images of 3 independent experiments. Scale bar length 10  $\mu$ M.

$\beta$  proteins targeted to cytoplasm and nucleus were then combined with the compartment-specific luciferase sensors. Targeting both proteins to the cytoplasm, the luciferase sensors were partially sequestered by cytoplasmic NES- $\beta$ 17 inclusions, surrounded by distributed NES-LucWT-EGFP.

However, the sensors remained completely homogeneously distributed over the cytoplasm, when NLS- $\beta$ 17 or  $\alpha$ S824 were coexpressed (Figure 64).

Directing luciferase sensors to the nucleus did not show any disturbance in presence of NLS- $\beta$ 17. In the majority of the cells, the sensors were homogeneously distributed over the nuclear matrix, even being excluded from the  $\beta$  protein aggregates (Figure 66). Only in a minor fraction (5-10 %) of cells, some nuclear luciferase sensors aggregated and got sequestered into the NLS- $\beta$ 17 aggregates. Very differently, the same sensors targeted to the nucleus were strongly recruited into NES- $\beta$ 17 aggregates in the cytoplasm (Figure 65). Most likely this happened directly after ribosomal synthesis, before the cells were able to deliver the luciferase sensors actively into the nucleus.

Very similar observations were made coexpressing NES- $\beta$ 23 or NLS- $\beta$ 23 with compartmental luciferase sensors.  $\beta$ 23 caused coaggregation with the sensors in the cytoplasm, whereas they were excluded from nuclear  $\beta$ 23 aggregates. Similar results were furthermore obtained combining the  $\beta$  proteins with the destabilized double mutants of the luciferase sensors. These occurred at lower cellular levels than the wildtype sensors in both compartments, indicating a potentially faster degradation.

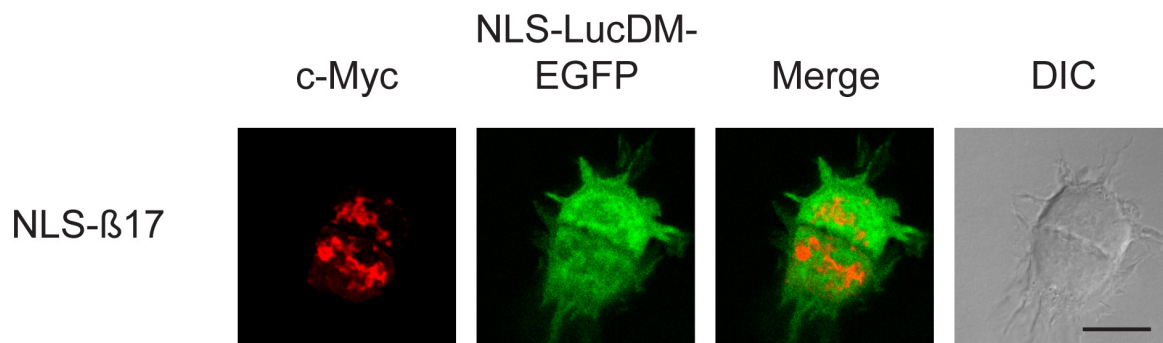


**Figure 66 | Exclusion of proteostasis sensor NLS-LucDM-EGFP (green) from nuclear  $\beta$  protein aggregates (red).** The proteostasis sensor was distributed over the nuclear matrix. The luciferase sensor did not overlap with, but surrounded nuclear  $\beta$ 17 aggregates.

Aberrant interactions between structurally unstable and misfolded proteins therefore occurred more prominently in the cytoplasm. Here we observed (co-)aggregation of both luciferase sensors, directed to cytoplasm or nucleus. In addition, as we will see later, cytoplasmic  $\beta$  proteins may inhibit the molecular machinery responsible for nuclear protein import, and therefore additionally decrease the efficiency of nuclear luciferase translocation. Interference with nucleo-cytoplasmic transport further increases the likelihood of aberrant interactions with NLS-Luc-EGFP in the cytoplasm.

The nuclear environment, and potentially the structural properties of the nuclear  $\beta$  proteins appeared in contrast to prevent aberrant interactions. Luciferase sensors and  $\beta$  proteins were left apparently unaffected from mutual interactions. Thus, cytoplasmic and nuclear aggregation and their aberrant interactions indicate elementary differences in the cytoplasmic and nuclear proteostasis with potentially severe consequences for the local misfolding and aggregation behavior.

## Inhibition of the proteasome causes a collapse of nuclear proteostasis

Levels and fluorescence of luciferase-EGFP double mutants (LucDM-EGFP) were significantly lower compared to the wildtype. An accelerated degradation of LucDM-EGFP due to conformational instability seemed plausible. Henceforth, we were interested in the fate of misfolded species under proteasomal inhibition. The proteasome is the main cytoplasmic and especially nuclear degradation machinery for the removal of monomeric proteins.

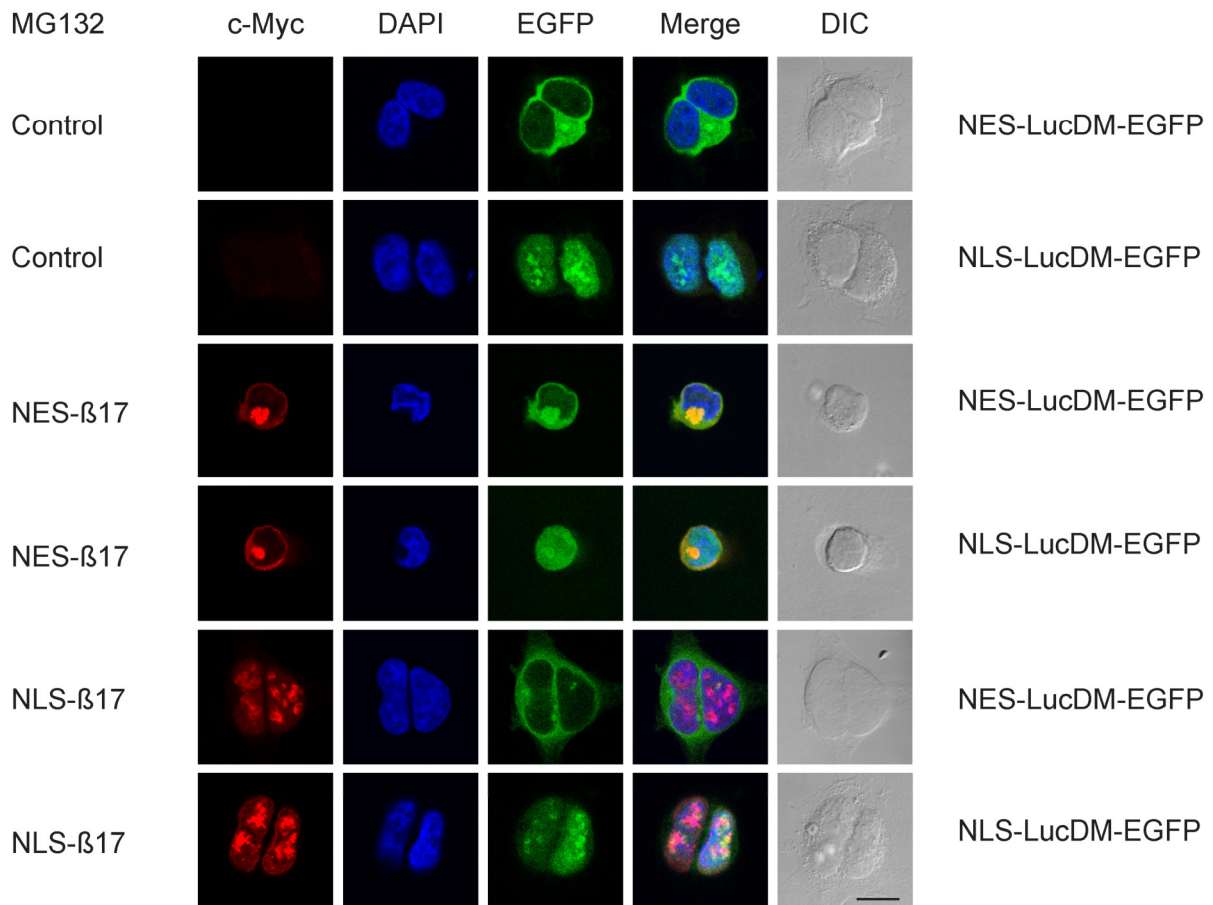


**Figure 67 | Proteasomal inhibition by MG132 and its influences on cytoplasmic and nuclear proteostasis and aggregation.** 24 h after cotransfection of LucDM-EGFP (green) targeted to cytoplasm or nucleus and  $\beta$  proteins or control vectors, the proteasome was inhibited for 5 h by MG132. Cells were fixed and stained with anti-c-Myc antibodies (red) and for nuclear DNA (DAPI, blue). Proteasomal inhibition caused an aggregation of the nuclear luciferase proteins, which accumulated in nuclear inclusions associated to, but not completely overlapping with nuclear  $\beta$  proteins aggregates. Cytoplasmic LucDM-EGFP was hardly influenced by proteasomal inhibition, rarely small aggregates were observed. Scale bar length 10  $\mu$ M.

MG132 is a potent and selective inhibitor of the proteasome, which causes a large reduction in the rates of cellular protein degradation (Kisselev 2011). Here we applied MG132 to HEK293T cells expressing LucDM-EGFP targeted to cytoplasm or nucleus. After 5 h of treatment, most cells transfected with NES-LucDM-EGFP showed a homogenous distribution of the sensor in the cytoplasm, while around 10% of cells contained a single cytoplasmic inclusion. Very differently, in cells expressing NLS-LucDM-EGFP multiple smaller aggregates appeared in the nucleus, overlapping with nucleolar structures (see also Gupta 2012, Thesis). Apparently, the nuclear proteostasis made

strong use of proteasomes to remove instable or misfolded proteins, which otherwise accumulated upon proteasomal inhibition.

The nuclear  $\beta$  proteins still accumulated in form of aggregates upon proteasomal inhibition. However,  $\beta$  proteins seemed in general not to be degraded by the proteasome, as they did not show any ubiquitination and did not accumulate further upon MG132 treatment (see also Olzscha 2010).

When coexpressed with NES- $\beta$ 17, the luciferase sensors behaved very similar with or without inhibition of the proteasome. In all cells expressing luciferase sensors and NES- $\beta$ 17, the luciferase sensors accumulated in perinuclear aggregates surrounded by homogenously distributed sensor protein.

As in absence of MG132 treatment, NLS-LucDM-EGFP was strongly recruited to NES- $\beta$ 17 aggregates. Nuclear luciferase aggregates were only seen in a minority of cells. The direct entrapment of luciferase sensors in the cytoplasm reduced the nuclear concentration of NLS-LucDM-EGFP, which presumably was a reason for the absence of nuclear aggregation in these cells. Another possibility might be that NES- $\beta$ 17 influenced the nuclear or overall proteostasis by additional means to prevent nuclear aggregation. Possible mechanisms could include e.g. an upregulation or nuclear localization of chaperones, or an inhibition of nuclear NLS-LucDM-EGFP import.

Proteasomal inhibition did not increase the aggregation of NES-LucDM-EGFP in presence of NLS- $\beta$ 17. As in the majority of cells before, the luciferase double mutant was homogeneously distributed over the cytoplasm. Only in rare cases, small cytoplasmic NES-LucDM-EGFP aggregates appeared. Proteasomal inhibition therefore does not seem to have a strong impact on the cytoplasmic proteostasis directly. Even in the presence of  $\beta$  proteins, NES-LucDM-EGFP remained soluble, rather indicating a strong stabilization by cytoplasmic chaperones. Therefore, misfolded species may rather be stabilized (at least temporarily) in the cytoplasm.

In contrast, NLS-LucDM-EGFP aggregated in presence as in absence of NLS- $\beta$ 17 aggregates under proteasomal inhibition. Both transfected proteins apparently were associated to the nucleoli. Despite not completely overlapping, they formed substructures very close to each other. Hence, the nuclear proteostasis appeared to be critically disturbed, when protein degradation through the proteasome was inhibited. These results demonstrate that aggregation at secure locations (such as the nucleoli) may offer an alternative to handle misfolded structures at least temporarily in case they cannot be directly degraded.

## Cytoplasmic $\beta$ proteins, Htt96Q, TDP-F4, and Parkin $\Delta$ C inhibit nuclear translocation of NF- $\kappa$ B

NF- $\kappa$ B is a ubiquitous transcription factor regulating cell type- and context-specific responses. NF- $\kappa$ B is also active in neurons and glial cells (O'Neill 1997, Salles 2014, Kaltschmidt 2009), but best understood for its regulatory functions in B lymphocytes and in inflammation (Sen 2011, Oeckinghaus 2011). The highly complex regulation of NF- $\kappa$ B integrates cross-signaling among numerous pathways and translates it into pro-survival or pro-apoptosis signals, which can finally decide about life and development or death of a cell (Oeckinghaus 2011).

NF- $\kappa$ B (a heterodimer of p50/p65) is directly controlled by binding to its inhibitor (I $\kappa$ B), which is phosphorylated by the I $\kappa$ B kinase (IKK), comprising IKK $\alpha$ , IKK $\beta$ , and its regulatory subunit NEMO (or IKK $\gamma$ ). Activation of NF- $\kappa$ B e.g. through TNF (tumor necrosis factor) receptor 1 mediated TNF $\alpha$  signaling induces phosphorylation and ubiquitination of I $\kappa$ B. This releases NF- $\kappa$ B into the cytoplasm and reveals its nuclear localization sequence (NLS). Recognized by importins, NF- $\kappa$ B is then actively translocated into the nucleus, where it binds to specific promoters and regulates gene transcription (Oeckinghaus 2011).

Intrigued by a defective stress signaling and distorted nuclear pore complexes, we became interested in assessing the functional activation and nucleo-cytoplasmic translocation of central signaling factors in cells challenged by misfolding and aggregation. Therefore, HEK293T cells were transfected with  $\beta$  proteins targeted to cytoplasm or nucleus, with Htt96Q, TDP-F4, Parkin $\Delta$ C,  $\alpha$ S824, or empty control vectors. After 40 h, NF- $\kappa$ B signaling was activated by TNF $\alpha$  treatment at 20 ng/mL for 30 min, and cells were fixed and immunostained for fluorescence microscopy.

Control cells demonstrated NF- $\kappa$ B translocation to the nucleus. Similarly, NF- $\kappa$ B translocated to the nucleus of cells expressing NLS- $\beta$ 17, NLS- $\beta$ 23, or  $\alpha$ S824. Therefore, activation and nuclear import were fully functional in the presence of nuclear  $\beta$  protein aggregates. Molecular signaling from the extracellular medium was recognized and processed within these cells.

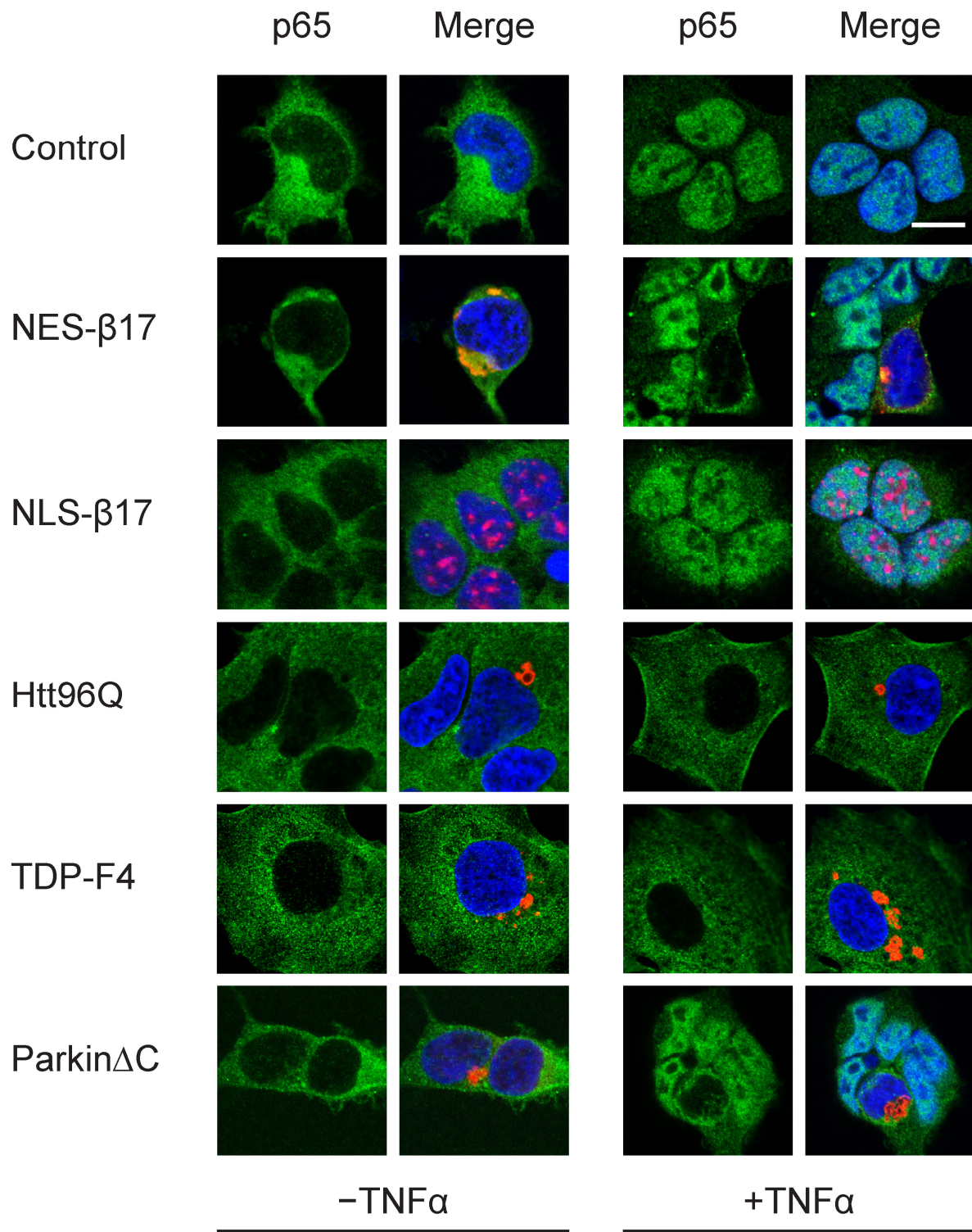


**Figure 68 | Protein aggregation in the cytoplasm interferes with nuclear NF-κB import after activation by TNFα.** 40 h after transfection of HEK293T cells with the indicated constructs, TNFα was applied for 30 min to activate NF-κB signaling. Cells were fixed and stained for protein aggregates (red), NF-κB (subunit p65, green), and nuclear DNA (DAPI, blue). Representative images from at least three independent experiments. Scale bar length 10 μM.

NES-β17, NES-β23, Htt96Q, TDP-F4, and ParkinΔC conversely prevented the nuclear import of NF-κB, which remained cytoplasmic. Partially, coaggregation between NF-κB and cytoplasmic β proteins occurred (especially for β23), but residual NF-κB was distributed over the cytoplasm. Thus, all tested cytoplasmic protein aggregates rendered the NF-κB activation dysfunctional. Almost all cells expressing cytoplasmic β proteins and around 70-80% of cells containing Htt96Q, TDP-F4, or ParkinΔC aggregates were affected by this translocation defect.

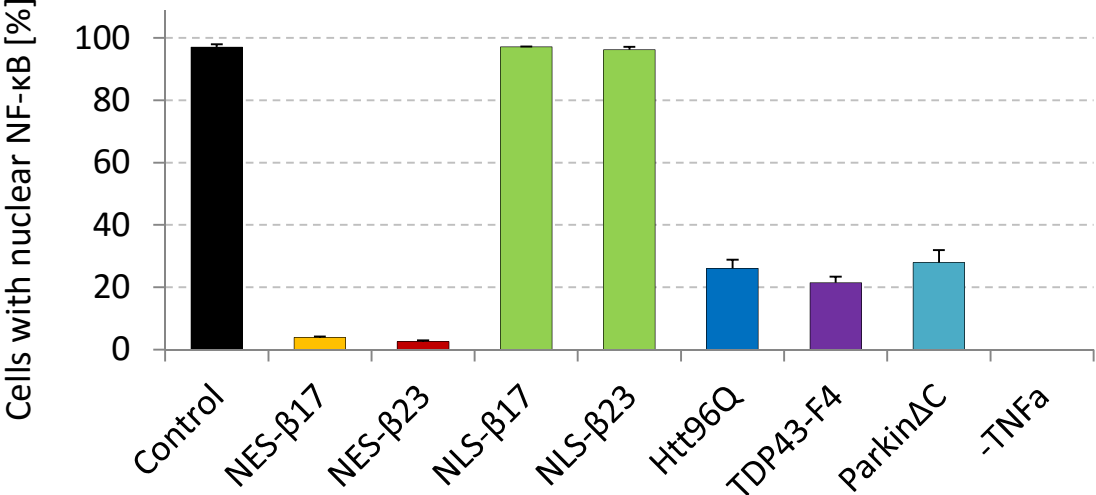


**Figure 69 | HEK293T cells examined for nuclear NF-κB (p65) after activation by TNFα, or without treatment (-TNFα).** Cells were analyzed and quantified for NF-κB translocation to the nucleus. Averages and SD from 3 independent experiments are shown; at least 100 cells were examined for every condition.

## Processing upstream of NF- $\kappa$ B is functional in cells expressing $\beta$ proteins

Before NF- $\kappa$ B is transported into the nucleus by cellular importins, a number of processing steps have to be completed. These include phosphorylation of NF- $\kappa$ B and I $\kappa$ B, followed by I $\kappa$ B ubiquitination and degradation. Only then, the p50/p65 dimer of NF- $\kappa$ B exposes its NLS, which is recognized by nuclear importins (Karin 2004).

Cells expressing  $\beta$  proteins were tested for NF- $\kappa$ B phosphorylation and I $\kappa$ B degradation. A phosphorylation specific antibody was applied (phospho-p65, Ser 536, Cell Signaling Technologies) to analyze HEK293T cells expressing  $\beta$  proteins,  $\alpha$ S824, or cells transfected with an empty vector. After expression for 40 h, followed by TNF $\alpha$  treatment for 15 min (optimal for p65 phosphorylation and I $\kappa$ B degradation), lysates were analyzed by SDS PAGE and immunoblotting, stained for phosphorylated NF- $\kappa$ B (p65), I $\kappa$ B, and GAPDH.

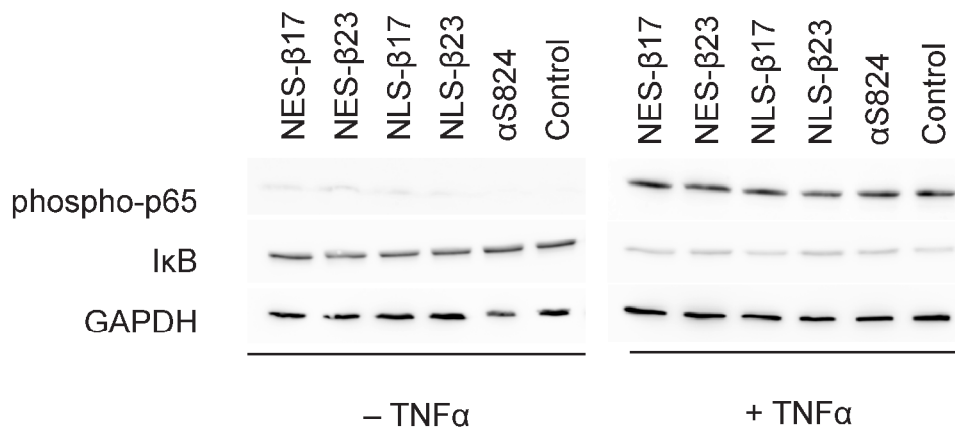


**Figure 70 | Immunoblot examining the phosphorylation of NF- $\kappa$ B (p65) and degradation of I $\kappa$ B before and after activation by TNF $\alpha$ .** Phosphorylation of p65 and degradation of I $\kappa$ B are prerequisites for the nuclear import of NF- $\kappa$ B. GAPDH levels demonstrate equal loading. Blots with the same antibody were generated with equal amounts of lysate and developed together to allow a comparative quantification.

NF- $\kappa$ B (p65) was phosphorylated and I $\kappa$ B was degraded in cells expressing cytoplasmic or nuclear  $\beta$  proteins. This occurred even when  $\beta$  proteins were aggregating in the cytoplasm and NF- $\kappa$ B translocation was inhibited. These results demonstrate that NF- $\kappa$ B was fully processed upon TNF $\alpha$  signaling, and in a competent state to be actively imported into the nucleus. All upstream processing in the NF- $\kappa$ B signaling pathway occurred efficiently, however, NF- $\kappa$ B failed to translocate to the nucleus, when cytoplasmic aggregates were present.

This observation indicates either a direct interference of cytoplasmic aggregation with the nucleocytoplasmic transport of proteins, or a novel mechanism of NF- $\kappa$ B regulation. Cytoplasmic misfolding and aggregation may prevent NF- $\kappa$ B activation through an inhibition of its nuclear import. At the current state of knowledge, such an inhibition would, however, likely occur rather upstream in the signaling pathway, e.g. through an influence on IKK or deactivated I $\kappa$ B release.



## Cytoplasmic $\beta$ proteins, Huntingtin96Q, and Parkin $\Delta$ C interfere with general nucleo-cytoplasmic protein transport

Expression of cytoplasmic  $\beta$  proteins, Huntingtin96Q, and TDP-F4 disturbed the nuclear envelope morphology and chromatin structure, and caused aggregation of FG-repeat proteins of the NPC. TNF $\alpha$  mediated NF- $\kappa$ B signaling and other stress response pathways (Hsf1/Hsp70 promoter activation) were abolished by cytoplasmic aggregates.

Disruption of the native localization and the active transport of essential cellular factors between nucleus and cytoplasm could lead to serious disturbances in cellular homeostasis and signaling in general. Consequently, we established an assay that allowed us to quantitatively analyze nucleo-cytoplasmic protein transport. Therefore, we fused EGFP (eukaryotic green fluorescent protein) to a nuclear localization sequence (NLS) followed by a nuclear export signal (NES). Due to the two targeting signals, the model protein is continuously being shuttled by active protein transporters between cytoplasm and nucleus. Thus we termed the resulting protein S-GFP (shuttling GFP, see Figure 71 A). Disturbances in the distribution of S-GFP could thus be quantified by its fluorescence in the respective compartment.

In cellular equilibrium, S-GFP was mainly cytoplasmic, indicating that the rate of nuclear export was higher than the rate of nuclear import. This circumstance allowed us to analyze the efficiency of general nuclear protein export in presence of misfolded proteins.

NES-mediated nuclear protein export by CRM1 can be inhibited by the small molecule drug Leptomycin B (LMB; Kudo 1998). In wildtype cells, addition of LMB causes a redistribution of S-GFP from cytoplasm to nucleus within minutes. Thus, under LMB conditions the active nuclear import can be examined and be compared to cells expressing aggregating proteins.

The relative concentrations of distributed S-GFP in the cytoplasm and nucleus were quantified by the fluorescence intensity of the protein in the respective compartment. The ratio of cytoplasmic to nuclear fluorescence describes the relative concentration of S-GFP in the two compartments.

S-GFP was cotransfected with  $\beta$  proteins, Htt96Q and Parkin $\Delta$ C in HEK293T cells. In control cells, S-GFP was strongly enriched in the cytoplasm (7.7-fold compared to nucleus). The efficiency of nuclear export decreased only marginally in the presence of NLS- $\beta$ 17 (5.8-fold cytoplasmic /nuclear gradient; see Figure 72). The effect of nuclear  $\beta$  proteins on the nuclear protein export was insignificant.

LMB treatment caused an inhibition of nuclear S-GFP export. 15 min were enough to redistribute the majority of the fluorescent protein to the nucleus. Control cells and cells expressing NLS- $\beta$ 17, both had a 6 fold concentration gradient of S-GFP between nucleus and cytoplasm. Nuclear import was completely undisturbed in presence of nuclear  $\beta$  proteins.

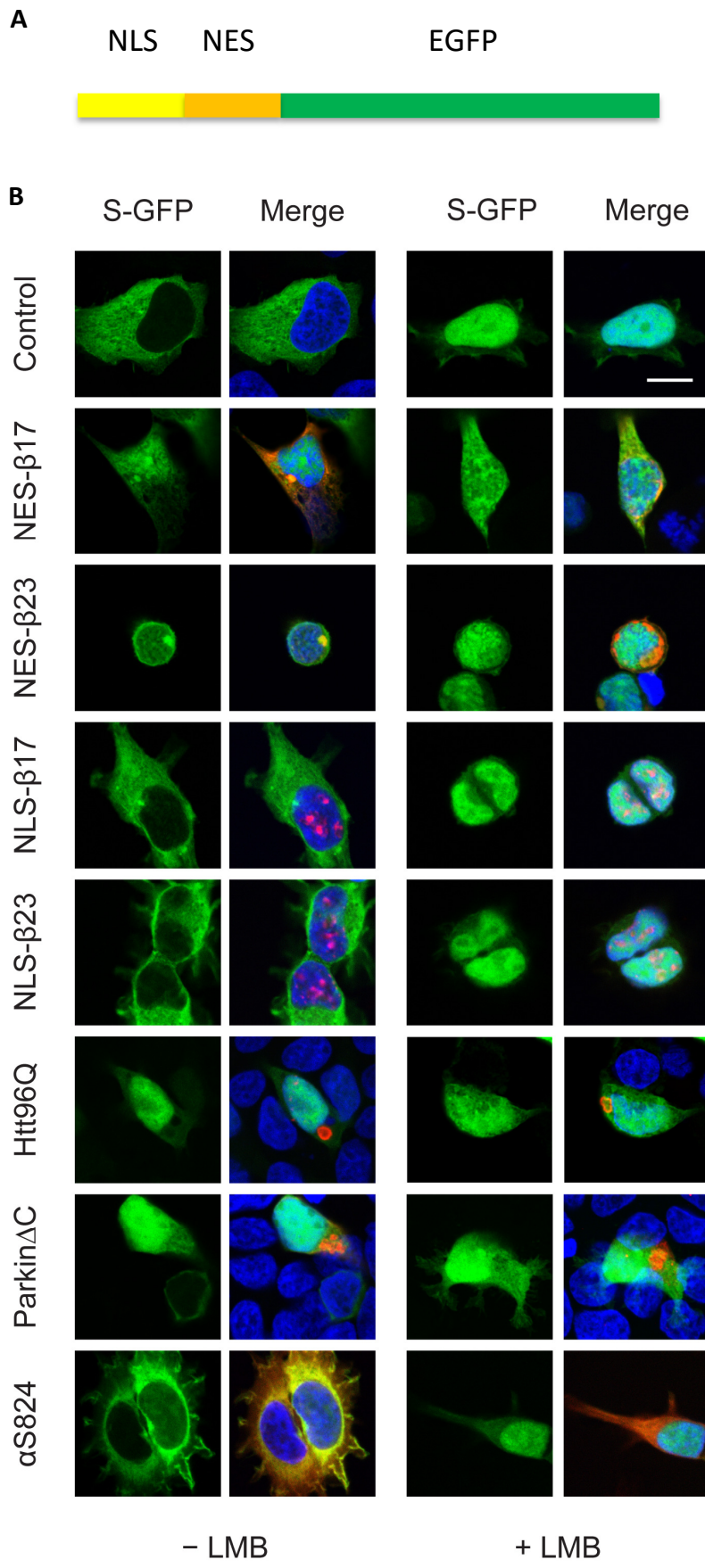


**Figure 71 | Cellular distribution of S-GFP in HEK293T cells, co-expressed with β proteins, Htt96Q, ParkinΔC, or αS824.** EGFP was fused to a nuclear localization sequence (NLS) and a nuclear export signal (NES), resulting in an EGFP permanently shuttling between cytoplasm and nucleus. **(A)** Construction of S-GFP. **(B)** In wildtype cells, S-GFP accumulated in the cytoplasm, most likely due to a higher nuclear export rate. This gradient is decreased in the presence of cytoplasmic β proteins, Htt96Q, or ParkinΔC. Nuclear β proteins did not disturb the distribution of S-GFP, nor did αS824. The small molecule drug Leptomycin B (LMB) inhibits the nuclear export of proteins, so that S-GFP redistributed to the nucleus within minutes. The efficiency of nuclear S-GFP import was significantly decreased in presence of cytoplasmic β proteins, Htt96Q, or ParkinΔC, but not by nuclear β proteins or αS824. Representative images of 3 independent experiments. Scale bar length 10 μM.

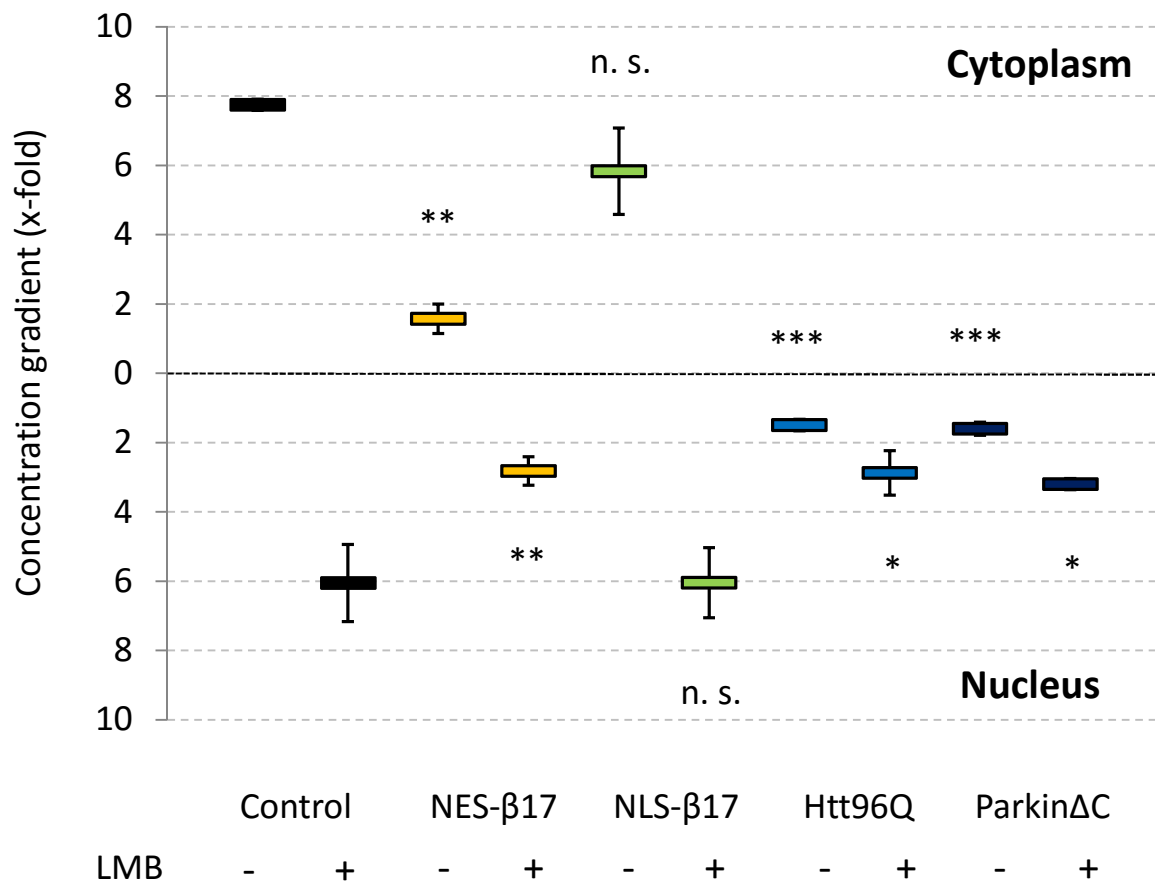


**Figure 72 | Cellular distribution of S-GFP in absence and in presence of  $\beta$  proteins, Htt96Q, or Parkin $\Delta$ C aggregates.** The nucleo-cytoplasmic concentration gradient of S-GFP was determined by its fluorescence intensity ratio between the two compartments in HEK293T cells 40 h after transfection. 75-150 cells were analyzed per condition. Averages and SD from 3 independent experiments. Significances compared to control cells under the same condition (+/- LMB), as determined by unpaired Student's t-test.

This situation changed when cytoplasmic  $\beta$  proteins, Htt96Q, or Parkin $\Delta$ C were coexpressed with S-GFP. The cellular localization of S-GFP generally drifted towards an equilibrated distribution between cytoplasm and nucleus. In other words, the concentration gradient between both compartments collapsed, the high import and export efficiencies achieved in control cells could not be reached any more. This was true for both transport directions, and occurred before and after inhibition of nuclear export by LMB.

In case of NES- $\beta$ 17, the cytoplasmic-nuclear concentration gradient of S-GFP fell below 2, corresponding to an export capacity of 25% compared to control cells. Moreover, the overall distribution of nuclear localization of S-GFP in this population of cells became much broader than in control cells, most likely due to differences in the progression and the probabilistic nature of protein aggregation. Whereas the majority of control cells exhibited a concentration gradient of S-GFP between 5-15 fold (on the level of individual cells), this gradient was reduced in cells accumulating NES- $\beta$ 17 to a range of 1 to 6. Therefore, a fraction of cells showed even an equal distribution of S-GFP between the two compartments. This result clearly demonstrated a severe interference of cytoplasmic  $\beta$  protein aggregation with nuclear protein export.

After inhibiting nuclear protein export by LMB, the nuclear concentration gradient of S-GFP decreased from 6-fold in control cells to around 3-fold in cells expressing NES- $\beta$ 17. Hence, in presence of NES- $\beta$ 17 aggregation, nuclear transport problems occurred in both directions. The relative decrease of nuclear S-GFP export (no LMB) was stronger than the nuclear import.

The breakdown of nuclear export became even more dramatic in cells with Htt96Q and Parkin $\Delta$ C aggregates. On average, S-GFP was even slightly concentrated in the nucleus (1.5-fold, without LMB treatment). In addition, the distribution of S-GFP in individual cells of the population appeared over a broad range, which might be related to the sudden outbreak of aggregate formation, as often observed for the polyglutamine-expanded huntingtin (Ossato 2010).

However, cells containing Htt96Q and Parkin $\Delta$ C aggregates were responding to LMB treatment. The average nuclear-cytoplasmic concentration gradient of S-GFP increased from 1.5 to 3 after nuclear export inhibition, a very comparable value to NES- $\beta$ 17. This rather subtle reaction demonstrated that the cells were still alive, harboring a residual transport capacity between two (still) separated compartments. However, the transport rates fell so low in the presence of cytoplasmic aggregates, that it appears unlikely that many protein gradients between the two compartments could be maintained in a physiological range.

NES- $\beta$ 23 had a very similar effect on S-GFP as NES- $\beta$ 17. However, NES- $\beta$ 23 coaggregated stronger with the fluorescent sensor S-GFP, impeding quantification. The soluble  $\alpha$ S824 had no apparent influence on the cellular distribution of S-GFP.

After discovering the inhibitory effect on N- $\kappa$ B activation, the experiments with S-GFP demonstrated that the presence of different kinds of cytoplasmic aggregates interfered with the active transport of proteins carrying a classical NES or NLS in both directions. Again,  $\beta$  protein aggregates in the nucleus behaved very inert.

## Cytoplasmic aggregation of importin $\alpha$ proteins

Importin  $\alpha$  proteins recognize and bind nuclear localization signals on proteins in the cytoplasm. Then the importins arrange Ran-dependent nuclear import through nuclear pore complexes. In the nucleus, substrates are released, and the importins become cargo of specific export complexes (CAS/Ran-GTP). Finally, the complex translocates back to the cytoplasm and dissociates (Cook 2007). Importin  $\alpha$ 1 (KpnA2) has been identified to interact with the  $\beta$  proteins (Olzscha 2011). Importin  $\alpha$ 3 (Kpna4) was reported to be the main import carrier of nuclear NF- $\kappa$ B translocation upon activation of the signaling pathway (Fagerlund 2005). As we observed major defects in NF- $\kappa$ B import and in general nucleo-cytoplasmic protein transport (S-GFP), we became interested in exploring the cellular distribution of importins in cells challenged with misfolding and aggregation.

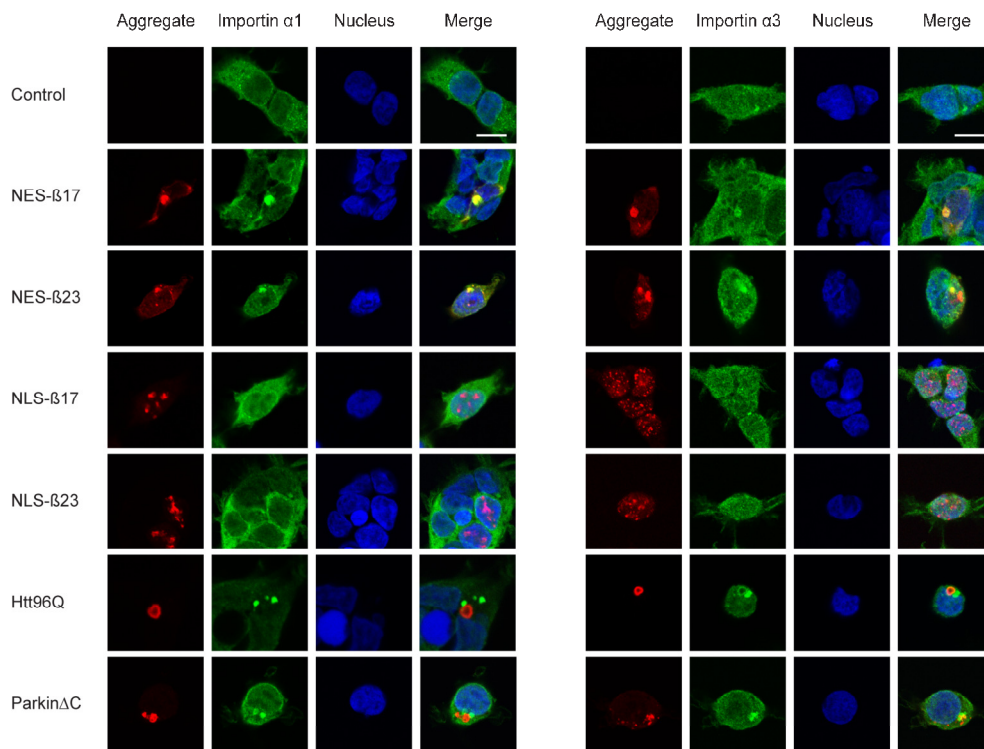


**Figure 73 | HEK293T cells expressing aggregation prone proteins (red) for 24 h, labeled for importin  $\alpha$ 1 (green, left panel) or importin  $\alpha$ 3 (green, right panel), and for nuclear DNA (DAPI, blue).** In wildtype cells, the importins were distributed over cytoplasm and nucleus, being enriched in the cytoplasm. In cells expressing cytoplasmic  $\beta$  proteins, importins were sequestered into aggregates. In cells with nuclear  $\beta$  proteins, the importins showed a wildtype-like distribution. In cells expressing Htt96Q or Parkin $\Delta$ C, the importins formed separate cytoplasmic inclusions. Representative images of 3 independent experiments. Scale bar length 10  $\mu$ M.

In wildtype HEK293T cells, importin  $\alpha$ 1 and importin  $\alpha$ 3 were distributed over cytoplasm and nucleus, being enriched in the cytoplasm. Expressing  $\beta$  proteins targeted to the cytoplasm for 24 h caused a significant fraction of both importins to become sequestered into the cytoplasmic  $\beta$  protein aggregates. In cells with Htt96Q or Parkin $\Delta$ C aggregates, the two importins formed separate inclusions in the cytoplasm, which did not overlap with the exogenous protein aggregates. Only in cells with nuclear  $\beta$  protein aggregates, the importins remained soluble and showed a wildtype-like distribution.

Conclusively, we found a clear association between inefficiencies of the active nucleo-cytoplasmic transport and (co-)aggregation of importin  $\alpha$  proteins, the executive molecular machinery carrying out active transport processes in cells.

## Nuclear mRNA accumulation in cells with cytoplasmic protein aggregation

Unsuccessful NF- $\kappa$ B translocation revealed nuclear import defects on the example of an essential cellular transcription factor. Experiments on S-GFP, a nucleo-cytoplasmic transport model protein, demonstrated transport inefficiencies occurring in both directions – into and out of the nucleus. Furthermore, the results suggested that the import defects we observed on NF- $\kappa$ B stand exemplary for many other transport inhibitions in cells with cytoplasmic protein aggregates. Consequently, the nuclear export of another central cellular molecule raised our attention: messenger RNA (mRNA).

mRNAs are synthesized in the nucleus as a transcript of genomic DNA by RNA polymerases. The resulting precursor mRNAs are then processed within small nuclear ribonucleoprotein particles (snRNPs). snRNPs consist of proteins and catalytically active RNAs (Wahl 2009). Noncoding introns are removed by the spliceosomes, and specific splice variants may appear in distinct cells and tissues. After several highly coupled processing steps, mature mRNAs are exported through the nuclear pore complexes to the cytoplasm. The whole process is mediated by mRNA processing and export proteins, among them the TREX (transcriptional export) machinery including the THO complex and Aly/REF (THOC4), which directly interacts with the mRNA export receptor TAP:p15 (Braun 2002, Köhler 2007, Carmody 2009).

In a SILAC based mass spectrometric analysis we previously identified mRNA processing and export factors as interactors of the  $\beta$  proteins in HEK293T cells (Olzscha 2011), and recently in primary mouse neurons (analysis performed by Li Rebekah Feng, Daniel Hornburg, Felix Meissner, and Matthias Mann). Especially proteins of the THO complex with extended low-complexity regions raised our awareness of potential interferences with mRNA export.

HEK293T and SH-SY5Y cells were transfected with  $\beta$  proteins, Htt96Q, TDP-F4, or Parkin $\Delta$ C. Cells were fixed and labeled for poly(A) RNA with a fluorescent Cy5-(d)<sub>30</sub> oligonucleotide probe (most mRNAs are polyadenylated after transcription). Aggregating proteins were labeled with respective antibodies.

In control cells, poly(A)-tailed RNA (corresponding to mRNA) was distributed fairly homogenously over the cytoplasm. The majority of nuclear mRNA concentrated in snRNPs, giving rise to small, fluorescently bright spots within the nuclear matrix (distinct from nucleoli). Remarkably, in cells expressing cytoplasmic  $\beta$  proteins, the vast majority of cellular mRNA accumulated in the nucleus, where numerous fluorescently bright structures appeared. These spherical structures did not reflect the tiny snRNPs of wildtype cells, but formed “nuclear mRNA bodies” of significantly increased size and brightness. Simultaneously, the cytoplasm was virtually free of mRNA.

The  $\beta$  proteins directed to the nucleus did not cause any nuclear accumulation of mRNAs, despite their neighborhood to mRNA processing and export functions. The cellular mRNA distribution appeared completely normal in form of distributed mRNA in the cytoplasm and snRNPs in the nucleus. Only in a few percent of cells, nuclear  $\beta$  proteins showed signs of nuclear mRNA accumulation.

NES-EGFP demonstrated that overexpression of NES-tagged proteins were not overloading the nuclear export capacity by itself.

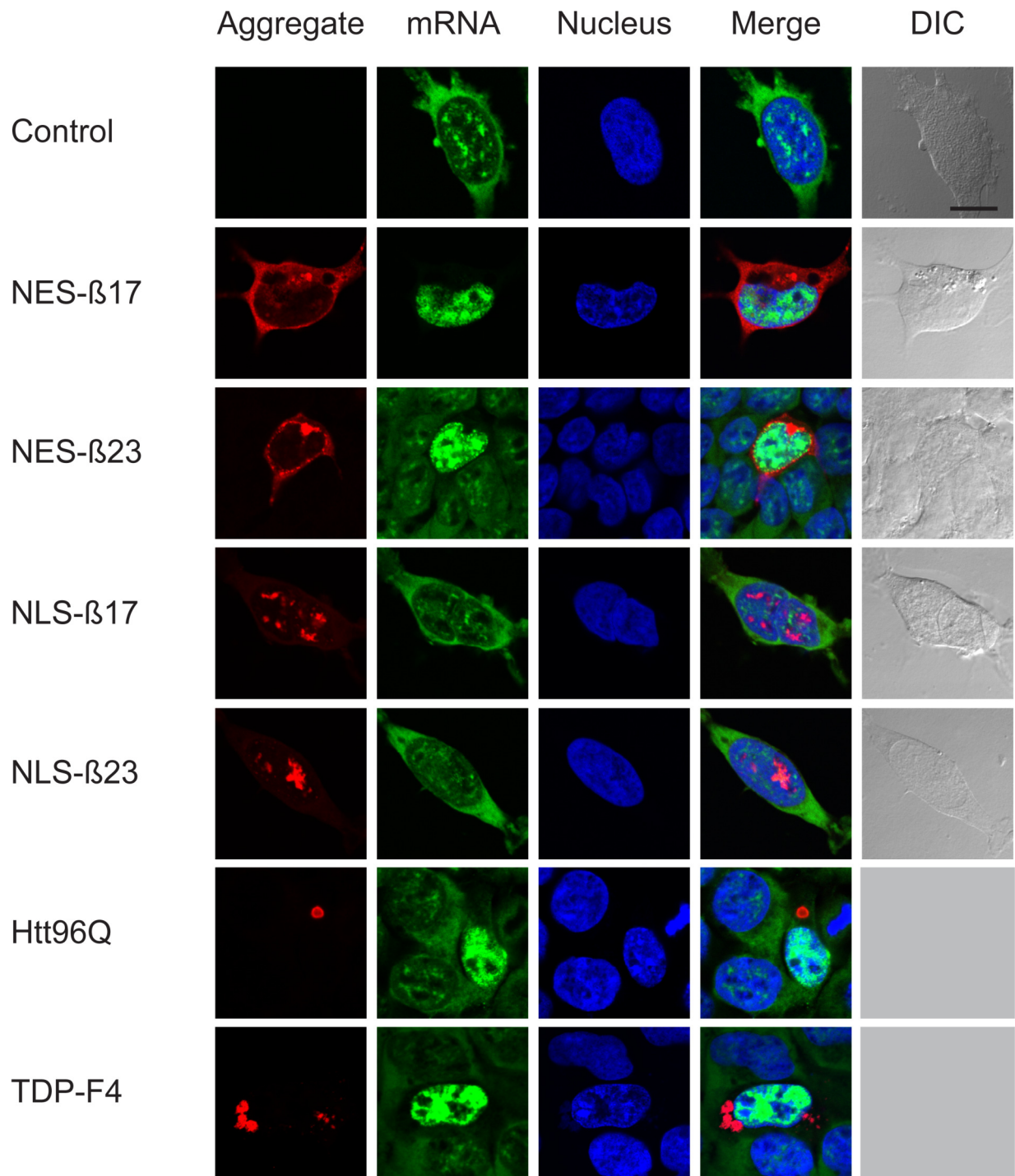


**Figure 74 | Cytoplasmic aggregation-prone proteins inhibit nuclear mRNA export and cause mRNA to accumulate in “nuclear mRNA bodies”.** HEK293T cells were analysed for their polyA RNA (green) distribution 24 h after transfection with  $\beta$  proteins, Htt96Q, TDP-F4 (red), or empty vectors (control). Nuclear DNA was stained with DAPI (blue). In control cells, the mRNA was distributed homogenously over the cytoplasm. In the nucleus, mRNA localized to snRNPs for processing of premature mRNAs. Cellular mRNA distribution was seriously disturbed in cells expressing cytoplasmic  $\beta$  proteins, Htt96Q, or TDP-F4. Here, the mRNA accumulated in “nuclear mRNA bodies” of clearly increased size compared to wildtype snRNPs. Cytoplasmic mRNA levels vanished. In contrast, cells expressing  $\beta$  proteins in the nucleus behaved very similar to control cells. The cellular distribution of mRNA appeared undisturbed. Representative images of at least 3 independent experiments. Scale bar length 10  $\mu$ M.

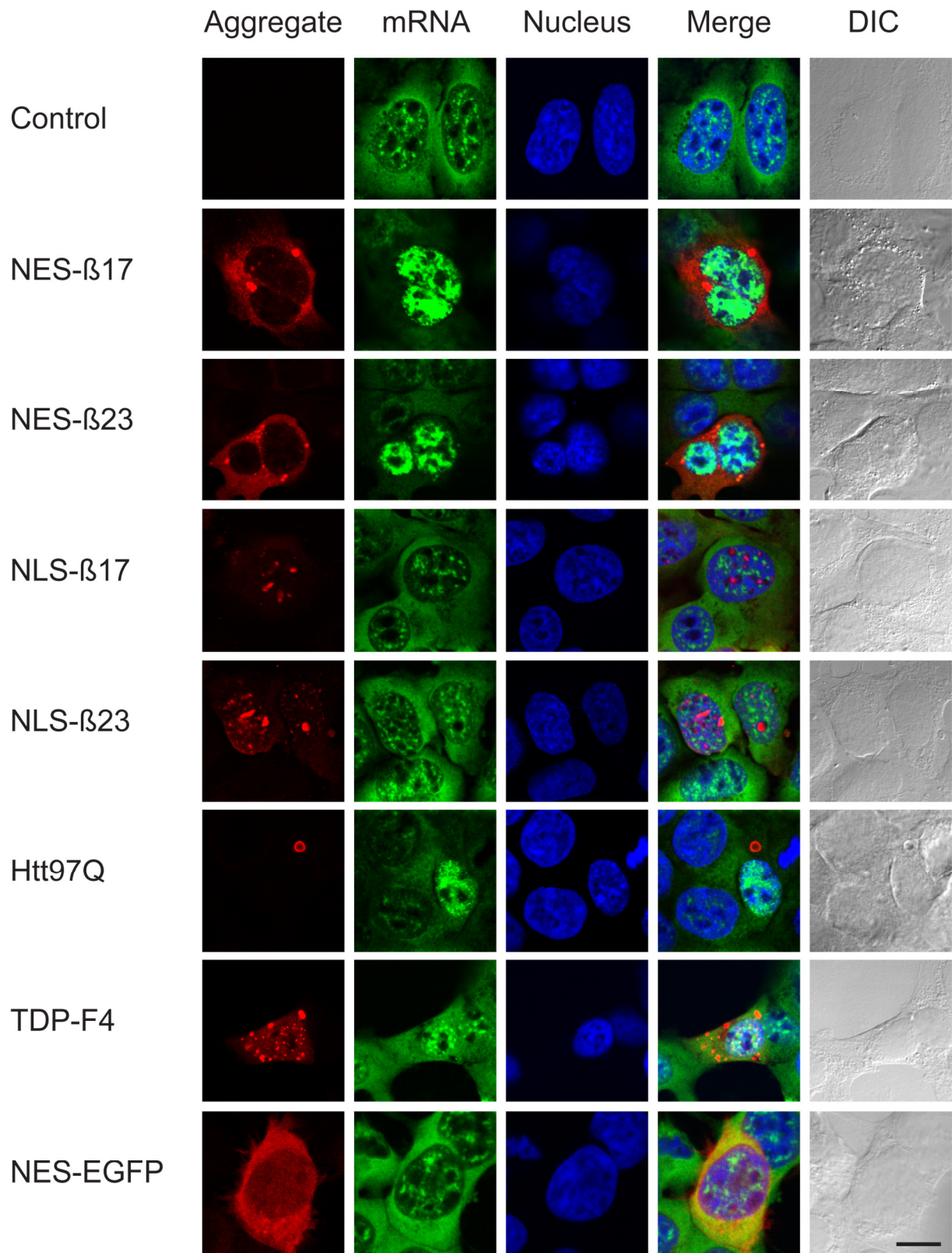


**Figure 75 | Cytoplasmic aggregation-prone proteins inhibit nuclear mRNA export and cause accumulation in “nuclear mRNA bodies” in SH-SY5Y (neuroblastoma) cells.** SH-SY5Y cells were analysed for their polyA RNA (green) distribution 24 h after transfection with  $\beta$  proteins, Htt96Q, TDP-F4 (red), or empty vectors (control). Nuclear DNA was stained with DAPI (blue). Similar to HEK293T cells, the cellular mRNA accumulated in nuclear bodies, and cytoplasmic mRNA levels vanished in cells with cytoplasmic  $\beta$  proteins, Htt96Q, or TDP-F4. mRNA was distributed wildtype-like in cells with nuclear  $\beta$  proteins, or NES-EGFP. Representative images of at least 3 independent experiments. Scale bar length 10  $\mu$ M.



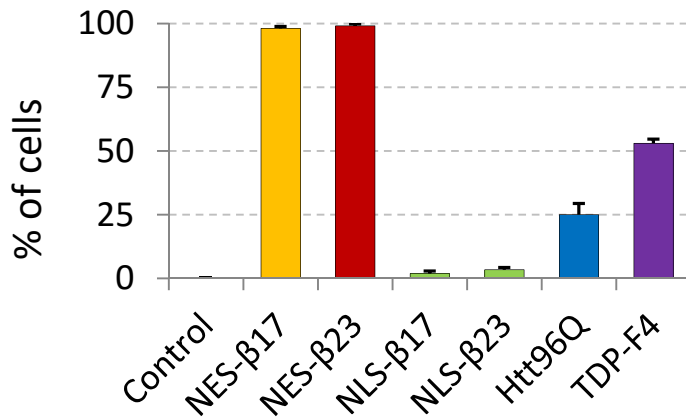


**Figure 76 | Quantification of HEK293T cells with nuclear mRNA accumulation upon expression of the indicated aggregation-prone proteins.** Cells were analyzed 24 h after transfection. Averages and SD from 3 independent experiments. At least 100 cells were analysed per experiment.

Nuclear accumulation of mRNA was furthermore observed in cells expressing Htt96Q and TDP-F4. However, here we observed a rather intermediate phenotype regarding the cellular distribution of mRNA: next to the presence of bright nuclear mRNA bodies, lower levels of residual mRNA remained distributed over the cytoplasm of many cells. Although a nuclear accumulation with mRNA bodies of increased size and brightness was present in cells with Htt96Q or TDP-F4 aggregates, not all cells were affected as strongly as in case of cytoplasmic  $\beta$  proteins.

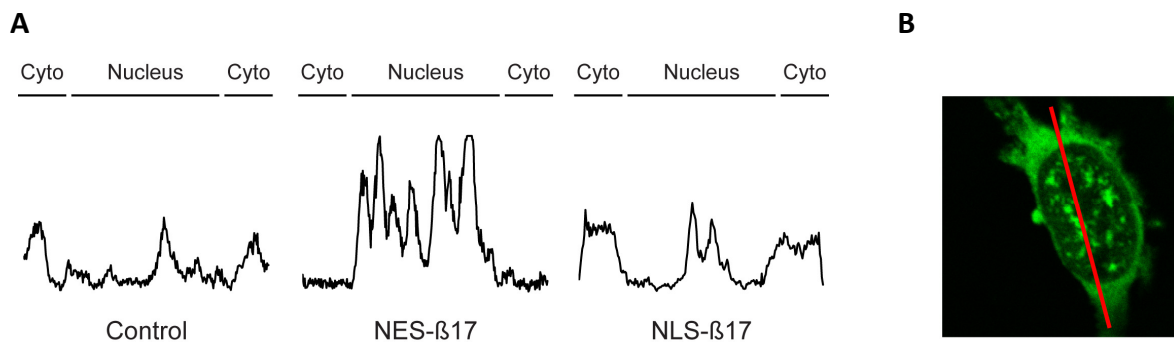


**Figure 77 | Cellular mRNA profiles presenting the distribution of mRNA along a route straight through the middle of a cell (red line).** (A) The fluorescence intensity (y-axis) along a path through a HEK293T cell (x-axis) represents the mRNA distribution. In control cells, mRNA levels are high in the cytoplasm (cyto), and generally lower in the nucleus, where “RNA spikes” corresponding to snRNPs appeared. Cells expressing nuclear  $\beta$  proteins showed a similar distribution, in contrast to cells expressing cytoplasmic  $\beta$  proteins. Here, the mRNA levels in the cytoplasm decreased strongly, while a high fluorescence in the nucleus indicated that mRNA accumulated in large nuclear mRNA bodies. Their size and fluorescence intensity reached far beyond those of wildtype snRNPs. (B) Exemplary route through a cell (red line), along which the polyA RNA fluorescence (green) was measured and plotted.

While the nuclear export of S-GFP was disturbed to a greater extent in cells with Htt96Q and Parkin $\Delta$ C aggregates, the  $\beta$  proteins caused a stronger nuclear mRNA accumulation. Although similar cellular pathways and functions were affected, the respective impact of different misfolding and aggregating proteins appeared to be of different strength. The distinct physicochemical nature of the individual aggregating sequence may be responsible for such variations. Individual sequence properties may thus aggravate or alleviate detrimental interactions and associated cellular malfunctions.

## Isolation and quantification confirms diminished cytoplasmic mRNA

To quantify cytoplasmic mRNA levels biochemically, cytoplasmic and nuclear fractions of transfected HEK293T cells were separated after lysis of the cellular membranes and sedimentation of preserved nuclei. PolyA RNA was purified from the separated cytoplasmic fraction by poly-d(T)-coupled beads (small uniform polystyrene-latex particles for improved quantification; Oligotex, Qiagen).

40 h after transfection, HEK293T cells were collected and cellular membranes were lysed in 4 °C cold PBS with 0.3% TritonX-100 and RNase inhibitor. Intact nuclei were sedimented. The cytoplasmic lysate (supernatant) was incubated with poly-d(T)-coupled beads for mRNA hybridization. The beads were washed and rehybridized to remove residual ribosomal RNAs. The mRNA was eluted at 70 °C. Quality and quantity of the mRNA were assessed on a NanoDrop spectrometer (absorption at 260/280 nm).

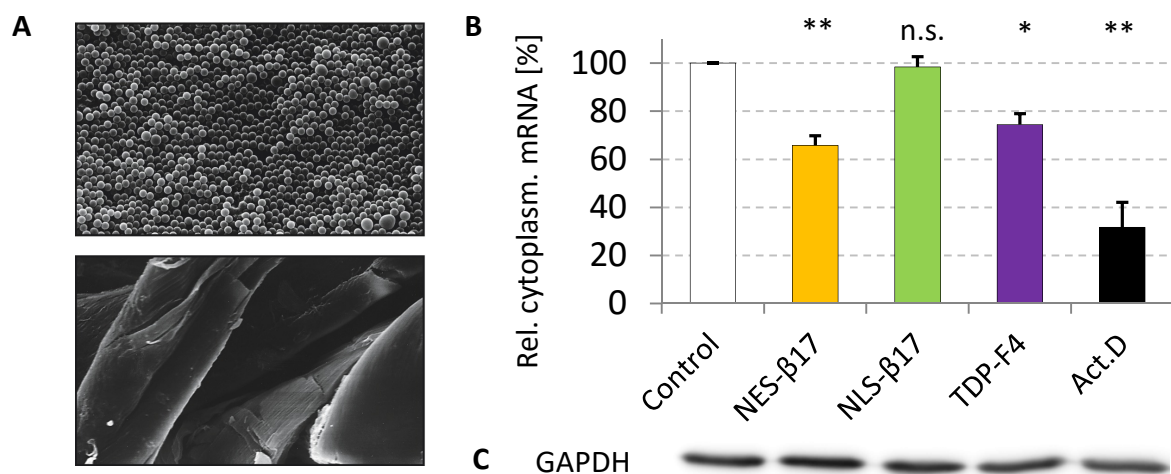


**Figure 78 | Purification of cytoplasmic mRNA by poly(T) DNA coupled Oligotex beads.** (A) Scanning electron micrographs of Oligotex particles (1 µm in diameter) and oligo-dT cellulose at the same magnification. The small and uniform Oligotex particles (Qiagen) allow a quantitative purification (figure from Qiagen). (B) Quantification of cytoplasmic mRNA purified from HEK293T cells expressing the indicated proteins, or treated with Actinomycin D, a general transcriptional inhibitor. NES-β17 and TDP-F4 show a significant reduction of cytoplasmic mRNA (averages and SD from 3 independent experiments). (C) GAPDH levels of HEK293T lysates (input).

Cytoplasmic mRNA levels were lowered in cells expressing NES-β17 and TDP-F4, as expected. mRNA levels decreased to 66% and 75% of control cells, respectively. For cells expressing NLS-β17, mRNA levels remained high at 98%. At a concentration of 5 µg/mL, Actinomycin D inhibits general transcription by RNA polymerase II. Cytoplasmic mRNA levels decreased to 32% in this control experiment. Equal GAPDH levels demonstrate that equal amounts of cells were lysed for the mRNA purification.

Since the proportion of cells expressing the transgenic proteins is limited by the transfection efficiency, while the whole cell population was analyzed, the measured values represent most likely an underestimation of the real decrease of cytoplasmic mRNA in single cells with cytoplasmic aggregates. Nevertheless, the biochemical analysis demonstrates a significant decrease of cytoplasmic mRNA levels in agreement with our observations by immunofluorescence.

## Proteasomal inhibition induces nuclear mRNA accumulation

Proteasomal inhibition by MG132 prevents the removal of misfolded proteins from cells. Misfolded structures accrue increasingly over time (Zhao 2010, Ros 2004, Obeng 2006) and might disturb the cellular proteostasis similarly to the expression of individual aggregating proteins.

The anticancer drug Bortezomib is a reversible 20S proteasome inhibitor causing a dose-dependent peripheral neuropathy. A study on the side effects of Bortezomib described unexpected nuclear retention and granule formation of polyA RNA in sensory ganglia neurons (Casafont 2010). Here we observed the distribution of mRNA in our system under proteasomal inhibition by MG132. Over time, MG132 treatment increasingly caused a cytoplasmic depletion and a nuclear accumulation of mRNA in SH-SY5Y cells.

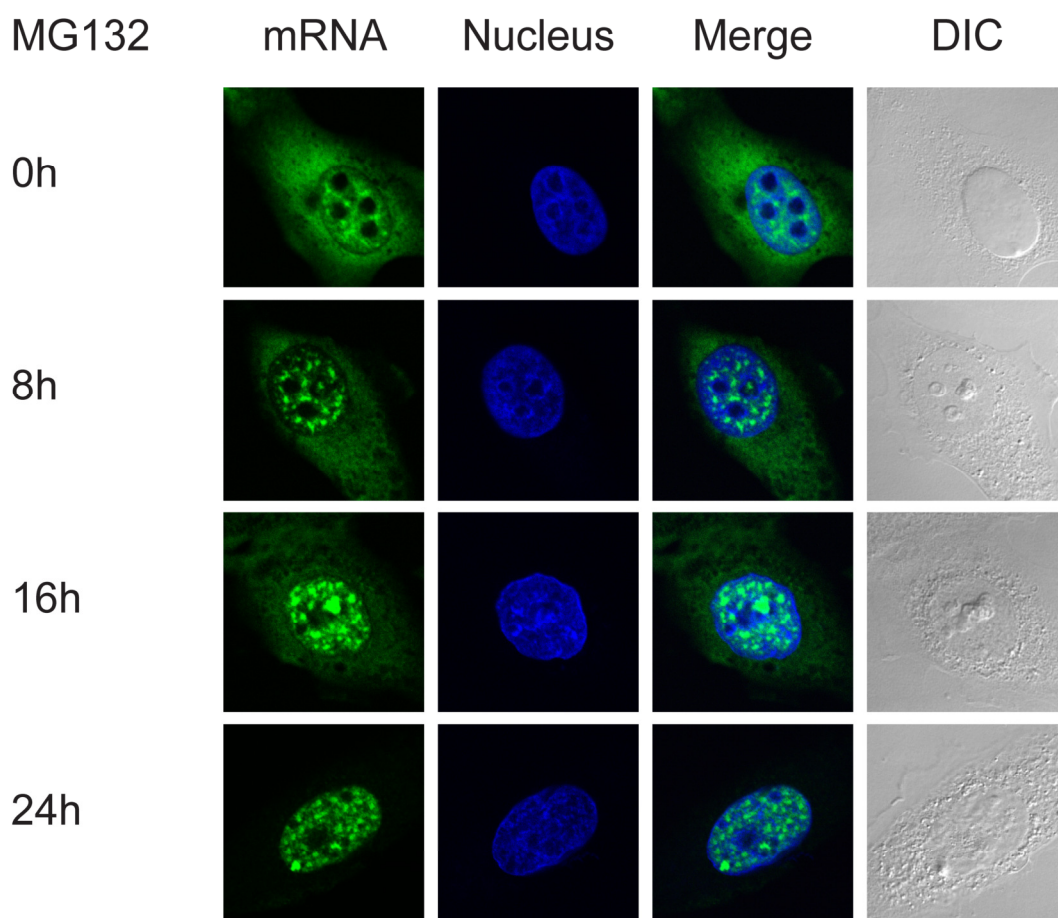


**Figure 79 | SH-SY5Y cells under proteasomal inhibition by MG132 for the indicated durations.** MG132 caused nuclear retention of mRNA (green) similar to cells expressing aggregation prone proteins in the cytoplasm. Representative images of 3 independent experiments.

These experiments demonstrate that nuclear mRNA accumulation appeared as a consequence of long-term stress in cells. Shorter stress, such as 2 h of heat shock at 43 °C, did not cause a nuclear accumulation of mRNA.

## mRNA disturbances in the R6/2 Huntington's disease mouse model

R6/2 mice are transgenic for exon 1 of human huntingtin, carrying an extended polyglutamine (polyQ) repeat of around 150 glutamines. R6/2 mice develop a progressive neurodegenerative phenotype, including involuntary stereotypic movements, tremor, epileptic seizures, brain shrinkage, and premature death (Mangiarini 1996).

First symptoms were observed in R6/2 mice starting between 9 and 11 weeks of age (Mangiarini 1996). The mice usually survive 13-14 weeks (Zhang 2003). Since we were interested in observing neurons suffering from early effects of huntingtin aggregation, but without major cell death yet, we decided to explore the distribution of mRNA in R6/2 mouse brains at 9 weeks of age. At this time, intraneuronal huntingtin aggregates were already forming, but symptoms just started to become apparent (Zhang 2003, Li 2005). Indeed, only one out of four R6/2 mice tested in this study showed initial tremors. The genotypes of R6/2 mice and littermates were confirmed by PCR.

Particularly cortical and striatal neurons were reportedly affected by aggregation of polyglutamine-expanded huntingtin in R6/2 mice (Mangiarini 1996), similar to human patients suffering from Huntington's disease (Graveland 1985, DiFiglia 1997, Li 2005). Different antibodies recognize a variety of cellular huntingtin inclusions, such as somatic, neutrophil, or nuclear oligomers or aggregates (Ko 2001, Miller 2011). These diverse observations suggest a coexistence of distinguishable, potentially compartment-specific fragments and conformations of the huntingtin protein or its fragments. We decided to apply the monoclonal 3B5H10 antibody in our study (Miller 2011). This antibody was selected to recognize specifically low-molecular-weight states of expanded polyQ proteins. These structures were strongly correlated to neuronal death *in situ*. 3B5H10 did not recognize polyQ repeats in higher molecular weight forms, as they appear in the major inclusion bodies (Miller 2011). Applying this antibody allowed us to observe specifically the early, potentially very toxic forms of huntingtin, and to correlate the appearance of these structures to the distribution of mRNA in neurons of R6/2 mice.

Brains of R6/2 mice and littermates (controls) were fixed by paraformaldehyde and cut into sections of 20  $\mu\text{m}$  thickness. In neurons of wildtype mice, the mRNA (hybridized to Cy5-(d)T<sub>30</sub>) was distributed over soma and neurites. The nuclear matrix appeared rather void of mRNA, which was concentrated in a small number of snRNPs, similar to cultured human cell lines.

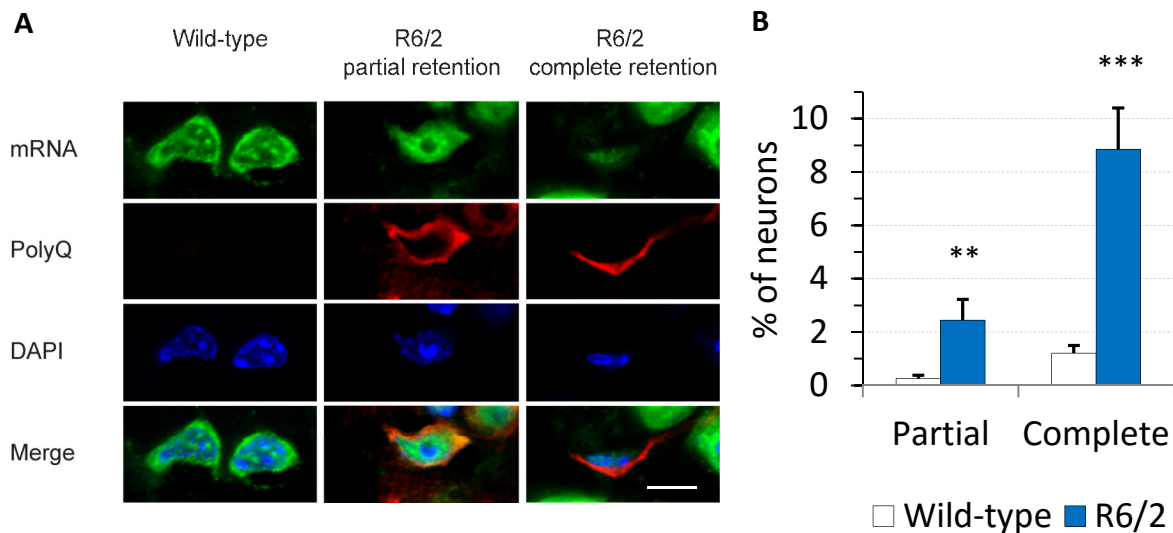


**Figure 80 | Distribution of mRNA (polyA RNA, green) in neurons of 9 week old wildtype and R6/2 mice, transgenic for human polyQ-expanded Htt exon 1. (A)** Brain slices of 20µm thickness were labelled with an antibody specific for extended polyQ sequences (3B5H10, red), and nuclear DNA was stained with DAPI (blue). Cells showed mRNA accumulations in the nucleus with residual mRNA remaining in the cytoplasm (*partial retention*), or with strongly reduced mRNA levels in the nucleus and vanished mRNA in the cytoplasm (*full retention*). Representative images from 3 wildtype and 4 R6/2 mice. Scale bar length 10 µM. **(B)** Quantification of neurons with *partial* or *complete nuclear mRNA retention* phenotypes in wildtype and R6/2 mice.

In cortical and striatal neurons of R6/2 mice, neuronal phenotypes could be classified into three groups regarding their cellular distribution of mRNA: firstly, neurons with a wildtype-like, healthy distribution; secondly, neurons with lowered mRNA fluorescence in the cytoplasm and increased mRNA fluorescence in a number of speckled nuclear particles (2.4% of total neurons; *partial nuclear mRNA accumulation*); thirdly, neurons with a very low fluorescence of residual mRNA in the cytoplasm, and lowered levels of nuclear mRNA, which appeared rather in speckled structures than in the classical snRNP morphology (8.9% of neurons; *complete nuclear mRNA accumulation*).

For most neurons showing a partial or complete nuclear mRNA accumulation, mainly cytoplasmic diffuse material or aggregates were stained by the 3B5H10 antibody, or cytoplasmic in combination with nuclear structures. Purely nuclear polyQ aggregates were hardly detected by 3B5H10.

An abnormal distribution with nuclear accumulation of mRNA originally discovered in cultures of immortalized human cells could thus not only be reproduced in primary mouse neurons (experiments by Li Rebekah Feng; Woerner 2016), but also in cerebral neurons of the R6/2 huntingtin mouse model. Aggregate formation and accompanying toxicity progresses in animals rather over days and weeks than over hours as in cell culture models. The two distinct mRNA related phenotypes in R6/2 mice may therefore correspond to variations in aggregation progression, which may appear chronologically in individual neurons. Observations at different mouse ages or other disease models may allow further insights into the mRNA related cell pathology.

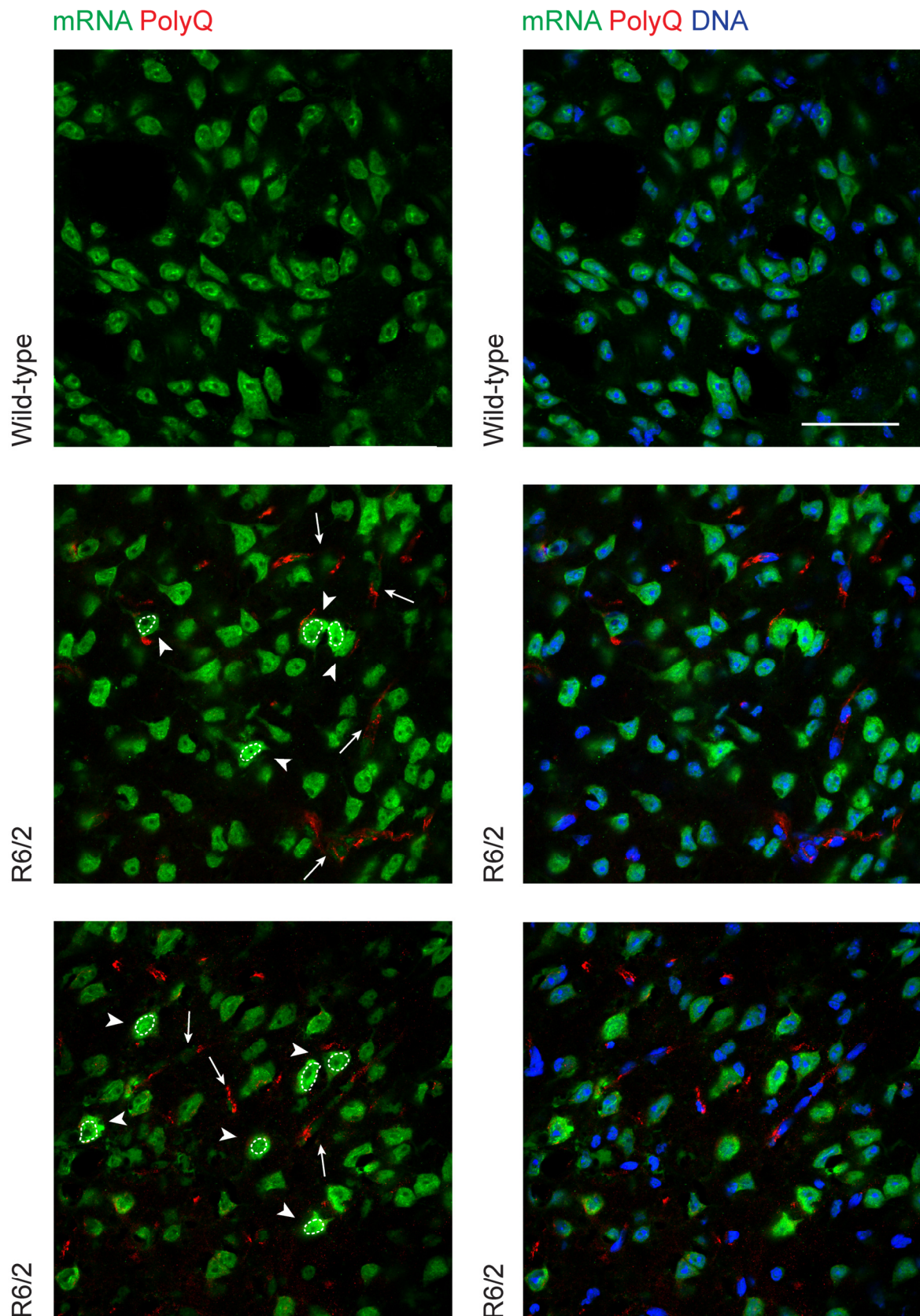


**Figure 81 | Brain sections of 9 week old wildtype and R6/2 mice were stained for mRNA (polyA RNA, green) and extended polyQ sequences (red).** PolyQ extended human Huntingtin was stained with an antibody specific for extended polyQ sequences (3B5H10, red), and nuclear DNA by DAPI (blue). Neurons with partial (arrowheads) and complete nuclear mRNA retention (arrows) are indicated. Representative images from 3 wildtype and 4 R6/2 mice. Scale bar, 50  $\mu$ m.

## Low apoptosis signaling in 9 week old R6/2 mice

As different populations of cells with distinct mRNA phenotypes were found in 9 week old R6/2 mice, their state of viability caught our interest. Especially cells with very low levels of cytoplasmic mRNA might have already been in a rather advanced stage towards cells death. Zhang et al. reported previously a sequential activation of caspases in R6/2 mice (Zhang 2003). They described a rather low activation of caspase-3 and caspase-9 in 9 weeks old R6/2 mice that significantly rose during the course of the following 3 weeks. At 12 weeks of age, caspase-8 and the pro-apoptotic mitochondrial Bax/Bim proteins became activated, concomitant to increased cell death by apoptosis triggering the mortality of R6/2 mice (Zhang 2003).

To analyze potential apoptosis signaling and cell death in association with the observed mRNA phenotypes, brain sections of R6/2 mice and littermates were stained for proteolytic activation of caspase-3. Therefore, a cleavage-specific antibody (cl.CAS-3) was applied to the brain slices of 9 week old R6/2 mice. Neurons displaying a partial or complete nuclear accumulation phenotype were generally not recognized by this antibody. A small fraction of cells stained positively for cleaved caspase-3 (< 0.1% of total neurons). These cells had almost undetectable levels of mRNA, which was likely already degraded at this stage. In wildtype mice, even fewer cells were recognized by antibodies against cl.CAS-3. Therefore, we conclude that the observed mRNA phenotypes (partial and complete mRNA accumulation) appear in an early stage towards cell death, which might rather appear as consequence of defective mRNA export and other malfunctions within the subsequent days.

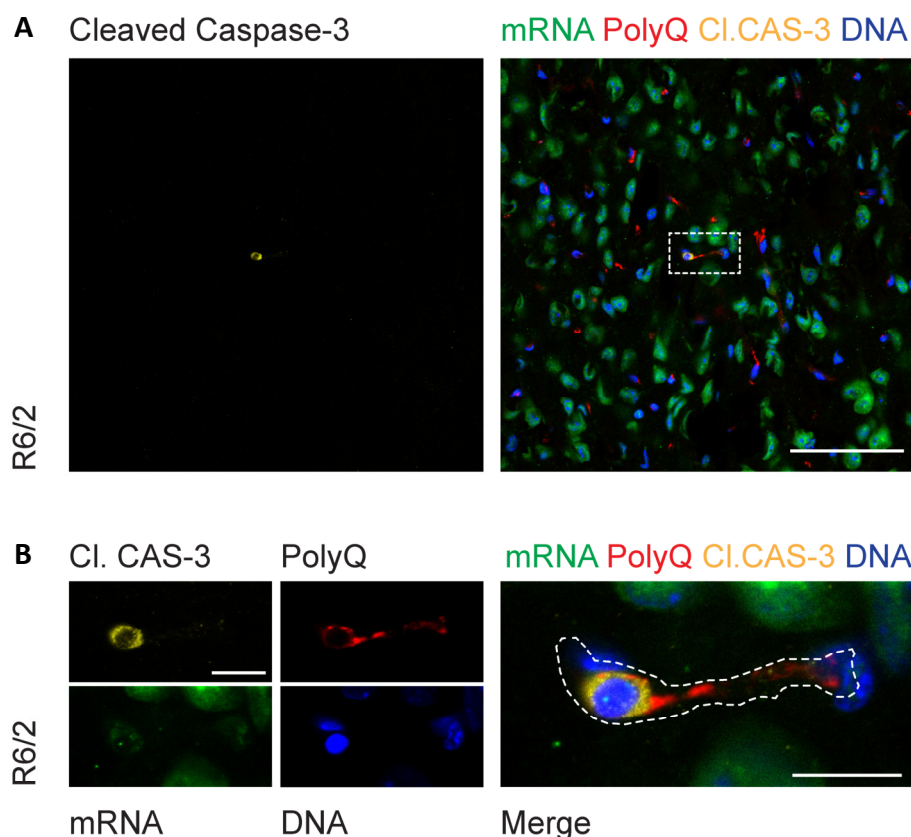


**Figure 82 |** Brain section from 9 week old R6/2 mouse stained for cleaved caspase-3 (cl.CAS-3, yellow), mRNA (polyA RNA, green), polyQ-expanded sequences (3B5H10, red), and nuclear DNA (DAPI, blue). **(A)** Overview over a brain section containing a single cleaved caspase-3 positive neuron. Scale bar length 50  $\mu$ m. **(B)** Magnification of the cleaved caspase-3 positive neuron marked in **(A)**. Scale bar length 10  $\mu$ m.

## Cytoplasmic mislocalization and aggregation of RNA exporter THOC2

The majority of mRNAs are transcribed by RNA polymerase II and undergo cotranscriptional processing in snRNPs (small nuclear ribonucleoprotein particles), before mature mRNAs are exported to the cytoplasm. Involved in processing and export are the exon-junction-complex (EJC) and the transcriptional export complex (TREX). TREX comprises the THO complex and numerous accessory factors (Chi 2013). One of the largest associated proteins is THOC2 (>180 kDa) with a disordered region of around 400 amino acids at its C-terminus (low complexity region, disorder predicted by IUPRed; Meszaros 2009). THOC2 has been identified as a major interactor of the  $\beta$  proteins in HEK293T cells and in murine primary neurons (Olzscha 2011, Woerner 2016).

Observing major mRNA distortions and mRNA accumulation in the nucleus, we became interested in the fate of THOC2 in cells with protein aggregation. In wildtype cells, the majority of THOC2 was distributed in the nuclear matrix. Similarly, in cells expressing nuclear  $\beta$  proteins, THOC2 was omitted from nuclear substructures, most likely nucleoli, as THOC2 surrounded the nuclear  $\beta$  protein aggregates.

However, in cells expressing cytoplasmic  $\beta$  proteins, THOC2 mislocalized to the cytoplasm, where it was partly distributed, and partly sequestered into  $\beta$  protein aggregates.

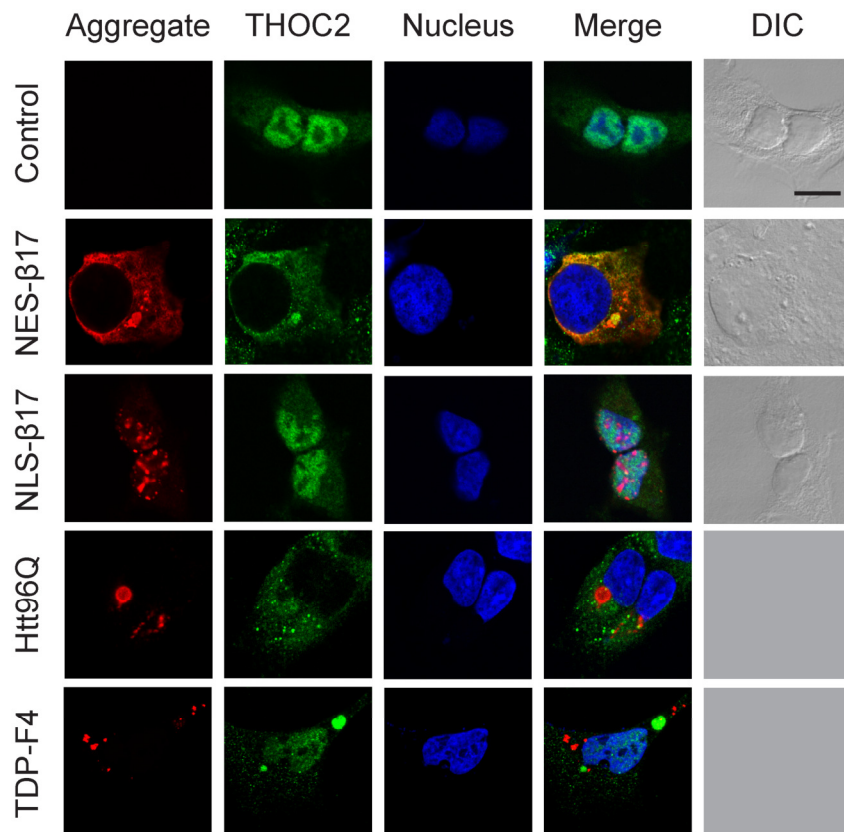


**Figure 83 | HEK293T cells labeled for the mRNA export protein THOC2 (green), which is a major factor of the transcriptional export (TREX) complex, in absence or presence of cytoplasmic or nuclear protein aggregates (red).** In control cells, THOC2 is distributed over the nuclear matrix, omitting certain substructures (supposedly nucleoli, see NLS- $\beta$ 17, with a wildtype-like distribution of THOC2). In cells expressing NES- $\beta$ 17 THOC2 was mislocalized to the cytoplasm and partially coaggregated with the  $\beta$  proteins. While THOC2 was also mislocalized to the cytoplasm in cells expressing Htt96Q and TDP-F4, here THOC2 formed separate inclusions in proximity to the aggregating proteins, contrary to the  $\beta$  proteins that directly recruited THOC2 into their own inclusions. Nuclear DNA stained with DAPI (blue). Representative images of 3 independent experiments. Scale bar length 10  $\mu$ M.



THOC2 likewise mislocalized to the cytoplasm of cells expressing Htt96Q or TDP-F4. Contrary to the  $\beta$  proteins, THOC2 now became sequestered into separate aggregates, distinct from the Htt96Q or TDP-F4 inclusions. Partly, a fraction of THOC2 remained nuclear, especially in case of TDP-F4. The mislocalization and aggregation of THOC2 occurred in all cases of nuclear mRNA retardation in presence of cytoplasmic protein aggregates, as described above.

In cells expressing cytoplasmic  $\beta$  proteins, Htt96Q, and in part TDP-F4, mislocalized THOC2 was obviously unable to (re-)enter the nucleus. This may either occur due to sequestration of THOC2 into misfolded low- or high-molecular-weight structures, or possibly, due to defects in nuclear import. Also nuclear mRNA processing and export proteins require a functional nuclear import on their own, at least once after their cytoplasmic synthesis, or continuously in case of shuttling factors.

Furthermore, cytoplasmic mislocalization of THOC2 was found in brains of R6/2 mice. Neurons that were recognized by antibodies against extended polyQ sequences (3B5H10) often contained cytoplasmic THOC2, which was missing at its natural nuclear localization.

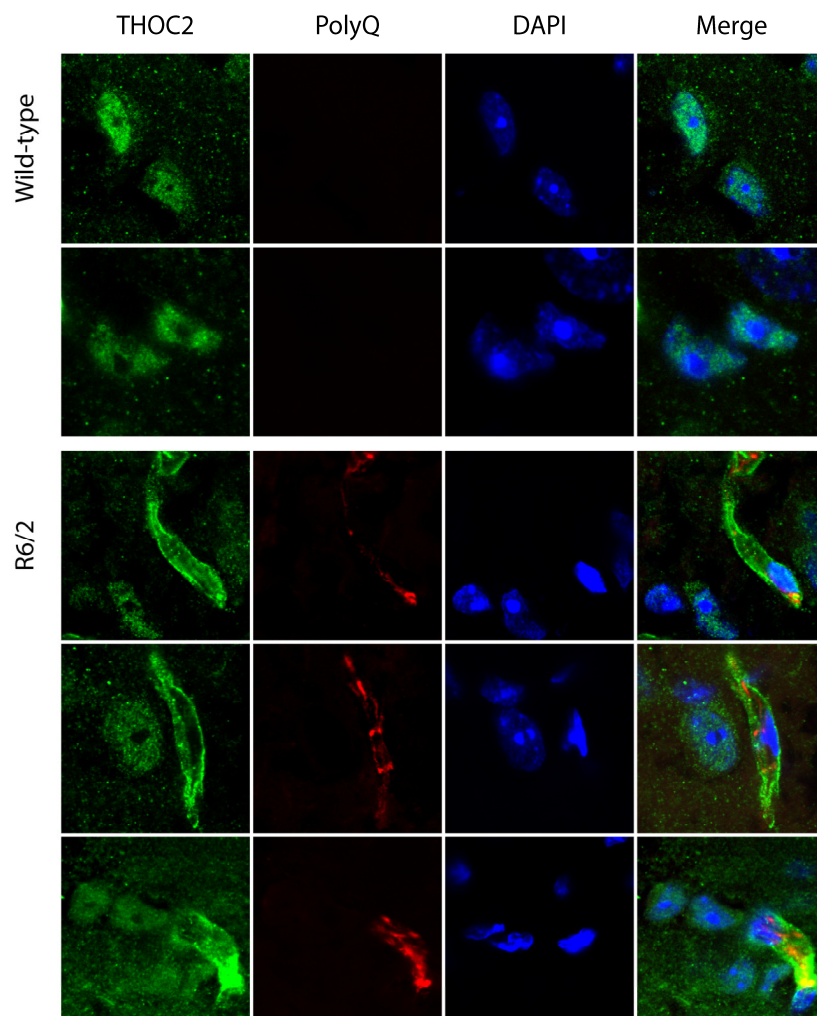


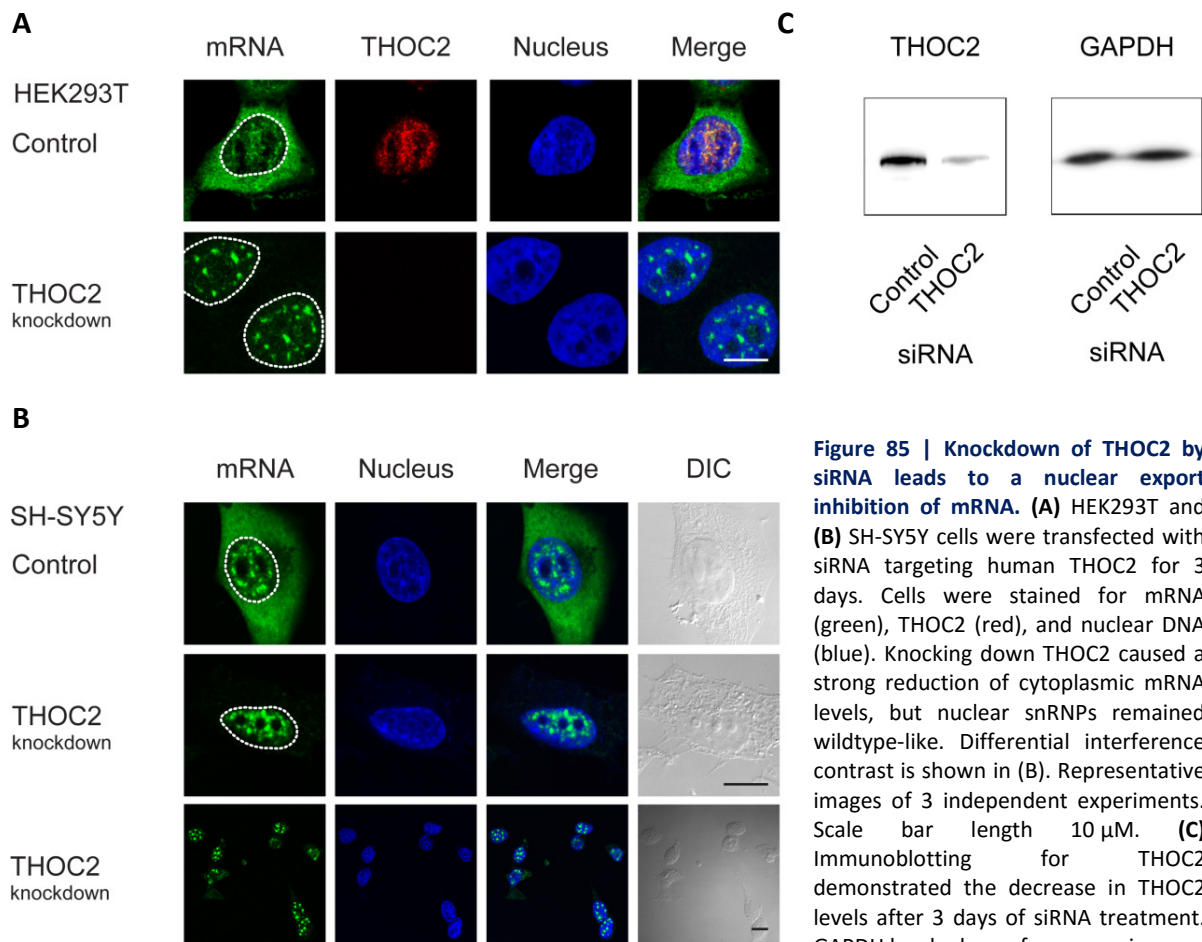
**Figure 84 | Brain sections of 9 week old wildtype and R6/2 mice were stained for THOC2 (green) with an antibody specific for extended polyQ sequences (3B5H10, red), and for nuclear DNA (blue). Neurons of R6/2 mice with visible aggregates often contain cytoplasmic THOC2, which is strongly enriched in the nuclei of unaffected cells. Representative images from 3 wildtype and 4 R6/2 mice.**

## siRNA-induced silencing of the transcriptional export complex protein THOC2

THOC2 is an essential protein of the transcriptional export complex (TREX). Inactivation of THOC2 e.g. through misfolding, mislocalization, or recruitment into aggregates likely causes severe mRNA processing and transport problems (Chi 2013). Therefore, we were interested in the phenotype of cells with low levels of functional THOC2.

3 days after transfection of siRNA targeting human THOC2, cellular THOC2 levels were decreased to  $13 \pm 3\%$  in HEK293T cells. At the same time, cytoplasmic mRNA levels vanished, while the nuclear mRNA speckles remained. Their size was comparable to snRNPs of wildtype cells (but significantly smaller compared to the protein aggregation-induced nuclear mRNA bodies; Figure 86).

However, silencing of THOC2 was sufficient to cause nuclear mRNA retention, resulting in a strong decrease of cytoplasmic mRNA levels. Control siRNA targeting firefly luciferase had no effect on cellular THOC2 levels or on mRNA distribution.



## Aggravated nuclear mRNA bodies in cells with pathogenic protein aggregation

The nuclear mRNA bodies observed in cells with cytoplasmic protein aggregation were of strongly increased size and brightness in comparison to wildtype or THOC2 siRNA-treated cells. This result suggests that the presence of toxic protein aggregates in the cytoplasm caused a more severe phenotype with a potentially different composition of the nuclear mRNA structures.

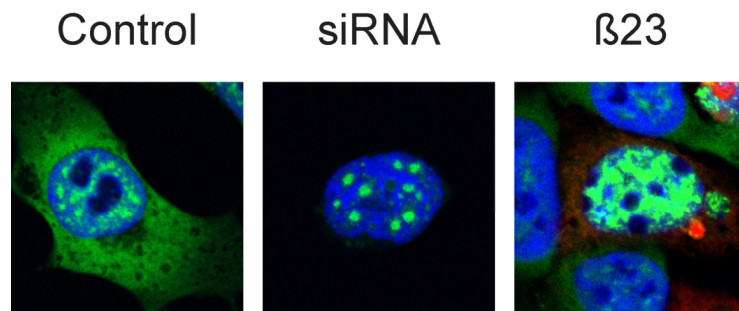


**Figure 86 | mRNA distribution (green) in SH-SY5Y cells transfected with empty control plasmids, siRNA against THOC2, or  $\beta$ 23-EGFP (red).** The mRNA is distributed over the cytoplasm and concentrated in nuclear snRNPs of control cells. The cytoplasmic mRNA vanished in cells lacking THOC2 or expressing  $\beta$ 23-EGFP. While the nuclear snRNPs in cells treated with siRNA against THOC2 appeared almost wildtype-like, size and brightness of the nuclear mRNA bodies were strongly increased in cells with protein aggregates.

Under selective knockdown of THOC2 by targeted siRNA, nuclear mRNA processing or cellular responses to missing mRNA export may still be functional. In the presence of toxic protein aggregation, additional defects such as insufficient processing of premature mRNAs or a disturbed nuclear RNA degradation may be an explanation for the increased size of the nuclear mRNA bodies. Associated (misfolded?) proteins might furthermore increase the volume of the nuclear mRNA bodies, e.g. RNA binding and processing proteins.

Sole nuclear mRNA export inhibitions might have different consequences for mRNA fate. The mRNA might be rapidly degraded, e.g. by the exosome, a nuclear quality control RNase (Houseley 2006). Or the mRNA may accumulate for longer times in the nucleus, accidentally or for temporal storage and subsequent export. Depending on the outcome, lowered or increased mRNA levels may be found.

To quantify the mRNA content of single cells, the complete mRNA fluorescence of was integrated (representing mainly nuclear mRNA in cells with cytoplasmic  $\beta$  protein aggregates) and compared to surrounding untransfected cells with a normal mRNA content and distribution. Compared to wildtype cells, the integrated mRNA fluorescence of cells expressing cytoplasmic  $\beta$  proteins roughly doubled. In addition, the mRNA content of cells expressing Htt96Q and TDP-F4 rose significantly (to ~160-175%; only cells with mRNA retention were analyzed for this quantification). Again, only a marginal increase in mRNA levels was found for cells expressing nuclear  $\beta$  proteins (~105-120%). The observed raise of cellular mRNA levels points towards a real, physical accumulation of mRNA in the nucleus. The mRNA was neither exported to the cytoplasm, nor immediately degraded in the nucleus. Protein misfolding and aggregation in the cytoplasm resulted in brightly fluorescent, nuclear bodies with substantially increased amounts of mRNA.

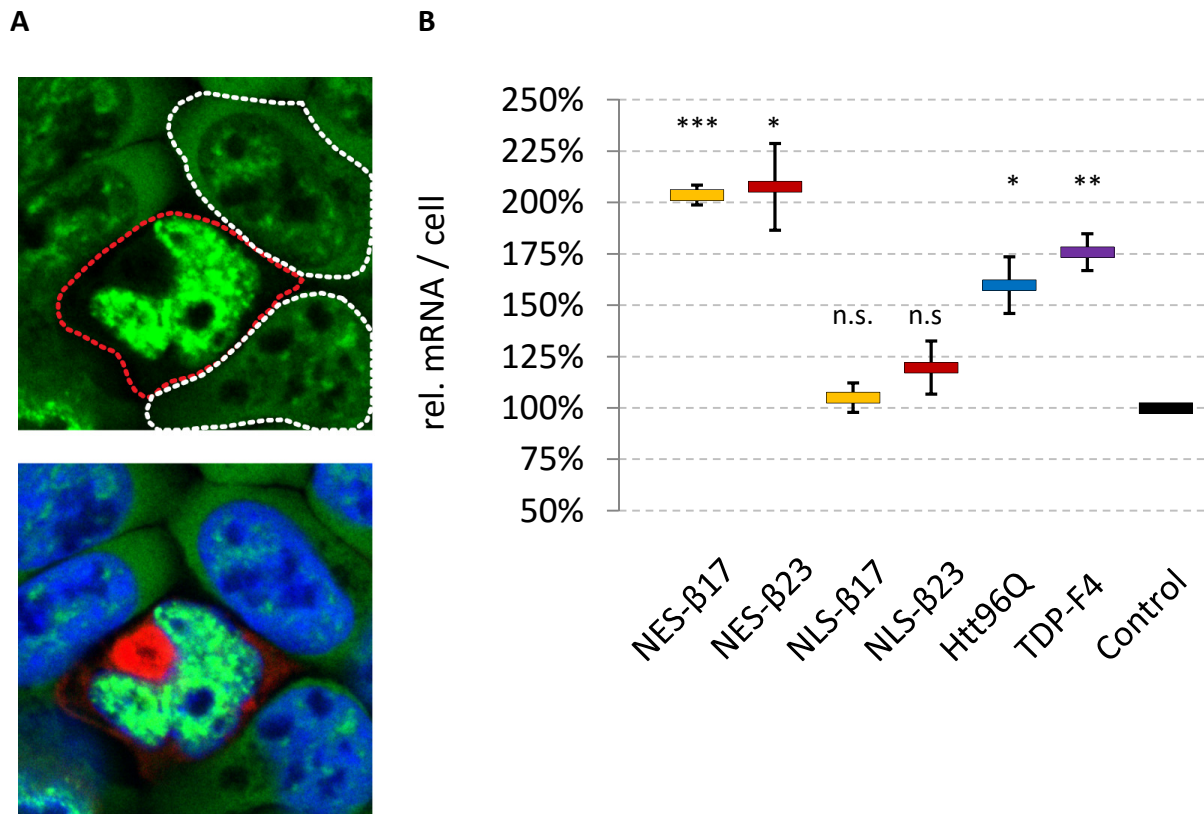


**Figure 87 | Single cell quantification of total mRNA.** (A) SH-SY5Y cells transfected with NES-β23 and stained for mRNA (polyA RNA, green), NES-β23 (c-Myc antibodies, red), and nuclear DNA (DAPI, blue) 24 h after transfection. The cellular polyA RNA fluorescence of cells with NES-β23 aggregates was integrated (red dashed line) and set in ratio to the integrated polyA RNA fluorescence of untransfected cells (white dashed lines) on the same focal area. (B) Quantification of total cellular mRNA content of single cells with the indicated protein aggregates and a nuclear mRNA accumulation phenotype, in relation to untransfected cells set to 100% ( $\geq 3$  independent experiments;  $n = 4-13$  cells, each). Cells with  $\beta$  proteins directed to the cytoplasm, Htt96Q, or TDP-F4 show an increase in cellular mRNA content, originating from an mRNA accumulation in the nucleus. Cells with nuclear  $\beta$  protein aggregates show no significant increase of cellular mRNA levels.

It would be highly interesting to analyze the RNA and protein content of the nuclear mRNA bodies in cells with cytoplasmic protein aggregates. A profound analysis of mRNA sequences may reveal functional and defective steps during mRNA processing. Especially mRNA splicing might be affected, while the polyA tail appeared to be synthesized due to the usage of a fluorescent poly(d)T probe. Identification of absent snRNP proteins or appearance of atypical factors should allow us to gain further insights into the mechanisms of nuclear mRNA body formation and associated cellular (dys-)functions.

## Cytoplasmic $\beta$ proteins inhibit the cellular protein synthesis

The loss of cytoplasmic mRNA should have immediate consequences on cellular protein synthesis. To examine the total translation, a  $^{35}\text{S}$ -Met pulse was performed in HEK293T cells. Methionine (Met) in newly synthesized proteins was labeled with the radioactive sulfur-35 isotope.

24 h after transfection with  $\beta$  proteins,  $\alpha\text{S824}$ , or empty plasmids, cells were treated with  $^{35}\text{S}$ -Met for 20 min, washed intensely with cold PBS (4°C), and lysed instantly. Cell lysates were separated by SDS-PAGE and evaluated by autoradiography and Coomassie Brilliant Blue staining. The incorporated  $^{35}\text{S}$ -Met reflected the relative amount of newly synthesized proteins during the pulse. Coomassie Brilliant Blue stained the total protein of the lysates. Expressing  $\beta$  proteins in the cytoplasm (NES- $\beta$ 17, NES- $\beta$ 23) drastically decreased the capacity of cells to synthesize new proteins, similar to  $\beta$ 23 without any targeting sequence (Olzscha 2011). Calculating with a transfection efficiency of 50%, the protein synthesis rate of cells expressing NES- $\beta$ 23 fell to 26% of control cells, and cells expressing NES- $\beta$ 17 reached a level of 50%. In contrast, the protein synthesis of cells expressing nuclear  $\beta$  proteins was only marginally decreased.

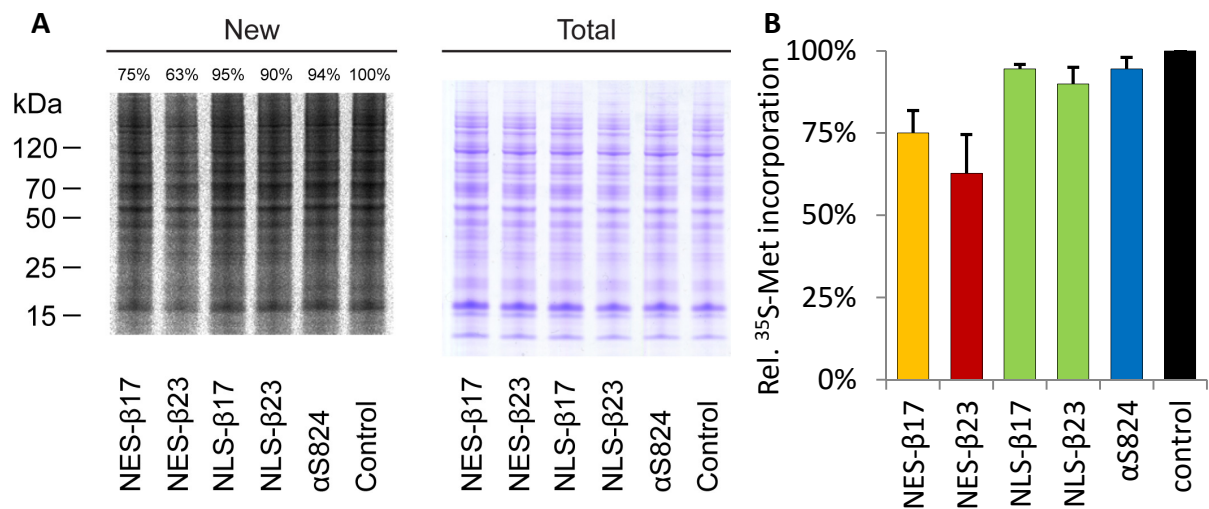


**Figure 88 | Inhibition of protein biosynthesis in presence of cytoplasmic aggregates.** (A) HEK293T cells were transfected with  $\beta$  proteins or control vectors. 24 h after transfection, cells were pulse-labelled with  $^{35}\text{S}$ -Met for 20 min. Cell lysates were analyzed by SDS PAGE, autoradiography, and Coomassie Brilliant Blue staining to detect newly synthesized proteins (left) and total proteins (right). (B) Quantification of relative  $^{35}\text{S}$ -Met incorporation from (A). Averages and SD from three independent experiments are shown. Only the cytoplasmic  $\beta$  proteins caused a significant decrease of protein translation.

The  $^{35}\text{S}$ -Met pulse experiments demonstrated that the general protein synthesis is strongly affected in cells expressing  $\beta$  proteins in the cytoplasm. Conversely,  $\beta$  proteins in the nucleus had only a minor impact. Defects in nuclear mRNA export and general nucleo-cytoplasmic transport inhibitions are therefore reflected in a strongly diminished protein synthesis rate. Consequently, cells become unresponsive towards external or internal signals and lose their capability of completing emergency responses to overcome stress situations.

## Translation initiation factors (eIFs) are trapped into cytoplasmic $\beta$ protein aggregates

In eukaryotes, enormous complexes of proteins come together with ribosomal subunits to form an elongation competent ribosome, making protein translation a highly complex and regulated process (Jackson 2010). Several protein translation initiation and elongation factors were found to interact with the  $\beta$  proteins in a co-immunoprecipitation experiment followed by a SILAC based mass spectrometric analysis (Olzscha 2011). The detected factors included subunits of the complexes eIF3, eIF4 and eEF1. Aberrant interactions with the  $\beta$  proteins might disturb their normal cellular activity or render them dysfunctional.

Immunocytochemistry and confocal fluorescence microscopy was applied to analyze possible interactions between the  $\beta$  proteins and translation initiation factors. HEK293T cells were labeled with antibodies for eIF3A and eIF4G. In control cells, the translation initiation factors uniformly distributed within the cytoplasm, as they did in cells expressing nuclear  $\beta$  proteins or  $\alpha$ S824. However, cytoplasmic  $\beta$  proteins partially coaggregated with the eIFs, especially NES- $\beta$ 17 and NES- $\beta$ 23. The only slightly toxic NES- $\beta$ 4 showed almost no colocalization with the two eIF proteins. Coaggregation of translation initiation factors as part of the cellular translation machinery may therefore contribute to toxicity and aggravate translational defects caused by nuclear mRNA retardation.

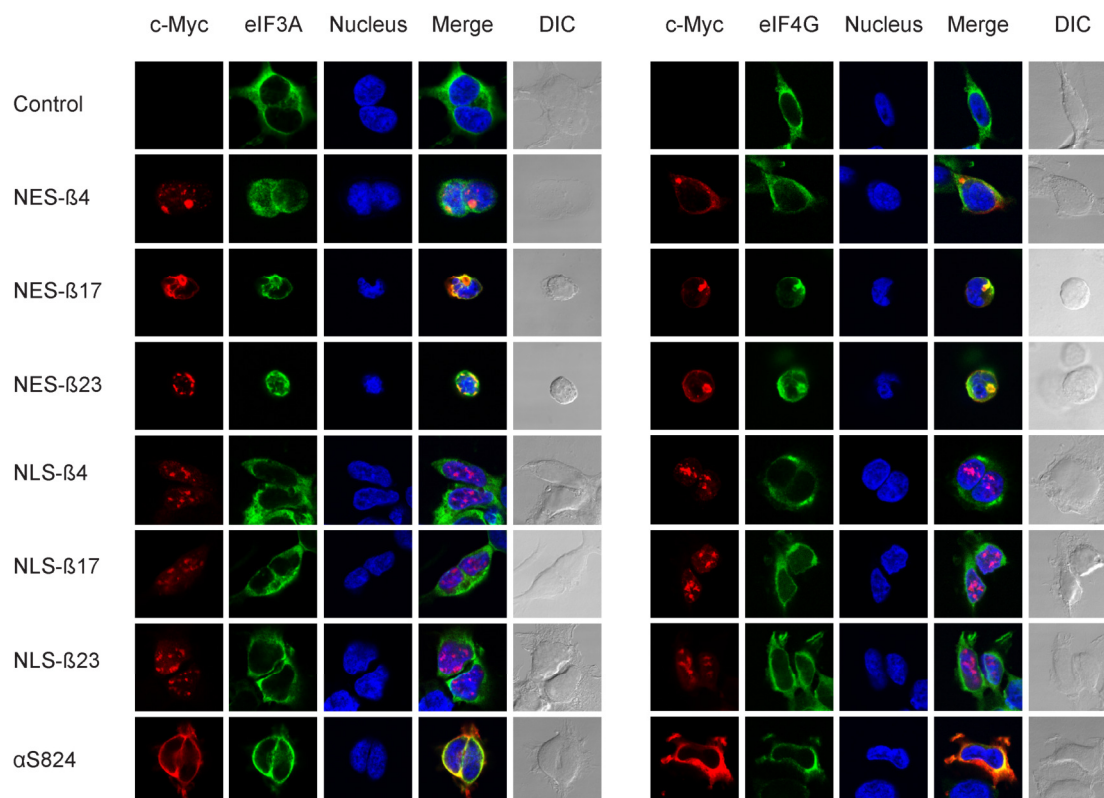


**Figure 89 | Eukaryotic translation initiation factors (eIF3A, eIF4G; green) interact and coaggregate with cytoplasmic  $\beta$  proteins NES- $\beta$ 17 and NES- $\beta$ 23 (red).** Neither the only slightly toxic NES- $\beta$ 4, nor the nuclear  $\beta$  proteins or  $\alpha$ S824 (red) disturbed the cytoplasmic homogenous distribution of eIF3A and eIF4G significantly. HEK293T cells were analysed 24 h after transfection with  $\beta$  proteins,  $\alpha$ S824, or empty vectors. Nuclear DNA was stained with DAPI (blue). Representative images of at least 3 independent experiments.

## Outlook: $\beta$ proteins targeted to mitochondria are toxic and cause mitochondrial swelling

To gain insights into mitochondrial proteostasis and the reaction of the organelles upon the appearance of local misfolding and aggregation,  $\beta$  proteins were fused to N-terminal mitochondrial targeting signals (originating from human COX8 or mitochondrial Hsp60, combined with a c-Myc sequence).

Mito- $\beta$ 4 and mito- $\beta$ 17 were successfully targeted to mitochondria. They appeared distributed over the mitochondrial matrix without visible aggregate formation.

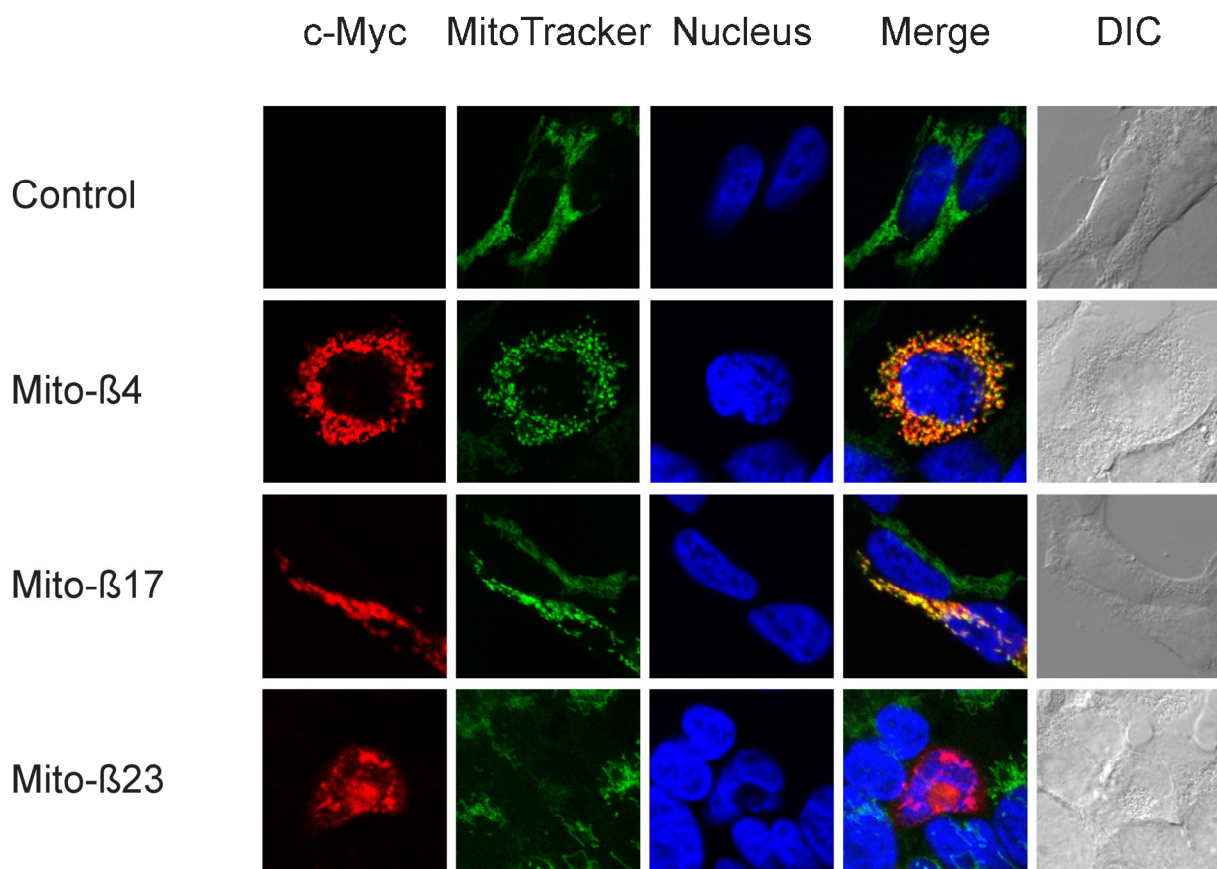


**Figure 90 |  $\beta$  proteins targeted into the mitochondrial matrix of HEK293T cells. Mitochondria were stained with fluorescent MitoTracker Red CMXRos that accumulates in living cells depending on their mitochondrial membrane potential.** Mito- $\beta$ 4 and mito- $\beta$ 17 were efficiently targeted to the mitochondria, which as consequence appeared swollen in size, forming visibly separated, highly fluorescent organelles (a phenotype described as “mitochondrial swelling”, typical for mitochondria initiating apoptosis/necrosis). In wildtype cells, a fine, interconnected mitochondrial network became apparent. Mito- $\beta$ 23 apparently formed cytoplasmic aggregates, whereby no mitochondria could be visualized by MitoTracker Red in these cells (24 h after transfection). The absence of mitochondria in these cells may suggest that mito- $\beta$ 23 already disrupted the organelles, potentially releasing their content to the cytoplasm, where the aggregation of  $\beta$ 23 proceeded. Representative images of 3 independent experiments.

Mitochondria were stained with the membrane potential dependent MitoTracker Red CMXRos. The dye stains mitochondria in living cells according to the physiological state of their mitochondria. While in wildtype cells mitochondria formed a fine tubular network, mitochondria were highly fluorescent, swollen in size and apparently rather separated from one another in cells expressing

mito- $\beta$ 4 or mito- $\beta$ 17. Such mitochondrial phenotypes have been known to occur under various forms of cellular stress (Blondin 1967), including high  $\text{Ca}^{2+}$  levels or increased amounts of reactive oxygen species. Swollen mitochondria are characteristic for cells undergoing apoptosis or necrosis. During the process of mitochondrial permeability transition, the mitochondrial inner membrane potential is rapidly lost due to an uncoupling channel. This channel is presumably formed by the c-subunit of the  $\text{F}_1\text{F}_0$  ATPase (Alavian 2014). Opening results in swollen, unconnected mitochondria with vanishing cristae, which consequently leads to cell death (Blondin 1967, Kim 2003).

Mito- $\beta$ 23 in contrast did not colocalize with mitochondria, but formed large cytoplasmic aggregates instead. Moreover, the membrane potential-dependent MitoTracker Red staining was entirely absent in cells expressing mito- $\beta$ 23 (24 h after transfection). Mito- $\beta$ 23 likely reached the mitochondria and caused their destruction already within this period (since the targeting of mito- $\beta$ 4 and mito- $\beta$ 17 was successful, and cytoplasmic/non-targeted  $\beta$ 23 did not cause obvious damage to mitochondria; see below). Mito- $\beta$ 23 aggregation might then have proceeded in the cytoplasm. Observing different time points of cells transfected with mito- $\beta$  proteins may be more conclusive.

However, targeting  $\beta$  proteins to mitochondria impaired cell viabilities in the classical sequence-dependent manner ( $\beta$ 23> $\beta$ 17> $\beta$ 4). Hence, the  $\beta$  proteins localized to mitochondria were harmful for cellular life and caused significant toxicity.

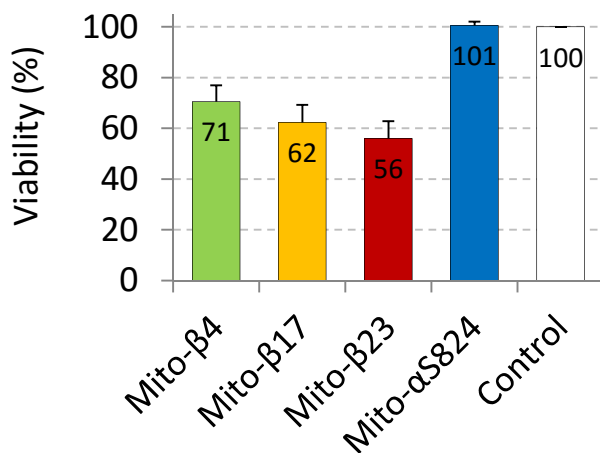


**Figure 91 | Viability of HEK293T cells expressing  $\beta$  proteins targeted to the mitochondrial matrix (here by fusion to the human mitochondrial-Hsp60 targeting sequence). Viability was determined by the capability of the cells to reduce MTT. Cells expressing  $\beta$  proteins fused to a COX8 mitochondrial targeting sequence showed equal phenotypes and similar toxicities. The relative, sequence-dependent toxicity of the  $\beta$  proteins remained preserved. Averages and SD from 4 independent experiments.**

Two mitochondrial interactors of the (non-targeted)  $\beta$  proteins were mitofilin (IMMT) and ChChd3 (Olzscha 2011). These proteins form a complex controlling and maintaining cristae formation. Upon downregulation of one of the proteins, mitochondria lose their morphology, cristae do not form any more, and mitochondria start to fragment (Darshi 2011, John 2005). Loss-of-function of these proteins results furthermore in mitochondrial swelling and dissociation of the mitochondrial network. A comparable phenotype was observed expressing mito- $\beta$ 4 or mito- $\beta$ 17. Deleterious interactions to these proteins might therefore contribute to the deleterious effects of  $\beta$  proteins targeted to the mitochondrial matrix. Deleterious interactions with mitochondrial proteins might happen in conjunction with or alternatively to the formation of the mitochondrial permeability transition pore.



However, expressing non-targeted  $\beta$  proteins aggregating in cytoplasm and nucleus did not cause any obvious deleterious effects to the mitochondria. Mitochondrial swelling was not observed, and mitochondrial morphology appeared wildtype-like.

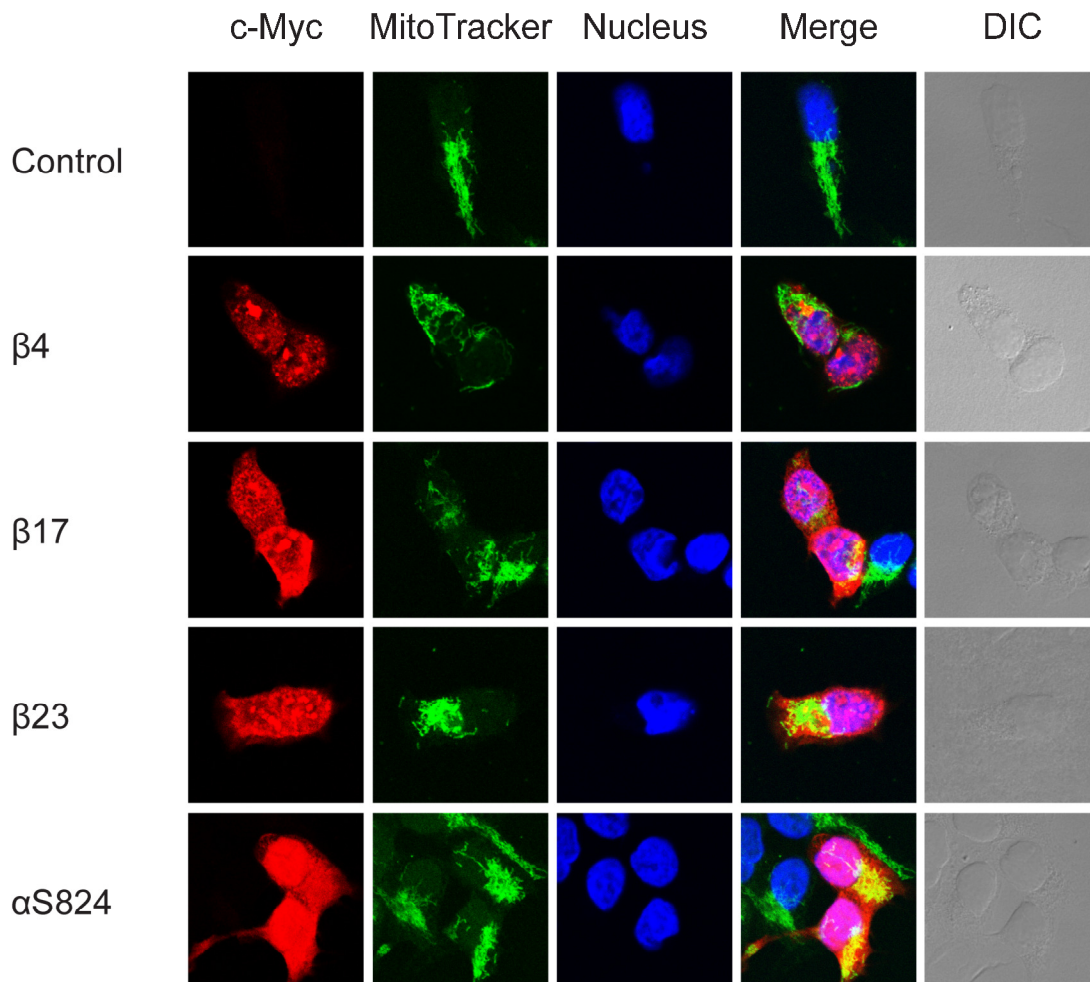


**Figure 92 |  $\beta$  proteins expressed in HEK293T cells, stained with the membrane potential dependent MitoTracker Red CMXRos.** Cells with  $\beta$  protein aggregates (red) showed a wildtype-like mitochondrial MitoTracker fluorescence (green), no mitochondrial swelling, but normal interconnected mitochondrial networks. Representative images of 3 independent experiments.

Targeting  $\beta$  proteins directly into the mitochondria increases the likelihood of interactions with local mitochondrial proteins, and thus to cause local damage. Most of the mitochondrial proteins are encoded in the nucleus and translocated into the mitochondrial matrix in an unfolded, chaperone-bound state (Hartl 1986, Hartl 1987, Neupert 2007). Non-targeted  $\beta$  proteins in the cytoplasm most likely interacted mainly with newly-synthesized mitochondrial proteins (Olzscha 2011), before these were able to reach the mitochondria. Immediate mitochondrial damage did not occur under these conditions.

# Discussion

## Rationally designed $\beta$ proteins are inherently toxic for cellular life

Rationally designed  $\beta$  proteins were expressed in *E. coli* (bacteria), *Saccharomyces cerevisiae* (yeast; as demonstrated by Matthias Antonin), HEK293T and SH-SY5Y cells (human neuronal precursor cells isolated from kidney (Shaw 2002, He 2010) and neuroblastoma cells), and in primary cortical neurons (mouse; experiments performed by Li Rebekah Feng). The  $\beta$  proteins formed inclusions and caused toxicity in all these organisms. The relative, sequence-dependent toxic impact was preserved over the different kingdoms of life ( $\beta_{23} > \beta_{17} > \beta_4$ ). The  $\beta$  proteins are no natural sequences, so that their proteotoxicity arises from their detrimental properties and interactions (toxic gain-of-function). When cellular proteins get recruited into  $\beta$  protein aggregates or otherwise lose their native functions, e.g. due to an imbalance in proteostasis, their absence certainly contributes to toxicity (secondary loss-of-function). The toxicity of the  $\beta$  proteins was not only maintained over the different life forms. Experiments on *E. coli* growth demonstrated furthermore that we could rationally modify the  $\beta$  protein sequences resulting in explainable effects on their toxicity. Mutations that disturbed oligomerization and fibril assembly significantly increased bacterial growth rates, while the addition of unpaired  $\beta$ -sheets offered “sticky” interaction surfaces and aggravated toxicity. The experiments confirm the notion that amyloid-like oligomer and fibril assembly impairs cellular life by general proteotoxic effects (e.g. Knowles 2014, Campioni 2010, Beerten 2012, Yang 2014 SciRep).

Purified  $\beta$  protein aggregates were added to the culture medium of HEK293T cells, where they caused toxicity from the extracellular space. Pretreatment by sonication may break extended fibrils and create oligomers with increased surface hydrophobicity (as demonstrated by ANS fluorescence). This observation is congruent with the idea that mature, growth-saturated fibrils behave rather inert inside as well as outside of cells, whereas small diffusible oligomers with unsaturated sticky surfaces are increasingly prone to erroneous interactions. Such interactions may also occur towards cellular membranes or membrane receptors, e.g. facilitating cellular uptake by endocytosis (Tomiya 2008, Haass 2007, Kaye 2003). We could show that the human prion receptor PrP<sup>C</sup> recognizes misfolded structures, such as the  $\beta$  proteins, A $\beta$ , or infectious prion proteins. Upon binding to extracellular sites, PrP<sup>C</sup> induced neurotoxic signaling leading to apoptosis (Resenberger 2011). While this very specific mechanism may also owe protective functions, many other unspecific interactions may induce erroneous signaling and thereby disturb the cellular homeostasis.

$\beta$  proteins targeted to the mitochondrial matrix or the endoplasmic reticulum (ER; Lisa Vincenz-Donnelly; Dolfe 2016) were toxic despite no visible aggregate formation. The  $\beta$  proteins may be held soluble by binding to factors, such as BRICHOS in the ER (Dolfe 2016). Nonetheless, vital functions were affected. Mitochondria fragmented and seemed to initiate apoptosis. Whether toxicity arose mainly through an overload of specific chaperones or other detrimental interactions, remains to be elucidated. Misfolded structures were toxic in all these compartments – but significantly less in the nucleus.

## $\beta$ proteins structurally resemble natural amyloid proteins

The  $\beta$  proteins were rationally designed to fold into  $\beta$ -sheet conformations by their polar-hydrophobic side-chain pattern. Indeed, they assembled into fibrils *in vitro* independently of their exact amino acid sequence (West 1999).

Purified from *E. coli* inclusion bodies in a denatured state, the  $\beta$  proteins reassembled in a physiological solution (salt, pH) into amyloid-like fibrils (Knowles 2014, Balbach 2002, Fowler 2007, Lindgren 2005). Electron microscopy demonstrated fibrils of several 100 nm length and around 3 nm in diameter. Especially  $\beta$ 23 assembled into spherical oligomers, potentially highly toxic structures in and on cells (Chiti 2006, Haass 2007, Tomiyama 2008). Higher order fibrils occurred increasingly under mildly acidic conditions, which counterbalanced the overall negative net charge of the  $\beta$  sequences. In highly crowded cells, this negative net charge may be compensated by surrounding biomolecules and ions, causing their sequestration into aggregates.

$\beta$ -sheet structure and amyloid-like nature of purified and reassembled  $\beta$  protein fibrils were demonstrated by their spectroscopic properties. The CD-spectroscopic analysis revealed that the polypeptide chains were folded into  $\beta$ -sheet structures. Up to 30% of the sequence may be rather unstructured, which represents a significant deviation from the design. However, it appears unlikely that a library of artificial sequences folds completely into a desired secondary structure, especially since the intramolecular complementarity of individual residues was not included in the design (West 1999). Non-complementary residues cause steric hindrances in the inner core of the  $\beta$  proteins, which may lay the foundation for the unstructured regions and potentially for cellular toxicity. If all hydrophobic residues were perfectly packed into the inner core of a six-stranded  $\beta$  protein monomer, the  $\beta$  proteins might still assemble into fibrils through hydrophobic interactions on the front and back surface of a monomer. However, such fibrils may behave rather inert within living cells. Completely surrounded by shielding polar residues, fibrils should not be very prone to engage in unspecific interactions (Mannini 2014, Bolognesi 2010, Beerten 2012, Sant'Anna 2014, Calamai 2003, Lazaridis 2013).

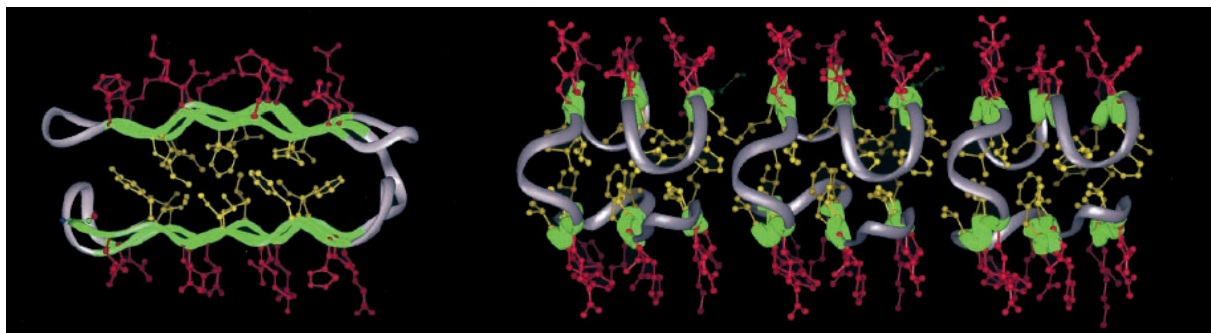


**Figure 93 | Schematic representation of an “ideal”  $\beta$  protein monomer, folded into a flat six-stranded  $\beta$ -sheet protein (left). The hydrophobic side chains (yellow) are perfectly packed into the interior, presenting open hydrophobic surfaces only on the front and back surfaces. Three  $\beta$  proteins monomers (turned by 90°, right) assemble into an amyloid-like fibril via their open hydrophobic surfaces. Only polar residues (red) remain on the surface. The structural model represents an ideal six-stranded  $\beta$ -sheet protein with a perfectly complementary hydrophobic core. In reality, the individual residues may not be matched so perfectly, resulting in structural deviations, such as partly twisted  $\beta$ -sheets or hydrophobic side-chains protruding to the surface of oligomeric or fibrillary assemblies. Such deviations may increasingly engage in aberrant interactions with metastable or unfolded proteins in the cell (figure adapted from Wang 2002).**

Cellular proteins may cover imperfections in the  $\beta$ -sheet design (hydrophobic and flexible surfaces), so that metastable or not fully folded proteins are sequestered in a misfolded state. They may expose sticky surfaces on their own and recruit other cellular proteins into the now growing aggregates. Indeed, hydrophobic side chains of  $\beta$ 23 occupied the highest volume, and ANS fluorescence revealed the largest hydrophobic surface patches on the most toxic among the  $\beta$  sequences. Structural deviations from the optimal cross- $\beta$ -sheet template may also influence the formation and stability of oligomers. They may arise from sudden ruptures in fibril growth or fibril truncations, or follow off-the-road pathways to fibril assembly. Also here, especially  $\beta$ 23 formed stable spherical oligomers from purified protein *in vitro*.

FTIR spectroscopy on the  $\beta$  proteins confirmed the presence of  $\beta$ -sheet structures in an antiparallel arrangement. The global maximum of the Amide I band revealed flat cross- $\beta$ -sheet structures, in contrast to rather twisted  $\beta$ -sheets occurring in many native proteins. The flat alignment of the  $\beta$ -sheets allows growth into continuous, linear fibrils. Detailed structures of spherical oligomeric assemblies as detected in the electron micrographs of  $\beta$ 23 remain to be elucidated. However, the spectroscopic properties indicated high  $\beta$ -sheet contents in the overall populations of *in vitro* refolded  $\beta$  proteins, including the oligomers.

Further evidence for the amyloid-like nature of the  $\beta$  protein assemblies came from their binding of amyloid-specific dyes, such as Thioflavin T, NIAD-4, and Congo Red. Thioflavin T and ANS allowed us to study the refolding of the  $\beta$  protein assemblies *in vitro* after dilution from denaturant (8 M guanidine). From denaturant, all three  $\beta$  proteins re-aggregated very rapidly into growing fibrils. The six-stranded  $\beta$ -sheet proteins fold most likely in an antiparallel orientation and form mostly short-ranging interactions, which allows similar  $\beta$ -sheet domains to fold within milliseconds (de Alba 1999, Kuwata 2001). This initial nucleation phase could not be followed by the applied methods of this study. Contrary to disease-related amyloid proteins, the  $\beta$  protein monomers directly fold into  $\beta$ -sheet rich conformations, and then oligomerize via their major hydrophobic surfaces. Monomers as building blocks of amyloid fibers appear therefore in a high concentration very rapidly, resulting in very fast fibril assembly (Thioflavin T, NIAD-4 binding). On electron micrographs, oligomers and short (proto-)fibrils appeared within minutes, but matured into longer amyloid fibrils over several hours.

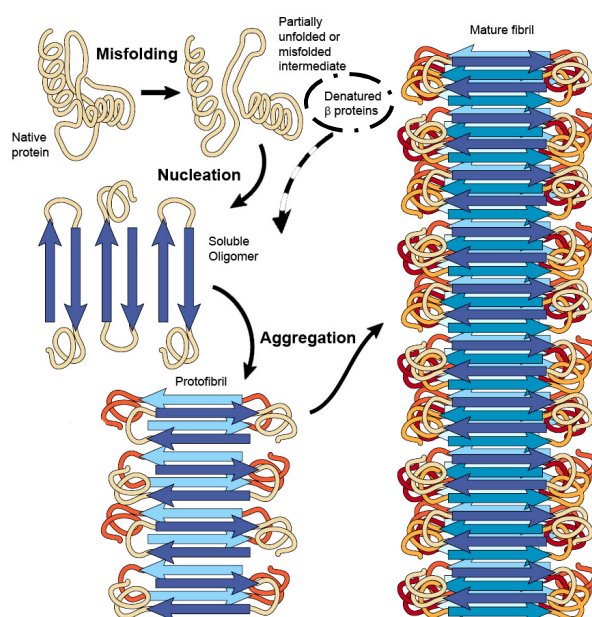


**Figure 94 | Process of protein aggregation leading through misfolding of native structures to nucleation, creating soluble on- or off-pathway oligomers. Some oligomers transform into smaller, ordered protofibrils, and consequently mature into bundled amyloid fibers.** The  $\beta$  proteins were designed to fold into amyloid-like  $\beta$ -sheet structures. They folded in a high concentration from an unfolded state (in guanidine) directly into a  $\beta$ -sheet rich conformation (the “native state” of the  $\beta$  protein monomers), likely similar to the structures present in soluble oligomers and protofibrils. Thus, they omit the usually extended nucleation time of functional cellular proteins, required for misfolding and oligomerization (figure adapted from Soto 2003).

## Hydrophobic surfaces, conformational flexibility, and low-molecular-weight structures correlate with cellular toxicity

Cerebral fibrils were recognized as the visible hallmarks of neurodegenerative diseases more than a century ago (Alzheimer 1907/1995). Meanwhile, molecular analyses demonstrated that most of these fibrils consist of one or a few major protein components, which may recruit further biomolecules into growing inclusions. It is generally expected that most sequences are in principle able to fold into stable cross- $\beta$ -sheet conformations (Dobson 2003, Hartl 2009). However, only a restricted set of proteins is associated with human misfolding diseases, while thousands of cellular proteins are synthesized, folded, and degraded without major problems. This raises questions about specific physicochemical and structural properties of such disease-related proteins, as well as of their interactors.

Toxicity caused by the  $\beta$  proteins correlated very well with their Thioflavin T and NIAD-4 binding *in vitro*, whereas the aggregation kinetics were equal for the three sequences. Thioflavin T supposedly forms tiny micelles that change their fluorescence properties upon binding to repetitive patterns along cross- $\beta$ -sheet fibrils (Khurana 2005, Krebs 2005, Biancalà 2010). High Thioflavin T and NIAD-4 fluorescence may relate to high binding affinities or to increased fibril formation of the highly toxic  $\beta$  proteins. However, quantifying insoluble fractions from cell lysates did not indicate quantitative differences regarding aggregate formation *in vivo* (Olzscha 2011). Electron micrographs rather suggested an increase in oligomeric structures by the most toxic  $\beta$ 23. As Thioflavin T is expected to bind along grooves parallel to the cross- $\beta$ -sheet axis, these grooves may occur in a more regular manner in the highly toxic  $\beta$  protein assemblies. The binding grooves of  $\beta$ 4 may be slightly distorted, a possibility supported by small deviations of the  $\beta$ 4 CD and FTIR spectra from ideal  $\beta$ -sheet spectra. NIAD-4 was developed for specifically binding A $\beta$  and other amyloid structures. The chemical structure of NIAD-4 (aromatic rings, aliphatic hydrocarbons) and its ability to cross the blood-brain barrier suggest that hydrophobic interactions may influence (increase) NIAD-4 binding, too. To interpret the relative differences of Thioflavin T and NIAD-4 binding regarding structural properties on proteotoxicity, high-resolution structures and more knowledge about the binding sites of the dyes would be helpful.

*In vivo*, the differential binding of NIAD-4 to cytoplasmic and nuclear  $\beta$  protein aggregates suggests structural alterations between the  $\beta$  proteins in the two compartments. Conformational differences may include a different degree of order within the amyloid core or different amounts of exposed hydrophobicity. Sequestration of cellular proteins may contribute to the NIAD-4 binding of amyloid fibrils in cells. The cytoplasmic aggregates proposedly sequester significantly more misfolded proteins into their structures (such as importin  $\alpha$ , THOC2, NF- $\kappa$ B, luciferase-EGFP, and others), while the nuclear  $\beta$  protein aggregates appeared rather protected from aberrant cellular interactions. Molecular shielding might further decrease the NIAD-4 binding e.g. through covering of binding sites on the amyloid fibers.

Low-molecular-weight oligomers formed by misfolded proteins are suspected to be highly detrimental. Protofibrils and spherical oligomers were detected on electron micrographs and by the A11 antibody. A11 was originally raised against an A $\beta$  fragment presenting oligomeric A $\beta$  epitopes. Interestingly, A11 recognizes specifically the oligomeric species of very different amyloid-associated proteins (Kayed 2003, Kaye 2006, Mamikonyan 2007). Extracts from human cells expressing  $\beta$  proteins were A11 reactive (Olzscha 2011), and  $\beta$  proteins refolded *in vitro* formed prefibrillar

species recognized by A11. Spherical oligomers were mainly visible on electron micrographs of  $\beta$ 23. The A11 reactivity was highly comparable between  $\beta$ 4,  $\beta$ 17, and  $\beta$ 23. Here, A11 may also have recognized short protofibrillar structures, which were visible on the electron micrographs of all  $\beta$  proteins.

Interesting results were achieved by size exclusion chromatography of lysates from HEK293T cells expressing cytoplasmic or nuclear  $\beta$  proteins, and the solubility analysis by sedimentation. Distributed low- to intermediate-molecular-weight oligomers were predominantly found in the cytoplasm with sizes of several hundred kilodaltons. An analysis of their composition may be especially interesting, since these highly mobile oligomers potentially interact with numerous cytoplasmic proteins of distinct properties. In the nucleus, most of the  $\beta$  proteins were sequestered in immobile megadalton structures. Whether these structures form by self-association or under the stringent control of cellular factors (such as NPM-1 or chaperones) remains to be explored further.

Soluble protein oligomers were described for many neurodegenerative and other protein misfolding diseases. Oligomeric particles were observed in affected tissues or forming *in vitro* (Ferreira 2008). The ability of oligomer-specific antibodies to neutralize toxicity in cell culture experiments speaks strongly for a pathogenicity of the soluble misfolded oligomers. Moreover, such sequence-independent antibodies potentially describe a general, common, hazardous protein backbone conformation that appears to be linked to proteotoxicity (Kayed 2003). In the case of Alzheimer's disease, various studies on patients and on *in vitro* assembled oligomers demonstrated their adverse effects on synaptic plasticity and neuronal function. In a group of Japanese patients, a mutation (APP E693 $\Delta$ , A $\beta$  E22 $\Delta$ ) caused enhanced oligomerization and prevented fibril formation. Even though the secretion of A $\beta$  was markedly reduced, these patients suffered from Alzheimer's-type dementia, and the mutant peptide inhibited hippocampal long-term potentiation in rats (Tomiyama 2008). The "arctic mutation" (APP E693G) strongly enhances oligomerization and causes familial AD (Nilsberth 2001).

Toxicity of oligomers may be based on their conformational dynamics, cellular mobility, or their interactive surfaces (Haass 2007, Campioni 2010, Miller 2011). The appearance of soluble A $\beta$  oligomers correlated in various studies much better with disease progression than of amyloid fibrils, which could not always be unambiguously related to dementia (Lue 1999, Haass 2007). While this does not relieve large fibers from any pathogenic influence, the results of this and other studies strongly suggest an increased hazardousness of small dynamic oligomers in cells.

The three  $\beta$  proteins showed very similar ANS binding kinetics during refolding. ANS fluorescence intensity and blueshift correlated positively with toxicity and is in general related to aggregation propensity (Chiti 2006), indicating the highly hydrophobic environment the  $\beta$  proteins exposed to their surroundings. Hydrophobic patches were not completely buried inside the fibrils, but remained partially exposed. For  $\beta$ 23, the ANS fluorescence was higher than for rhodanese or the extremely slowly folding MBP double mutant, refolding from denaturant in absence of GroEL. Harmful hydrophobic surface patches may aggravate with an increased occurrence of the highly flexible hydrophobic side-chain isoleucine in the sequence of  $\beta$ 23 (see Table 1).  $\beta$ 4,  $\beta$ 17, and  $\beta$ 23 hardly vary regarding their number of aromatic residues (1 Tyr, 3 Phe; 2 His in  $\beta$ 17 and  $\beta$ 23). Formation of aromatic moieties may increase the "stickiness" of misfolded structures, due to their hydrophobicity and repetitive  $\pi$ -stacking interactions (as in double stranded DNA; Bemporad 2006, Gazit 2005). The  $\beta$  proteins offer an interesting basis for a more sophisticated mutational analysis to correlate structural details to general proteotoxicity.

Uncovered hydrophobic surfaces likely engage in cellular interactions with (partially) unfolded or misfolded proteins. Occurring in a limited number, such ANS positive patches can be shielded by cellular chaperones. Hsp110 increasingly recognized the more toxic  $\beta$  proteins offering more ANS binding sites, even in absence of additional co-factors (Hsp70/40). Hydrophobic stretches play an important role in substrate recognition of the closely related Hsp70 (Rudiger 1997, Polier 2010). When misfolded proteins with hydrophobic surfaces occur persistently in large amounts, chaperones become increasingly recruited to sites of misfolding. In pathologic cases, this may initiate a vicious cycle overloading the cellular chaperone capacity, which eventually might lead to proteostasis collapse. Surface accessible hydrophobicity on the  $\beta$  proteins strongly correlated with their toxicity, and may thus represent a major structural origin of the toxic gain-of-function of misfolded proteins.

Structural analyses of the purified  $\beta$  proteins refolded *in vitro* identified hydrophobic surface patches and a high aggregation propensity (in terms of amyloid marker binding) as the major determinants correlating to *in vivo* toxicity. Unstructured regions, even though enriched in  $\beta$  protein interactors (Olzscha 2011), and conformational flexibility remain rather unaddressed for the  $\beta$  proteins so far. Experiments detecting hydrogen exchange (by mass spectrometry, FTIR, or NMR) or spin relaxation measurements (by NMR) may allow insights into structural dynamics of the different  $\beta$  protein sequences and structural assemblies (Konrat 2014).

So what are the major risk factors of misfolded sequences for causing toxicity in cells? Our studies on the  $\beta$  proteins and their interactors as well as other studies on protein aggregation suggest that exceeding certain thresholds of hydrophobicity on the surface of proteins in combination with an overall conformational flexibility of the native state enables proteins to convert from native to misfolded states with a stable, mostly hydrophobic core. Polar zippers of extended polyglutamine sequences or the yeast prion Ure2p are examples for hydrophilic cores in amyloid fibrils, too (Perutz 1994, Chan 2005). Stable fibril cores surrounded by flexible tails may then support stable but non-native interactions e.g. via induced fit(-like) mechanisms (Koshland 1958) to a broader range of cellular interactors that become sequestered into the inclusions. While one or a few major protein components mostly form the fundament of such aggregates, sequestered cellular proteins subsequently lose their native functions and aggravate the aggregation process on their own.

Agreeing with the fact that  $\beta$  protein interactors were not especially hydrophobic overall (Olzscha 2011), a certain length of continuous hydrophobicity may be enough to form a stable aggregation core, even though the rest of the sequence contains less hydrophobicity (Sawaya 2007). The total hydrophobicity may therefore not be very conclusive, but rather its concentration at specific sites together with dynamics and physicochemical properties of surrounding side-chains (Goldschmidt 2010, Beerten 2012). Hydrophobicity should mainly stabilize non-native cellular interactions, while conformational flexibility promotes the “kinetic energy” to expose such hydrophobic patches. Structural flexibility facilitates the evolution of protein function and arises from a complex balance act between several evolutionary pressures (Bloom 2004). Experiments on different types of HypF-N oligomers directly support the hazardous nature of combining hydrophobicity with flexibility, strengthening “structural flexibility and hydrophobic exposure” as the “primary determinants [] to cause cellular dysfunctions” (Campioni 2010).

“Proteins comprise of a general toxic potential” is the conclusion emerging from these studies. Evolution limited hazardous sequences and conformations, strongly restricting the available sequence space for cellular life. Examples include alternating polar-hydrophobic side-chains (Broome

2000) and steric complementary zippers (Goldschmidt 2010), typical properties supporting amyloid formation. Hazardous conformations may however come to the surface in an aging population that was never subject to evolution before, in cases of sporadic missense mutations that continuously appear, or under the general influence of stressors of the cellular proteostasis (such as chemical toxins or irradiation).

## Aggregation and toxicity in cytoplasm and nucleus

$\beta$  proteins without cellular targeting signals formed cytoplasmic and nuclear inclusions; none of those were associated with mitochondria or the secretory pathway. 100-150 metastable proteins enriched in disordered regions preferentially interacted with these  $\beta$  proteins (Olzscha 2011). The selection of interactors raises questions about each individual's contribution to the overall toxicity in cells. Sequestration of non-essential proteins may cause toxicity only under specific conditions, if at all. Recruitment into aggregates may not necessarily affect the cellular level of functional proteins, or only to a non-harmful degree. So which pathways and functions are seriously affected?

Cytoplasm and nucleus are connected through selective pores permeable for most ions, metabolites, and proteins below 30-40 kDa (Mohr 2009). The two compartments fulfill very distinct cellular functions and contain adapted proteostasis machineries. Many components have been described, partly in high detail, but their complex interplay and further functions are still under investigation, especially for the nucleus (Kim 2013). To increase our understanding of nuclear and cytoplasmic proteostasis, we directed the  $\beta$  proteins specifically into the two compartments. Cytoplasmic  $\beta$  proteins aggregated in juxtannuclear spherical inclusions surrounded by distributed oligomers. In the nucleus, several larger, morphologically irregular aggregates were confined to the nucleoli and associated to NPM-1. The three human disease-associated proteins Htt96Q, TDP-F4, and Parkin $\Delta$ C formed mainly spherical, juxtannuclear inclusion in the cytoplasm, accompanied by several smaller aggregates. Even when fused to a nuclear localization sequence, Htt96Q aggregated already in the cytoplasm in HEK293T and SH-SY5Y cells. On the contrary, Htt96Q without targeting sequence formed nuclear inclusions in murine neurons. Here, Htt96Q fragments may have been actively transported into the neuronal nucleus as a protective mechanism (Park 2013), demonstrating the variability and specificity of handling misfolded structures by different cell types.

Strikingly, all cytoplasmic protein aggregates caused an aggregation of FG-repeat proteins (residing at the interior lining of the nuclear pore complex (NPC)). Either the NPC proteins were sequestered into the  $\beta$  protein aggregates, or they aggregated separately next to cytoplasmic inclusions of Htt96Q, TDP-F4, or Parkin $\Delta$ C. The fluorescence intensity around the nuclear envelope decreased significantly, indicating a real loss of functional proteins. The nuclear  $\beta$  proteins in contrast had no visible influence on NPC proteins, and the nuclear morphology appeared wildtype-like. Nuclear envelope and chromatin structure was often disturbed by cytoplasmic aggregation. Irregularities of nuclear pores and NPC proteins were previously reported for cells expressing extended polyglutamine proteins and on biopsies of Alzheimer's patients (Suhr 2001, Sheffield 2006). Interfering with the nuclear pores might be especially harmful in view of the findings that a part of the NPC proteins are extremely long-lived and insufficiently replaced after cell differentiation. Functional NPC levels indeed decrease during aging, which may lie behind an age-dependent deterioration of nucleo-cytoplasmic transport (Toyama 2013). These initial findings attracted our attention to study the nucleo-cytoplasmic transport in presence of misfolding and aggregation in the two respective compartments.



## **Inhibition of NF- $\kappa$ B by cytoplasmic protein aggregation may shift the balance between neuronal life and death**

We studied active nucleo-cytoplasmic transport on three different substrates: the transcription factor NF- $\kappa$ B, the general transport model S-GFP, and messenger RNA. In all cases examined here, cytoplasmic misfolding and aggregation generated severe transport inefficiencies in and out of the nucleus, whereas nuclear  $\beta$  proteins remained unreactive and caused virtually no disturbances.

NF- $\kappa$ B is a ubiquitous transcription factor present in practically all cell types and tissues. NF- $\kappa$ B is widely known for its central role in immune cells, in the inflammatory response, in developmental processes, and for its influence on the balance between survival and apoptosis (Oeckinghaus 2011, Sen 2011).

In neurons, NF- $\kappa$ B reportedly plays a role in neuronal plasticity, long-term memory formation, neuronal development, and survival. Brain-specific activators including glutamate (via both AMPA/KA and NMDA receptors) and neurotrophins point towards an involvement of NF- $\kappa$ B in synaptic plasticity. NF- $\kappa$ B (p50  $-/-$ ) knockout mice had low learning abilities and were sensitive to neurotoxins (O'Mahony 2006, Kaltschmidt 2009, O'Neill 1997). "NF- $\kappa$ B can therefore be considered as one of the most important transcription factors characterized in brain to date and it might be as crucial for neuronal and glial cell function as it is for immune cells" (O'Neill 1997). The deep involvement of NF- $\kappa$ B signaling in neuronal processes described over the past decade highlights the importance of effective NF- $\kappa$ B activation. Transcriptional regulation requires its translocation from cytoplasm (including distant parts of neurites) into the nucleus – for learning, long-term memory, neuronal plasticity, and, strongly connected to all that, neuronal survival (Salles 2014).

As long as being functional, NF- $\kappa$ B signaling induced by e.g. A $\beta$  complexes leads to neuronal protection and enhanced cell survival, however only in early disease states. In contrast to that, missing activation of NF- $\kappa$ B sensitized cells towards apoptosis, e.g. in knockout animals or inhibited model systems (O'Neill 1997). Thus, it may behave similarly in neurons of AD patients.

NF- $\kappa$ B signaling is mainly regulated by binding to inhibitor  $\kappa$ B (I $\kappa$ B) and upstream signaling arriving at the I $\kappa$ B kinase complex in conjunction with the NF- $\kappa$ B essential modulator (IKK/NEMO). NF- $\kappa$ B resides in its inhibited state in the cytoplasm, in neurites and synapses. NF- $\kappa$ B contains an NLS and a DNA binding site, which are both covered by complexing with I $\kappa$ B. Steps of activation e.g. by TNF $\alpha$  through the TNF receptor include phosphorylation and ubiquitination of IKK/NEMO. Then I $\kappa$ B and p65 (NF- $\kappa$ B) become phosphorylated, and I $\kappa$ B is ubiquitinated and degraded. Released NF- $\kappa$ B then is translocated through the nuclear pore for transcriptional regulation. Nuclear import is mediated by RanGTPase dependent karyopherins (importin  $\alpha$ ; Karin 2000, Salles 2014).

NF- $\kappa$ B signaling is highly influenced by crosstalk among several signaling pathways, and many receptors send signals in opposing directions. The TNF receptor simultaneously induces a caspase-8 dependent proapoptotic response that is usually outbalanced by prosurvival signaling of NF- $\kappa$ B. The highly integrating response changes from acute to chronic situations, so that a defective nuclear translocation of NF- $\kappa$ B preventing a transcriptional regulation can directly shift the equilibrium from prosurvival to apoptosis and cell death (Oeckinghaus 2011). NF- $\kappa$ B and upstream factors are target of many post-translational modifications (Salles 2014). The E3 ubiquitin ligase Parkin promotes survival through linear ubiquitination of NEMO, which prevents the induction of premature, stress-induced apoptosis and shifts the complex equilibrium towards prosurvival signaling (Müller-Rischart 2013).

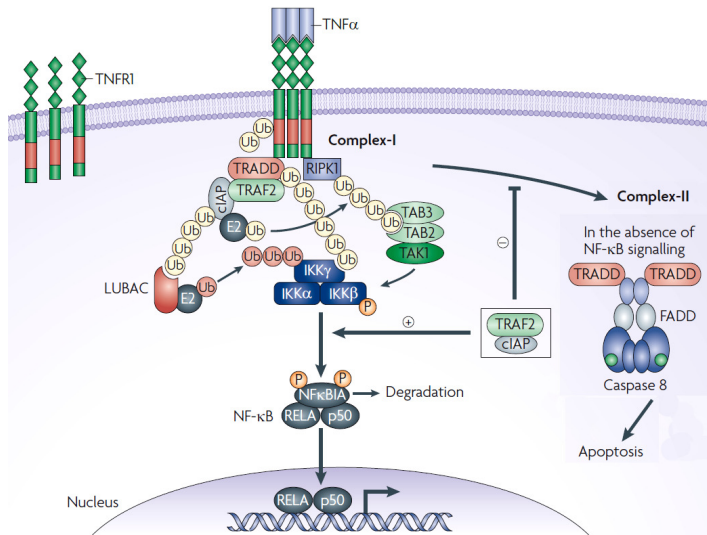


**Figure 95 | Activation of NF-κB by tumor necrosis factor receptor 1 (TNFR1) and its crosstalk to apoptosis signaling via caspase-8.** Activation of TNFR e.g. by TNFα causes the ubiquitin-dependent recruitment of linear ubiquitin chain assembly complex (LUBAC), which conjugates ubiquitin chains onto IKK. Phosphorylation and ubiquitination of IκB results in its release from NF-κB. Itself phosphorylated, NF-κB reveals its NLS and is actively translocated into the nucleus. If not simultaneously inhibited by a transcriptional response of NF-κB, TNFR-associated via death domain (TRADD) activates the platform for caspase-8, finally inducing cell death through apoptosis (figure adapted from Gyrd-Hansen 2010).

The nuclear import of NF-κB was inhibited in practically all HEK293T cells with β proteins aggregating in the cytoplasm, and in most cells with Htt96Q, TDP-F4, or ParkinΔC inclusions (Figure 68). The translocation of NF-κB was prevented by the β proteins despite a functional upstream signaling up to p65 phosphorylation and IκB degradation. NF-κB levels were comparable to wildtype cells, demonstrating a strong blockage of nuclear NF-κB import. The fraction of cells with aggregates of Htt96Q or TDP-F4 was too low to quantify accurately p65 phosphorylation and IκB degradation by immunoblotting. Single-cell observations or improved expression conditions may clarify the situation for these proteins. In contrast, cells with β proteins aggregating in the nucleus promoted quantitative nuclear NF-κB import.

As described above, inhibition of transcriptional regulation through NF-κB shifts the signaling equilibrium towards apoptosis. Initiator caspase-8 is activated through TNFR-1, and caspase-8 transmits its signaling to downstream effector caspases directly in the cytoplasm. Once activated, caspase-9 and caspase-3 further inactivate nuclear transport and permeabilize the nuclear envelope, allowing caspases to enter the nucleus even by passive diffusion (Faleiro 2000). Once a certain threshold or duration is reached, protein misfolding interfering with nucleo-cytoplasmic transport may therefore cause a vicious cycle that ultimately leads to cell death. This appears particularly harmful to neurons under proteome stress, especially if NF-κB is supposed to promote neuronal development and memory formation.

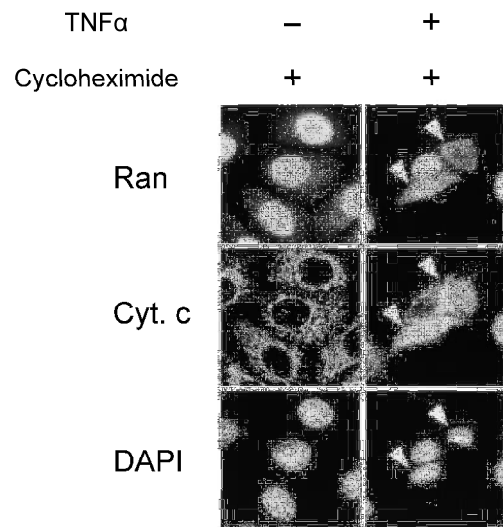


**Figure 96 | Induction of apoptosis by TNFα in the presence of cycloheximide.** Cycloheximide inhibits protein synthesis and thereby prevents a response of activated NF-κB (amongst other effects). TNFα treatment in presence of cycloheximide prevents a regulated NF-κB through missing protein synthesis, but activates cellular apoptosis in absence of counteracting signals. Consequently, nuclear transport becomes inhibited (cytoplasmic RAN) and the nuclear membrane are permeabilized, allowing apoptotic factors such as cytochrome c or caspase-3 to enter the nucleus (figure adapted from Faleiro 2000).

## General defects in nucleo-cytoplasmic protein transport

NF- $\kappa$ B is a highly regulated transcription factor influenced by complex signaling networks. To investigate the general nucleo-cytoplasmic protein transport we created S-GFP (NES-NLS-EGFP), which is continually transported in both directions through the nuclear pores. Quantifying the fluorescence of S-GFP in the two compartments revealed its inter-compartmental concentration gradient. These gradients were significantly decreased from 6-8 in wildtype cells (+/- nuclear export inhibitor, Leptomycin B) to only 3 fold in cells with  $\beta$ 17 aggregates in the cytoplasm (Figure 72). The export efficiency went further down in cells expressing Htt96Q or Parkin $\Delta$ C. Again, the  $\beta$  proteins targeted to the nucleus did not significantly interfere with the nucleo-cytoplasmic transport of S-GFP.

Quantification of the S-GFP gradients demonstrated a significant loss of efficiency in general nuclear protein import and export, but not a complete blockage. UV irradiation and oxidative or other forms of stress have been reported to cause inhibitions of nucleo-cytoplasmic protein transport and to translocate only specific stress proteins, such as Hsc70 (Miyamoto 2004, Velazquez 1984, Kose 2012). The sequence of events and causal relationships remained however elusive so far. Depending on the circumstances, the loss of transport capacities might be a cellular accident, resulting from a damage caused by specific stressors (such as protein misfolding). Or cellular transport may be prevented as part of a cellular response mechanism, trying to overcome detrimental impacts and to recover cellular homeostasis. Located at “predetermined breaking points”, even metastable sequences might then appear during evolution to induce a specific response, corresponding to a switch between the normal functional and a stress-triggered conformation.

## Interferences with nuclear mRNA export

The experiments on S-GFP revealed serious protein transport inhibitions in and out of the nucleus in cells with cytoplasmic protein aggregation. These experiments generalize the inhibition of NF- $\kappa$ B translocation, since a set of karyopherins (importins and CRM-1) mediates the nucleo-cytoplasmic transport of most targeted proteins. Lowered cytoplasmic levels of S-GFP indicated that nuclear export of proteins is similarly affected as nuclear import. Messenger RNAs (mRNAs) are transported through the nuclear pores by a multitude of proteins and protein-RNA complexes. Many of these proteins are especially enriched in low-complexity regions that form disordered stretches, which supposedly mediate inducible protein-RNA interactions (Spolar 1994, Dyson 2002). Such proteins with prolonged disordered regions were shown to be prone for misfolding and aggregation, especially under a challenged proteostasis or in an unsuitable cellular environment (Raychaudhuri 2009, Olzscha 2011).

Consequently, we became interested in the efficiency of nuclear mRNA export. In HEK293T and SH-SY5Y cells and in murine cortical neurons with cytoplasmic aggregates of the  $\beta$  proteins, Htt96Q, or TDP-F4, we observed a strong accumulation of mRNA in the nucleus, and simultaneously a reduction of cytoplasmic mRNA. No interferences were observed between mRNA export and nuclear  $\beta$  proteins or nuclear Htt96Q in murine cortical neurons (experiments performed by Li Rebekah Feng; Woerner 2016).

The morphology of the aggregation induced nuclear polyA-RNA-rich bodies was clearly distinct from the structure of polyA stained snRNPs in wildtype cells. The nuclear mRNA bodies were of significantly increased size and bright fluorescence, corresponding to an increase of nuclear mRNA levels beyond the total mRNA levels of control cells, which we confirmed by single cell quantification.

Similarly, a prolonged inhibition of the proteasome accumulated misfolded, polyubiquitinated proteins (Zhao 2010, Ros 2004, Obeng 2006) and caused an accumulation of mRNA in the nucleus with decreasing levels in the cytoplasm. Accumulation of nuclear mRNA was previously described in sensory ganglia neurons due to a dose-limiting neurotoxicity causing sensory ataxia, which appeared as a side-effect of the proteasomal inhibitor Bortezomib applied in cancer therapy (Casafont 2010). Polyubiquitinated proteins and a reduction of transcriptional activity were associated with nuclear mRNA granules. These granules contained several RNA-binding proteins, but lacked the mRNA export factors THOC4 (Aly/Ref) and Y14. The mechanistic origins of the nuclear polyA RNA granule formation remained unresolved in this case. It occurred however under a disturbed removal of misfolded proteins, and RNA export proteins were missing at their functional sites (Casafont 2010).

THOC2 and the whole THO complex have been identified to interact with the  $\beta$  proteins in HEK293T cells and murine cortical neurons (Olzscha 2011, Woerner 2016). Confocal microscopy revealed cytoplasmic mislocalization and coaggregation of THOC2 in cells with cytoplasmic  $\beta$  proteins, or separate cytoplasmic aggregation of THOC2 next to Htt96Q or TDP-F4 inclusions. siRNA-mediated knockdown of THOC2 reduced cytoplasmic mRNA levels, while nuclear RNA appeared relatively wildtype-like. The knockdown demonstrated that THOC2 is an essential factor for mRNA export to the cytoplasm. Defective mRNA export can thus reproduce a similar, although less severe mRNA-related phenotype as caused by protein misfolding and aggregation. Next to THOC2, knockdown of several individual THO proteins have recently been shown to cause a nuclear accumulation of mRNA. Thereby, the strong coupling of mRNA processing and export and its dependence on mRNA quality control was again demonstrated (Chi 2013).

Huntington's disease (HD) is a genetic disorder caused by an extended polyglutamine (polyQ) sequence in the first exon of Huntingtin. Transgenic R6/2 mice express this exon of human huntingtin with approximately 150 glutamines driven by the endogenous human Huntingtin promoter (Mangiarini 1996). R6/2 mice display a progressive neurological phenotype mimicking many features of HD in humans. Aggregation proceeds in the mouse brains over weeks in a physiological environment accompanied by aging phenomena. At weaning, the R6/2 mice were indistinguishable from their wildtype littermates. Starting from week 9-11 initial symptoms such as involuntary movements, shaking, and increased stress sensitivity appeared. After exhibiting increasingly severe symptoms for 2-3 weeks the mice died (Mangiarini 1996, Zhang 2003).

In many neurons of 9 week old R6/2 mice, the mRNA was distributed equally to wildtype litter mates. The mRNA was distributed over the neuronal soma (cytoplasm) reaching out into neurites, while the mRNA was concentrated in distinct snRNPs in the nucleus. Nevertheless, a fraction of cells in R6/2 mice developed phenotypes with disturbed mRNA distributions. About 2.5% of neurons showed a *partial nuclear mRNA retention* with increased levels of nuclear mRNA, accompanied by lowered mRNA levels in the cytoplasm. These neurons appeared similar to HEK293T and SH-SY5Y cells expressing Htt96Q, where the cytoplasmic mRNA was not as strongly depleted as in presence of  $\beta$  proteins or TDP-F4. In about 9% of neurons with a *complete nuclear mRNA retention*, cytoplasmic mRNA was virtually lost in addition to strongly decreased nuclear mRNA levels.

The R6/2 mice thereby exhibited phenotypes with reduced mRNA levels in the nucleus that were not observed in this form after 1-2 days of transient Htt96Q expression in HEK293T or SH-SY5Y cells. Thus, mRNA degradation may occur in the mouse brain, potentially as a consequence of nuclear mRNA export defects. Addition of the polyA tail may also become affected, hiding the mRNA from poly(d)T probes. A third phenotype was detected in cells with cleaved caspase-3, which was hardly present in 9 weeks old R6/2 mice. Neurons positively stained for activated caspase-3 had almost entirely lost their cellular mRNA. As studied by Zhang et al., activation of caspases highly increased in

R6/2 mice beyond 12 weeks of age (Zhang 2003). Neurons of 9 week old R6/2 mice did not yet reach this stage.

A cell cannot survive and keep up its normal functions, if significant amounts of mRNAs are not exported to the cytoplasm. A breakdown of most cellular functions has to follow, as proteins are continuously turned over. Cells lose their ability to respond to stimuli or stress situations, when translations of new transcripts vanish. Therefore, two scenarios are possible: either mRNA export to the cytoplasm is restored after an acute stress phase, or ongoing mRNA export defects will ultimately lead to cell death. Accordingly, it may be reasonable to assume that the different phenotypes observed in R6/2 neurons represent snap-shots of a development over time. The low frequency of neurons exhibiting decreased cytoplasmic and high nuclear mRNA levels (*partial nuclear mRNA accumulation*) might suggest a transient phenomenon that develops into a state defined by vanished cytoplasmic and low nuclear mRNA (*complete nuclear mRNA accumulation*). Finally, caspases are activated, inducing apoptosis and neuronal death, accompanied by a complete degradation of mRNA (Bushell 2004).

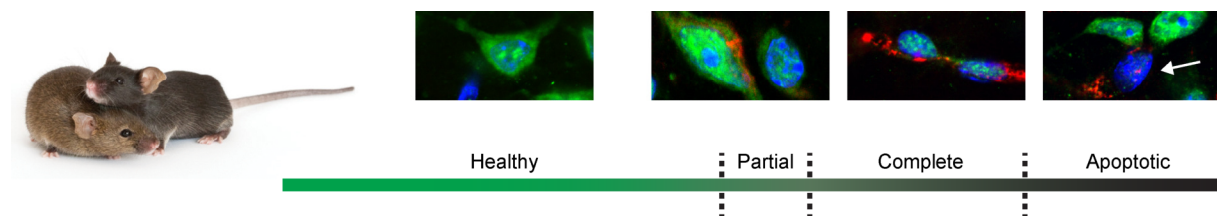


**Figure 97 | Possible chronology of events during nuclear mRNA accumulation caused by polyglutamine expanded Huntingtin in neurons of R6/2 mice.** The distinct neuronal states were observed at 9 weeks of age, but they may appear chronologically in individual cells. Neurons expressing polyglutamine expanded Huntingtin start to accumulate increasing amounts of mRNA in the nucleus, whereas cytoplasmic levels decline. Consequently, the nuclear mRNA is degraded, or general transcription ceases. Apoptosis is induced in a later stage of disease progression. mRNA (green), polyglutamine expanded human Huntingtin exon 1 (red), and nuclear DNA (blue) are labeled in representative images. R6/2 mice image from The Jackson Laboratory (left).

## Reduced cytoplasmic RNA and nucleolar volumes in dementia patients

It would be highly interesting to observe interferences of protein aggregation with mRNA export and turnover during aging of different disease-related model animals, but even more in cerebral neurons of human patients. This should shed a light on the real chronology of events and the incidence of such mRNA processing and export interferences in human neurodegenerative disorders.

First indications of a reduced cytoplasmic RNA content in neurons of patients suffering from senile dementia have been observed in the cerebral cortex in 1975 (Oksova 1975 AA Gist Embr/ Z Nevropat Psikhiat ISS Korsakova). Another group confirmed this finding two years later and determined mean losses of cytoplasmic RNA of often 30% in various regions of the brain (Mann 1977). The authors applied cytometric assays with the RNA binding fluorescent dyes azure A or B (Bennion 1975, Khan 2016). In subsequent studies, similar reductions in cytoplasmic RNA have been described in conjunction with reduced nucleolar diameters in the neurons of patients of senile dementia or Alzheimer's disease (Mann 1978, Mann 1983, Neary 1986). These observations are highly interesting in the context of our findings that misfolded proteins associated to nucleolar structures, while partially altering their morphology (NPM-1). Nowadays, advanced techniques offer studying proteins and RNAs involved in this process in much higher detail. This should enable us to resolve the cellular mechanisms behind the findings from the 70s, which were hardly followed during the last decades any more.

## Localization of Huntingtin aggregates in cell cultures, mouse models, and human patients

Cortical and striatal neurons of R6/2 mice were analyzed regarding disturbances of mRNA homeostasis (mRNAstasis). Beyond these brain regions, Huntingtin aggregates as well as the described mRNA phenotypes were found practically throughout the whole R6/2 brain. Already before, Huntingtin pathology has been described not to be restricted to certain brain areas in R6/2 mice (Rattray 2013), possibly due to the extreme expansion of around 150 glutamines. Huntingtin in human patients comprises mostly of 37-60 glutamines. In humans, cortex and striatum were reported to be most sensitive and to become most strongly affected during disease progression (DiFiglia 1997).

Under experimental conditions, the intracellular distribution of mutant Huntingtin strongly depends on cell types, specific constructs (fragments, GFP fusions, flanking sequences), and the selective visibility caused by the applied detection method. Many anti-Huntingtin antibodies are selective for certain species or conformations (Ko 2001, Miller 2011). In HEK293T and SH-SY5Y cells, Htt69Q mostly formed aggresome-like inclusions in the cytoplasm (even when fused to an NLS), while in murine embryonic neuronal cultures mostly nuclear aggregates were observed.

In human patients and in HD mouse models, Huntingtin aggregates were distributed over cytoplasm and nucleus in a dynamic equilibrium (DiFiglia 1997, Hodgson 1999, Liu 2015). Overall, especially short N-terminal fragments are imported into the nucleus, whereas larger fragments or the full length protein accumulate preferentially in the cytoplasm (Sieradzan 1999, Hodgson 1999, Lunkes 2002). Most likely, aggregation in both compartments contributes to neuronal toxicity, although the general omnipresence of the misfolded structures and the selectivity of the applied detection methods often challenge a clear, meaningful analysis (Hackam 1999 *HuMolGen*, Cooper 1998, Hackam 1999 *PhilosTrans BiolSci*). Toxicity of mutant Huntingtin was even described in the absence of visible aggregate formation. In R6/2 mice and in cell culture, we observed some cases of nuclear mRNA accumulation in the absence of Htt96Q or TDP-F4 aggregates, but in presence of distributed, presumably oligomeric material, so that distributed oligomerization might furthermore obscure the real origin of cellular toxicity (Hodgson 1999).

In other studies, amelioration of symptoms in R6/2 mice could be achieved by a reduction of proteins that coaggregate with or modulate cytoplasmic Huntingtin (Mielcarek 2013). Intracellular antibodies selectively directed against cytoplasmic Huntingtin aggregates promoted their ubiquitination and degradation (Wang 2008), furthermore attesting a toxic role of cytoplasmic mutant Huntingtin.

Intracellular aggregates of polyglutamine expressing cells were reported to sequester proteins of the nuclear pore complex and envelope, among them Nup62 and Lamin B (Suhr 2001). Recently, in R6/2 mice and in HEK293T cells cytoplasmic, perinuclear Huntingtin inclusions were found to interact with and possibly disrupt parts of the nuclear envelope (Liu 2015). As consequence, the cell cycle of terminally differentiated neurons was reactivated, leading to cell death and progressive neuronal loss (Liu 2015). Similar to our observations, distorted nuclear membranes and a loss of nuclear pore complex proteins (the FG-repeat rich Nup-62) around the nuclear envelope appeared in HEK293T cells.

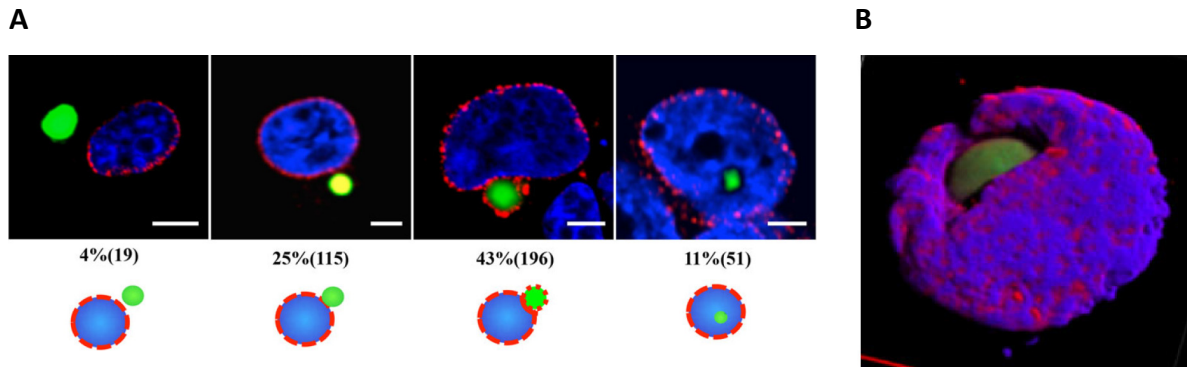


**Figure 98 |** Huntingtin-exon1-97Q-GFP (green) in HEK293T cells formed either cytoplasmic, perinuclear aggregates surrounded by nuclear pore proteins (Nup62, red) or inclusions within the nucleus (blue, DAPI). **(A)** Different classes of Huntingtin inclusions observed 24 h after transfection. **(B)** 3D reconstruction of a perinuclear Huntingtin aggregate that penetrated into the nucleus and caused severe deformations of the nuclear morphology from the cytoplasmic side, still being separated by the nuclear lamina (visible on individual z-stack images). Scale bar length 5 μM (figures from Liu 2015).

In their study, Huntingtin inclusions formed in the cytoplasm and to a small percentage in the nucleus (10-25%; Liu 2015). Live cell imaging showed that these inclusions maintained their location and grew in the respective compartment of initial formation. Perinuclear inclusions came into close contact and were surrounded by nuclear envelope proteins, but never crossed the nuclear envelope entirely. Intranuclear inclusions were never covered in nuclear pore proteins, suggesting their local formation (Liu 2015). When misfolded Huntingtin oligomers reached a seeding threshold at one site, rapid growth accumulated the vast majority of distributed mutant huntingtin within minutes (Ossato 2010). There is no evidence for any endocytosis-like processes at the nuclear envelope, which could transport whole inclusions into or out of the nucleus e.g. for degradation. In agreement with our studies, increased mortality strictly correlated with perinuclear inclusions. They caused damage to the nuclear envelopes followed by cell death. Neurons with nuclear aggregates remained post-mitotic and viable (Liu 2015).

## Cytoplasmic proteostasis – how does it promote misfolding and toxicity?

The cytoplasm is the site of protein synthesis and the compartment most associated with protein folding, signaling, and metabolism, while in the nucleus genetic information is stored and transcribed. Cytoplasm and nucleus are connected through large nuclear pore complexes (NPCs). These are not only selection filters for large proteins (> 30-40 kDa), but also serve as platform for the nucleo-cytoplasmic transport machinery to actively enrich all kind of biomolecules in the two compartments.

In our experiments on the consequences of cytoplasmic and nuclear aggregation, we observed many differences between these two compartments. Aggregation occurring in the cytoplasm was much more harmful to cells than in the nucleus. The toxicity of cytoplasmic aggregation became not only apparent by reduced viability and growth, but also by concrete cellular malfunctions including nucleo-cytoplasmic transport inhibitions, failing stress responses, mislocalization and coaggregation of proteins, and formation of nuclear mRNA bodies.

Distributed, lower-molecular-weight structures mainly formed in the cytoplasm. Conformational differences between cytoplasmic and nuclear aggregates were indicated by an increased cytoplasmic solubility and a differential staining of the aggregates by the amyloid sensor NIAD-4. Aggregation appears to be strongly modulated by the compartment-specific environment. Additional factors regulating local aggregation and proteostasis remain to be explored, especially for the nucleus.

Cytoplasmic aggregates recruited many cellular proteins and caused their mislocalization or separate aggregation, even of primarily nuclear proteins. Nuclear aggregates on the contrary appeared very unreactive, did not interfere with surrounding proteins, even those that were sequestered into cytoplasmic inclusions. Nuclear  $\beta$  proteins accumulated at nucleolar sites apparently isolated from the nuclear matrix and from chromatin.

Nuclear luciferase-EGFP only aggregated under proteasomal inhibition, while under the same conditions cytoplasmic luciferase-EGFP remained largely soluble. This observation indicates the significance of proteasomal degradation of misfolded and unstable structures in the nuclear environment, where such structures otherwise rapidly accumulate. Nuclear proteostasis is characterized by the absence of autophagy and by lower chaperones levels. Beyond, this observation also demonstrates the influence of the local proteostasis machinery on the stabilization of misfolded structures in the cytoplasm. This may prevent their aggregation, but does also prevent their degradation and promote their distribution?

Several mechanisms investigated in this study revealed how cytoplasmic aggregation disturbs fundamental cellular processes such as signaling transduction and the regulated translation of genetic information into new proteins. Mislocalization and (co-)aggregation of transport-related proteins likely contribute to the multiplicity of toxicity described for so many protein misfolding disorders (Soto 2003 and many others).

However, especially proteins with extended polyglutamine sequences potentially appear to cause additional damage in the nucleus. Expanded polyglutamine proteins show a distinct aggregation mechanism (mainly driven by hydrogen bonds, forming polar zippers). Transcriptional dysregulations were ascribed to the high affinity of polyglutamine sequences towards RNA-binding proteins and transcription factors in the nucleus (Schaffar 2004, Sugars 2003, Perutz 1994, Woulfe 2007).



## **Protein folding environment in the cytoplasm – keeping unstable structures alive?**

One of the potentially most hazardous situations may occur when newly synthesized and not yet fully folded proteins come into contact to misfolded proteins with hydrophobic or unstructured surface regions. A large number of newly synthesized proteins were found to interact with the  $\beta$  proteins, likely trapped before the structures folded and reached their cellular destination (Olzscha 2011).

Similarly, large proteins with prolonged unstructured regions were prone to interact with misfolded and aggregated structures in the cytoplasm (Olzscha 2011). However, this does not seem to happen in the nucleus, where many, especially RNA-binding proteins, naturally contain extended unstructured regions. However, newly synthesized proteins do not appear here, and misfolded structures such as the  $\beta$  proteins are secluded to nucleoli. In the cytoplasm in contrast, partially unfolded structures have to be stabilized – to promote protein synthesis and folding and to prevent their immediate aggregation. This stabilization may however also increase the concentration of vulnerable, premature, or temporarily misfolded structures. While this may not be a problem under the control of a highly sophisticated chaperone and proteostasis machinery in a healthy cell, it may potentially turn harmful during aging, cellular stress, or the appearance of protein mutants or toxins that may overload or defeat the cytoplasmic proteostasis capacity, especially under chronic conditions.

Several sub-compartmental structures harboring misfolded proteins with distinct properties were described for the cytoplasm. While a proteasome rich “juxtannuclear quality control” compartment (JUNQ) contains ubiquitinated proteins and the disaggregase Hsp104, terminally aggregated structures including mutated Huntingtin and prions were sequestered into “insoluble protein deposits” (IPOD), as described for *S. cerevisiae* (Kaganovich 2008). Precise properties of comparable misfolded structures in human neurons remain to be detailed. However, as observed also in this study, cellular proteins either were sequestered into major aggregates or formed separate inclusions, confirming the notion that their structural properties might influence their aggregation behavior. The number of distinct inclusions and their characteristics under typical disease conditions remain intriguing research questions.

## **Efficient degradation or secluded deposition – a new role of the nucleus in proteostasis**

It is becoming clearer now that the nucleus may play an important role in the degradation and storage of misfolded protein structures, and thereby in the overall proteostasis of the cell. The protein folding environment of the cytoplasm is absent in the nucleus. Instead of nascent chains and not-yet fully folded proteins we find high concentration of proteasomes (Wojcik 2003, Chowdhury 2015, Kleinschmidt 1983). Unstable structures may thus either be degraded directly, or be secluded from the nuclear matrix into insoluble localized particles. Both mechanisms need to be analyzed in more detail in future. A very rapid degradation of thermally misfolding luciferase supports the idea of a highly efficient removal of misfolded structures in the nucleus, compared to other compartments (Hageman 2007). Recent observations indicate that the cytoplasm even takes advantage of these nuclear characteristics, as distinct misfolded structures were specifically transported into the nucleus for degradation (Park 2013, Nielsen 2014).

Nuclear chaperone levels increase during cellular misfolding stress (Velazquez 1984, Welch 1984, Kose 2012). Downregulation of a stress-specific nuclear Hsp70 importer (Hikeshi) “delays the attenuation and reversion of multiple heat shock-induced nuclear phenotypes”, a finding that clearly demonstrates the positive influence of molecular chaperones on nuclear proteostasis under stress (Kose 2012).

## Cellular transport systems – high susceptibility towards misfolding?

Between cytoplasm and nucleus, many proteins and some RNAs are actively transported by members of the karyopherin  $\beta$  family, regulated by the GTPase Ran (Cook 2010). Other proteins and complexes involved in molecular transport through the nuclear pore complexes (NPCs) include TAP:p15 and the THO complex for mRNAs (Braun 2002, Chi 2013), Xpot for tRNAs, and Xpo5 for snRNAs. The major transport proteins share structural similarities. They are large proteins (>100 kDa) with multiple binding sites. They contain prolonged disordered regions, which may become structured upon substrate binding (Kobe 1999, Cook 2007). They transit through multiple conformations and several compartments (Cook 2007, Cook 2010). Most likely, the interconnection of structural and functional features increases the vulnerability of transport proteins towards aberrant interactions or aggregation. Large proteins with tolerant multi-substrate binding sites, hydrophobic surface patches, conformational flexibility, and multiple native states are highly endangered species, especially when challenged with an unbalanced proteostasis (Chiti 2006, Olzscha 2011). Molecular transport factors adopt various distinct conformations, such as empty vs. substrate bound, import vs. export competent, or cofactor bound vs. released states. Different chemical and biological environments additionally challenge the structural stability of nucleo-cytoplasmic transporters. While newly synthesized proteins cross the borders of most compartments in an unfolded and chaperone escorted state, large molecular complexes including associated transport proteins travel between nucleus and cytoplasm (Cook 2007).

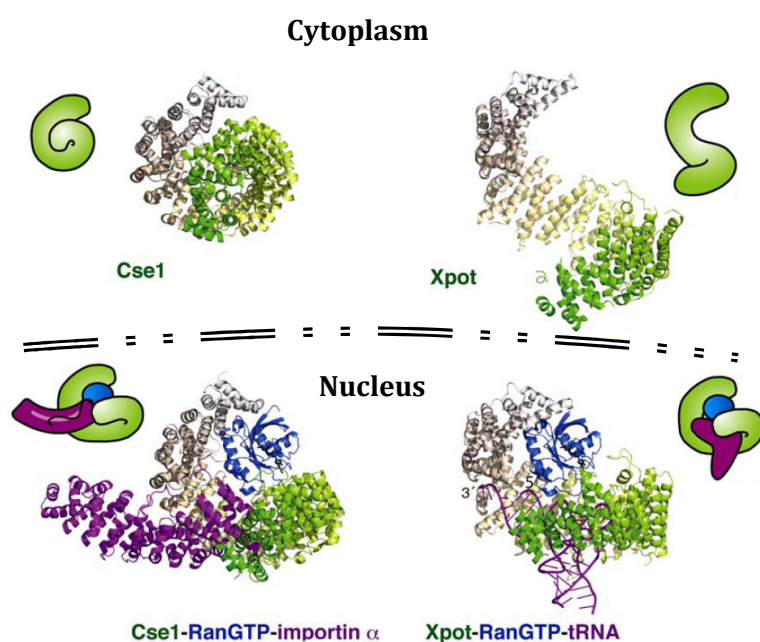


**Figure 99 | Structures and drawings illustrate the large conformational adjustments of nuclear exporters of importin  $\alpha$  (Cse1) and tRNA (Xpot) in a cytoplasmic, free vs. a nuclear, substrate bound state.** Large conformational rearrangements accompany the transition from the autoinhibitory (Cse1) or open (Xpot) conformation in the cytoplasm to cargo and RanGTP association in the nucleus. While Cse1 folds back on itself in the cytoplasm in a compact state, RanGTP binding causes Cse1 to open up, revealing its importin  $\alpha$  binding site. Differently, Xpot remains in a closed conformation until tRNA and RanGTP bind in the nucleus, whereas Xpot opens up for substrate release in the cytoplasm. Especially open conformations in a substrate-free state reveal large binding surfaces, which may explain the increased vulnerability of transport proteins towards deleterious interactions with misfolded species (figure adapted from Cook 2010).

RNA processing and export proteins contain even longer disordered polypeptide regions. Apparently, these low complexity sequences of almost exclusively polar side chains create unique properties that keep these proteins soluble in the nuclear environment. But are they compatible with the presence of misfolded structures or a disturbed proteostasis in the cytoplasm? Here, such proteins may become trapped, engage in detrimental interactions, or aggregate. Once mislocalized, they may further aggravate transport inefficiencies. Several THOC proteins contain extended intrinsically unstructured regions, as predicted by different algorithms (IUPred, ANCHOR, DisProt). Many unstructured regions are potentially stabilized upon binding to cellular factors or complex formation in cells. Certain conditions may attract unstructured regions to engage in unspecific interactions, especially if their native interaction partners are missing. An abnormal cellular environment under

proteostasis stress may furthermore support erroneous interactions. Intrinsically unstructured regions that were predicted to gain stabilization energy upon binding are common among the THOC proteins (Figure 100). With ~400 residues THOC2 contains next to an especially long unstructured region, which might be a reason why the protein was preferentially sequestered into aggregates of the  $\beta$  proteins (Olzscha 2011).

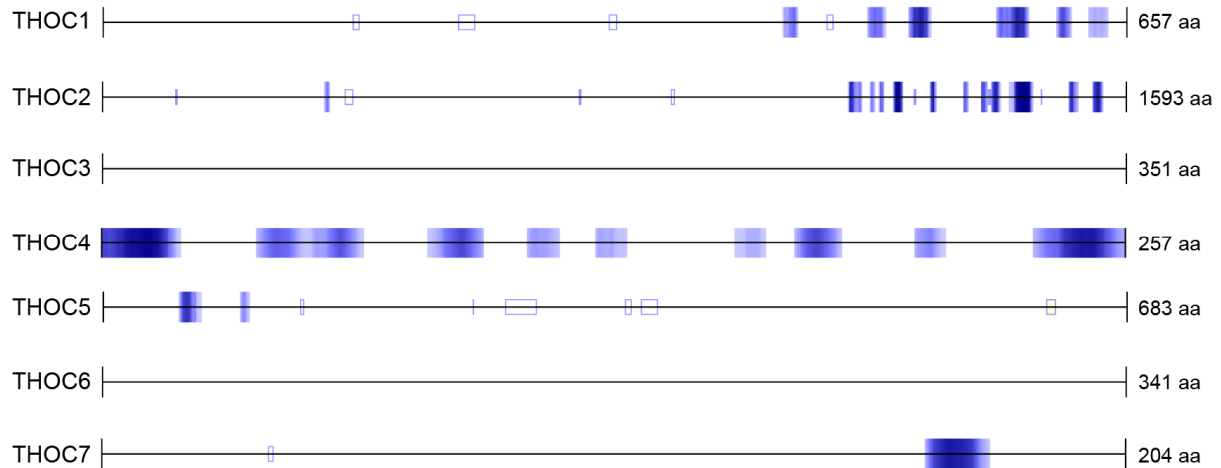


**Figure 100 | Human THOC proteins contain multiple intrinsically unstructured regions predicted to be energetically stabilized upon binding** (blue regions; ANCHOR algorithm, Meszaros 2009). Intrinsically unstructured regions are present in many nuclear nucleic acid binding proteins. Such regions preferentially interact with proteins prone to misfolding and aggregation (Olzscha 2011, Raychaudhuri 2009, Meszaros 2009).

Nucleo-cytoplasmic and other forms of molecular transport steadily keep up cellular gradients of proteins, RNAs, and other biomolecules. For a cell with an already overloaded chaperone capacity, defects in a second, such essential system as the molecular transport undoubtedly risks losing cellular homeostasis, once a threshold of malfunction has been crossed. Interferences in cellular transport have been observed quite early in the cellular pathology here. Thus, they may be very crucial for the whole disease pathogenesis, and beyond lay the foundation for numerous further malfunctions that have been associated with protein misfolding and aggregation in neurons and other cells.

Induction of cellular responses is central to regenerate homeostasis in cellular stress situations (Schröder 2005, Chakrabarti 2011). The defective Hsp70 promoter induction demonstrated that cytoplasmic  $\beta$  proteins strongly inhibited stress responses upon heat shock and cytoplasmic protein misfolding stress. Defects in stress response induction and regulated termination have been implicated in numerous neurodegenerative disorders. Consequences are ineffective chronic stress responses that are unable to restore homeostasis (Cowan 2003, Prahlad 2011, Halliday 2014). For example in mouse models of Parkinson's disease, phosphorylation of eIF2 $\alpha$  reduced the burden of newly synthesized proteins, but further limited the cellular capabilities to react upon chronic misfolding (Colla 2012, Parlato 2014). Ineffective transport inevitably interferes with signaling pathways and thereby potentially multiplies the original damage.

Remarkably, deficiencies in subcellular protein targeting are even applied by nature in cellular stress sensors. The mitochondrial stress reporter ATFS-1 contains a mitochondrial and a nuclear localization sequence (equivalent to our S-GFP). ATFS-1 is usually imported into mitochondria, where it is degraded. Deficiencies in mitochondrial import adjust the nuclear concentration, which results in a mitochondrial unfolded protein response (Nargund 2012, Wolff 2014). This stress response system beautifully describes how evolution utilizes cellular malfunctions for stress sensing, finding nature's own way of circumventing problems. If not now, then at some point in the future.

## What makes neurons especially vulnerable?

Many protein misfolding diseases are neurodegenerative disorders. They destroy distinct regions of the brain and give rise to specific symptoms of dementia (Ryan 2013, Braak 1991, Finkbeiner 2011, Clavaguera 2009, Levenson 2014). Additionally, protein misfolding has recently been associated to several non-neuronal disorders, such as diabetes (Mukherjee 2015), cancer (Silva 2014), and various other forms of systemic amyloidoses (Blancas-Mejia 2013). In case of damage, individual cells are in general easier to replace outside of the nervous system, so that a loss of single cells does not directly accrue in a dysfunctional organ. Terminally differentiated neurons and glia cells connect during embryonic development and childhood in an extremely complex and unique way, which explains their irreplaceable nature. Despite recent reports about cerebral stem cells (Gage 2013, Ming 2011), neuronal connectivity is essential for an efficient cognition and cannot easily be reproduced by neuronal replacement (Geerlings 2014, Meunier 2014, Williams 2013, Thompson 2004, Wen 2011). When irreplaceability encounters increased vulnerability in neurons of an aging organism, certain areas of the brain accumulate increasingly damage, until the first symptoms of dementia appear.

In our studies on the fundamentals of protein misfolding in cells we focused on the structural properties of proteins that are especially prone to interact and become recruited into misfolded assemblies (Olzscha 2011). Proteins interacting with the toxic  $\beta$  proteins were often at central (hub) positions within cellular interactions networks. Such proteins often contain hydrophobic patches at interaction sites, in contrast to polar surfaces that shield proteins from their surroundings and keep the structures soluble. Many interactors of the  $\beta$  proteins contain prolonged unstructured regions (Olzscha 2011). These occur to an increased number in nuclear proteins. Many of these are RNA binding and processing proteins that may become structured upon substrate binding (Dyson 2002, Dyson 2005). Determining the cellular interactors of the  $\beta$  proteins should help to identify cellular functions and pathways that become disturbed early in cells affected from aggregation. Among the interactors were proteins involved in subcellular transport. Such proteins contain many and extensive interaction surfaces, as they bind not only numerous substrates, but also cofactors within large transport complexes, NPC proteins, release factors, and retrograde transporters that return the transporters to their original location (Cook 2007).

Neurons are connected to each other with up to 60,000 connections in an extremely complex, self-regulated manner. The longest cells of the human body with axons of up to one meter length are part of the neuronal system (Debanne 2011). Establishing activity-dependent connections strongly relies on the transmission of signals, which includes electric signaling as well as extensive molecular transport of proteins, RNA, and small organic signaling molecules or peptides to site-specific locations. Key areas of molecular trafficking include long distance transports between nucleus, soma, neurites, and synapses. For example, mRNA is specifically located for targeted protein expression at the synapse (Kanai 2005, Moon 2009, Hirokawa 2010). Signaling molecules are retrotranslocated from the synapse to the nucleus, a central mechanism for mediating neuronal plasticity (Castillo 2012). And at least certain misfolded proteins are transported to the nucleus for clearance by the proteasome, a pathway that itself is susceptible to aggregation (Park 2013). In neurons, such misfolded proteins may have to travel over extremely long distances, along which they can spread misfolding and damage cellular systems. Beyond nucleo-cytoplasmic, neuron-wide transport is essential for neuronal activity and survival.

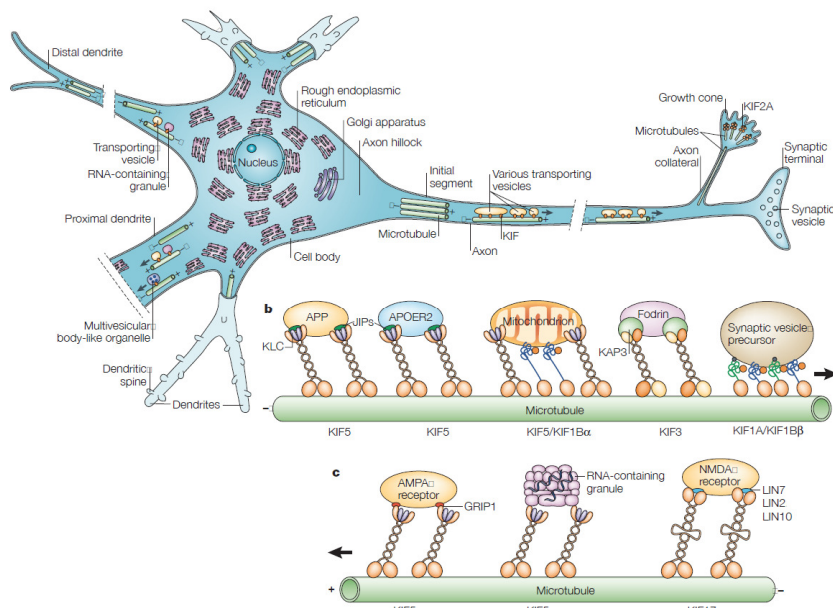


**Figure 101 | Dendritic and axonal trafficking of protein complexes, RNA granules, vesicles, and organelles.** In a typical neuron, numerous dendrites and a single axon (on the right) extend from the cell body. Molecular motors of mostly the kinesin and dynein families transport cargo along microtubules in the anterograde and retrograde direction, respectively. Dendrites, axons, and synapses strongly depend on a defined local environment and the delivery of site-specific cargos, e.g. for local translation of membrane receptors or other signaling-related molecules. RNA is thereby transported in the form of ribonucleoprotein granules (Kanai 2004) in both directions with the help of kinesin or dynein motors (figure adapted from Hirokawa 2005).

In *Drosophila*, expression of cytoplasmic polyQ proteins disrupted axonal transport by titrating out soluble motor proteins (*Drosophila* huntingtin). By a different mechanism, nuclear polyQ proteins induced neuronal apoptosis in the absence of axonal blockages, most likely caused by transcriptional dysregulation (Gunawardena 2003, Long 2014). Cytoskeletal transport problems caused synaptic loss in early stages of Alzheimer's disease and mild cognitive impairment (Scheff 2006, Knobloch 2008). Especially the damage of synaptic terminals was described as early structural correlate to dementia progression and an early cause of injury in the neuronal network (Serrano-Pozo 2011).

For neurons, effective communication among the extensive cytoplasmic protrusions and the nucleus is fundamental for neuronal activity, plasticity, and survival (Chevalier-Larsen 2006). Neuronal plasticity, brain wiring, and higher brain functions strongly depend on nuclear import and export, which we described to be compromised multifaceted through cytoplasmic misfolding and aggregation. Recently, mutant huntingtin has been shown to inhibit mitochondrial protein import by interacting directly with the TIM23 mitochondrial import complex. The mitochondrial import defects and subsequent neuronal cell deaths was attenuated by overexpression of TIM23 (Yano 2014). These findings further demonstrate the high vulnerability of protein transport factors towards aberrant interactions.

Additional reasons for a high neuronal susceptibility may originate from a different role of autophagy in these highly complex cells. Neurons mainly live on glucose and protect their proteomes. Even under starvation, neurons show only limited autophagy. While artificially enhancing protein turnover by autophagy caused serious neuronal damage, inhibiting autophagy under stress increased their survival. Unspecific protein turnover may be too harmful for the complex neuronal architecture, so that neurons cannot fully make use of autophagy without damaging themselves (Koike 2008, Yamamoto 2014).

Perturbation of cellular transport seems to be an early and widespread event in the multifactorial disease pathology of neurodegenerative disorders. Transport problems consequently trigger a cascade of cellular malfunctions that ultimately lead to neuronal failure and death, spreading over non-replaceable regions of our brain (Gunawardena 2003, Soto 2003).

## Therapeutic strategies

Exploring the fundamentals of protein misfolding and aggregation and corresponding cellular defense mechanisms may lead us to novel starting points in drug development or for innovative therapies. This study revealed that intracellular molecular transport inefficiencies likely contribute early in the pathogenesis of neurodegenerative and other protein misfolding diseases. Defects in nucleo-cytoplasmic transport have been furthermore implicated in dipeptide repeat disorders and in cancer development (Jovicic 2015, Zhang 2015, Freibaum 2015; Mor 2014). An early recovery of this central function may prevent many detrimental consequences arising from the loss of cellular gradients and of a correct localization of biomolecules in the cell.

However, reversing the pathologic defects resulting from protein misfolding and consequent aberrant interactions is highly challenging if not impossible, since malfunctions are not limited to a single factor or pathway. Toxicity arising from misfolded proteins interferes with the activity of numerous metastable proteins that are often part of large protein complexes or interaction networks (Olzscha 2011). A significant part of the cellular proteome and other biomolecules may be functionally deactivated, destroyed, or even gain toxic functions on its own (Oskarsson 2015, Olzscha 2011, Kretschmar 2013, Butterfield 2010). This includes the nucleo-cytoplasmic transport and the large, highly coupled mRNA processing and export machinery. Avoiding a single or few of these detrimental interactions or trying to repair their consequences leaves behind a variety of remaining dysfunctions. A classical single target - single molecule strategy may therefore never be able to reverse the dysfunctions originating from gain-of-function related proteotoxicity.

### A new role for the nucleus in the prevention of toxic protein aggregation?

Avoiding damage therefore seems especially advisable for all neurodegenerative and other amyloidoses. Priority lies in the removal of the “toxic compound”, referring to all aberrant toxic protein species and aggregated assemblies that may give rise to further misfolding, as interferences in the aggregation process or attempts to dissolve cellular aggregates may distribute even more toxic material (Sperling 2011, Campioni 2010, Haass 2007). Thus, the whole range of misfolded states and their potential recognition signatures need to be characterized in high detail, attempting e.g. an early removal via cellular degradation pathways. Innovative strategies may thereby include cellular proteins that recognize hazardous species, transport them to less sensitive (sub-)compartments, or hand them over to degradation machineries directly. The nucleus may thereby move into the focus of basic and therapeutical research, as this study demonstrated the high tolerance of the compartment towards misfolded structures. Moreover, recent work indicated the targeted translocation of cytoplasmic misfolded proteins into the nucleus for degradation (Park 2013). A similar approach may be based on chaperone-mediated autophagy, where potentially toxic conformations are specifically recognized and targeted to autophagosomes (Filimonenko 2010). Despite the single factors that have been described, such as the misfolding selective Hsp40 chaperone Sis1p and the autophagy adaptor complex ALFY, respective cellular machineries remain largely to be explored (Park 2013, Filimonenko 2010). Therefore, the specific nuclear or autophagosomal targeting of defined misfolded structures represents a promising approach to release the cytoplasm from an overwhelming burden of hazardous conformations. Ideally, this may lead to preventive therapies, removing misfolded structures long before they accumulate and cause serious damage to cells.

## Increasing proteostatic resilience

In all cells, misfolded protein conformations are continuously forming and being removed. A novel therapeutic strategy may lie in enhancing the proteostasis machinery to increase cellular resilience towards the occurrence of misfolded species. This includes their removal and turnover, but furthermore the cellular capabilities of protein folding, maintenance, and aggregation prevention.

Indeed, aging seems to be accompanied by an accumulation of misfolded soluble and insoluble proteins (Gupta 2011, De Cecco 2011, David 2010). While protein synthesis and oxidative phosphorylation decline, including the levels of the respective cellular machineries, protein degradation and the activity of small heat shock proteins seem to gain in significance (Walther 2015, Jonker 2013, Li 2013). Age-dependent adaptations of the proteostasis network already occur naturally, which may be protective or harmful. The intriguing question remains, whether targeted modulations may help to reduce the damage of toxic conformations, increasing cellular viability and finally life expectancy of humans. In a long-lived mutant of *Caenorhabditis elegans*, increased levels of small heat shock proteins sequestered misfolded proteins into chaperone-enriched aggregates, accumulating potentially highly toxic soluble structures into less harmful insoluble aggregates (Walther 2015, Lu 2014). Despite such strategies may not ultimately heal neurodegenerative disease patients yet, a sophisticated intervention into the proteostasis network may help one day to significantly improve neuronal proteostasis in aging humans and to improve the quality of life for many years.

Neurodegenerative damage associated to protein misfolding can barely be repaired once it reached a certain threshold. A powerful and therapeutically fine-tuned proteostasis machinery is required (Morimoto 2008), equipping cells with the capabilities to proactively prevent exceedingly harmful misfolding damage. Recent research as well as our studies have shown that cells may be either unable to mount stress responses under conditions of neurodegenerative diseases, or misfolding might result in a chronic response that is unable to clear the aggregation load and finally leads to chronic inflammation, apoptosis and cell death (Roth 2014, Roberts 2014, Zhang 2008, Hoozemans 2005). Strategies investigated so far include the induction of a full, Hsf-1 regulated heat shock, which simultaneously increases the levels of multiple molecular chaperones, or the activation of autophagy e.g. by the mTOR inhibitor rapamycin. However, these approaches were accompanied by respective side-effects (Scheper 2015). A hyperactive heat shock response may induce cancer or even other protein misfolding disorders.

The nuclear proteostasis machinery and its connection to the whole proteostasis network remains to be explored in detail (Nielsen 2014, Hipp 2014, Labbadia 2015). Finding and understanding new key members that mediate proteostasis balance between the different cellular compartments may offer a great potential for a therapeutic refinement. More subtle, targeted interventions into the proteostasis network include a specific induction of individual effectors or of specific arms of stress response pathways. Such strategies may shift the balance from irreversible to reversible aggregation (Kaganovich 2008) and enable an early and efficient refolding or removal of misfolded proteins, long before proteostasis is at serious risk. Maintaining cellular proteostasis hopefully may allow us one day to keep our memories and skills in forms of neuronal and glial networks viable for many more years.

# Experimental procedures

## Molecular genetics

### Expression systems

For expression in mammalian cells, all  $\beta$ -proteins, S-GFP (NES-NLS-EGFP), and the cytoplasmic, nuclear or mitochondrial targeted versions of Luciferase-EGFP (Gupta 2011) were cloned into pcDNA3.1 Myc-His A vectors (Invitrogen) via KpnI and XbaI. All sequences were followed directly by a stop codon, excluding the expression of any 3' c-Myc- and His-tags of the vector.

Myc-Htt96Q was cloned into pcDNA3.1 Hygro(+) by Gregor Schaffar (Schaffar 2004).

TDP-F4 was received from the nonprofit repository Addgene (TDP-43-EGFP construct 4; Yang 2010).

Parkin $\Delta$ C (ParkinW453X) was kindly provided by Dr. Konstanze Winklhofer (Winklhofer 2003).

For bacterial expression (*E. coli*), the N-terminally c-Myc-tagged  $\beta$  proteins and  $\alpha$ S824 were cloned into pTrcHis (IPTG inducible; Invitrogen) or pBad (titratable expression by carbon sources such as arabinose, glucose, glycerol), excluding expression of His-tags included in the vector. For purification,  $\alpha$ S824 was cloned into the pProEx HT vector N-terminal of the His tag, which was cleaved off by TEV protease during purification of the protein.

### Sequence design

The  $\beta$  proteins and  $\alpha$ S824 were fused to an N-terminal c-Myc tag (MCEQKLISEEDLG) directly followed by (Olzscha 2011, West 1999):

#### $\beta$ 4

MQISMDYQLEIEFGNDNKVELQLNDSSGGEVKLQIRGPGGRVHFNVHSSGSNLEVNFNNDGGEVQFHMH

#### $\beta$ 17

MQISMDYEIKFHGDGDNFDLNLDDSSGGDLQLQIRGPGGRVHVHIHSSSGKVDFHVNNDGGDVEVKMH

#### $\beta$ 23

MQISMDYNIQFHNNGNEIQFEIDDSSGGDIEIEIRGPGGRVHIQLNDGHGHIKVDFHNDGGELQIDMH

#### $\alpha$ S824

MYGRNDLLEDLEVLKNEHKNWGGKDNLHDVDNHLQNVIEDIHDFMQGGSSGGKLQEMMKEFQVLDDELNNHLQGGKHTVHHIEQNIKEIFHHLEELVHR

NES- $\beta$ 4/ $\beta$ 17/ $\beta$ 23/ $\alpha$ S824 were generated by integrating a consensus NES (LELLEDLTLG; la Cour 2004) behind the c-Myc tag of the  $\beta$  proteins and  $\alpha$ S824, resulting in (MCEQKLISEEDLELLEDLTLG).

NLS- $\beta$ 4/ $\beta$ 17/ $\beta$ 23/ $\alpha$ S824 were generated by inserting two repeats of the SV40 derived NLS (DPKKRKRKV) N-terminal of c-Myc tagged  $\beta$  proteins or  $\alpha$ S824, resulting in (MAADPKKRKRKVDPPKKRKRKVDTYGAGEQKLISEEDLNGASS).



Mito- $\beta$ 4/ $\beta$ 17/ $\beta$ 23/ $\alpha$ S824 I and II were generated by inserting either the mitochondrial leader sequence of human mtHsp60 (MLRLPTVFRQMRPVSRLAPHLTRAYAKDVKFGCEQKLISEEDLGMQIS) or of human COX8 (MSVLTPLLLRGLTGSARRLPVPRAKIHSLCEQKLISEEDLG) followed by a c-Myc sequence N-terminal to the  $\beta$  proteins or  $\alpha$ S824. Both leader sequences were functional.

To generate EGFP fusion proteins, the N-terminally c-Myc tagged  $\beta$  proteins or  $\alpha$ S824 were fused N-terminal to EGFP (amplified from pEGFP-N1), connected via a flexible 16 amino acid long linker sequence (TSGSAASAAGAGEAAA; Chang JMB 2005) and cloned via KpnI and XbaI into pcDNA3.1 Myc-His A (Invitrogen). Any 3' tags of the vector are not expressed, omitted by a stop codon directly behind the EGFP sequence.

The NLS- $\beta$ 23 (K7T, K15T) and NLS-EGFP (K7T, K15T) nuclear import mutants were generated by site-directed mutagenesis, amplifying the respective NLS plasmids by PCR with an oligonucleotide carrying the nucleobases to be exchanged (Kalderon 1984, Hodel 2001).

S-GFP was generated by inserting the described NLS and NES connected via short linkers with an **HA tag** (MAADPKKKRKVDPKKRKVDTYGAG**YPYDVDPDYA**LELLEDLTTLGSDI) N-terminal to EGFP (from pEGFP-N1) via KpnI and XbaI into pcDNA3.1 Myc-His A (Invitrogen), omitting other tags of the vector.

Targeting versions of the  $\beta$  proteins and  $\alpha$ S824 and constructs fused to EGFP were created by PCR amplification, fusing oligonucleotides with overlapping sequences and amplifying the fused constructs with short 5' oligonucleotides for both strands. Integrated KpnI and XbaI restriction sites allowed restriction and ligation into the described vectors. See below for details of the individual steps of cloning.

American firefly luciferase, in form of the wild type protein or including a single or a double point mutation selected for thermal destabilization of luciferase, was fused to EGFP for use as fluorescent proteostasis sensors (Gupta 2011). Here, the luciferase-EGFP proteins were combined with nuclear export signals, nuclear localization sequences, or mitochondrial targeting sequences (as described for the  $\beta$  proteins, excluding the c-Myc tag) to direct the sensors specifically into these compartments. The targeting signals were fused N-terminally by PCR and ligated into pcDNA3.1 vectors using KpnI and XbaI restriction sites.

## Agarose gel electrophoresis

DNA fragments were separated in 0.8-1.5% agarose gels (LE agarose, Biozym) casted in TAE buffer (50x stock per liter: 242 g TRIS base, 57 mL acetic acid, 37 g EDTA), including 0.01% SYBR Safe DNA Gel Stain (Invitrogen). Samples were applied in DNA loading buffer (6x stock solution: 30% glycerol, 0.25% bromophenol blue) with a 1 kb DNA ladder (Promega) and run at 100 V in TAE. For visualizing, the gel was illuminated using blue light (Sage Imager 2.0, Invitrogen).

## Polymerase chain reaction (PCR)

For molecular cloning or sequence analysis, DNA fragments were amplified by PCR (Mullis 1986). The components of a standard PCR are described below. In case of inefficiency, concentrations of primers, template, magnesium ions, or the annealing temperature were modified.

The PCR reaction was run including Herculase DNA Polymerase (Agilent Technologies) or Pfu DNA Polymerase (Promega) in T3 Thermocyclers (Biometra). For mutagenesis, the complete plasmids were amplified in 20-25 cycles, syntheses of inserts for cloning or fusion of DNA fragments were performed in up to 30 cycles.

**Table 2 | Standard PCR setup.**

Reagent	Volume
DNA template (50-300 ng/ $\mu$ L)	1 $\mu$ L
5'-Primer 0.1 $\mu$ M	5 $\mu$ L
3'-Primer 0.1 $\mu$ M	5 $\mu$ L
dNTPs (2.5 mM each nucleotide)	5 $\mu$ L
10x Herculase buffer	5 $\mu$ L
Herculase (5 U/ $\mu$ L)	1 $\mu$ L
ddH <sub>2</sub> O added to a final volume of	50 $\mu$ L

**Table 3 | Standard PCR cycling program.**

Reaction Step	Temperature	Time
Initial denaturation	95°C	2 min
Denaturation	95°C	30 sec
Annealing	40-60°C	30-60 sec
Elongation	72°C	1 min/kb
Final Elongation	72°C	10 min
Storage	4°C	$\infty$

PCR products were purified with the Wizard SV Gel and PCR Clean-Up System (Promega).

### Site-directed mutagenesis (mutations, insertions, and fusion proteins)

Site-directed modifications of genetic sequences were created by PCR.

Site-directed mutations, such as an exchange of single codons in the SV40 nuclear localization signal rendering it functionally ineffective, were introduced by amplifying the complete gene or the entire plasmids with synthetic oligonucleotide primers carrying the desired modifications (exchange of a single or a few nucleotides). Afterwards, the original methylated plasmids were digested by DpnI (NEB) for 60 min at 37 °C, and the remaining solution was added to chemically competent *DH5 $\alpha$*  cells for transformation.

For insertions or deletions of e.g. protein targeting signals or antibody binding sites, similar oligonucleotide primers were applied containing the desired sequences including restriction sites.

Fusion proteins (such as EGFP fusions, introduction of protein targeting signals) were created by amplifying DNA sequences carrying overlapping sequences. Overlapping sequences were therefore introduced running a PCR with primers containing the respective sites at their 5' or 3' ends. These PCR products were purified and fused in a second PCR reaction, where the overlapping sequences bind to each other so that DNA polymerase can prolong residual complementary sequences.

Additional short primers at the 5' ends of the complete fusion sequence allowed amplifying the entire fused sequences selectively in the same reaction. The fusion sequences were then purified, restricted and ligated into desired vectors.

### **Molecular cloning (restriction, ligation)**

The restriction of plasmids and linear DNA inserts was performed applying site-specific restriction enzymes (NEB or Fermentas). Restricted plasmid backbones were dephosphorylated to prevent self-religation (Calf Intestinal Alkaline Phosphatase, NEB). Concentrations, buffers, and incubation times were chosen according to the manufacturers' instructions or modified, if necessary. Results were controlled by agarose gel electrophoresis. DNA fragments of interest were selected and purified for further processing (Wizard SV Gel and PCR Clean-Up System, Promega).

For ligation, 0.5  $\mu\text{L}$  of T4 DNA ligase (Promega) was added to a total volume of 30  $\mu\text{L}$  reaction mix, containing 50-200 ng restricted vector, 3-7 times (molar ratio) restricted inserts, and ligation buffer (Promega). Restrictions were carried out overnight at 16 °C under agitation. Up to 5  $\mu\text{L}$  of the ligated sample were added to chemically competent *DH5 $\alpha$*  cells for transformation.

### **Preparation and transformation of chemically competent *E. coli* cells**

An appropriate *E. coli* strain (*DH5 $\alpha$*  for plasmid preparations or BL21 (DE3) for protein purification) was plated out on LB agar. From this, a single colony was grown in a small pre-culture to inoculate 1 L LB medium growing to an  $\text{OD}_{600}$  of < 0.5. Cells were centrifuged at 6,000 x g for 10 min at 4 °C and resuspended in ice-cold sterile  $\text{Ca}^{2+}$ /glycerol solution (60 mM  $\text{CaCl}_2$ , 10 mM Pipes, 15% glycerol, pH 7.0). After a second centrifugation and resuspension, cells were kept on ice for 30 min. A third centrifugation followed, cells were resuspended in 10 mL ice-cold  $\text{Ca}^{2+}$ /glycerol buffer and dispensed in e.g. 200  $\mu\text{L}$  aliquots. Cells were immediately frozen in liquid nitrogen and stored at -80 °C (adapted from Davis 1994).

For transformation, 50  $\mu\text{L}$  chemically competent cells per sample were thawed on ice, and 10-500 ng plasmid DNA or up to 5  $\mu\text{L}$  of a ligation reaction mix were added. After incubation on ice or at 4 °C for 20 min, cells were heat shocked at 42 °C for 45 sec and cooled on ice for further 5 min. 1 mL of LB medium was added, and the cells were incubated at 37 °C shaking for 1 h. Cells were sedimented and 400  $\mu\text{L}$  of fresh LB medium was added. The cells were plated on LB agar plates containing antibiotics for selection (100  $\mu\text{g}/\text{mL}$  ampicillin or 50  $\mu\text{g}/\text{mL}$  kanamycin) and incubated overnight at 37 °C.

### **Plasmid preparation**

Plasmids were prepared from selective LB cultures starting from a single colony of *DH5 $\alpha$*  cells transformed recently.

Plasmids for bacterial transformation or cloning applications were prepared using the Wizard Plus SV Minipreps kit (Promega). Endotoxin free plasmids for human cell culture were prepared utilizing the EndoFree Plasmid Maxi Kit (Qiagen) according to the supplier's instruction.

Concentration and quality of purified DNA was determined by UV spectroscopy (260/280 nm), and sequences were confirmed by DNA sequencing (core facility, MPI of Biochemistry).

## Protein purification

### De novo $\beta$ proteins

To purify  $\beta$  proteins from *E. coli* BL21 (DE3) cells, single colonies were picked and grown in selective LB medium at 37 °C overnight. On the next morning, precultures were diluted and grown at 37 °C until an OD<sub>600</sub> of 1.0 was reached, induced with 0.5 mM isopropyl-D-thiogalactoside (IPTG), and grown for protein expression for 4 h. Cells were harvested by centrifugation at 5000 x g for 10 min and resuspended in 25% sucrose, 50 mM Tris (pH 8.0), 1 mM EDTA, supplemented with complete protease inhibitor (Roche) and 1 mg/mL lysozyme (Sigma). The cells were lysed by repeated freeze-thaw cycles and DNA was digested by Benzonase (Novagen).

Inclusion bodies were isolated by repeated washing in 0.5% Triton X-100, 1 mM EDTA, and centrifugation at 20,000 x g for 15 min. The pellet was dissolved in 8 M urea and separated on a MonoQ 10/100 HR16/10 column in 8 M urea, 25 mM Tris pH 7.5, applying a gradient from 0 to 1 M NaCl. The fractions containing  $\beta$  proteins were further purified by size exclusion chromatography on Sephacryl S-300 HiPreP 26/60 in 8 M urea, 0.1 M NaCl, 25 mM Tris pH 7.5. After dialysis into 150 mM KCl, 0.5 mM MgCl<sub>2</sub>, 25 mM HEPES pH 7.5 (or originally 0.1 M NaCl, 25 mM sodium phosphate, pH 7.5) overnight, the proteins formed invisible soluble oligomers, which eluted shortly after the excluded volume of Sephacryl S-300 size-exclusion columns run on the same buffer solution. All protein samples were stored at -80°C (based on West 1999).

### De novo $\alpha$ -helical protein $\alpha$ S824

The soluble 6 x His-tagged  $\alpha$ S824 protein was purified after expression for 3 h from *E. coli* cells, lysed (lysis buffer see above) and centrifuged at 20,000 x g for 15 min. The supernatant was applied to Ni-NTA agarose for 30 min at 4 °C under agitation. The material was loaded on a column and washed with 300 mM NaCl, 30 mM Imidazol in 25 mM phosphate buffer, pH 8, until the eluate showed an OD<sub>280</sub> < 0.05. The pure protein was finally eluted in the same buffer containing 250 mM Imidazol and dialyzed into 100 mM NaCl, 25 mM sodium phosphate, pH 7.5.

### Hsp110 (Hsp105)

Purification of 6 x His-tagged Hsp110 (cloned into pProEx) was performed from *E. coli* BL21 (DE3) cod+ RLI cells (Novagen). Hsp110 expression was induced at an OD<sub>600nm</sub> of 0.6 with 1 mM IPTG, accompanied by a temperature shift from 37°C to 18°C. After overnight expression, cells were harvested and resuspended in 350 mM KCl, 25 mM HEPES (pH 7.5), 5 mM imidazole, 1 mM PMSF, and 0.5 mg/mL lysozyme incubating at RT for 20 min, followed by lysis through repeated freeze-thaw cycles. After sedimentation of cell debris by centrifugation at 20,000 g for 15 min at 4°C, the resulting supernatant was loaded onto a Ni-NTA charged 5 mL HiTrap Chelating HP column at 4 °C. After washing with 350 mM KCl, 25 mM HEPES (pH 7.5), 5 mM imidazole, including 1 mM PMSF (until OD<sub>280</sub> < 0.05), 6 x His-tagged Hsp110 was eluted by a gradient from 5-200 mM imidazole in the same buffer. This gradient resulted in a separation of full length 6 x His-Hsp110 and cleavage products present in the lysate. For cleavage of the 6 x His-tag, the eluted full length protein was incubated for 60 min at RT with TEV protease at a molar ratio of 20:1 in the presence of 5 mM  $\beta$ -mercaptoethanol. After dilution into the same buffer containing 5 mM imidazol, the solution was again applied to a Ni-NTA column to remove uncleaved 6 x His-Hsp110 and 6 x His-TEV protease. In a final purification

step, Hsp110 was passed through a Sephacryl S-300 HiPreP 26/60 size exclusion column equilibrated in 150 mM KCl, 0.5 mM MgCl<sub>2</sub>, 25 mM HEPES pH 7.5. Eventually, Hsp110 containing fractions were concentrated in a Vivaspin 50000 MWCO ultrafiltration tube (modified from Dragovic 2006).

## Protein analytics

### Determination of protein concentration

The concentration of the purified  $\beta$  proteins was determined by UV absorbance of the protein backbone at 210 nm, since the  $\beta$  proteins do not contain any tryptophan. The peptide bond absorbs at 210 nm with an extinction coefficient of 20 for 1 mg/mL protein solution (up to 24, in case of a protein containing tryptophan; Scopes 1974). The molar concentration depends on the length of the polypeptide chain (number of peptide bonds).

The concentration of the purified, His-tagged  $\alpha$ S824 protein was determined by its UV absorbance at 280 nm. The extinction coefficient ( $\epsilon_{280} = 12,950 \text{ M}^{-1} \text{ cm}^{-1}$ ) was calculated using the ProtParam tool at the ExPaSy Bioinformatics Resource Portal (<http://web.expasy.org/cgi-bin/protparam/protparam>; Edelhoch 1967, Pace 1995) based on the amino acid sequence of  $\alpha$ S824 (three tryptophans).

### Discontinuous, denatured SDS-PAGE

Discontinuous SDS-PAGE (sodium dodecylsulfate polyacrylamide gel electrophoresis) under denaturing and reducing conditions (including SDS and  $\beta$ -mercaptoethanol) is widely used to separate proteins (Laemmly 1970). The binding of negatively charged SDS molecules to polypeptides allows a separation according to the mass of proteins, since the number of binding detergent molecules is relatively proportional to the length of the polypeptide chains, and therefore determines their charge in the electrical field. Electrophoresis was performed on a Mini-Protean 3 System (BioRad).

**Table 4 | Polyacrylamide gel formulation for SDS-PAGE (for 2 gels / 10 mL solution)**

Acrylamide gel	dd H <sub>2</sub> O (mL)	30% Acrylamide/ Bis-acrylamide (mL)	Gel buffer solution (mL)	10% SDS (w/v) (mL)
4%	6.1	1.3	2.5	0.1
5%	5.7	1.7	2.5	0.1
6%	5.4	2.0	2.5	0.1
7%	5.1	2.3	2.5	0.1
8%	4.7	2.7	2.5	0.1
9%	4.4	3.0	2.5	0.1
10%	4.1	3.3	2.5	0.1
11%	3.7	3.7	2.5	0.1
12%	3.4	4.0	2.5	0.1
13%	3.1	4.3	2.5	0.1
14%	2.7	4.7	2.5	0.1
15%	2.4	5.0	2.5	0.1
16%	2.1	5.3	2.5	0.1
17%	1.7	5.7	2.5	0.1

Up to 2.5 mL of dd H<sub>2</sub>O was replaced by 2 M sucrose. The resolving gel buffer consists of 1.5 M Tris (pH 8.8), the stacking gel buffer of 0.5 M Tris (pH 6.8). The polymerization was started by the addition of 50 µL 10% APS (ammonium persulfate) and 5 µL TEMED (resolving gel) or 50 µL 10% APS and 10 µL TEMED (stacking gel).

Discontinuous gels concentrate the protein sample at the border between the highly permeable stacking gel and the lower permeable resolving gel, which leads to a high resolution of protein separation. Assuring a high quality, resolving gels were covered in dd H<sub>2</sub>O until complete polymerization, before stacking gels were casted.

Protein samples were dissolved in 2x SDS loading buffer (60 mM Tris (pH 6.8), 2% SDS, 25% glycerol (v/v), 0.01% bromphenolblue (w/v); 5% β-mercaptoethanol (v/v) added prior to use), heated to 95 °C for 5 min, and immediately vortexed to achieve complete denaturation. Gel electrophoresis was performed using SDS-PAGE running buffer (5x stock/L: 15 g Tris, 75 g glycine, 5 g SDS, pH ~8.4) at initially 70 V (protein sample in stacking gel), later 100-250 V (running gel). Prestained Protein Marker (Fermentas) was added as a size marker. Protein samples were stored at -80 °C.

### **Coomassie Brilliant Blue staining**

Gels were quickly washed in dd H<sub>2</sub>O after electrophoresis, proteins were fixed (10% acetic acid), stained (50% ethanol, 10% acetic acid, 0.25% Serva Blue R) and destained (50% methanol or ethanol, 10% acetic acid), leading to a specific blue coloration of protein bands. The gels were scanned electronically or dried on filter paper.

### **Immunoblotting**

Electrophoretically separated proteins were blotted from polyacrylamide gels on nitrocellulose or (methanol activated) PVDF membranes for immunodetection (Towbin 1979) with a Mini Trans-Blot Cell Western blotting device (Bio-Rad). According to the setup, the protein was transferred at a constant electrical voltage (100V) for 90-120 min in Western Blot Transfer Buffer (25 mM Tris, 192 mM glycine, 20% ethanol, pH ~8.4). After transfer, membranes were washed quickly in TBS-T (25 mM Tris (pH7.6), 150 mM NaCl, 0.1% Tween 20) and then incubated with primary antibodies against a desired epitope in TBS-T containing 5% (w/v) skimmed milk (Saliter) for blocking unspecific interactions for 1 h at room temperature up to overnight at 4°C. After extensive washing with TBS-T, a secondary antibody (standard dilution 1:3000) directed against the primary species and conjugated to horseradish peroxidase was incubated for 1-3 h at room temperature. After extensive washing in TBS-T, the immunoblots were developed using the chemiluminescence Rodeo ECL solutions (USB) and analyzed on a LAS-3000 image reader (Fujifilm) and by AIDA software (Raytest). If desired, the blots were stripped (Restore Western Blot Stripping Buffer, 21059, ThermoFisher Scientific) for 15-30 min and washed in TBS-T for another immunolabeling.

### **Native dot blots for immunodetection of A11 reactive species**

The β-sheet proteins were freshly refolded from denaturant (8 M guanidine hydrochloride or 10 M urea) into physiological buffer (150 mM KCl, 0.5 mM MgCl<sub>2</sub>, 25 mM HEPES (pH 7.5)) for several hours. 3 µL of 20 µM protein solutions were pipetted on a nitrocellulose membrane, which was incubated with A11 antibodies (1:2000, Prof. C.Glabé) or anti-c-Myc (9E10, Santa Cruz; 1:3000) in 25 mM Tris,

150 mM NaCl, 0.1% Tween 20 and 1% BSA at pH 7.6 overnight. After extensive washing with TBS-T, a secondary antibody conjugated to horseradish peroxidase was incubated for 1 h. The blots were developed after extensive washing with TBS-T. The A11 reactivity was compared to control proteins such as the  $\alpha$ -helical  $\alpha$ S824, BSA, or MBP.

For analyzing the effect of sonication on  $\beta$  protein structures, the protein solutions were sonicated at 2  $\mu$ M concentrations in physiological buffer for 2-60 sec with a microtip (intensity level 5, Ultrasonic Processor XL, Misonix Inc.), directly pipetted on a nitrocellulose membrane, and developed as described.

## Spectroscopy

### Fluorescence spectroscopy

The fluorescence spectroscopic measurements were accomplished on a FluoroLog-3 Spectrofluorometer (HORIBA Jobin Yvon).

The refolding and aggregation kinetics were recorded by diluting denatured  $\beta$  proteins out of 8 M guanidine hydrochloride 1:400 into physiological buffer (150 mM KCl, 0.5 mM MgCl<sub>2</sub>, 25 mM HEPES, pH 7.5) at a final protein concentration of 3  $\mu$ M protein.

For steady state measurements, the protein concentration was kept at 3  $\mu$ M in physiological buffer containing 20  $\mu$ M of the fluorescent dyes Thioflavin T (Sigma) or ANS (8-Anilino-1-naphthalenesulfonic acid, Sigma), or 1  $\mu$ M of NIAD-4 (ICX Nomadics). Thioflavin T fluorescence was excited at 440 nm, NIAD-4 fluorescence at 475 nm, and ANS fluorescence at 375 nm. Refolding kinetics were analyzed by Thioflavin T emission observed at 482 nm, NIAD-4 emission at 590 nm, or ANS emission at 490 nm.

### Circular dichroism (CD) spectroscopy

CD measurements were performed on a Jasco CD Spectrometer J-715 at 25°C in 6 mM HEPES, 25 mM KCl, pH 7.5 at a protein concentration of 0.1 mg/mL. Spectra were recorded in a 0.1 mm quartz cuvette between 197 and 250 nm (with a bandwidth of 1 nm and a scanning speed of 50 nm/min). Each single spectrum was averaged from 3 accumulative scans. Secondary structure content was analyzed by the CDSSTR algorithm (Johnson 1999; Jasco software).

### Fourier transform infrared spectroscopy (FTIR)

The  $\beta$ -sheet proteins were dialyzed overnight against 10 mM potassium phosphate, 10 mM NaCl, pH 6.0,  $\alpha$ -S824 was dialyzed against 10 mM potassium phosphate, 10 mM NaCl, pH 7.5. Infrared spectra were measured in the Vertex 70 spectrophotometer (Bruker, Germany) equipped with a TGS detector using attenuated total reflection (ATR) with parallelogram-shaped Germanium crystals as internal reflection plates (Korth Kristalle, Germany). A thin film of 50-100 mg of the respective protein was dried under N<sub>2</sub> on one side of the Germanium crystal that was placed in a homemade gas-tight chamber (Heinz et al., 2003). H-D exchange was performed by flushing D<sub>2</sub>O-saturated N<sub>2</sub> through the chamber and monitored every 1 to 3 min until the spectra were stable (usually after 45 min). Spectra were recorded before and after H-D exchange with a nominal resolution of 2 cm<sup>-1</sup> in

the double-sided, forward-backward mode, collecting 1024 scans per sample. Water vapor and CO<sub>2</sub> contributions were corrected for using the atmospheric compensation of the OPUS software (version 6.5) from Bruker. The spectral region of the amide I band (1705 to 1595 cm<sup>-1</sup>) was extracted, corrected for the base line, and scaled so as to obtain a constant integral value for comparison. Peak positions of spectral components were analyzed using Fourier-self deconvolution and the second derivative of the spectra.

## **Electron microscopy**

Carbon-coated copper grids were covered in  $\beta$  protein aggregates either in 25 mM HEPES, 150 mM KCl, 0.5 mM MgCl<sub>2</sub>, pH 7.5 or 10 mM potassium phosphate buffer at pH 6.0 (after overnight dialysis into the respective buffer) for 1 min, washed 3 times, stained for 1 min in 2% uranyl acetate, and air-dried. A CM200 FEG transmission electron microscope (FEI, Eindhoven) with a CCD-camera was used at an accelerating voltage of 160 kV and at a magnification of 55,000 x.

## **Human cells: culture and transfection**

### **Cultivation and passage of human cells**

Cell lines utilized in this study were grown in cell culture flasks with a hydrophilic surface of carboxy- and hydroxygroups (Cellstar, Greiner Bio-One). Cells were cultured in supplemented DMEM (Dulbecco's Modified Eagle Medium, Gibco) containing 2 mM L-glutamine, 0.1 mM MEM non-essential amino acids and 100 U/mL penicillin and 100  $\mu$ g/mL streptomycin (all from Gibco), enriched by 10% FBS (fetal bovine serum, Gibco). Cells were grown at 37 °C and 5% CO<sub>2</sub> in a water vapor saturated atmosphere.

For subcultivation, cells were washed with PBS (Gibco), and for dissociation treated for 3 min in TrypLe Express (Gibco) at 37 °C. Fractions of 5-50% of the cells were transferred into cell culture flasks with supplemented enriched medium.

### **Cryopreservation**

During exponential growth (80-90 % confluence), cells were washed (PBS), treated with TrypLe Express (Gibco) and centrifuged at 300 x g. After aspiration of the medium cells were suspended in freezing medium comprising 10% sterile DMSO, 25% FBS (Gibco), and 65% DMEM (Gibco). Cells were then transferred into sterile cryovials and placed at -20 °C for 2 h and at -80 °C overnight, before keeping them at -80 °C for several months or in liquid nitrogen for long time storage.

For revitalizing, the cryovials were taken out of the liquid nitrogen and immediately warmed up in a 37 °C water bath. The cellular suspension was transferred into 37 °C prewarmed medium and centrifuged at 300 x g, the medium was aspirated. Resuspended in fresh supplemented enriched medium, the cells were cultured under standard conditions.

### **Determining cell numbers**

For cellular counts, a fraction of cells were stained for dead cells with 0.4% Trypan Blue Solution (Sigma) and pipetted on a Neubauer counting chamber. All living cells of one large square (1 mm<sup>2</sup> or



0.1 mm<sup>3</sup>), comprising 25 small squares, were counted (at least 100 cells) and multiplied by 10,000 to calculate the cell number per milliliter.

### **Transient transfection by electroporation**

For electroporation, HEK293T cells were washed, treated with TrypLe express, counted, and resuspended in electroporation medium (25% FBS and 75% non-supplemented DMEM, Gibco). Cells were then mixed with expression plasmids prepared utilizing the EndoFree Plasmid Maxi Kit (Qiagen). 2-30 µg of plasmids were added to 2-10x10<sup>6</sup> cells in 400 µL electroporation medium, and the mix was transferred to 0.4 cm electroporation cuvettes (Bio-Rad). The electroporation was conducted at 225 V, ∞ Ω, 950 µF exponential wave for HEK293T cells (modified from Barry 2004 and Jordan 2008) with the GenePulser XCell System (Bio-Rad), optimized on our distinct device. After electroporation, cells were kept at room temperature for 10 min for recovery, and then resuspended in 5 mL supplemented DMEM. After centrifugation at 300 x g for 3 min, cell pellets were resuspended in an appropriate volume of fresh supplemented DMEM to remove dead cells or detrimental cellular factors released during the pulse. The cells were cultivated for several hours up to 3 days for protein expression (based on Barry 2004, Jordan 2008).

Electroporation conditions were adapted for neuroblastoma cell lines (SH-SY5Y or SK-N-SH). For these cells, optimal conditions for protein expression and a strong cytotoxicity of β proteins relative to control cells transfected with empty vectors were found at a 225 V, 20 ms square wave pulse (similar to Jordan 2008).

### **Transient transfection by lipofection**

HEK293T or SH-SY5Y cells were seeded one or two days before transfection in appropriate cell culture vessels for equilibration and growth. For lipofection, 1 µg of plasmid in 300 µL OptiMem I (Life Technologies) was mixed with 2.5 µL Lipofectamine 2000 (Life Technologies) diluted in 300 µL OptiMem I after 5 min of incubation, gently vortexed, and incubated for 20 min at room temperature. The mixture was added to cells growing on a surface of 4 cm<sup>2</sup> (standard 12 well plate). For other cultivation areas, measures were adapted linearly to the surface. After 3 h, the transfection mix was replaced by supplemented DMEM omitting antibiotics.

## **Confocal fluorescence microscopy**

### **Fixation and immunostaining of human cells**

Cells from mammalian tissue culture were grown on poly-L-Lysine coated coverslips (German glass, BD BioCoat, BD Biosciences) for 24-72 h, fixed in 4% formaldehyde/PBS for 10 min, permeabilized in 0.1% (v/v) Triton X-100/PBS for 5 min, and washed with PBS. Cells were treated with primary antibodies against a target epitope at dilutions of 1:200 to 1:3000 in 1% BSA/PBS for 1 h at room temperature up to overnight at 4 °C, followed by secondary antibodies conjugated to fluorescent dyes for one or several hours at room temperature. Cells were then incubated in DAPI/PBS at 0.25 µg/mL for 10 min, washed in PBS, and dipped shortly in dd H<sub>2</sub>O before mounting them in fluorescence mounting medium (DAKO) on a glass slide. To detect amyloid species, cells were additionally stained with 100 nM NIAD-4 (ICX Nomadics) in PBS for 30 min after fixation and permeabilization. The specimens were kept at 4 °C.

## Confocal immunofluorescence and image acquisition

Image acquisition was performed on a LEICA TCS SP2 AOBS or on a LEICA TCS SP8 AOBS confocal laser scanning microscope equipped with LEICA HCX PL APO 63x/NA1.4 oil immersion objectives.

Up to four different fluorescent dyes were applied for cellular localization of proteins, DNA, or RNA. In multicolor samples, emission bandwidth settings and signal amplification intensities were set to exclude erroneous co-localizations. Therefore, single stained controls were prepared.

## Fluorescence in situ hybridization (RNA FISH)

HEK293T or SH-SY5Y cells were grown on poly-L-Lysine coated coverslips (German glass, BD BioCoat, BD Biosciences) for 24-72 hours, fixed in 4% paraformaldehyde in ultrapure SSC solution (15 mM saline-sodium citrate, 150 mM NaCl, pH 7.0 (UltraPure SSD, ThermoFisher Scientific), DEPC treated dd H<sub>2</sub>O) for 10 min, permeabilized with 0.1% (v/v) Triton X-100 in ultrapure SSC for 5 min, and washed in FISH buffer (UltraPure SSC, 10% formamide) for 10 min at 37 °C. Fluorescently labeled Cy5-(d)T<sub>30</sub> (desoxythymidine) oligonucleotides were applied at 0.1 μM in FISH buffer including 10% dextran sulfate (average molecular weight > 500 kDa, Sigma) for 2-3 h in a humidified chamber at 37 °C. Cells were washed 2 times with FISH buffer at 37 °C. Antibody and DAPI staining followed subsequently as described in PBS based buffers.

## Fluorescence in situ hybridization on murine brain sections (RNA FISH)

Animal experiments were performed in compliance with institutional and governmental regulations.

R6/2 mice and wildtype litter mates were received from The Jackson Laboratory (B6CBA-Tg(HDexon1)62Gpb/1J). Mice were anaesthetized with 5% chloral hydrate in PBS and transcardially perfused with 4% paraformaldehyde/PBS. The brains were post-fixed for 2 h in 4% paraformaldehyde/PBS at 4 °C and cryoprotected in 30% sucrose/PBS for 24 h at 4 °C. Brains were embedded in Tissue-Tek O.C.T. Compound (Sakura) at -20 °C, 20 μm coronal sections were cut on a freezing microtome (Leica), dried on glass slides overnight on air and stored at -20°C until usage.

Sections were thawed and washed in prewarmed FISH tissue buffer (15 mM saline-sodium citrate, 150 mM NaCl, pH 7.0 (ultrapure SSD, ThermoFisher Scientific), 10% formamide, 0.3% Triton X-100 (v/v)) at 45 °C. A higher hybridization temperature than for cultured cells was necessary to prevent background binding to nuclear DNA. Hybridization to Cy5-(d)T<sub>30</sub> oligonucleotides was performed in a humidified chamber in prewarmed fish tissue buffer including 10% dextran sulfate (average molecular weight > 500 kDa, Sigma) for 1-3 h at 43 °C. Afterwards, sections were washed with FISH tissue buffer for 10 min at 45 °C.

For immunostaining, the hybridized sections were washed in 0.3% TritonX-100/PBS, and stained for extended polyQ tracts (monoclonal anti-polyglutamines antibody, mouse, clone 3B5H10, Sigma, P1874; Miller 2011) in 1% BSA, 0.3% TritonX-100/PBS), for active apoptosis (cleaved Caspase-3 Asp75 antibody, rabbit, Cell Signaling Technology, #9661), or for THOC2 (HPA047921, Sigma) overnight at 4 °C, followed by fluorescently labeled secondary antibodies. Sections were subsequently incubated in DAPI/PBS at 0.25 μg/mL for 10 min and washed 2 times in PBS before covering them under a glass slide (Menzel Gläser #1, Thermo Scientific) in fluorescence mounting medium (DAKO).

## Fixation and staining of mitochondrial matrix proteins

The cell-permeant MitoTracker Red CM-H<sub>2</sub>XRos (M7513, Invitrogen) is a reduced, non-fluorescent dye that fluorescents upon oxidation and accumulates in mitochondria in living cells in a membrane potential dependent manner. MitoTracker Red was added to HEK293T cells 24 h after transient transfection, growing on poly-L-Lysine coated coverslips, at 100 nM in DMEM (including glutamate) for 1 h at 37 °C. Cells were washed with PBS and subsequently treated as described for immunostaining. After paraformaldehyde fixation, cells were additionally permeabilized in ice-cold methanol at -20 °C for 10 min, enabling an antibody staining of mitochondrial matrix proteins.

## Cellular experiments and assays

### Cytotoxicity measurements by MTT assay

MTT (3-(4,5-Dimethylthiazol-2-yl)-2,5-diphenyltetrazoliumbromid) is a yellow, water soluble dye, which upon reduction by cellular enzymes becomes a water insoluble, blue formazan product. The viability of the cells is reflected in their capacity to reduce MTT by cellular reducing agents.

### Intracellular expression of $\beta$ proteins

Transiently transfected cells were incubated (usually 25x, 40x, and 70x10<sup>5</sup> cells in 3 replicates in 24 well plates) for 72 hours under standard conditions. The culture medium was aspirated and 0.5 mL of 0.5 mg/mL MTT dissolved in non-supplemented DMEM was added for 1 h at 37 °C. Cells were lysed by addition of 0.5 mL of 20% SDS (w/v) and 50% DMF (v/v) in water and repeated pipetting. Absorbance was detected at 570 nm (KC4 software, Synergy-HT, BioTek) and compared to empty-vector control cells and cell-free control wells (Shearman 1995).

### Extracellular addition of purified $\beta$ proteins to the culture medium

Untransfected cells were incubated with purified  $\beta$  proteins (usually 25x, 40x, and 70x10<sup>5</sup> cells in 3 replicates in 24 well plates) for 24-48 hours in supplemented DMEM. Immediately before addition to the culture medium, purified  $\beta$  proteins (in form of soluble, non-precipitated oligomers in physiological buffer) were sonicated with a tip sonicator (Ultrasonic Processor XL, Misonix Inc.) at level 5 for 5-10 sec, and applied in concentrations of 20 nM up to 2  $\mu$ M in supplemented DMEM.

### *E. coli* growth inhibition

BL21 cells were freshly transformed with pTrcHis vectors containing  $\beta$  proteins or  $\alpha$ -helical proteins and grown overnight on selective LB agar plates. Single colonies were selected and grown in selective 6 mL LB liquid cultures overnight. On the next morning, cultures were diluted to an OD<sub>600nm</sub> of 0.15 into fresh selective 100 mL LB. Protein expression was induced after an initial recovery from stationary phase at an OD<sub>600nm</sub> of 0.4. Growth of the cultures was followed photometric (OD<sub>600nm</sub>) until a plateau was reached after ~4 h. The growth of BL21 cells carrying an expression plasmid was compared to control cells transformed with an empty vector control.

## NF- $\kappa$ B activation and translocation

HEK293T cells were transiently transfected with 25  $\mu$ g of pcDNA3.1 plasmids encoding  $\beta$  proteins, Htt96Q, TDP-F4, Parkin $\Delta$ C, or with control vectors (empty or  $\alpha$ S824) by electroporation or lipofection, and incubated for 40 hours. NF- $\kappa$ B signaling was then activated by the addition of 20 ng/mL human TNF $\alpha$  (recombinant *E.coli* cytokine from Jena Bioscience (PR-430) or Biomol GmbH (50435)). TNF $\alpha$  was added for 15 min before cells were collected for immunoblotting (best timing to observe p65 phosphorylation and I $\kappa$ B degradation) or for 30 min for immunofluorescence (best timing for nuclear translocation of p65). Samples were fixed and immunostained as described above.

## Compartmental quantification of S-GFP

S-GFP carries a combined N-terminal NES and NLS and is therefore permanently actively shuttled between cytoplasm and nucleus. HEK293T cells were transfected (by electroporation) with 3  $\mu$ g pcDNA3.1 encoding S-GFP in addition to 25  $\mu$ g of plasmids encoding the  $\beta$  proteins, Htt96Q, Parkin $\Delta$ C, or with empty control vectors and incubated for 40 h in enriched DMEM. Cells were treated with either 10 ng/mL CMR1 inhibitor Leptomycin B (LMB) or DMSO for 15 min before fixation and immunostaining of aggregates.

The relative concentration of S-GFP in the cytoplasm and nucleus were quantified by the fluorescence intensity ratio of around 75-150 cells per sample and condition, and three independent repetitions each. The fluorescence intensities in the cytoplasm and nucleus were quantified using ImageJ (Rasband, W.S., ImageJ, U. S. National Institutes of Health, Bethesda, Maryland, USA, <http://imagej.nih.gov/ij/>, 1997-2012.). The cytoplasmic/nuclear concentration gradient corresponds directly to the cytoplasmic/nuclear fluorescence ratio. The relative nuclear localization (N) or relative cytoplasmic localization (C) of S-GFP was calculated from the fluorescence ratio (R) nucleus/cytoplasm by  $N=100/(1+1/R)$ , assuming that  $N+C=100\%$  and  $N/C=R$ , and that cytoplasm and nucleus similar volumes.

## THOC2 knockdown by siRNA

HEK293T or SH-SY5Y cells were seeded on poly-L-Lysine coated coverslips and grown overnight. Cells were transfected with siRNA targeting human THOC2 (Thermo Scientific, ON-TARGET plus human THOC2 siRNA L-025006-01) or by non-targeting control siRNA targeting firefly luciferase mRNA (Thermo Scientific, SMARTpool ON-TARGETplus non-targeting siRNA #2, D-001810-02-05). The transfection was performed at 50 nM (5  $\mu$ L of 5  $\mu$ M) siRNA and 2.5  $\mu$ L DharmaFECT1 (Thermo Scientific) in 500  $\mu$ L Opti-Mem I Reduced Serum Media (Gibco) for 3 h. Cells were incubated for 24 h, 48 h, and 72 h in enriched DMEM and subsequently fixed, permeabilised (0.1% TritonX-100 in PBS) and (immuno-)stained for poly(A) RNA and THOC2, as described. The cellular knockdown of THOC2 was verified by immunoblotting.

## Cellular distribution of mRNA after proteasome inhibition by MG132

HEK293T or SH-SY5Y cells were seeded on poly-L-Lysine coated coverslips and grown overnight. Cells were treated with 5  $\mu$ M MG132 in enriched DMEM for 0 h, 8 h, and 16 h. Cells were fixed, permeabilized (0.1% TritonX-100 in PBS), and (immuno-)stained for poly(A) RNA, as described.

## Single cell quantification of total polyA RNA

24 h after transfection with  $\beta$  protein, Htt97Q, TDP-F4 or control plasmids on poly-L-Lysine coated coverslips, HEK293T cells were fixed, permeabilized and (immuno-)stained for polyA RNA, aggregating proteins, and nuclear DNA (as described). The relative total polyA RNA fluorescence intensities of single cells containing aggregates and showing nuclear polyA RNA retention was quantified and set in ratio to untransfected cells on the same coverslip with wildtype-like distribution of polyA RNA ( $\geq 3$  independent experiments,  $n = 4-13$  cells in each experiment). The ratio describes a potential accumulation or degradation of polyA RNA in cells with protein aggregates compared to wildtype cells.

## Absolute quantification of cytoplasmic mRNA

$1.5 \times 10^6$  HEK293T cells were seeded in round 10 cm cell culture dishes for 24 h of growth. Cultures were transfected with 15  $\mu\text{g}$  DNA (pcDNA3.1) and 40  $\mu\text{L}$  Lipofectamin 2000 (Invitrogen) in 6 mL Opti-Mem I Reduced Serum Media (Gibco) for 3 h, afterwards being replaced by 10% FBS supplemented DMEM (including glutamate, non-essential amino acids, antibiotics, as described above). After 40 h of protein expression, cells were trypsinized and collected at 500 x g by centrifugation. Resuspended in PBS, one third of the cells were processed for mRNA quantification, residual cells were lysed in SDS loading buffer (see SDS PAGE) for quantification of protein levels (GAPDH by immunoblotting).

Cellular membranes were lysed in cytoplasmic extraction buffer (140 mM NaCl, 5 mM KCl, 10 mM Tris, pH 7.5, 0.3% TritonX-100, 1mM DTT and 1000 U/mL RNase inhibitor (RNasin, Promega)) at 4 °C for 10 min, keeping nuclei intact. Nuclei were sedimented by centrifugation for 2 min at 500 x g at 4 °C and separated from the cytoplasmic lysate (supernatant). After addition of an equal volume of mRNA binding buffer (1 M LiCl, 20 mM Tris, 2 mM EDTA, pH 7.5, 1% SDS), the supernatant containing the cytoplasmic lysate was incubated with polyA+ RNA polystyrene-latex particles of uniform size (1  $\mu\text{m}$  diameter, Oligotex, Qiagen), covalently linked to dC<sub>10</sub>T<sub>30</sub> oligonucleotides at 70 °C for 3 min, followed by mRNA hybridization at 25 °C for 10 min.

The following mRNA purification was performed based on the manufacturers' instructions (Oligotex Handbook, Qiagen), modified to keep the procedure highly quantitative. Oligotex-mRNA complexes were sedimented at 16,000 x g, rehybridised, and washed to remove residually bound ribosomal RNAs. For elution, the oligotex-mRNA complexes were resuspended in 85  $\mu\text{L}$  elution buffer at 70 °C (OEB, Qiagen) to release the bound mRNA, followed by a quick sedimentation of Oligotex particles (16,000 x g, 30 sec). For a precise quantification and different to manufacturer's instructions, no spin columns were used during the elution. The supernatant containing the purified cytoplasmic mRNA was transferred to a separate tube for photometric quantification of concentration and purity (absorption at 260/280 nm, NanoDrop 1000 spectrophotometer, ThermoScientific).

Actinomycin D was applied for general transcriptional inhibition by RNA Polymerase II at 5  $\mu\text{g}/\text{mL}$  for 16 h (Jablonski 2009) on cells transfected with an empty control plasmid. In a similar way, cells were treated with Actinomycin D and hybridized to Cy5-(d)T<sub>30</sub> for labeling poly(A) RNA to demonstrate nuclear retention of cellular mRNAs microscopically.

## Solubility of cytoplasmic and nuclear $\beta$ proteins

24 h after transfection of an equal amount of around  $1 \times 10^6$  HEK293T cells with plasmids encoding  $\beta$  proteins or empty control plasmids, cells were collected by trypsination and centrifugation (300 x g for 2 min), and resuspended in (200  $\mu$ L) PBS on ice. Samples were split 1:1 (v/v) for total lysate and fractionation. Cells were lysed by the addition of an equal volume of 2 x lysis buffer (2% TritonX-100, 750 mM NaCl, 1 mM  $\text{KH}_2\text{PO}_4$ , 3 mM  $\text{Na}_2\text{HPO}_4$ , pH 7.4, Complete Protease Inhibitor Cocktail (Roche), and Benzonase Nuclease (Novagen)) under rotation at 4 °C for 15 min. Samples for fractionation were centrifuged at 20,000 x g for 5 min, the supernatant was completely taken off, and the pellet was resuspended in an equal volume of 1 x lysis buffer (200  $\mu$ L). Total lysate samples were processed without centrifugation.

For SDS-PAGE, 2 x SDS loading buffer (60 mM Tris, pH 6.8, 2% SDS, 25% glycerol (v/v), 0.01% Bromophenolblue (w/v); 5%  $\beta$ -mercaptoethanol (v/v) freshly added) was mixed with the sample before denaturation at 95 °C for 5 min and vortexing for 10 sec. Samples were run on a 15% SDS PAGE and transferred on PVDF membranes for immunoblotting against c-Myc, GAPDH, and Histone H3.

## Size exclusion chromatography of HEK293T lysates

HEK293T cells were transiently transfected with NES- $\beta$ 17, NLS- $\beta$ 17, or empty plasmids (control). After 24 h, cells were lysed in 1% Triton X-100, 420 mM NaCl, 1 mM  $\text{KH}_2\text{PO}_4$ , 3 mM  $\text{Na}_2\text{HPO}_4$ , pH 7.4, Complete Protease Inhibitor Cocktail (Roche), and Benzonase Nuclease (Novagen). The ionic strength was increased to enable a complete nuclear lysis. Debris was removed at 2,000 x g, and 1-2  $\mu$ g of total protein was separated on a Superpose 6 column (30 mL, Pharmazia Biotech). Fractions were concentrated by TCA precipitation (15% TCA final concentration) at 4°C for 1 h. Resulting pellets were washed twice in ice-cold acetone (-20°C) and resuspended in PBS. 5x SDS-sample buffer was added (10% SDS, 10%  $\beta$ -mercaptoethanol, 60% glycerol, 0.1 M Tris, pH 6.8) and the pH was neutralized by addition of 1M Tris pH 6.8, as necessary. Samples were heated to 95 °C for 5 min and vortexed. SDS PAGE was performed on a NuPAGE 4-12% gradient BisTris SDS Mini Gel (Invitrogen), which was blotted on methanol activated PVDF membranes.

## Proteostasis sensors

HEK293T cells were cotransfected by electroporation with 25  $\mu$ g of plasmids encoding  $\beta$ -sheet proteins or of control plasmids in addition to 3  $\mu$ g of plasmids encoding American firefly luciferase-EGFP, targeted to cytoplasm or nucleus. After 24 h of protein expression, samples were fixed and immunostained.

Examining the concentration dependent tendency of aggregation of the luciferase-EGFP sensors, 15  $\mu$ g of plasmids (5 times more than before) were transfected by electroporation and aggregation was evaluated. For proteasomal inhibition, cells were treated with 5  $\mu$ M MG132 for 5 h in supplemented DMEM.

## FRAP (fluorescence recovery after photo bleaching)

HEK293T cells were transiently transfected with vectors expressing C-terminally EGFP tagged  $\beta$  proteins, or EGFP. After 24 h, spherical ROIs (region of interests) were bleached for  $\sim$ 1 s reaching 5-

20% of original fluorescence intensity in the respective ROI, and recovery was followed over time (at 37 °C). Fluorescence intensities were normalized to 100% before and 0% after bleaching (first recording after bleaching).

### **<sup>35</sup>S-Met radioactive pulse labeling of newly translated proteins**

2x10<sup>6</sup> HEK293T cells were transfected by electroporation with  $\beta$  proteins and control plasmids, grown in a 6 well plate for 24 h, and transferred to prewarmed Cysteine-/Methionine-free DMEM without FBS. 20 min later, 50  $\mu$ Ci/mL <sup>35</sup>S-Met was added and incubated for 20 min at 37 °C. The pulse was stopped by aspirating the radioactive medium and washing with 4 °C cold PBS. Cells were collected and lysed in 1% Triton X-100/PBS including Complete Protease Inhibitor Cocktail (Roche) and Benzonase (Novagen), rocking for 30 min. After removal of insoluble parts by centrifugation at 500 x g for 2 min, 2x SDS PAGE loading buffer (60 mM Tris, pH 6.8, 2% SDS, 25% Glycerol (v/v), 0.01% Bromphenolblue (w/v); 5% freshly added  $\beta$ -mercaptoethanol (v/v)) was mixed with the supernatant. The samples were denatured at 95 °C for 5 min, immediately vortexed and separated on a NuPAGE 4-12% gradient BisTris SDS Mini Gel (Invitrogen). The gel was stained with Serva Blue G (Serva), dried on a filter paper (Whatman) and analyzed by fluorography.

### **Hsp70 promoter activation**

3x10<sup>6</sup> HEK293T cells were transiently cotransfected by electroporation with 25  $\mu$ g of plasmids carrying genes of  $\beta$  proteins or controls (empty vector,  $\alpha$ S824) and 2  $\mu$ g of plasmid expressing *Firefly* luciferase, controlled by the Hsp70 promoter (Olzscha 2011). 7x10<sup>5</sup> cells per well were grown overnight in enriched DMEM in 12 well plates. After 20 h, cells were either kept at 37 °C or heat shocked for 2 h at 43.5 °C followed by a recovery for 2 h at 37 °C. Cells were then lysed with 300  $\mu$ L of Cell Culture Lysis Reagent (Promega) for 15 min of incubation and gentle shaking. The luciferase activity measurement was performed after addition of 50  $\mu$ L of luciferase substrate solution (Luciferase Assay System, Promega) to 20  $\mu$ L of cell lysate on a Lumat LB9507 (EG&G Berthold).

### **Observing mitotic cells**

HEK293T cells were transiently transfected with NES- $\beta$ 17, NLS- $\beta$ 17, or empty control plasmids. After 48 h, cells were fixed, permeabilized, and stained with antibodies against aggregates (c-Myc) and NPM-1, and finally for nuclear DNA (DAPI). Cells of different mitotic states were selected by the distribution and morphology of their DNA, and the distribution of aggregates was observed.

### **Statistics**

In general, for all experiments, at least three biologically independent repeats were performed. Means and standard deviations were calculated.

Significance was analyzed by the two-tailed, heteroscedastic student's t-test (significance levels: (\*) for  $p < 0.05$ , (\*\*) for  $p < 0.01$ , (\*\*\*) for  $p < 0.001$ ).

## Antibodies

Antibody	Epitope	Host, clonality	Source
A11 (Anti-A $\beta$ -1-11)	Soluble amyloid oligomers (A $\beta$ 1-11)	Rabbit, polyclonal	Prof. Dr. Charles Glabe (University of California)
c-Myc (9E10)	p62 c-Myc, res. 408-439	Mouse, monoclonal	Santa Cruz, Sc-40
c-Myc-Cy3 (9E10)	p62 c-Myc, res. 408-439	Mouse, monoclonal	Sigma, C6594
GAPDH (6C5)	GAPDH	Mouse, monoclonal	Millipore, MAB374
Histone-H3	Histone-H3	Rabbit, polyclonal	Abcam, ab1791
Polyglutamine (3B5H10) (Miller 2011)	Early oligomerig forms of polyQ extended Htt	Mouse, monoclonal	Sigma, P1874
Cleaved caspase-3 Asp175	Proteolytically activated caspase-3	Rabbit, polyclonal	Cell Signaling Technology, #9661
Nucleophosmin-1	NPM-1 (B23)	Mouse, monoclonal	Invitrogen, 32-5200
Importin $\alpha$ 1	Kpna2	Rabbit, polyclonal	Abcam, ab70160
Importin $\alpha$ 3	Kpna4	Rabbit, polyclonal	Abcam, ab84735
THOC2	THOC2	Rabbit, polyclonal	Sigma, HPA047921
NF- $\kappa$ B (XP, D14E12)	p65	Rabbit, monoclonal	Cell Signaling Technology, #8242
Phospho-NF- $\kappa$ B (93H1)	Phospho-p65 (Ser 536)	Rabbit, monoclonal	Cell Signaling Technology, #3033
I $\kappa$ B- $\alpha$ (L35A5)	I $\kappa$ B- $\alpha$	Mouse, monoclonal	Cell Signaling Technology, #4814
eIF3 $\alpha$ (D51F4)	eIF3 $\alpha$	Rabbit, monoclonal	Cell Signaling Technology, #3411
eIF4G	eIF4G	Rabbit, polyclonal	Cell Signaling Technology, #2498
Nuclear Pore Complex Proteins (Mab414)	Nuclear pore complex proteins, recognizes FXFG-repeat domains	Mouse, monoclonal	Abcam, ab24609
Hsp105 (B-7)	Hsp105 (Hsp110)	Mouse, monoclonal	Santa Cruz, sc-74550
Mouse IgG-Alexa488	Mouse IgG	Goat, F(ab') <sub>2</sub> fragments	Cell Signaling Technology, #4408
Mouse IgG-Alexa555	Mouse IgG	Goat, F(ab') <sub>2</sub> fragments	Cell Signaling Technology, #4409
Rabbit IgG-FITC	Rabbit IgG	Goat, polyclonal	Sigma, F9887
Rabbit IgG-Atto488	Rabbit IgG	Goat, polyclonal	Sigma, 18772
Rabbit IgG-Alexa555	Rabbit IgG	Goat, F(ab') <sub>2</sub> fragments	Cell Signaling Technology, #4413
Mouse IgG Peroxidase	Mouse IgG	Goat, polyclonal	Sigma, A4416
Rabbit IgG Peroxidase	Rabbit IgG	Goat, polyclonal	Sigma, A9169



## Sequences of utilized constructs

### c-Myc tagged $\beta$ proteins

$\beta$ 4

>MCEQKLISEEDLGMQISM~~MDYQLEIE~~GNDNKV~~ELQL~~NDSSGGEV~~KLQIR~~GPGG~~RVHFN~~VHSSSGSN~~LEVN~~FNDGGEV~~QFHM~~

$\beta$ 17

>MCEQKLISEEDLGMQISM~~MDYEIKF~~HGDGDN~~FDLNL~~DDSSGGL~~QLQIR~~GPGG~~RVHVIH~~SSSSGK~~VDFH~~VNNDGGD~~VEVKM~~H

$\beta$ 23

>MCEQKLISEEDLGMQISM~~MDYNIQF~~HNNGN~~EIQFEI~~DDSSGD~~IEIEI~~RGPGG~~RVHIQ~~LDG~~HGH~~IK~~VDFH~~NDGGEL~~QIDM~~H

$\alpha$ S824

>MCEQKLISEEDLGMYGK~~INDLLED~~Q~~EVLK~~NLHKN~~WH~~GGKDN~~LHDV~~DNH~~LQNV~~IEDI~~HDFM~~QGGGSGGK~~LQEM~~MKEF~~QQVLD~~  
EL~~NNHL~~QGGK~~HTV~~H~~TEQ~~NIKEIF~~HHLE~~ELVHR

### Targeting signals and tags

c-Myc tag

### Sequences

>MCEQKLISEEDLGMQIS+

**NES** nuclear export sequence

>MCEQKLISEEDL~~LELLED~~LT~~LG~~MQIS+

**NLS** nuclear localization signal

>MAAD~~PKKKR~~KVD~~PKKKR~~KVDTYGAGEQKLISEEDLNGASS+

**NLS** K7T, K15T

>MAAD~~PKTKR~~KVD~~PKTKR~~KVDTYGAGEQKLISEEDLNGASS+

inefficient NLS

**COX8** mitochondrial targeting signal

>MSVLTPLLLRGLTGSARRLPVPRAKIHSLCEQKLISEEDLGMQIS+

**mtHsp60** mitochondrial targeting signal

>LRLPTVFRQMRPVSRLAPHLTRAYAKDVKFGCEQKLISEEDLGMQIS+

**Prenylation** sequence

>+GGGGSGGGGSCVIM

Maurer-Stroh 2005

$\beta$  proteins-Linker16-EGFP (c-Myc+ $\beta$  proteins+16 a.a. linker+EGFP; Chang 2005)

+TSGSAASAAGAGEAAA~~VSKG~~EELFTGVVPI~~LV~~ELDGDVNGHKFSVSGEGEGDATY~~GKLT~~LKFICTTGKLPVWP  
TLVTTLT~~YGVQ~~CF~~SRYP~~DHMKQ~~HDF~~FKSAMPEGYVQERTIFFKDDGNYKTRAEV~~KFEG~~DTLVNRIELK~~GID~~FKED  
GNILGHKLEYNYN~~SHNV~~YIMADKQKNGIKVNF~~KIRH~~NIEDGSVQLADHYQ~~QNT~~PIGDGPVLLPD~~NHYL~~STQSALS  
KDPNEKRDH~~MVLL~~EFVTAAGITLGMDELYK

$\beta$  proteins - monomerizing lysine mutants (K) for *E. coli* growth inhibition

$\beta$ 4 >MCEQKLISEEDLGMQISM~~MDYQKEI~~E~~EG~~NDNKV~~ELQL~~NDSSGGEV~~KLQIR~~GPGG~~RVHFN~~VHSSSGSN~~LEVN~~FNDGGEV~~QKHM~~H

$\beta$ 17 >MCEQKLISEEDLGMQISM~~MDYEKKF~~HGDGDN~~FDLNL~~DDSSGGL~~QLQIR~~GPGG~~RVHVIH~~SSSSGK~~VDFH~~VNNDGGD~~VEKKM~~H

$\beta$ 23 >MCEQKLISEEDLGMQISM~~MDYNIQF~~HNNGN~~EIQFEI~~DDSSGD~~IEIEI~~RGPGG~~RVHIQ~~LDG~~HGH~~IK~~VDFH~~NDGGEL~~QKDM~~H

$\beta$  proteins - odd number of  $\beta$ -sheets for *E. coli* growth inhibition

$\beta$ 17+4 >MCEQKLISEEDLGMQISM~~MDYEIKF~~HGDGDN~~FDLNL~~DDSSGGL~~QLQIR~~GPGG~~RVHVIH~~SSSSGK~~VDFH~~VNNDGGD~~VEVKM~~HNDGGEV~~QFHM~~H

$\beta$ 17+23 >MCEQKLISEEDLGMQISM~~MDYEIKF~~HGDGDN~~FDLNL~~DDSSGGL~~QLQIR~~GPGG~~RVHVIH~~SSSSGK~~VDFH~~VNNDGGD~~VEVKM~~HNDGGEV~~QIDM~~H

$\beta$ 23<sub>short</sub> >MCEQKLISEEDLGMQISM~~MDYNIQF~~HNNGN~~EIQFEI~~DDSSGD~~IEIEI~~RGPGG~~RVHIQ~~LDG~~HGH~~IK~~VDFH~~

**S-GFP** (shuttling EGFP, NLS-HA-NES-Linker16-EGFP)

>MAAD~~PKKKR~~KVD~~PKKKR~~KVDTYGAGY~~PYD~~V~~PDYA~~LL~~ELLE~~DLTI~~SG~~SDLTSGSAASAAGAGEAAA~~VSKG~~EELFT  
GVVPI~~LV~~ELDGDVNGHKFSVSGEGEGDATY~~GKLT~~LKFICTTGKLPVWP~~TLV~~TTLT~~YGVQ~~CF~~SRYP~~DHMKQ~~HDF~~FK  
KSAMPEGYVQERTIFFKDDGNYKTRAEV~~KFEG~~DTLVNRIELK~~GID~~FKEDGNILGHKLEYNYN~~SHNV~~YIMADKQK  
GIKVNF~~KIRH~~NIEDGSVQLADHYQ~~QNT~~PIGDGPVLLPD~~NHYL~~STQSALS~~KDP~~NEKRDH~~MVLL~~EFVTAAGITLGM  
DELYK



# Literature

- Aguzzi, A., and Rajendran, L. (2009). The transcellular spread of cytosolic amyloids, prions, and prionoids. *Neuron* 64, 783-790.
- Aitken, A., and Learmonth, M. (1996). Article "Protein Determination by UV Absorption" in "The protein protocols handbook" (Towota, N.J.: Humana Press).
- Akopian, D., Shen, K., Zhang, X., and Shan, S.O. (2013). Signal recognition particle: an essential protein-targeting machine. *Annu Rev Biochem* 82, 693-721.
- Alavian, K.N., Beutner, G., Lazrove, E., Sacchetti, S., Park, H.A., Licznanski, P., Li, H., Nabili, P., Hockensmith, K., Graham, M., *et al.* (2014). An uncoupling channel within the c-subunit ring of the F1FO ATP synthase is the mitochondrial permeability transition pore. *Proc Natl Acad Sci U S A* 111, 10580-10585.
- Alonso, A., Zaidi, T., Novak, M., Grundke-Iqbal, I., and Iqbal, K. (2001). Hyperphosphorylation induces self-assembly of tau into tangles of paired helical filaments/straight filaments. *Proc Natl Acad Sci U S A* 98, 6923-6928.
- Alonso, A.C., Grundke-Iqbal, I., and Iqbal, K. (1996). Alzheimer's disease hyperphosphorylated tau sequesters normal tau into tangles of filaments and disassembles microtubules. *Nat Med* 2, 783-787.
- Alzheimer, A. (1907). Über eine eigenartige Erkrankung der Hirnrinde. *Allgemeine Zeitschrift für Psychiatrie und psychisch-gerichtliche Medizin* 64, 146-148.
- Alzheimer, A., Stelzmann, R.A., Schnitzlein, H.N., and Murtagh, F.R. (1995). An English translation of Alzheimer's 1907 paper, "Über eine eigenartige Erkrankung der Hirnrinde". *Clinical anatomy* 8, 429-431.
- Anfinsen, C.B. (1973). Principles that govern the folding of protein chains. *Science* 181, 223-230.
- Armstrong, R.A., Lantos, P.L., and Cairns, N.J. (2008). What determines the molecular composition of abnormal protein aggregates in neurodegenerative disease? *Neuropathology* 28, 351-365.
- Aronsson, G., Brorsson, A.C., Sahlman, L., and Jonsson, B.H. (1997). Remarkably slow folding of a small protein. *FEBS Lett* 411, 359-364.
- Astbury, W.T., Beighton, E., and Parker, K.D. (1959). The cross-beta configuration in supercontracted proteins. *Biochim Biophys Acta* 35, 17-25.
- Atwal, R.S., Desmond, C.R., Caron, N., Maiuri, T., Xia, J., Sipione, S., and Truant, R. (2011). Kinase inhibitors modulate huntingtin cell localization and toxicity. *Nat Chem Biol* 7, 453-460.
- Auer, S., Dobson, C.M., and Vendruscolo, M. (2007). Characterization of the nucleation barriers for protein aggregation and amyloid formation. *HFSP J* 1, 137-146.
- Bakthisaran, R., Tangirala, R., and Rao Ch, M. (2015). Small heat shock proteins: Role in cellular functions and pathology. *Biochim Biophys Acta* 1854, 291-319.
- Balbach, J.J., Ishii, Y., Antzutkin, O.N., Leapman, R.D., Rizzo, N.W., Dyda, F., Reed, J., and Tycko, R. (2000). Amyloid fibril formation by A beta 16-22, a seven-residue fragment of the Alzheimer's beta-amyloid peptide, and structural characterization by solid state NMR. *Biochemistry* 39, 13748-13759.
- Balch, W.E., Morimoto, R.I., Dillin, A., and Kelly, J.W. (2008). Adapting proteostasis for disease intervention. *Science* 319, 916-919.
- Ballinger, C.A., Connell, P., Wu, Y., Hu, Z., Thompson, L.J., Yin, L.Y., and Patterson, C. (1999). Identification of CHIP, a novel tetratricopeptide repeat-containing protein that interacts with heat shock proteins and negatively regulates chaperone functions. *Mol Cell Biol* 19, 4535-4545.
- Bancher, C., Brunner, C., Lassmann, H., Budka, H., Jellinger, K., Wiche, G., Seitelberger, F., Grundke-Iqbal, I., Iqbal, K., and Wisniewski, H.M. (1989). Accumulation of abnormally phosphorylated tau precedes the formation of neurofibrillary tangles in Alzheimer's disease. *Brain Res* 477, 90-99.
- Bano, D., Dinsdale, D., Cabrera-Socorro, A., Maida, S., Lambacher, N., McColl, B., Ferrando-May, E., Hengartner, M.O., and Nicotera, P. (2010). Alteration of the nuclear pore complex in Ca(2+)-mediated cell death. *Cell death and differentiation* 17, 119-133.
- Bano, D., Hengartner, M.O., and Nicotera, P. (2010). Nuclear pore complex during neuronal degeneration: cracking the last barrier! *Nucleus* 1, 136-138.
- Barry, P.A. (2004). Efficient electroporation of mammalian cells in culture. *Methods Mol Biol* 245, 207-214.
- Bartlett, A.I., and Radford, S.E. (2009). An expanding arsenal of experimental methods yields an explosion of insights into protein folding mechanisms. *Nat Struct Mol Biol* 16, 582-588.

- Beerten, J., Jonckheere, W., Rudyak, S., Xu, J., Wilkinson, H., De Smet, F., Schymkowitz, J., and Rousseau, F. (2012). Aggregation gatekeepers modulate protein homeostasis of aggregating sequences and affect bacterial fitness. *Protein Eng Des Sel* 25, 357-366.
- Behrends, C., Langer, C.A., Boteva, R., Bottcher, U.M., Stemp, M.J., Schaffar, G., Rao, B.V., Giese, A., Kretzschmar, H., Siegers, K., *et al.* (2006). Chaperonin TRiC promotes the assembly of polyQ expansion proteins into nontoxic oligomers. *Mol Cell* 23, 887-897.
- Bemporad, F., Taddei, N., Stefani, M., and Chiti, F. (2006). Assessing the role of aromatic residues in the amyloid aggregation of human muscle acylphosphatase. *Protein Sci* 15, 862-870.
- Bennion, P.J., Horobin, R.W., and Murgatroyd, L.B. (1975). The use of a basic dye (azure A or toluidine blue) plus a cationic surfactant for selective staining of RNA: a technical and mechanistic study. *Stain Technol* 50, 307-313.
- Berliner, L.M. (1992). Statistics, Probability and Chaos. *Statistical Science* 7, 69-90.
- Bhushan, S., Gartmann, M., Halic, M., Armache, J.P., Jarasch, A., Mielke, T., Berninghausen, O., Wilson, D.N., and Beckmann, R. (2010). alpha-Helical nascent polypeptide chains visualized within distinct regions of the ribosomal exit tunnel. *Nat Struct Mol Biol* 17, 313-317.
- Biamonti, G., and Vourc'h, C. (2010). Nuclear stress bodies. *Cold Spring Harb Perspect Biol* 2, a000695.
- Biancalana, M., and Koide, S. (2010). Molecular mechanism of Thioflavin-T binding to amyloid fibrils. *Biochim Biophys Acta* 1804, 1405-1412.
- Blancas-Mejia, L.M., and Ramirez-Alvarado, M. (2013). Systemic amyloidoses. *Annu Rev Biochem* 82, 745-774.
- Blondin, G.A., and Green, D.E. (1967). The mechanism of mitochondrial swelling. *Proc Natl Acad Sci U S A* 58, 612-619.
- Bloom, J.D., Wilke, C.O., Arnold, F.H., and Adami, C. (2004). Stability and the evolvability of function in a model protein. *Biophys J* 86, 2758-2764.
- Boisvert, F.M., van Koningsbruggen, S., Navascues, J., and Lamond, A.I. (2007). The multifunctional nucleolus. *Nat Rev Mol Cell Biol* 8, 574-585.
- Bolognesi, B., Kumita, J.R., Barros, T.P., Esbjorner, E.K., Luheshi, L.M., Crowther, D.C., Wilson, M.R., Dobson, C.M., Favrin, G., and Yerbury, J.J. (2010). ANS binding reveals common features of cytotoxic amyloid species. *ACS Chem Biol* 5, 735-740.
- Borjesson-Hanson, A., Edin, E., Gislason, T., and Skoog, I. (2004). The prevalence of dementia in 95 year olds. *Neurology* 63, 2436-2438.
- Boulon, S., Westman, B.J., Hutten, S., Boisvert, F.M., and Lamond, A.I. (2010). The nucleolus under stress. *Mol Cell* 40, 216-227.
- Boutell, J.M., Thomas, P., Neal, J.W., Weston, V.J., Duce, J., Harper, P.S., and Jones, A.L. (1999). Aberrant interactions of transcriptional repressor proteins with the Huntington's disease gene product, huntingtin. *Hum Mol Genet* 8, 1647-1655.
- Braak, H., and Braak, E. (1991). Neuropathological staging of Alzheimer-related changes. *Acta Neuropathol* 82, 239-259.
- Brandenburg, E., von Berlepsch, H., and Koksich, B. (2012). Specific in situ discrimination of amyloid fibrils versus alpha-helical fibres by the fluorophore NIAD-4. *Mol Biosyst* 8, 557-564.
- Braun, I.C., Herold, A., Rode, M., and Izaurralde, E. (2002). Nuclear export of mRNA by TAP/NXF1 requires two nucleoporin-binding sites but not p15. *Mol Cell Biol* 22, 5405-5418.
- Brinker, A., Pfeifer, G., Kerner, M.J., Naylor, D.J., Hartl, F.U., and Hayer-Hartl, M. (2001). Dual function of protein confinement in chaperonin-assisted protein folding. *Cell* 107, 223-233.
- Broome, B.M., and Hecht, M.H. (2000). Nature disfavors sequences of alternating polar and non-polar amino acids: implications for amyloidogenesis. *J Mol Biol* 296, 961-968.
- Bryan, P., Alexander, P., Strausberg, S., Schwarz, F., Lan, W., Gilliland, G., and Gallagher, D.T. (1992). Energetics of folding subtilisin BPN'. *Biochemistry* 31, 4937-4945.
- Buckingham, S.D., Jones, A.K., Brown, L.A., and Sattelle, D.B. (2009). Nicotinic acetylcholine receptor signalling: roles in Alzheimer's disease and amyloid neuroprotection. *Pharmacol Rev* 61, 39-61.
- Bushell, M., Stoneley, M., Sarnow, P., and Willis, A.E. (2004). Translation inhibition during the induction of apoptosis: RNA or protein degradation? *Biochem Soc Trans* 32, 606-610.
- Butterfield, S.M., and Lashuel, H.A. (2010). Amyloidogenic protein-membrane interactions: mechanistic insight from model systems. *Angew Chem Int Ed Engl* 49, 5628-5654.
- Calamai, M., Taddei, N., Stefani, M., Ramponi, G., and Chiti, F. (2003). Relative influence of hydrophobicity and net charge in the aggregation of two homologous proteins. *Biochemistry* 42, 15078-15083.

- Calloni, G., Chen, T., Schermann, S.M., Chang, H.C., Genevoux, P., Agostini, F., Tartaglia, G.G., Hayer-Hartl, M., and Hartl, F.U. (2012). DnaK functions as a central hub in the E. coli chaperone network. *Cell Rep* 1, 251-264.
- Campioni, S., Mannini, B., Zampagni, M., Pensalfini, A., Parrini, C., Evangelisti, E., Relini, A., Stefani, M., Dobson, C.M., Cecchi, C., *et al.* (2010). A causative link between the structure of aberrant protein oligomers and their toxicity. *Nat Chem Biol* 6, 140-147.
- Carmody, S.R., and Wenthe, S.R. (2009). mRNA nuclear export at a glance. *J Cell Sci* 122, 1933-1937.
- Casafont, I., Berciano, M.T., and Lafarga, M. (2010). Bortezomib induces the formation of nuclear poly(A) RNA granules enriched in Sam68 and PABPN1 in sensory ganglia neurons. *Neurotox Res* 17, 167-178.
- Castillo, P.E., Younts, T.J., Chavez, A.E., and Hashimoto, Y. (2012). Endocannabinoid signaling and synaptic function. *Neuron* 76, 70-81.
- Cattaneo, E., Zuccato, C., and Tartari, M. (2005). Normal huntingtin function: an alternative approach to Huntington's disease. *Nat Rev Neurosci* 6, 919-930.
- Chakrabarti, A., Chen, A.W., and Varner, J.D. (2011). A review of the mammalian unfolded protein response. *Biotechnol Bioeng* 108, 2777-2793.
- Chakraborty, K., Chatila, M., Sinha, J., Shi, Q., Poschner, B.C., Sikor, M., Jiang, G., Lamb, D.C., Hartl, F.U., and Hayer-Hartl, M. (2010). Chaperonin-catalyzed rescue of kinetically trapped states in protein folding. *Cell* 142, 112-122.
- Chan, J.C., Oyler, N.A., Yau, W.M., and Tycko, R. (2005). Parallel beta-sheets and polar zippers in amyloid fibrils formed by residues 10-39 of the yeast prion protein Ure2p. *Biochemistry* 44, 10669-10680.
- Chang, H.C., Kaiser, C.M., Hartl, F.U., and Barral, J.M. (2005). De novo folding of GFP fusion proteins: high efficiency in eukaryotes but not in bacteria. *J Mol Biol* 353, 397-409.
- Chevalier-Larsen, E., and Holzbaur, E.L. (2006). Axonal transport and neurodegenerative disease. *Biochim Biophys Acta* 1762, 1094-1108.
- Chi, B., Wang, Q., Wu, G., Tan, M., Wang, L., Shi, M., Chang, X., and Cheng, H. (2013). Aly and THO are required for assembly of the human TREX complex and association of TREX components with the spliced mRNA. *Nucleic Acids Res* 41, 1294-1306.
- Chiti, F., and Dobson, C.M. (2006). Protein misfolding, functional amyloid, and human disease. *Annu Rev Biochem* 75, 333-366.
- Chiti, F., Stefani, M., Taddei, N., Ramponi, G., and Dobson, C.M. (2003). Rationalization of the effects of mutations on peptide and protein aggregation rates. *Nature* 424, 805-808.
- Cho, Y., Seong, J.K., Jeong, Y., and Shin, S.Y. (2012). Individual subject classification for Alzheimer's disease based on incremental learning using a spatial frequency representation of cortical thickness data. *Neuroimage* 59, 2217-2230.
- Chothia, C., and Janin, J. (1981). Relative orientation of close-packed beta-pleated sheets in proteins. *Proc Natl Acad Sci U S A* 78, 4146-4150.
- Chowdhury, M., and Enekel, C. (2015). Intracellular Dynamics of the Ubiquitin-Proteasome-System. *F1000Research* 4, 367.
- Chu, C.T., Plowey, E.D., Wang, Y., Patel, V., and Jordan-Sciutto, K.L. (2007). Location, location, location: altered transcription factor trafficking in neurodegeneration. *J Neuropathol Exp Neurol* 66, 873-883.
- Chung, K.K., Zhang, Y., Lim, K.L., Tanaka, Y., Huang, H., Gao, J., Ross, C.A., Dawson, V.L., and Dawson, T.M. (2001). Parkin ubiquitinates the alpha-synuclein-interacting protein, synphilin-1: implications for Lewy-body formation in Parkinson disease. *Nat Med* 7, 1144-1150.
- Ciechanover, A., Hod, Y., and Hershko, A. (1978). A heat-stable polypeptide component of an ATP-dependent proteolytic system from reticulocytes. *Biochem Biophys Res Commun* 81, 1100-1105.
- Clavaguera, F., Bolmont, T., Crowther, R.A., Abramowski, D., Frank, S., Probst, A., Fraser, G., Stalder, A.K., Beibel, M., Staufenbiel, M., *et al.* (2009). Transmission and spreading of tauopathy in transgenic mouse brain. *Nature cell biology* 11, 909-913.
- Colla, E., Coune, P., Liu, Y., Pletnikova, O., Troncoso, J.C., Iwatsubo, T., Schneider, B.L., and Lee, M.K. (2012). Endoplasmic reticulum stress is important for the manifestations of alpha-synucleinopathy in vivo. *J Neurosci* 32, 3306-3320.
- Connell, P., Ballinger, C.A., Jiang, J., Wu, Y., Thompson, L.J., Hohfeld, J., and Patterson, C. (2001). The co-chaperone CHIP regulates protein triage decisions mediated by heat-shock proteins. *Nature cell biology* 3, 93-96.
- Cook, A., Bono, F., Jinek, M., and Conti, E. (2007). Structural biology of nucleocytoplasmic transport. *Annu Rev Biochem* 76, 647-671.
- Cook, A.G., and Conti, E. (2010). Nuclear export complexes in the frame. *Curr Opin Struct Biol* 20, 247-252.

- Cooper, J.K., Schilling, G., Peters, M.F., Herring, W.J., Sharp, A.H., Kaminsky, Z., Masone, J., Khan, F.A., Delanoy, M., Borchelt, D.R., *et al.* (1998). Truncated N-terminal fragments of huntingtin with expanded glutamine repeats form nuclear and cytoplasmic aggregates in cell culture. *Hum Mol Genet* 7, 783-790.
- Cowan, K.J., Diamond, M.I., and Welch, W.J. (2003). Polyglutamine protein aggregation and toxicity are linked to the cellular stress response. *Hum Mol Genet* 12, 1377-1391.
- Cuervo, A.M., Stefanis, L., Fredenburg, R., Lansbury, P.T., and Sulzer, D. (2004). Impaired degradation of mutant alpha-synuclein by chaperone-mediated autophagy. *Science* 305, 1292-1295.
- Darshi, M., Mendiola, V.L., Mackey, M.R., Murphy, A.N., Koller, A., Perkins, G.A., Ellisman, M.H., and Taylor, S.S. (2011). ChChd3, an inner mitochondrial membrane protein, is essential for maintaining crista integrity and mitochondrial function. *J Biol Chem* 286, 2918-2932.
- David, D.C., Ollikainen, N., Trinidad, J.C., Cary, M.P., Burlingame, A.L., and Kenyon, C. (2010). Widespread protein aggregation as an inherent part of aging in *C. elegans*. *PLoS Biol* 8, e1000450.
- Davis, L.G., Kuehl, W.M., and Battey, J.F. (1994). Basic methods on molecular biology (Appleton & Lange).
- de Alba, E., Santoro, J., Rico, M., and Jimenez, M.A. (1999). De novo design of a monomeric three-stranded antiparallel beta-sheet. *Protein Sci* 8, 854-865.
- De Cecco, M., Jeyapalan, J., Zhao, X., Tamamori-Adachi, M., and Sedivy, J.M. (2011). Nuclear protein accumulation in cellular senescence and organismal aging revealed with a novel single-cell resolution fluorescence microscopy assay. *Aging* 3, 955-967.
- De Strooper, B., Iwatsubo, T., and Wolfe, M.S. (2012). Presenilins and gamma-secretase: structure, function, and role in Alzheimer Disease. *Cold Spring Harb Perspect Med* 2, a006304.
- Debanne, D., Campanac, E., Bialowas, A., Carlier, E., and Alcaraz, G. (2011). Axon physiology. *Physiol Rev* 91, 555-602.
- Dehay, B., and Bertolotti, A. (2006). Critical role of the proline-rich region in Huntingtin for aggregation and cytotoxicity in yeast. *J Biol Chem* 281, 35608-35615.
- Dekker, C., Stirling, P.C., McCormack, E.A., Filmore, H., Paul, A., Brost, R.L., Costanzo, M., Boone, C., Leroux, M.R., and Willison, K.R. (2008). The interaction network of the chaperonin CCT. *EMBO J* 27, 1827-1839.
- del Alamo, M., Hogan, D.J., Pechmann, S., Albanese, V., Brown, P.O., and Frydman, J. (2011). Defining the specificity of cotranslationally acting chaperones by systematic analysis of mRNAs associated with ribosome-nascent chain complexes. *PLoS Biol* 9, e1001100.
- DeSantis, M.E., Leung, E.H., Sweeny, E.A., Jackrel, M.E., Cushman-Nick, M., Neuhaus-Follini, A., Vashist, S., Sochor, M.A., Knight, M.N., and Shorter, J. (2012). Operational plasticity enables hsp104 to disaggregate diverse amyloid and nonamyloid clients. *Cell* 151, 778-793.
- Deshai, R.J., and Joazeiro, C.A. (2009). RING domain E3 ubiquitin ligases. *Annu Rev Biochem* 78, 399-434.
- Deuerling, E., Schulze-Specking, A., Tomoyasu, T., Mogk, A., and Bukau, B. (1999). Trigger factor and DnaK cooperate in folding of newly synthesized proteins. *Nature* 400, 693-696.
- Dias, C.L., Ala-Nissila, T., Wong-ekkabut, J., Vattulainen, I., Grant, M., and Karttunen, M. (2010). The hydrophobic effect and its role in cold denaturation. *Cryobiology* 60, 91-99.
- DiFiglia, M., Sapp, E., Chase, K.O., Davies, S.W., Bates, G.P., Vonsattel, J.P., and Aronin, N. (1997). Aggregation of huntingtin in neuronal intranuclear inclusions and dystrophic neurites in brain. *Science* 277, 1990-1993.
- Dill, K.A. (1990). Dominant Forces in Protein Folding. *Biochemistry* 29, 7133-7155.
- Dill, K.A., and MacCallum, J.L. (2012). The protein-folding problem, 50 years on. *Science* 338, 1042-1046.
- Dobson, C.M. (2003). Protein folding and misfolding. *Nature* 426, 884-890.
- Dolfe, L., Winblad, B., Johansson, J., and Presto, J. (2016). BRICHOS binds to a designed amyloid-forming beta-protein and reduces proteasomal inhibition and aggregates formation. *The Biochemical journal* 473, 167-178.
- Doyle, S.M., and Wickner, S. (2009). Hsp104 and ClpB: protein disaggregating machines. *Trends Biochem Sci* 34, 40-48.
- Dragovic, Z., Broadley, S.A., Shomura, Y., Bracher, A., and Hartl, F.U. (2006). Molecular chaperones of the Hsp110 family act as nucleotide exchange factors of Hsp70s. *EMBO J* 25, 2519-2528.
- Dunker, A.K., Silman, I., Uversky, V.N., and Sussman, J.L. (2008). Function and structure of inherently disordered proteins. *Curr Opin Struct Biol* 18, 756-764.
- Duyao, M.P., Auerbach, A.B., Ryan, A., Persichetti, F., Barnes, G.T., McNeil, S.M., Ge, P., Vonsattel, J.P., Gusella, J.F., Joyner, A.L., *et al.* (1995). Inactivation of the mouse Huntington's disease gene homolog Hdh. *Science* 269, 407-410.

- Dyson, H.J., and Wright, P.E. (2002). Coupling of folding and binding for unstructured proteins. *Curr Opin Struct Biol* 12, 54-60.
- Dyson, H.J., and Wright, P.E. (2005). Intrinsically unstructured proteins and their functions. *Nat Rev Mol Cell Biol* 6, 197-208.
- Edelhoch, H., and Osborne, J.C., Jr. (1976). The thermodynamic basis of the stability of proteins, nucleic acids, and membranes. *Adv Protein Chem* 30, 183-250.
- Eisert, R., Felau, L., and Brown, L.R. (2006). Methods for enhancing the accuracy and reproducibility of Congo red and thioflavin T assays. *Anal Biochem* 353, 144-146.
- El Albani, A., Bengtson, S., Canfield, D.E., Bekker, A., Macchiarelli, R., Mazurier, A., Hammarlund, E.U., Boulvais, P., Dupuy, J.J., Fontaine, C., *et al.* (2010). Large colonial organisms with coordinated growth in oxygenated environments 2.1 Gyr ago. *Nature* 466, 100-104.
- Englander, S.W., Mayne, L., and Krishna, M.M. (2007). Protein folding and misfolding: mechanism and principles. *Q Rev Biophys* 40, 287-326.
- Erkmann, J.A., and Kutay, U. (2004). Nuclear export of mRNA: from the site of transcription to the cytoplasm. *Exp Cell Res* 296, 12-20.
- Eroglu, B., Moskophidis, D., and Mivechi, N.F. (2010). Loss of Hsp110 leads to age-dependent tau hyperphosphorylation and early accumulation of insoluble amyloid beta. *Mol Cell Biol* 30, 4626-4643.
- Eyles, S.J., and Gierasch, L.M. (2010). Nature's molecular sponges: small heat shock proteins grow into their chaperone roles. *Proc Natl Acad Sci U S A* 107, 2727-2728.
- Fagerlund, R., Kinnunen, L., Kohler, M., Julkunen, I., and Melen, K. (2005). NF- $\kappa$ B is transported into the nucleus by importin  $\alpha$ 3 and importin  $\alpha$ 4. *J Biol Chem* 280, 15942-15951.
- Faleiro, L., and Lazebnik, Y. (2000). Caspases disrupt the nuclear-cytoplasmic barrier. *J Cell Biol* 151, 951-959.
- Fedyukina, D.V., and Cavagnero, S. (2011). Protein folding at the exit tunnel. *Annu Rev Biophys* 40, 337-359.
- Ferbitz, L., Maier, T., Patzelt, H., Bukau, B., Deuerling, E., and Ban, N. (2004). Trigger factor in complex with the ribosome forms a molecular cradle for nascent proteins. *Nature* 431, 590-596.
- Filimonenko, M., Isakson, P., Finley, K.D., Anderson, M., Jeong, H., Melia, T.J., Bartlett, B.J., Myers, K.M., Birkeland, H.C., Lamark, T., *et al.* (2010). The selective macroautophagic degradation of aggregated proteins requires the PI3P-binding protein Alfy. *Mol Cell* 38, 265-279.
- Findeis, M.A. (2007). The role of amyloid beta peptide 42 in Alzheimer's disease. *Pharmacol Ther* 116, 266-286.
- Finder, V.H., Vodopivec, I., Nitsch, R.M., and Glockshuber, R. (2010). The recombinant amyloid-beta peptide Abeta1-42 aggregates faster and is more neurotoxic than synthetic Abeta1-42. *J Mol Biol* 396, 9-18.
- Finkbeiner, S. (2011). Huntington's Disease. *Cold Spring Harb Perspect Biol* 3.
- Fornerod, M., Ohno, M., Yoshida, M., and Mattaj, I.W. (1997). CRM1 is an export receptor for leucine-rich nuclear export signals. *Cell* 90, 1051-1060.
- Fowler, D.M., Koulov, A.V., Balch, W.E., and Kelly, J.W. (2007). Functional amyloid--from bacteria to humans. *Trends Biochem Sci* 32, 217-224.
- Francastel, C., Schubeler, D., Martin, D.I., and Groudine, M. (2000). Nuclear compartmentalization and gene activity. *Nat Rev Mol Cell Biol* 1, 137-143.
- Frank Walter, E.W. (2002). *Catalytic RNA*. eLS John Wiley & Sons Ltd, Chichester.
- Freibaum, B.D., Lu, Y., Lopez-Gonzalez, R., Kim, N.C., Almeida, S., Lee, K.H., Badders, N., Valentine, M., Miller, B.L., Wong, P.C., *et al.* (2015). GGGGCC repeat expansion in C9orf72 compromises nucleocytoplasmic transport. *Nature* 525, 129-133.
- Frisoni, G.B., Fox, N.C., Jack, C.R., Jr., Scheltens, P., and Thompson, P.M. (2010). The clinical use of structural MRI in Alzheimer disease. *Nat Rev Neurol* 6, 67-77.
- Fulda, S., Gorman, A.M., Hori, O., and Samali, A. (2010). Cellular stress responses: cell survival and cell death. *International journal of cell biology* 2010, 214074.
- Gage, F.H., and Temple, S. (2013). Neural stem cells: generating and regenerating the brain. *Neuron* 80, 588-601.
- Gallagher, P.S., Oeser, M.L., Abraham, A.C., Kaganovich, D., and Gardner, R.G. (2014). Cellular maintenance of nuclear protein homeostasis. *Cell Mol Life Sci* 71, 1865-1879.
- Galvan, V., Gorostiza, O.F., Banwait, S., Ataie, M., Logvinova, A.V., Sitaraman, S., Carlson, E., Sagi, S.A., Chevallier, N., Jin, K., *et al.* (2006). Reversal of Alzheimer's-like pathology and behavior in human APP transgenic mice by mutation of Asp664. *Proc Natl Acad Sci U S A* 103, 7130-7135.
- Gazit, E. (2005). Mechanisms of amyloid fibril self-assembly and inhibition. Model short peptides as a key research tool. *The FEBS journal* 272, 5971-5978.

- Geerligs, L., Maurits, N.M., Renken, R.J., and Lorist, M.M. (2014). Reduced specificity of functional connectivity in the aging brain during task performance. *Hum Brain Mapp* 35, 319-330.
- Geisler, S., Holmstrom, K.M., Skujat, D., Fiesel, F.C., Rothfuss, O.C., Kahle, P.J., and Springer, W. (2010). PINK1/Parkin-mediated mitophagy is dependent on VDAC1 and p62/SQSTM1. *Nature cell biology* 12, 119-131.
- Giasson, B.I., Forman, M.S., Higuchi, M., Golbe, L.I., Graves, C.L., Kotzbauer, P.T., Trojanowski, J.Q., and Lee, V.M. (2003). Initiation and synergistic fibrillization of tau and alpha-synuclein. *Science* 300, 636-640.
- Glenner, G.G., and Wong, C.W. (1984). Alzheimer's disease: initial report of the purification and characterization of a novel cerebrovascular amyloid protein. *Biochem Biophys Res Commun* 120, 885-890.
- Goldschmidt, L., Teng, P.K., Riek, R., and Eisenberg, D. (2010). Identifying the amyloids, proteins capable of forming amyloid-like fibrils. *Proc Natl Acad Sci U S A* 107, 3487-3492.
- Gomez-Isla, T., Price, J.L., McKeel, D.W., Jr., Morris, J.C., Growdon, J.H., and Hyman, B.T. (1996). Profound loss of layer II entorhinal cortex neurons occurs in very mild Alzheimer's disease. *J Neurosci* 16, 4491-4500.
- Graveland, G.A., Williams, R.S., and DiFiglia, M. (1985). Evidence for degenerative and regenerative changes in neostriatal spiny neurons in Huntington's disease. *Science* 227, 770-773.
- Grimm, M.O., Zimmer, V.C., Lehmann, J., Grimm, H.S., and Hartmann, T. (2013). The impact of cholesterol, DHA, and sphingolipids on Alzheimer's disease. *Biomed Res Int* 2013, 814390.
- Group, T.H.s.D.C.R. (1993). A novel gene containing a trinucleotide repeat that is expanded and unstable on Huntington's disease chromosomes. The Huntington's Disease Collaborative Research Group. *Cell* 72, 971-983.
- Gunawardena, S., Her, L.S., Bruschi, R.G., Laymon, R.A., Niesman, I.R., Gordesky-Gold, B., Sintasath, L., Bonini, N.M., and Goldstein, L.S. (2003). Disruption of axonal transport by loss of huntingtin or expression of pathogenic polyQ proteins in *Drosophila*. *Neuron* 40, 25-40.
- Gupta, R. (2012). Firefly Luciferase Mutants as Sensors of Proteome Stress. In Fakultät für Chemie und Pharmazie (Ludwig-Maximilians-Universität München).
- Gupta, R., Kasturi, P., Bracher, A., Loew, C., Zheng, M., Vilella, A., Garza, D., Hartl, F.U., and Raychaudhuri, S. (2011). Firefly luciferase mutants as sensors of proteome stress. *Nat Methods* 8, 879-884.
- Guttinger, S., Laurell, E., and Kutay, U. (2009). Orchestrating nuclear envelope disassembly and reassembly during mitosis. *Nat Rev Mol Cell Biol* 10, 178-191.
- Gyrd-Hansen, M., and Meier, P. (2010). IAPs: from caspase inhibitors to modulators of NF-kappaB, inflammation and cancer. *Nat Rev Cancer* 10, 561-574.
- Haass, C., and Selkoe, D.J. (2007). Soluble protein oligomers in neurodegeneration: lessons from the Alzheimer's amyloid beta-peptide. *Nat Rev Mol Cell Biol* 8, 101-112.
- Hackam, A.S., Hodgson, J.G., Singaraja, R., Zhang, T., Gan, L., Gutekunst, C.A., Hersch, S.M., and Hayden, M.R. (1999). Evidence for both the nucleus and cytoplasm as subcellular sites of pathogenesis in Huntington's disease in cell culture and in transgenic mice expressing mutant huntingtin. *Philos Trans R Soc Lond B Biol Sci* 354, 1047-1055.
- Hackam, A.S., Singaraja, R., Zhang, T., Gan, L., and Hayden, M.R. (1999). In vitro evidence for both the nucleus and cytoplasm as subcellular sites of pathogenesis in Huntington's disease. *Hum Mol Genet* 8, 25-33.
- Hageman, J., Vos, M.J., van Waarde, M.A., and Kampinga, H.H. (2007). Comparison of intra-organellar chaperone capacity for dealing with stress-induced protein unfolding. *J Biol Chem* 282, 34334-34345.
- Halliday, M., and Mallucci, G.R. (2014). Targeting the unfolded protein response in neurodegeneration: A new approach to therapy. *Neuropharmacology* 76 Pt A, 169-174.
- Hardy, J., and Selkoe, D.J. (2002). The amyloid hypothesis of Alzheimer's disease: progress and problems on the road to therapeutics. *Science* 297, 353-356.
- Hardy, S.J., and Randall, L.L. (1991). A kinetic partitioning model of selective binding of nonnative proteins by the bacterial chaperone SecB. *Science* 251, 439-443.
- Hartl, F.U. (1996). Molecular chaperones in cellular protein folding. *Nature* 381, 571-579.
- Hartl, F.U., Bracher, A., and Hayer-Hartl, M. (2011). Molecular chaperones in protein folding and proteostasis. *Nature* 475, 324-332.
- Hartl, F.U., and Hayer-Hartl, M. (2009). Converging concepts of protein folding in vitro and in vivo. *Nat Struct Mol Biol* 16, 574-581.
- Hartl, F.U., Ostermann, J., Guiard, B., and Neupert, W. (1987). Successive translocation into and out of the mitochondrial matrix: targeting of proteins to the intermembrane space by a bipartite signal peptide. *Cell* 51, 1027-1037.



- Hartl, F.U., Schmidt, B., Wachter, E., Weiss, H., and Neupert, W. (1986). Transport into mitochondria and intramitochondrial sorting of the Fe/S protein of ubiquinol-cytochrome c reductase. *Cell* *47*, 939-951.
- Hawe, A., Sutter, M., and Jiskoot, W. (2008). Extrinsic fluorescent dyes as tools for protein characterization. *Pharm Res* *25*, 1487-1499.
- Haynes, C.M., and Ron, D. (2010). The mitochondrial UPR - protecting organelle protein homeostasis. *J Cell Sci* *123*, 3849-3855.
- Haynes, C.M., Yang, Y., Blais, S.P., Neupert, T.A., and Ron, D. (2010). The matrix peptide exporter HAF-1 signals a mitochondrial UPR by activating the transcription factor ZC376.7 in *C. elegans*. *Mol Cell* *37*, 529-540.
- Haynie, D.T., and Freire, E. (1993). Structural energetics of the molten globule state. *Proteins* *16*, 115-140.
- He, B., and Soderlund, D.M. (2010). Human embryonic kidney (HEK293) cells express endogenous voltage-gated sodium currents and Na v 1.7 sodium channels. *Neuroscience letters* *469*, 268-272.
- Hecht, M.H., Das, A., Go, A., Bradley, L.H., and Wei, Y. (2004). De novo proteins from designed combinatorial libraries. *Protein Sci* *13*, 1711-1723.
- Heinz, C., Engelhardt, H., and Niederweis, M. (2003). The core of the tetrameric mycobacterial porin MspA is an extremely stable beta-sheet domain. *J Biol Chem* *278*, 8678-8685.
- Henn, I.H., Bouman, L., Schlehe, J.S., Schlierf, A., Schramm, J.E., Wegener, E., Nakaso, K., Culmsee, C., Berninger, B., Krappmann, D., *et al.* (2007). Parkin mediates neuroprotection through activation of I $\kappa$ B kinase/nuclear factor- $\kappa$ B signaling. *J Neurosci* *27*, 1868-1878.
- Hernandez-Verdun, D. (2011). Assembly and disassembly of the nucleolus during the cell cycle. *Nucleus* *2*, 189-194.
- Hipp, M.S., Park, S.H., and Hartl, F.U. (2014). Proteostasis impairment in protein-misfolding and -aggregation diseases. *Trends in cell biology* *24*, 506-514.
- Hirokawa, N., Niwa, S., and Tanaka, Y. (2010). Molecular motors in neurons: transport mechanisms and roles in brain function, development, and disease. *Neuron* *68*, 610-638.
- Hirokawa, N., and Takemura, R. (2005). Molecular motors and mechanisms of directional transport in neurons. *Nat Rev Neurosci* *6*, 201-214.
- Hodel, M.R., Corbett, A.H., and Hodel, A.E. (2001). Dissection of a nuclear localization signal. *J Biol Chem* *276*, 1317-1325.
- Hodgson, J.G., Agopyan, N., Gutekunst, C.A., Leavitt, B.R., LePiane, F., Singaraja, R., Smith, D.J., Bissada, N., McCutcheon, K., Nasir, J., *et al.* (1999). A YAC mouse model for Huntington's disease with full-length mutant huntingtin, cytoplasmic toxicity, and selective striatal neurodegeneration. *Neuron* *23*, 181-192.
- Hoop, C.L., Lin, H.K., Kar, K., Hou, Z., Poirier, M.A., Wetzell, R., and van der Wel, P.C. (2014). Polyglutamine amyloid core boundaries and flanking domain dynamics in huntingtin fragment fibrils determined by solid-state nuclear magnetic resonance. *Biochemistry* *53*, 6653-6666.
- Hoozemans, J.J., Veerhuis, R., Van Haastert, E.S., Rozemuller, J.M., Baas, F., Eikelenboom, P., and Scheper, W. (2005). The unfolded protein response is activated in Alzheimer's disease. *Acta Neuropathol* *110*, 165-172.
- Hortschansky, P., Schroeckh, V., Christopeit, T., Zandomenighi, G., and Fandrich, M. (2005). The aggregation kinetics of Alzheimer's beta-amyloid peptide is controlled by stochastic nucleation. *Protein Sci* *14*, 1753-1759.
- Houseley, J., LaCava, J., and Tollervey, D. (2006). RNA-quality control by the exosome. *Nat Rev Mol Cell Biol* *7*, 529-539.
- Hsu, A.L., Murphy, C.T., and Kenyon, C. (2003). Regulation of aging and age-related disease by DAF-16 and heat-shock factor. *Science* *300*, 1142-1145.
- Hua, Z., and Vierstra, R.D. (2011). The cullin-RING ubiquitin-protein ligases. *Annual review of plant biology* *62*, 299-334.
- Huang, G.S., and Oas, T.G. (1995). Submillisecond folding of monomeric lambda repressor. *Proc Natl Acad Sci U S A* *92*, 6878-6882.
- Huang, H.C., and Jiang, Z.F. (2009). Accumulated amyloid-beta peptide and hyperphosphorylated tau protein: relationship and links in Alzheimer's disease. *J Alzheimers Dis* *16*, 15-27.
- Huang, H.C., and Jiang, Z.F. (2011). Amyloid-beta protein precursor family members: a review from homology to biological function. *J Alzheimers Dis* *26*, 607-626.
- Hubbard, R.E., and Kamran Haider, M. (2010). Hydrogen Bonds in Proteins: Role and Strength. *Encyclopedia of Life Sciences*.

- Huber, E.M., Basler, M., Schwab, R., Heinemeyer, W., Kirk, C.J., Groettrup, M., and Groll, M. (2012). Immuno- and constitutive proteasome crystal structures reveal differences in substrate and inhibitor specificity. *Cell* *148*, 727-738.
- Hutton, M., Lendon, C.L., Rizzu, P., Baker, M., Froelich, S., Houlden, H., Pickering-Brown, S., Chakraverty, S., Isaacs, A., Grover, A., *et al.* (1998). Association of missense and 5'-splice-site mutations in tau with the inherited dementia FTDP-17. *Nature* *393*, 702-705.
- Iacono, D., O'Brien, R., Resnick, S.M., Zonderman, A.B., Pletnikova, O., Rudow, G., An, Y., West, M.J., Crain, B., and Troncoso, J.C. (2008). Neuronal hypertrophy in asymptomatic Alzheimer disease. *J Neuropathol Exp Neurol* *67*, 578-589.
- Ishida, Y., and Nagata, K. (2011). Hsp47 as a collagen-specific molecular chaperone. *Methods Enzymol* *499*, 167-182.
- Jablonski, J.A., and Caputi, M. (2009). Role of cellular RNA processing factors in human immunodeficiency virus type 1 mRNA metabolism, replication, and infectivity. *J Virol* *83*, 981-992.
- Jackson, R.J., Hellen, C.U., and Pestova, T.V. (2010). The mechanism of eukaryotic translation initiation and principles of its regulation. *Nat Rev Mol Cell Biol* *11*, 113-127.
- Jaiswal, H., Conz, C., Otto, H., Wolfle, T., Fitzke, E., Mayer, M.P., and Rospert, S. (2011). The chaperone network connected to human ribosome-associated complex. *Mol Cell Biol* *31*, 1160-1173.
- Jaroniec, C.P., MacPhee, C.E., Astrof, N.S., Dobson, C.M., and Griffin, R.G. (2002). Molecular conformation of a peptide fragment of transthyretin in an amyloid fibril. *Proc Natl Acad Sci U S A* *99*, 16748-16753.
- Jewett, A.I., Baumketner, A., and Shea, J.E. (2004). Accelerated folding in the weak hydrophobic environment of a chaperonin cavity: creation of an alternate fast folding pathway. *Proc Natl Acad Sci U S A* *101*, 13192-13197.
- John, G.B., Shang, Y., Li, L., Renken, C., Mannella, C.A., Selker, J.M., Rangell, L., Bennett, M.J., and Zha, J. (2005). The mitochondrial inner membrane protein mitofilin controls cristae morphology. *Mol Biol Cell* *16*, 1543-1554.
- Johnson, A.P., Cleaves, H.J., Dworkin, J.P., Glavin, D.P., Laczano, A., and Bada, J.L. (2008). The Miller volcanic spark discharge experiment. *Science* *322*, 404.
- Johnson, W.C. (1999). Analyzing protein circular dichroism spectra for accurate secondary structures. *Proteins* *35*, 307-312.
- Jonker, M.J., Melis, J.P., Kuiper, R.V., van der Hoeven, T.V., Wackers, P.F., Robinson, J., van der Horst, G.T., Dolle, M.E., Vijg, J., Breit, T.M., *et al.* (2013). Life spanning murine gene expression profiles in relation to chronological and pathological aging in multiple organs. *Aging cell* *12*, 901-909.
- Jonsson, T., Atwal, J.K., Steinberg, S., Snaedal, J., Jonsson, P.V., Bjornsson, S., Stefansson, H., Sulem, P., Gudbjartsson, D., Maloney, J., *et al.* (2012). A mutation in APP protects against Alzheimer's disease and age-related cognitive decline. *Nature* *488*, 96-99.
- Jordan, E.T., Collins, M., Terefe, J., Ugozzoli, L., and Rubio, T. (2008). Optimizing electroporation conditions in primary and other difficult-to-transfect cells. *J Biomol Tech* *19*, 328-334.
- Jovaisaite, V., Mouchiroud, L., and Auwerx, J. (2014). The mitochondrial unfolded protein response, a conserved stress response pathway with implications in health and disease. *The Journal of experimental biology* *217*, 137-143.
- Jovicic, A., Mertens, J., Boeynaems, S., Bogaert, E., Chai, N., Yamada, S.B., Paul, J.W., 3rd, Sun, S., Herdy, J.R., Bieri, G., *et al.* (2015). Modifiers of C9orf72 dipeptide repeat toxicity connect nucleocytoplasmic transport defects to FTD/ALS. *Nat Neurosci* *18*, 1226-1229.
- Kaganovich, D., Kopito, R., and Frydman, J. (2008). Misfolded proteins partition between two distinct quality control compartments. *Nature* *454*, 1088-1095.
- Kaiser, C.M., Chang, H.C., Agashe, V.R., Lakshminpathy, S.K., Etchells, S.A., Hayer-Hartl, M., Hartl, F.U., and Barral, J.M. (2006). Real-time observation of trigger factor function on translating ribosomes. *Nature* *444*, 455-460.
- Kalderon, D., Roberts, B.L., Richardson, W.D., and Smith, A.E. (1984). A short amino acid sequence able to specify nuclear location. *Cell* *39*, 499-509.
- Kalim, K.W., Basler, M., Kirk, C.J., and Groettrup, M. (2012). Immunoproteasome subunit LMP7 deficiency and inhibition suppresses Th1 and Th17 but enhances regulatory T cell differentiation. *J Immunol* *189*, 4182-4193.
- Kaltschmidt, B., and Kaltschmidt, C. (2009). NF-kappaB in the nervous system. *Cold Spring Harb Perspect Biol* *1*, a001271.
- Kamtekar, S., Schiffer, J.M., Xiong, H., Babik, J.M., and Hecht, M.H. (1993). Protein design by binary patterning of polar and nonpolar amino acids. *Science* *262*, 1680-1685.

- Kanai, Y., Dohmae, N., and Hirokawa, N. (2004). Kinesin transports RNA: isolation and characterization of an RNA-transporting granule. *Neuron* *43*, 513-525.
- Kang, J., Lemaire, H.G., Unterbeck, A., Salbaum, J.M., Masters, C.L., Grzeschik, K.H., Multhaup, G., Beyreuther, K., and Muller-Hill, B. (1987). The precursor of Alzheimer's disease amyloid A4 protein resembles a cell-surface receptor. *Nature* *325*, 733-736.
- Karin, M., and Ben-Neriah, Y. (2000). Phosphorylation meets ubiquitination: the control of NF-[kappa]B activity. *Annu Rev Immunol* *18*, 621-663.
- Kayed, R., and Glabe, C.G. (2006). Conformation-dependent anti-amyloid oligomer antibodies. *Methods Enzymol* *413*, 326-344.
- Kayed, R., Head, E., Thompson, J.L., McIntire, T.M., Milton, S.C., Cotman, C.W., and Glabe, C.G. (2003). Common structure of soluble amyloid oligomers implies common mechanism of pathogenesis. *Science* *300*, 486-489.
- Kerner, M.J., Naylor, D.J., Ishihama, Y., Maier, T., Chang, H.C., Stines, A.P., Georgopoulos, C., Frishman, D., Hayer-Hartl, M., Mann, M., *et al.* (2005). Proteome-wide analysis of chaperonin-dependent protein folding in *Escherichia coli*. *Cell* *122*, 209-220.
- Khan, A.Y., and Suresh Kumar, G. (2016). Spectroscopic studies on the binding interaction of phenothiazinium dyes, azure A and azure B to double stranded RNA polynucleotides. *Spectrochim Acta A Mol Biomol Spectrosc* *152*, 417-425.
- Khosravani, H., Zhang, Y., Tsutsui, S., Hameed, S., Altier, C., Hamid, J., Chen, L., Villemaire, M., Ali, Z., Jirik, F.R., *et al.* (2008). Prion protein attenuates excitotoxicity by inhibiting NMDA receptors. *J Cell Biol* *181*, 551-565.
- Khurana, R., Coleman, C., Ionescu-Zanetti, C., Carter, S.A., Krishna, V., Grover, R.K., Roy, R., and Singh, S. (2005). Mechanism of thioflavin T binding to amyloid fibrils. *J Struct Biol* *151*, 229-238.
- Kim, J.S., He, L., and Lemasters, J.J. (2003). Mitochondrial permeability transition: a common pathway to necrosis and apoptosis. *Biochem Biophys Res Commun* *304*, 463-470.
- Kim, S.J., Born, B., Havenith, M., and Gruebele, M. (2008). Real-time detection of protein-water dynamics upon protein folding by terahertz absorption spectroscopy. *Angew Chem Int Ed Engl* *47*, 6486-6489.
- Kim, Y.E., Hipp, M.S., Bracher, A., Hayer-Hartl, M., and Ulrich Hartl, F. (2013). Molecular chaperone functions in protein folding and proteostasis. *Annu Rev Biochem* *82*, 323-355.
- King, M.L., Zhou, Y., and Bubunenko, M. (1999). Polarizing genetic information in the egg: RNA localization in the frog oocyte. *Bioessays* *21*, 546-557.
- Kisselev, A.F., and Goldberg, A.L. (2001). Proteasome inhibitors: from research tools to drug candidates. *Chem Biol* *8*, 739-758.
- Kleinschmidt, J.A., Hugle, B., Grund, C., and Franke, W.W. (1983). The 22 S cylinder particles of *Xenopus laevis*. I. Biochemical and electron microscopic characterization. *European journal of cell biology* *32*, 143-156.
- Knobloch, M., and Mansuy, I.M. (2008). Dendritic spine loss and synaptic alterations in Alzheimer's disease. *Mol Neurobiol* *37*, 73-82.
- Knowles, T.P., Vendruscolo, M., and Dobson, C.M. (2014). The amyloid state and its association with protein misfolding diseases. *Nat Rev Mol Cell Biol* *15*, 384-396.
- Ko, J., Ou, S., and Patterson, P.H. (2001). New anti-huntingtin monoclonal antibodies: implications for huntingtin conformation and its binding proteins. *Brain Res Bull* *56*, 319-329.
- Kobe, B. (1999). Autoinhibition by an internal nuclear localization signal revealed by the crystal structure of mammalian importin alpha. *Nat Struct Biol* *6*, 388-397.
- Kohler, A., and Hurt, E. (2007). Exporting RNA from the nucleus to the cytoplasm. *Nat Rev Mol Cell Biol* *8*, 761-773.
- Koike, M., Shibata, M., Tadakoshi, M., Gotoh, K., Komatsu, M., Waguri, S., Kawahara, N., Kuida, K., Nagata, S., Kominami, E., *et al.* (2008). Inhibition of autophagy prevents hippocampal pyramidal neuron death after hypoxic-ischemic injury. *Am J Pathol* *172*, 454-469.
- Kojro, E., Gimpl, G., Lammich, S., Marz, W., and Fahrenholz, F. (2001). Low cholesterol stimulates the nonamyloidogenic pathway by its effect on the alpha -secretase ADAM 10. *Proc Natl Acad Sci U S A* *98*, 5815-5820.
- Komander, D., and Rape, M. (2012). The ubiquitin code. *Annu Rev Biochem* *81*, 203-229.
- Konno, T. (2001). Amyloid-induced aggregation and precipitation of soluble proteins: an electrostatic contribution of the Alzheimer's beta(25-35) amyloid fibril. *Biochemistry* *40*, 2148-2154.
- Konrat, R. (2014). NMR contributions to structural dynamics studies of intrinsically disordered proteins. *J Magn Reson* *241*, 74-85.

- Koplin, A., Preissler, S., Ilina, Y., Koch, M., Scior, A., Erhardt, M., and Deuerling, E. (2010). A dual function for chaperones SSB-RAC and the NAC nascent polypeptide-associated complex on ribosomes. *J Cell Biol* 189, 57-68.
- Korgaonkar, C., Hagen, J., Tompkins, V., Frazier, A.A., Allamargot, C., Quelle, F.W., and Quelle, D.E. (2005). Nucleophosmin (B23) targets ARF to nucleoli and inhibits its function. *Mol Cell Biol* 25, 1258-1271.
- Kose, S., Furuta, M., and Imamoto, N. (2012). Hikeshi, a nuclear import carrier for Hsp70s, protects cells from heat shock-induced nuclear damage. *Cell* 149, 578-589.
- Koshland, D.E. (1958). Application of a Theory of Enzyme Specificity to Protein Synthesis. *Proc Natl Acad Sci U S A* 44, 98-104.
- Kovacs, I.A., Szalay, M.S., and Csermely, P. (2005). Water and molecular chaperones act as weak links of protein folding networks: energy landscape and punctuated equilibrium changes point towards a game theory of proteins. *FEBS Lett* 579, 2254-2260.
- Kraus, A., Groveman, B.R., and Caughey, B. (2013). Prions and the potential transmissibility of protein misfolding diseases. *Annu Rev Microbiol* 67, 543-564.
- Krebs, M.R., Wilkins, D.K., Chung, E.W., Pitkeathly, M.C., Chamberlain, A.K., Zurdo, J., Robinson, C.V., and Dobson, C.M. (2000). Formation and seeding of amyloid fibrils from wild-type hen lysozyme and a peptide fragment from the beta-domain. *J Mol Biol* 300, 541-549.
- Krem, M.M., and Di Cera, E. (1998). Conserved water molecules in the specificity pocket of serine proteases and the molecular mechanism of Na<sup>+</sup> binding. *Proteins* 30, 34-42.
- Kretzschmar, H., and Tatzelt, J. (2013). Prion disease: a tale of folds and strains. *Brain Pathol* 23, 321-332.
- Krishnan, R., and Lindquist, S.L. (2005). Structural insights into a yeast prion illuminate nucleation and strain diversity. *Nature* 435, 765-772.
- Kroemer, G., Galluzzi, L., and Brenner, C. (2007). Mitochondrial membrane permeabilization in cell death. *Physiol Rev* 87, 99-163.
- Kudlicki, W., Coffman, A., Kramer, G., and Hardesty, B. (1997). Ribosomes and ribosomal RNA as chaperones for folding of proteins. *Fold Des* 2, 101-108.
- Kudo, N., Wolff, B., Sekimoto, T., Schreiner, E.P., Yoneda, Y., Yanagida, M., Horinouchi, S., and Yoshida, M. (1998). Leptomycin B inhibition of signal-mediated nuclear export by direct binding to CRM1. *Exp Cell Res* 242, 540-547.
- Kurata, T., Miyazaki, K., Kozuki, M., Morimoto, N., Ohta, Y., Ikeda, Y., and Abe, K. (2012). Atorvastatin and pitavastatin reduce senile plaques and inflammatory responses in a mouse model of Alzheimer's disease. *Neurol Res* 34, 601-610.
- Kuwata, K., Shastry, R., Cheng, H., Hoshino, M., Batt, C.A., Goto, Y., and Roder, H. (2001). Structural and kinetic characterization of early folding events in beta-lactoglobulin. *Nat Struct Biol* 8, 151-155.
- la Cour, T., Kiemer, L., Molgaard, A., Gupta, R., Skriver, K., and Brunak, S. (2004). Analysis and prediction of leucine-rich nuclear export signals. *Protein Eng Des Sel* 17, 527-536.
- Labbadia, J., and Morimoto, R.I. (2015). The biology of proteostasis in aging and disease. *Annu Rev Biochem* 84, 435-464.
- Laemmli, U.K. (1970). Cleavage of structural proteins during the assembly of the head of bacteriophage T4. *Nature* 227, 680-685.
- Lahdenpera, M., Lummaa, V., Helle, S., Tremblay, M., and Russell, A.F. (2004). Fitness benefits of prolonged post-reproductive lifespan in women. *Nature* 428, 178-181.
- Lakshminpathy, S.K., Tomic, S., Kaiser, C.M., Chang, H.C., Genevoux, P., Georgopoulos, C., Barral, J.M., Johnson, A.E., Hartl, F.U., and Etchells, S.A. (2007). Identification of nascent chain interaction sites on trigger factor. *J Biol Chem* 282, 12186-12193.
- Lashuel, H.A., Hartley, D., Petre, B.M., Walz, T., and Lansbury, P.T., Jr. (2002). Neurodegenerative disease: amyloid pores from pathogenic mutations. *Nature* 418, 291.
- Latonen, L., Moore, H.M., Bai, B., Jaamaa, S., and Laiho, M. (2011). Proteasome inhibitors induce nucleolar aggregation of proteasome target proteins and polyadenylated RNA by altering ubiquitin availability. *Oncogene* 30, 790-805.
- Lawrence, M.S., Phillips, K.J., and Liu, D.R. (2007). Supercharging proteins can impart unusual resilience. *J Am Chem Soc* 129, 10110-10112.
- Lazaridis, T. (2013). HydrophobicEffect. eLS.

- Leavitt, B.R., van Raamsdonk, J.M., Shehadeh, J., Fernandes, H., Murphy, Z., Graham, R.K., Wellington, C.L., Raymond, L.A., and Hayden, M.R. (2006). Wild-type huntingtin protects neurons from excitotoxicity. *J Neurochem* 96, 1121-1129.
- Lee, N., Bessho, Y., Wei, K., Szostak, J.W., and Suga, H. (2000). Ribozyme-catalyzed tRNA aminoacylation. *Nat Struct Biol* 7, 28-33.
- Lee, R.J., Liu, C.W., Harty, C., McCracken, A.A., Latterich, M., Romisch, K., DeMartino, G.N., Thomas, P.J., and Brodsky, J.L. (2004). Uncoupling retro-translocation and degradation in the ER-associated degradation of a soluble protein. *EMBO J* 23, 2206-2215.
- Levenson, R.W., Sturm, V.E., and Haase, C.M. (2014). Emotional and behavioral symptoms in neurodegenerative disease: a model for studying the neural bases of psychopathology. *Annu Rev Clin Psychol* 10, 581-606.
- Levinthal, C. (1969). How to Fold Graciously. University of Illinois Press *Mossbauer Spectroscopy in Biological Systems: Proceedings of a meeting held at Allerton House, Monticello, Illinois, 22-24*.
- Levy, Y., and Onuchic, J.N. (2006). Water mediation in protein folding and molecular recognition. *Annu Rev Biophys Biomol Struct* 35, 389-415.
- Li, H., Kumar Sharma, L., Li, Y., Hu, P., Idowu, A., Liu, D., Lu, J., and Bai, Y. (2013). Comparative bioenergetic study of neuronal and muscle mitochondria during aging. *Free radical biology & medicine* 63, 30-40.
- Li, J.Y., Popovic, N., and Brundin, P. (2005). The use of the R6 transgenic mouse models of Huntington's disease in attempts to develop novel therapeutic strategies. *NeuroRx* 2, 447-464.
- Li, S.H., Cheng, A.L., Zhou, H., Lam, S., Rao, M., Li, H., and Li, X.J. (2002). Interaction of Huntington disease protein with transcriptional activator Sp1. *Mol Cell Biol* 22, 1277-1287.
- Lindgren, M., Sorgjerd, K., and Hammarstrom, P. (2005). Detection and characterization of aggregates, prefibrillar amyloidogenic oligomers, and protofibrils using fluorescence spectroscopy. *Biophys J* 88, 4200-4212.
- Liu, K.Y., Shyu, Y.C., Barbaro, B.A., Lin, Y.T., Chern, Y., Thompson, L.M., James Shen, C.K., and Marsh, J.L. (2015). Disruption of the nuclear membrane by perinuclear inclusions of mutant huntingtin causes cell-cycle re-entry and striatal cell death in mouse and cell models of Huntington's disease. *Hum Mol Genet* 24, 1602-1616.
- Lo Bianco, C., Schneider, B.L., Bauer, M., Sajadi, A., Brice, A., Iwatsubo, T., and Aebischer, P. (2004). Lentiviral vector delivery of parkin prevents dopaminergic degeneration in an alpha-synuclein rat model of Parkinson's disease. *Proc Natl Acad Sci U S A* 101, 17510-17515.
- Lodish, H.F. (2000). *Molecular cell biology*, 4th edn (New York: W.H. Freeman).
- Long, Z., Tang, B., and Jiang, H. (2014). Alleviating neurodegeneration in Drosophila models of PolyQ diseases. *Cerebellum & Ataxias* 1.
- Lu, J., and Deutsch, C. (2005). Folding zones inside the ribosomal exit tunnel. *Nat Struct Mol Biol* 12, 1123-1129.
- Lu, T., Aron, L., Zullo, J., Pan, Y., Kim, H., Chen, Y., Yang, T.H., Kim, H.M., Drake, D., Liu, X.S., *et al.* (2014). REST and stress resistance in ageing and Alzheimer's disease. *Nature* 507, 448-454.
- Lue, L.F., Kuo, Y.M., Roher, A.E., Brachova, L., Shen, Y., Sue, L., Beach, T., Kurth, J.H., Rydel, R.E., and Rogers, J. (1999). Soluble amyloid beta peptide concentration as a predictor of synaptic change in Alzheimer's disease. *Am J Pathol* 155, 853-862.
- Lunkes, A., Lindenberg, K.S., Ben-Haiem, L., Weber, C., Devys, D., Landwehrmeyer, G.B., Mandel, J.L., and Trottier, Y. (2002). Proteases acting on mutant huntingtin generate cleaved products that differentially build up cytoplasmic and nuclear inclusions. *Mol Cell* 10, 259-269.
- Luthi-Carter, R., Hanson, S.A., Strand, A.D., Bergstrom, D.A., Chun, W., Peters, N.L., Woods, A.M., Chan, E.Y., Kooperberg, C., Krainc, D., *et al.* (2002). Dysregulation of gene expression in the R6/2 model of polyglutamine disease: parallel changes in muscle and brain. *Hum Mol Genet* 11, 1911-1926.
- Lyubchenko, Y.L., Krasnoslobodtsev, A.V., and Luca, S. (2012). Fibrillogenesis of huntingtin and other glutamine containing proteins. *Sub-cellular biochemistry* 65, 225-251.
- Maggi, L.B., Jr., Kuchenruether, M., Dadey, D.Y., Schwoppe, R.M., Grisendi, S., Townsend, R.R., Pandolfi, P.P., and Weber, J.D. (2008). Nucleophosmin serves as a rate-limiting nuclear export chaperone for the Mammalian ribosome. *Mol Cell Biol* 28, 7050-7065.
- Magner, L.N. (2002). *A History of the Life Sciences, Revised and Expanded* (CRC Press).
- Maji, S.K., Perrin, M.H., Sawaya, M.R., Jessberger, S., Vadodaria, K., Rissman, R.A., Singru, P.S., Nilsson, K.P., Simon, R., Schubert, D., *et al.* (2009). Functional amyloids as natural storage of peptide hormones in pituitary secretory granules. *Science* 325, 328-332.
- Makkerh, J.P., Dingwall, C., and Laskey, R.A. (1996). Comparative mutagenesis of nuclear localization signals reveals the importance of neutral and acidic amino acids. *Curr Biol* 6, 1025-1027.

- Mallette, F.A., and Richard, S. (2012). K48-linked ubiquitination and protein degradation regulate 53BP1 recruitment at DNA damage sites. *Cell research* 22, 1221-1223.
- Mamikonian, G., Necula, M., Mkrtichyan, M., Ghochikyan, A., Petrushina, I., Movsesyan, N., Mina, E., Kiyatkin, A., Glabe, C.G., Cribbs, D.H., *et al.* (2007). Anti-A beta 1-11 antibody binds to different beta-amyloid species, inhibits fibril formation, and disaggregates preformed fibrils but not the most toxic oligomers. *J Biol Chem* 282, 22376-22386.
- Mandelkow, E.M., and Mandelkow, E. (2012). Biochemistry and cell biology of tau protein in neurofibrillary degeneration. *Cold Spring Harb Perspect Med* 2, a006247.
- Mangiarini, L., Sathasivam, K., Seller, M., Cozens, B., Harper, A., Hetherington, C., Lawton, M., Trotter, Y., Lehrach, H., Davies, S.W., *et al.* (1996). Exon 1 of the HD gene with an expanded CAG repeat is sufficient to cause a progressive neurological phenotype in transgenic mice. *Cell* 87, 493-506.
- Mann, D.M., and Sinclair, K.G. (1978). The quantitative assessment of lipofuscin pigment, cytoplasmic RNA and nucleolar volume in senile dementia. *Neuropathol Appl Neurobiol* 4, 129-135.
- Mann, D.M., and Yates, P.O. (1983). Serotonin nerve cells in Alzheimer's disease. *J Neurol Neurosurg Psychiatry* 46, 96.
- Mann, D.M., Yates, P.O., and Barton, C.M. (1977). Cytophotometric mapping of neuronal changes in senile dementia. *J Neurol Neurosurg Psychiatry* 40, 299-302.
- Marciniak, S.J., Yun, C.Y., Oyadomari, S., Novoa, I., Zhang, Y., Jungreis, R., Nagata, K., Harding, H.P., and Ron, D. (2004). CHOP induces death by promoting protein synthesis and oxidation in the stressed endoplasmic reticulum. *Genes Dev* 18, 3066-3077.
- Mashaghi, A., Kramer, G., Bechtluft, P., Zachmann-Brand, B., Driessen, A.J., Bukau, B., and Tans, S.J. (2013). Reshaping of the conformational search of a protein by the chaperone trigger factor. *Nature* 500, 98-101.
- Masters, C.L., and Selkoe, D.J. (2012). Biochemistry of amyloid beta-protein and amyloid deposits in Alzheimer disease. *Cold Spring Harb Perspect Med* 2, a006262.
- Masuda, S., Das, R., Cheng, H., Hurt, E., Dorman, N., and Reed, R. (2005). Recruitment of the human TREX complex to mRNA during splicing. *Genes Dev* 19, 1512-1517.
- Matera, A.G., Izaguire-Sierra, M., Praveen, K., and Rajendra, T.K. (2009). Nuclear bodies: random aggregates of sticky proteins or crucibles of macromolecular assembly? *Dev Cell* 17, 639-647.
- Matsumura, H., Mizohata, E., Ishida, H., Kogami, A., Ueno, T., Makino, A., Inoue, T., Yokota, A., Mae, T., and Kai, Y. (2012). Crystal structure of rice Rubisco and implications for activation induced by positive effectors NADPH and 6-phosphogluconate. *J Mol Biol* 422, 75-86.
- Mattoo, R.U., Sharma, S.K., Priya, S., Finka, A., and Goloubinoff, P. (2013). Hsp110 is a bona fide chaperone using ATP to unfold stable misfolded polypeptides and reciprocally collaborate with Hsp70 to solubilize protein aggregates. *J Biol Chem* 288, 21399-21411.
- Maurer-Stroh, S., and Eisenhaber, F. (2005). Refinement and prediction of protein prenylation motifs. *Genome Biol* 6, R55.
- Mayer, M.P. (2010). Gymnastics of molecular chaperones. *Mol Cell* 39, 321-331.
- McCracken, A.A., and Brodsky, J.L. (1996). Assembly of ER-associated protein degradation in vitro: dependence on cytosol, calnexin, and ATP. *J Cell Biol* 132, 291-298.
- McGuffee, S.R., and Elcock, A.H. (2010). Diffusion, crowding & protein stability in a dynamic molecular model of the bacterial cytoplasm. *PLoS Comput Biol* 6, e1000694.
- Medalia, O., Weber, I., Frangakis, A.S., Nicastro, D., Gerisch, G., and Baumeister, W. (2002). Macromolecular architecture in eukaryotic cells visualized by cryoelectron tomography. *Science* 298, 1209-1213.
- Mercer, T.R., Dinger, M.E., and Mattick, J.S. (2009). Long non-coding RNAs: insights into functions. *Nat Rev Genet* 10, 155-159.
- Meszaros, B., Simon, I., and Dosztanyi, Z. (2009). Prediction of protein binding regions in disordered proteins. *PLoS Comput Biol* 5, e1000376.
- Metz, A., Soret, J., Vourc'h, C., Tazi, J., and Jolly, C. (2004). A key role for stress-induced satellite III transcripts in the relocalization of splicing factors into nuclear stress granules. *J Cell Sci* 117, 4551-4558.
- Meunier, D., Stamatakis, E.A., and Tyler, L.K. (2014). Age-related functional reorganization, structural changes, and preserved cognition. *Neurobiol Aging* 35, 42-54.
- Meyer, P. (1994). Bi-logistic Growth. *Technological Forecasting and Social Change* 47, 89-102.
- Mielcarek, M., Landles, C., Weiss, A., Bradaia, A., Seredenina, T., Inuabasi, L., Osborne, G.F., Wadel, K., Toullier, C., Butler, R., *et al.* (2013). HDAC4 reduction: a novel therapeutic strategy to target cytoplasmic huntingtin and ameliorate neurodegeneration. *PLoS Biol* 11, e1001717.

- Miller, J., Arrasate, M., Brooks, E., Libeu, C.P., Legleiter, J., Hatters, D., Curtis, J., Cheung, K., Krishnan, P., Mitra, S., *et al.* (2011). Identifying polyglutamine protein species in situ that best predict neurodegeneration. *Nat Chem Biol* 7, 925-934.
- Miller, S.L. (1953). A production of amino acids under possible primitive earth conditions. *Science* 117, 528-529.
- Miller, S.L., and Urey, H.C. (1959). Organic compound synthesis on the primitive earth. *Science* 130, 245-251.
- Ming, G.L., and Song, H. (2011). Adult neurogenesis in the mammalian brain: significant answers and significant questions. *Neuron* 70, 687-702.
- Mironov, A.S., Gusarov, I., Rafikov, R., Lopez, L.E., Shatalin, K., Kreneva, R.A., Perumov, D.A., and Nudler, E. (2002). Sensing small molecules by nascent RNA: a mechanism to control transcription in bacteria. *Cell* 111, 747-756.
- Miyamoto, Y., Saiwaki, T., Yamashita, J., Yasuda, Y., Kotera, I., Shibata, S., Shigeta, M., Hiraoka, Y., Haraguchi, T., and Yoneda, Y. (2004). Cellular stresses induce the nuclear accumulation of importin alpha and cause a conventional nuclear import block. *J Cell Biol* 165, 617-623.
- Mohr, D., Frey, S., Fischer, T., Guttler, T., and Gorlich, D. (2009). Characterisation of the passive permeability barrier of nuclear pore complexes. *EMBO J* 28, 2541-2553.
- Monsellier, E., Ramazzotti, M., de Laureto, P.P., Tartaglia, G.G., Taddei, N., Fontana, A., Vendruscolo, M., and Chiti, F. (2007). The distribution of residues in a polypeptide sequence is a determinant of aggregation optimized by evolution. *Biophys J* 93, 4382-4391.
- Moon, I.S., Cho, S.J., Seog, D.H., and Walikonis, R. (2009). Neuronal activation increases the density of eukaryotic translation initiation factor 4E mRNA clusters in dendrites of cultured hippocampal neurons. *Exp Mol Med* 41, 601-610.
- Moore, S., and Stein, W.H. (1948). Photometric ninhydrin method for use in the chromatography of amino acids. *J Biol Chem* 176, 367-388.
- Moore, S., and Stein, W.H. (1951). Chromatography of amino acids on sulfonated polystyrene resins. *J Biol Chem* 192, 663-681.
- Mor, A., White, M.A., and Fontoura, B.M. (2014). Nuclear trafficking in health and disease. *Current opinion in cell biology* 28, 28-35.
- Morimoto, R.I. (2008). Proteotoxic stress and inducible chaperone networks in neurodegenerative disease and aging. *Genes Dev* 22, 1427-1438.
- Mosmann, T. (1983). Rapid colorimetric assay for cellular growth and survival: application to proliferation and cytotoxicity assays. *J Immunol Methods* 65, 55-63.
- Mossuto, M.F., Dhulesia, A., Devlin, G., Frare, E., Kumita, J.R., de Laureto, P.P., Dumoulin, M., Fontana, A., Dobson, C.M., and Salvatella, X. (2010). The non-core regions of human lysozyme amyloid fibrils influence cytotoxicity. *J Mol Biol* 402, 783-796.
- Mukherjee, A., Morales-Scheihing, D., Butler, P.C., and Soto, C. (2015). Type 2 diabetes as a protein misfolding disease. *Trends Mol Med*.
- Mukhopadhyay, D., and Riezman, H. (2007). Proteasome-independent functions of ubiquitin in endocytosis and signaling. *Science* 315, 201-205.
- Mulkijanian, A.Y., Bychkov, A.Y., Dibrova, D.V., Galperin, M.Y., and Koonin, E.V. (2012). Origin of first cells at terrestrial, anoxic geothermal fields. *Proc Natl Acad Sci U S A* 109, E821-830.
- Müller-McNicoll, M., and Neugebauer, K.M. (2013). How cells get the message: dynamic assembly and function of mRNA-protein complexes. *Nat Rev Genet* 14, 275-287.
- Muller-Rischart, A.K., Pilsl, A., Beaudette, P., Patra, M., Hadian, K., Funke, M., Peis, R., Deinlein, A., Schweimer, C., Kuhn, P.H., *et al.* (2013). The E3 ligase parkin maintains mitochondrial integrity by increasing linear ubiquitination of NEMO. *Mol Cell* 49, 908-921.
- Mullis, K., Faloona, F., Scharf, S., Saiki, R., Horn, G., and Erlich, H. (1986). Specific enzymatic amplification of DNA in vitro: the polymerase chain reaction. *Cold Spring Harb Symp Quant Biol* 51 Pt 1, 263-273.
- Munch, C., O'Brien, J., and Bertolotti, A. (2011). Prion-like propagation of mutant superoxide dismutase-1 misfolding in neuronal cells. *Proc Natl Acad Sci U S A* 108, 3548-3553.
- Murakami, H., Ohta, A., Ashigai, H., and Suga, H. (2006). A highly flexible tRNA acylation method for non-natural polypeptide synthesis. *Nat Methods* 3, 357-359.
- Nagai, K., Muto, Y., Pomeranz Krummel, D.A., Kambach, C., Ignjatovic, T., Walke, S., and Kuglstatter, A. (2001). Structure and assembly of the spliceosomal snRNPs. *Novartis Medal Lecture. Biochem Soc Trans* 29, 15-26.
- Nair, S.K., and Burley, S.K. (2003). X-ray structures of Myc-Max and Mad-Max recognizing DNA. Molecular bases of regulation by proto-oncogenic transcription factors. *Cell* 112, 193-205.

- Nargund, A.M., Pellegrino, M.W., Fiorese, C.J., Baker, B.M., and Haynes, C.M. (2012). Mitochondrial import efficiency of ATFS-1 regulates mitochondrial UPR activation. *Science* 337, 587-590.
- Nasir, J., Floresco, S.B., O'Kusky, J.R., Diewert, V.M., Richman, J.M., Zeisler, J., Borowski, A., Marth, J.D., Phillips, A.G., and Hayden, M.R. (1995). Targeted disruption of the Huntington's disease gene results in embryonic lethality and behavioral and morphological changes in heterozygotes. *Cell* 81, 811-823.
- Nath, S., Agholme, L., Kurudenkandy, F.R., Granseth, B., Marcusson, J., and Hallbeck, M. (2012). Spreading of neurodegenerative pathology via neuron-to-neuron transmission of beta-amyloid. *J Neurosci* 32, 8767-8777.
- Neary, D., Snowden, J.S., Mann, D.M., Bowen, D.M., Sims, N.R., Northen, B., Yates, P.O., and Davison, A.N. (1986). Alzheimer's disease: a correlative study. *J Neurol Neurosurg Psychiatry* 49, 229-237.
- Neckers, L. (2007). Heat shock protein 90: the cancer chaperone. *J Biosci* 32, 517-530.
- Nesterov, E.E., Skoch, J., Hyman, B.T., Klunk, W.E., Bacskaï, B.J., and Swager, T.M. (2005). In vivo optical imaging of amyloid aggregates in brain: design of fluorescent markers. *Angew Chem Int Ed Engl* 44, 5452-5456.
- Neupert, W. (2012). A mitochondrial odyssey. *Annu Rev Biochem* 81, 1-33.
- Neupert, W., and Herrmann, J.M. (2007). Translocation of proteins into mitochondria. *Annu Rev Biochem* 76, 723-749.
- Ni, R., Marutle, A., and Nordberg, A. (2013). Modulation of alpha7 nicotinic acetylcholine receptor and fibrillar amyloid-beta interactions in Alzheimer's disease brain. *J Alzheimers Dis* 33, 841-851.
- Nielsen, S.V., Poulsen, E.G., Rebola, C.A., and Hartmann-Petersen, R. (2014). Protein quality control in the nucleus. *Biomolecules* 4, 646-661.
- Nilsberth, C., Westlind-Danielsson, A., Eckman, C.B., Condrón, M.M., Axelman, K., Forsell, C., Stenh, C., Luthman, J., Teplow, D.B., Younkin, S.G., *et al.* (2001). The 'Arctic' APP mutation (E693G) causes Alzheimer's disease by enhanced Abeta protofibril formation. *Nat Neurosci* 4, 887-893.
- Noda, T., Suzuki, K., and Ohsumi, Y. (2002). Yeast autophagosomes: de novo formation of a membrane structure. *Trends in cell biology* 12, 231-235.
- Obeng, E.A., Carlson, L.M., Gutman, D.M., Harrington, W.J., Jr., Lee, K.P., and Boise, L.H. (2006). Proteasome inhibitors induce a terminal unfolded protein response in multiple myeloma cells. *Blood* 107, 4907-4916.
- Oeckinghaus, A., Hayden, M.S., and Ghosh, S. (2011). Crosstalk in NF-kappaB signaling pathways. *Nat Immunol* 12, 695-708.
- Okada, T., Haze, K., Nadanaka, S., Yoshida, H., Seidah, N.G., Hirano, Y., Sato, R., Negishi, M., and Mori, K. (2003). A serine protease inhibitor prevents endoplasmic reticulum stress-induced cleavage but not transport of the membrane-bound transcription factor ATF6. *J Biol Chem* 278, 31024-31032.
- Oksova, E.E. (1975). [Correlation of the volume of the perineural oligodendroglia of the cerebral cortex with their RNA level]. *Arkh Anat Gistol Embriol* 68, 11-14.
- Oksova, E.E. (1975). [Glio-neuronal relationships in the cerebral cortex in senile dementia]. *Zh Nevropatol Psikhiatr Im S S Korsakova* 75, 1026-1030.
- Olzscha, H. (2010). Analyse struktureller Determinanten der toxischen Wirkung amyloider Proteine. In Fakultät für Chemie und Pharmazie (Ludwig-Maximilians-Universität München).
- Olzscha, H., Schermann, S.M., Woerner, A.C., Pinkert, S., Hecht, M.H., Tartaglia, G.G., Vendruscolo, M., Hayer-Hartl, M., Hartl, F.U., and Vabulas, R.M. (2011). Amyloid-like aggregates sequester numerous metastable proteins with essential cellular functions. *Cell* 144, 67-78.
- O'Mahony, A., Raber, J., Montano, M., Foehr, E., Han, V., Lu, S.M., Kwon, H., LeFevour, A., Chakraborty-Sett, S., and Greene, W.C. (2006). NF-kappaB/Rel regulates inhibitory and excitatory neuronal function and synaptic plasticity. *Mol Cell Biol* 26, 7283-7298.
- Ondrejčák, T., Klyubin, I., Hu, N.W., Barry, A.E., Cullen, W.K., and Rowan, M.J. (2010). Alzheimer's disease amyloid beta-protein and synaptic function. *Neuromolecular Med* 12, 13-26.
- O'Neill, L.A., and Kaltschmidt, C. (1997). NF-kappa B: a crucial transcription factor for glial and neuronal cell function. *Trends Neurosci* 20, 252-258.
- Oro, J., and Kimball, A.P. (1961). Synthesis of purines under possible primitive earth conditions. I. Adenine from hydrogen cyanide. *Arch Biochem Biophys* 94, 217-227.
- Oskarsson, M.E., Paulsson, J.F., Schultz, S.W., Ingelsson, M., Westermark, P., and Westermark, G.T. (2015). In vivo seeding and cross-seeding of localized amyloidosis: a molecular link between type 2 diabetes and Alzheimer disease. *Am J Pathol* 185, 834-846.
- Ossato, G., Digman, M.A., Aiken, C., Lukacsovich, T., Marsh, J.L., and Gratton, E. (2010). A two-step path to inclusion formation of huntingtin peptides revealed by number and brightness analysis. *Biophys J* 98, 3078-3085.



- Otto, H., Conz, C., Maier, P., Wolfle, T., Suzuki, C.K., Jenö, P., Rucknagel, P., Stahl, J., and Rospert, S. (2005). The chaperones MPP11 and Hsp70L1 form the mammalian ribosome-associated complex. *Proc Natl Acad Sci U S A* *102*, 10064-10069.
- Pace, C.N., Vajdos, F., Fee, L., Grimsley, G., and Gray, T. (1995). How to measure and predict the molar absorption coefficient of a protein. *Protein Sci* *4*, 2411-2423.
- Palop, J.J., Jones, B., Kekoni, L., Chin, J., Yu, G.Q., Raber, J., Masliah, E., and Mucke, L. (2003). Neuronal depletion of calcium-dependent proteins in the dentate gyrus is tightly linked to Alzheimer's disease-related cognitive deficits. *Proc Natl Acad Sci U S A* *100*, 9572-9577.
- Park, S.H., Kukushkin, Y., Gupta, R., Chen, T., Konagai, A., Hipp, M.S., Hayer-Hartl, M., and Hartl, F.U. (2013). PolyQ proteins interfere with nuclear degradation of cytosolic proteins by sequestering the Sis1p chaperone. *Cell* *154*, 134-145.
- Park, S.J., Sohn, H.Y., and Park, S.I. (2013). TRAIL regulates collagen production through HSF1-dependent Hsp47 expression in activated hepatic stellate cells. *Cell Signal* *25*, 1635-1643.
- Parker, D.S., Davis, A., and Taniuchi, H. (1981). Further study of the conformation of nuclease-(1-126) in relation to intrinsic enzymatic activity. *J Biol Chem* *256*, 4557-4569.
- Parlato, R., and Liss, B. (2014). How Parkinson's disease meets nucleolar stress. *Biochim Biophys Acta* *1842*, 791-797.
- Perona, J.J., Craik, C.S., and Fletterick, R.J. (1993). Locating the catalytic water molecule in serine proteases. *Science* *261*, 620-622.
- Perutz, M. (1994). Polar zippers: their role in human disease. *Protein Sci* *3*, 1629-1637.
- Pesiridis, G.S., Lee, V.M., and Trojanowski, J.Q. (2009). Mutations in TDP-43 link glycine-rich domain functions to amyotrophic lateral sclerosis. *Hum Mol Genet* *18*, R156-162.
- Pickart, C.M. (2001). Mechanisms underlying ubiquitination. *Annu Rev Biochem* *70*, 503-533.
- Polier, S., Hartl, F.U., and Bracher, A. (2010). Interaction of the Hsp110 molecular chaperones from *S. cerevisiae* with substrate protein. *J Mol Biol* *401*, 696-707.
- Poorkaj, P., Bird, T.D., Wijsman, E., Nemens, E., Garruto, R.M., Anderson, L., Andreadis, A., Wiederholt, W.C., Raskind, M., and Schellenberg, G.D. (1998). Tau is a candidate gene for chromosome 17 frontotemporal dementia. *Ann Neurol* *43*, 815-825.
- Posner, M., Kiss, A.J., Skiba, J., Drossman, A., Dolinska, M.B., Hejtmancik, J.F., and Sergeev, Y.V. (2012). Functional validation of hydrophobic adaptation to physiological temperature in the small heat shock protein alphaA-crystallin. *PLoS One* *7*, e34438.
- Prahlad, V., and Morimoto, R.I. (2011). Neuronal circuitry regulates the response of *Caenorhabditis elegans* to misfolded proteins. *Proc Natl Acad Sci U S A* *108*, 14204-14209.
- Pratt, A.J., and MacRae, I.J. (2009). The RNA-induced silencing complex: a versatile gene-silencing machine. *J Biol Chem* *284*, 17897-17901.
- Preissler, S., and Deuerling, E. (2012). Ribosome-associated chaperones as key players in proteostasis. *Trends Biochem Sci* *37*, 274-283.
- Prince, M., Guerchet, M., and Prina, M. (2013). The Global Impact of Dementia 2013–2050 (Alzheimer's Disease International).
- Pringsheim, T., Wiltshire, K., Day, L., Dykeman, J., Steeves, T., and Jette, N. (2012). The incidence and prevalence of Huntington's disease: a systematic review and meta-analysis. *Mov Disord* *27*, 1083-1091.
- Qian, S.B., McDonough, H., Boellmann, F., Cyr, D.M., and Patterson, C. (2006). CHIP-mediated stress recovery by sequential ubiquitination of substrates and Hsp70. *Nature* *440*, 551-555.
- Raina, P., Santaguida, P., Ismail, A., Patterson, C., Cowan, D., Levine, M., Booker, L., and Oremus, M. (2008). Effectiveness of cholinesterase inhibitors and memantine for treating dementia: evidence review for a clinical practice guideline. *Ann Intern Med* *148*, 379-397.
- Ramachandran, G.N., Ramakrishnan, C., and Sasisekharan, V. (1963). Stereochemistry of polypeptide chain configurations. *J Mol Biol* *7*, 95-99.
- Ramirez, O.A., and Couve, A. (2011). The endoplasmic reticulum and protein trafficking in dendrites and axons. *Trends in cell biology* *21*, 219-227.
- Rampelt, H., Kirstein-Miles, J., Nillegoda, N.B., Chi, K., Scholz, S.R., Morimoto, R.I., and Bukau, B. (2012). Metazoan Hsp70 machines use Hsp110 to power protein disaggregation. *EMBO J* *31*, 4221-4235.
- Rape, M., Hoppe, T., Gorr, I., Kalocay, M., Richly, H., and Jentsch, S. (2001). Mobilization of processed, membrane-tethered SPT23 transcription factor by CDC48(UFD1/NPL4), a ubiquitin-selective chaperone. *Cell* *107*, 667-677.

- Rapoport, M., Dawson, H.N., Binder, L.I., Vitek, M.P., and Ferreira, A. (2002). Tau is essential to beta -amyloid-induced neurotoxicity. *Proc Natl Acad Sci U S A* 99, 6364-6369.
- Ratray, I., Smith, E.J., Crum, W.R., Walker, T.A., Gale, R., Bates, G.P., and Modo, M. (2013). Correlations of behavioral deficits with brain pathology assessed through longitudinal MRI and histopathology in the R6/1 mouse model of Huntington's disease. *PLoS One* 8, e84726.
- Raychaudhuri, S., Dey, S., Bhattacharyya, N.P., and Mukhopadhyay, D. (2009). The role of intrinsically unstructured proteins in neurodegenerative diseases. *PLoS One* 4, e5566.
- Redfield, C. (2004). Using nuclear magnetic resonance spectroscopy to study molten globule states of proteins. *Methods* 34, 121-132.
- Refolo, L.M., Pappolla, M.A., LaFrancois, J., Malester, B., Schmidt, S.D., Thomas-Bryant, T., Tint, G.S., Wang, R., Mercken, M., Petanceska, S.S., *et al.* (2001). A cholesterol-lowering drug reduces beta-amyloid pathology in a transgenic mouse model of Alzheimer's disease. *Neurobiol Dis* 8, 890-899.
- Reisberg, B., and Franssen, E.H. (1999). Clinical stages of Alzheimer's disease. An atlas of Alzheimer's disease New York, London: The Parthenon Publishing Group, 11-29.
- Resenberger, U.K., Harmeier, A., Woerner, A.C., Goodman, J.L., Muller, V., Krishnan, R., Vabulas, R.M., Kretschmar, H.A., Lindquist, S., Hartl, F.U., *et al.* (2011). The cellular prion protein mediates neurotoxic signalling of beta-sheet-rich conformers independent of prion replication. *EMBO J* 30, 2057-2070.
- Richly, H., Rape, M., Braun, S., Rumpf, S., Hoege, C., and Jentsch, S. (2005). A series of ubiquitin binding factors connects CDC48/p97 to substrate multiubiquitylation and proteasomal targeting. *Cell* 120, 73-84.
- Ring, D., Wolman, Y., Friedmann, N., and Miller, S.L. (1972). Prebiotic synthesis of hydrophobic and protein amino acids. *Proc Natl Acad Sci U S A* 69, 765-768.
- Riudavets, M.A., Iacono, D., Resnick, S.M., O'Brien, R., Zonderman, A.B., Martin, L.J., Rudow, G., Pletnikova, O., and Troncoso, J.C. (2007). Resistance to Alzheimer's pathology is associated with nuclear hypertrophy in neurons. *Neurobiol Aging* 28, 1484-1492.
- Roberts, R.G. (2014). Living in constant crisis--when stress management becomes the problem. *PLoS Biol* 12, e1001999.
- Rock, K.L., Gramm, C., Rothstein, L., Clark, K., Stein, R., Dick, L., Hwang, D., and Goldberg, A.L. (1994). Inhibitors of the proteasome block the degradation of most cell proteins and the generation of peptides presented on MHC class I molecules. *Cell* 78, 761-771.
- Romisch, K. (2005). Endoplasmic reticulum-associated degradation. *Annual review of cell and developmental biology* 21, 435-456.
- Ros, C., and Kempf, C. (2004). The ubiquitin-proteasome machinery is essential for nuclear translocation of incoming minute virus of mice. *Virology* 324, 350-360.
- Roth, D.M., Hutt, D.M., Tong, J., Boucheccareilh, M., Wang, N., Seeley, T., Dekkers, J.F., Beekman, J.M., Garza, D., Drew, L., *et al.* (2014). Modulation of the maladaptive stress response to manage diseases of protein folding. *PLoS Biol* 12, e1001998.
- Rothman, J.E. (1989). Polypeptide chain binding proteins: catalysts of protein folding and related processes in cells. *Cell* 59, 591-601.
- Rubinsztein, D.C., Marino, G., and Kroemer, G. (2011). Autophagy and aging. *Cell* 146, 682-695.
- Rudiger, S., Germeroth, L., Schneider-Mergener, J., and Bukau, B. (1997). Substrate specificity of the DnaK chaperone determined by screening cellulose-bound peptide libraries. *EMBO J* 16, 1501-1507.
- Runkel, E.D., Liu, S., Baumeister, R., and Schulze, E. (2013). Surveillance-activated defenses block the ROS-induced mitochondrial unfolded protein response. *PLoS Genet* 9, e1003346.
- Rüßmann, F., Stemp, M.J., Monkemeyer, L., Etchells, S.A., Bracher, A., and Hartl, F.U. (2012). Folding of large multidomain proteins by partial encapsulation in the chaperonin TRiC/CCT. *Proc Natl Acad Sci U S A* 109, 21208-21215.
- Rutherford, S.L. (2003). Between genotype and phenotype: protein chaperones and evolvability. *Nat Rev Genet* 4, 263-274.
- Rutherford, S.M., and Gilani, G.S. (2009). Amino acid analysis. *Curr Protoc Protein Sci Chapter 11*, Unit 11 19.
- Ryan, N.S., Keihaninejad, S., Shakespeare, T.J., Lehmann, M., Crutch, S.J., Malone, I.B., Thornton, J.S., Mancini, L., Hyare, H., Yousry, T., *et al.* (2013). Magnetic resonance imaging evidence for presymptomatic change in thalamus and caudate in familial Alzheimer's disease. *Brain* 136, 1399-1414.
- Sabatini, D.D., Blobel, G., Nonomura, Y., and Adelman, M.R. (1971). Ribosome-membrane interaction: Structural aspects and functional implications. *Adv Cytopharmacol* 1, 119-129.
- Sagan, L. (1967). On the origin of mitosing cells. *J Theor Biol* 14, 255-274.

- Saganich, M.J., Schroeder, B.E., Galvan, V., Bredesen, D.E., Koo, E.H., and Heinemann, S.F. (2006). Deficits in synaptic transmission and learning in amyloid precursor protein (APP) transgenic mice require C-terminal cleavage of APP. *J Neurosci* 26, 13428-13436.
- Salles, A., Romano, A., and Freudenthal, R. (2014). Synaptic NF-kappa B pathway in neuronal plasticity and memory. *J Physiol Paris* 108, 256-262.
- Sansom, S.N., Griffiths, D.S., Faedo, A., Kleinjan, D.J., Ruan, Y., Smith, J., van Heyningen, V., Rubenstein, J.L., and Livesey, F.J. (2009). The level of the transcription factor Pax6 is essential for controlling the balance between neural stem cell self-renewal and neurogenesis. *PLoS Genet* 5, e1000511.
- Sant'Anna, R., Braga, C., Varejao, N., Pimenta, K.M., Grana-Montes, R., Alves, A., Cortines, J., Cordeiro, Y., Ventura, S., and Foguel, D. (2014). The importance of a gatekeeper residue on the aggregation of transthyretin: implications for transthyretin-related amyloidoses. *J Biol Chem* 289, 28324-28337.
- Sarikas, A., Hartmann, T., and Pan, Z.Q. (2011). The cullin protein family. *Genome Biol* 12, 220.
- Sawaya, M.R., Sambashivan, S., Nelson, R., Ivanova, M.I., Sievers, S.A., Apostol, M.I., Thompson, M.J., Balbirnie, M., Wiltzius, J.J., McFarlane, H.T., *et al.* (2007). Atomic structures of amyloid cross-beta spines reveal varied steric zippers. *Nature* 447, 453-457.
- Schaffar, G., Breuer, P., Boteva, R., Behrends, C., Tzvetkov, N., Strippel, N., Sakahira, H., Siegers, K., Hayer-Hartl, M., and Hartl, F.U. (2004). Cellular toxicity of polyglutamine expansion proteins: mechanism of transcription factor deactivation. *Mol Cell* 15, 95-105.
- Scheff, S.W., and Price, D.A. (2006). Alzheimer's disease-related alterations in synaptic density: neocortex and hippocampus. *J Alzheimers Dis* 9, 101-115.
- Scheff, S.W., Price, D.A., Schmitt, F.A., and Mufson, E.J. (2006). Hippocampal synaptic loss in early Alzheimer's disease and mild cognitive impairment. *Neurobiol Aging* 27, 1372-1384.
- Scheper, W., and Hoozemans, J.J. (2015). The unfolded protein response in neurodegenerative diseases: a neuropathological perspective. *Acta Neuropathol*.
- Scheufler, C., Brinker, A., Bourenkov, G., Pegoraro, S., Moroder, L., Bartunik, H., Hartl, F.U., and Moarefi, I. (2000). Structure of TPR domain-peptide complexes: critical elements in the assembly of the Hsp70-Hsp90 multichaperone machine. *Cell* 101, 199-210.
- Schindler, T., Herrler, M., Marahiel, M.A., and Schmid, F.X. (1995). Extremely rapid protein folding in the absence of intermediates. *Nat Struct Biol* 2, 663-673.
- Schroder, M., Chang, J.S., and Kaufman, R.J. (2000). The unfolded protein response represses nitrogen-starvation induced developmental differentiation in yeast. *Genes Dev* 14, 2962-2975.
- Schroder, M., and Kaufman, R.J. (2005). The mammalian unfolded protein response. *Annu Rev Biochem* 74, 739-789.
- Scopes, R.K. (1974). Measurement of protein by spectrophotometry at 205 nm. *Anal Biochem* 59, 277-282.
- Sen, R. (2011). The origins of NF-kappaB. *Nat Immunol* 12, 686-688.
- Serrano-Pozo, A., Frosch, M.P., Masliah, E., and Hyman, B.T. (2011). Neuropathological alterations in Alzheimer disease. *Cold Spring Harb Perspect Med* 1, a006189.
- Shaw, G., Morse, S., Ararat, M., and Graham, F.L. (2002). Preferential transformation of human neuronal cells by human adenoviruses and the origin of HEK 293 cells. *FASEB journal : official publication of the Federation of American Societies for Experimental Biology* 16, 869-871.
- Shearman, M.S., Hawtin, S.R., and Taylor, V.J. (1995). The intracellular component of cellular 3-(4,5-dimethylthiazol-2-yl)-2, 5-diphenyltetrazolium bromide (MTT) reduction is specifically inhibited by beta-amyloid peptides. *J Neurochem* 65, 218-227.
- Sheffield, L.G., Miskiewicz, H.B., Tannenbaum, L.B., and Mirra, S.S. (2006). Nuclear pore complex proteins in Alzheimer disease. *J Neuropathol Exp Neurol* 65, 45-54.
- Shimohata, T., Onodera, O., and Tsuji, S. (2000). Interaction of expanded polyglutamine stretches with nuclear transcription factors leads to aberrant transcriptional regulation in polyglutamine diseases. *Neuropathology* 20, 326-333.
- Shorter, J. (2011). The mammalian disaggregase machinery: Hsp110 synergizes with Hsp70 and Hsp40 to catalyze protein disaggregation and reactivation in a cell-free system. *PLoS One* 6, e26319.
- Siegel, A. (2011). Why are most alpha helices in proteins right handed? (Quora; <http://www.quora.com/Why-are-most-alpha-helices-in-proteins-right-handed>).
- Sieradzan, K.A., Mechan, A.O., Jones, L., Wanker, E.E., Nukina, N., and Mann, D.M. (1999). Huntington's disease intranuclear inclusions contain truncated, ubiquitinated huntingtin protein. *Exp Neurol* 156, 92-99.

- Silva, J.L., De Moura Gallo, C.V., Costa, D.C., and Rangel, L.P. (2014). Prion-like aggregation of mutant p53 in cancer. *Trends Biochem Sci* 39, 260-267.
- Somero, G.N. (1995). Proteins and temperature. *Annu Rev Physiol* 57, 43-68.
- Soto, C. (2003). Unfolding the role of protein misfolding in neurodegenerative diseases. *Nat Rev Neurosci* 4, 49-60.
- Sperling, R.A., Jack, C.R., Jr., and Aisen, P.S. (2011). Testing the right target and right drug at the right stage. *Sci Transl Med* 3, 111cm133.
- Spolar, R.S., and Record, M.T., Jr. (1994). Coupling of local folding to site-specific binding of proteins to DNA. *Science* 263, 777-784.
- Sreerama, N., and Woody, R.W. (2000). Estimation of protein secondary structure from circular dichroism spectra: comparison of CONTIN, SELCON, and CDSSTR methods with an expanded reference set. *Anal Biochem* 287, 252-260.
- Steiner, H., Fluhrer, R., and Haass, C. (2008). Intramembrane proteolysis by gamma-secretase. *J Biol Chem* 283, 29627-29631.
- Stickle, D.F., Presta, L.G., Dill, K.A., and Rose, G.D. (1992). Hydrogen bonding in globular proteins. *J Mol Biol* 226, 1143-1159.
- Stryer, L. (1965). The interaction of a naphthalene dye with apomyoglobin and apohemoglobin. A fluorescent probe of non-polar binding sites. *J Mol Biol* 13, 482-495.
- Sugars, K.L., and Rubinsztein, D.C. (2003). Transcriptional abnormalities in Huntington disease. *Trends Genet* 19, 233-238.
- Suhr, S.T., Senut, M.C., Whitelegge, J.P., Faull, K.F., Cuizon, D.B., and Gage, F.H. (2001). Identities of sequestered proteins in aggregates from cells with induced polyglutamine expression. *J Cell Biol* 153, 283-294.
- Szabo, I., and Zoratti, M. (1991). The giant channel of the inner mitochondrial membrane is inhibited by cyclosporin A. *J Biol Chem* 266, 3376-3379.
- Szebeni, A., and Olson, M.O. (1999). Nucleolar protein B23 has molecular chaperone activities. *Protein Sci* 8, 905-912.
- Taipale, M., Jarosz, D.F., and Lindquist, S. (2010). HSP90 at the hub of protein homeostasis: emerging mechanistic insights. *Nat Rev Mol Cell Biol* 11, 515-528.
- Taipale, M., Krykbaeva, I., Koeva, M., Kayatekin, C., Westover, K.D., Karras, G.I., and Lindquist, S. (2012). Quantitative analysis of HSP90-client interactions reveals principles of substrate recognition. *Cell* 150, 987-1001.
- Tanzi, R.E. (2012). The genetics of Alzheimer disease. *Cold Spring Harb Perspect Med* 2.
- Tartaglia, G.G., and Vendruscolo, M. (2008). The Zyggregator method for predicting protein aggregation propensities. *Chem Soc Rev* 37, 1395-1401.
- Teske, B.F., Wek, S.A., Bunpo, P., Cundiff, J.K., McClintick, J.N., Anthony, T.G., and Wek, R.C. (2011). The eIF2 kinase PERK and the integrated stress response facilitate activation of ATF6 during endoplasmic reticulum stress. *Mol Biol Cell* 22, 4390-4405.
- Thompson, P.M., Hayashi, K.M., Sowell, E.R., Gogtay, N., Giedd, J.N., Rapoport, J.L., de Zubicaray, G.I., Janke, A.L., Rose, S.E., Semple, J., *et al.* (2004). Mapping cortical change in Alzheimer's disease, brain development, and schizophrenia. *Neuroimage* 23 Suppl 1, S2-18.
- Tomiya, T., Nagata, T., Shimada, H., Teraoka, R., Fukushima, A., Kanemitsu, H., Takuma, H., Kuwano, R., Imagawa, M., Ataka, S., *et al.* (2008). A new amyloid beta variant favoring oligomerization in Alzheimer's-type dementia. *Ann Neurol* 63, 377-387.
- Towbin, H., Staehelin, T., and Gordon, J. (1979). Electrophoretic transfer of proteins from polyacrylamide gels to nitrocellulose sheets: procedure and some applications. *Proc Natl Acad Sci U S A* 76, 4350-4354.
- Toyama, B.H., Savas, J.N., Park, S.K., Harris, M.S., Ingolia, N.T., Yates, J.R., 3rd, and Hetzer, M.W. (2013). Identification of long-lived proteins reveals exceptional stability of essential cellular structures. *Cell* 154, 971-982.
- Tran, H.T., Mao, A., and Pappu, R.V. (2008). Role of backbone-solvent interactions in determining conformational equilibria of intrinsically disordered proteins. *J Am Chem Soc* 130, 7380-7392.
- Tsang, W.Y., and Lemire, B.D. (2002). Mitochondrial genome content is regulated during nematode development. *Biochem Biophys Res Commun* 291, 8-16.
- Tuck, A.C., and Tollervey, D. (2013). A transcriptome-wide atlas of RNP composition reveals diverse classes of mRNAs and lncRNAs. *Cell* 154, 996-1009.
- Tyedmers, J., Mogk, A., and Bukau, B. (2010). Cellular strategies for controlling protein aggregation. *Nat Rev Mol Cell Biol* 11, 777-788.
- Tyler, S.J., Dawbarn, D., Wilcock, G.K., and Allen, S.J. (2002). alpha- and beta-secretase: profound changes in Alzheimer's disease. *Biochem Biophys Res Commun* 299, 373-376.

- Ulmer, T.S., Bax, A., Cole, N.B., and Nussbaum, R.L. (2005). Structure and dynamics of micelle-bound human alpha-synuclein. *J Biol Chem* *280*, 9595-9603.
- Um, J.W., Park, H.J., Song, J., Jeon, I., Lee, G., Lee, P.H., and Chung, K.C. (2010). Formation of parkin aggregates and enhanced PINK1 accumulation during the pathogenesis of Parkinson's disease. *Biochem Biophys Res Commun* *393*, 824-828.
- Um, J.W., Stichel-Gunkel, C., Lubbert, H., Lee, G., and Chung, K.C. (2009). Molecular interaction between parkin and PINK1 in mammalian neuronal cells. *Molecular and cellular neurosciences* *40*, 421-432.
- Unverdorben, P., Beck, F., Sledz, P., Schweitzer, A., Pfeifer, G., Plitzko, J.M., Baumeister, W., and Forster, F. (2014). Deep classification of a large cryo-EM dataset defines the conformational landscape of the 26S proteasome. *Proc Natl Acad Sci U S A* *111*, 5544-5549.
- Uversky, V.N., Gillespie, J.R., and Fink, A.L. (2000). Why are "natively unfolded" proteins unstructured under physiological conditions? *Proteins* *41*, 415-427.
- Vassar, P.S., and Culling, C.F. (1959). Fluorescent stains, with special reference to amyloid and connective tissues. *Arch Pathol* *68*, 487-498.
- Velazquez, J.M., and Lindquist, S. (1984). hsp70: nuclear concentration during environmental stress and cytoplasmic storage during recovery. *Cell* *36*, 655-662.
- Vembar, S.S., and Brodsky, J.L. (2008). One step at a time: endoplasmic reticulum-associated degradation. *Nat Rev Mol Cell Biol* *9*, 944-957.
- Vijay-Kumar, S., Bugg, C.E., and Cook, W.J. (1987). Structure of ubiquitin refined at 1.8 Å resolution. *J Mol Biol* *194*, 531-544.
- Vilchez, D., Boyer, L., Morantte, I., Lutz, M., Merkwirth, C., Joyce, D., Spencer, B., Page, L., Masliah, E., Berggren, W.T., *et al.* (2012). Increased proteasome activity in human embryonic stem cells is regulated by PSMD11. *Nature* *489*, 304-308.
- Viphakone, N., Hautbergue, G.M., Walsh, M., Chang, C.T., Holland, A., Folco, E.G., Reed, R., and Wilson, S.A. (2012). TREX exposes the RNA-binding domain of Nxf1 to enable mRNA export. *Nat Commun* *3*, 1006.
- Voges, D., Zwickl, P., and Baumeister, W. (1999). The 26S proteasome: a molecular machine designed for controlled proteolysis. *Annu Rev Biochem* *68*, 1015-1068.
- Waelter, S., Boeddrich, A., Lurz, R., Scherzinger, E., Lueder, G., Lehrach, H., and Wanker, E.E. (2001). Accumulation of mutant huntingtin fragments in aggresome-like inclusion bodies as a result of insufficient protein degradation. *Mol Biol Cell* *12*, 1393-1407.
- Wahl, M.C., Will, C.L., and Luhrmann, R. (2009). The spliceosome: design principles of a dynamic RNP machine. *Cell* *136*, 701-718.
- Waldburger, C.D., Jonsson, T., and Sauer, R.T. (1996). Barriers to protein folding: formation of buried polar interactions is a slow step in acquisition of structure. *Proc Natl Acad Sci U S A* *93*, 2629-2634.
- Walther, D.M., Kasturi, P., Zheng, M., Pinkert, S., Vecchi, G., Ciryam, P., Morimoto, R.I., Dobson, C.M., Vendruscolo, M., Mann, M., *et al.* (2015). Widespread Proteome Remodeling and Aggregation in Aging *C. elegans*. *Cell* *161*, 919-932.
- Wang, C.E., Zhou, H., McGuire, J.R., Cerullo, V., Lee, B., Li, S.H., and Li, X.J. (2008). Suppression of neuropil aggregates and neurological symptoms by an intracellular antibody implicates the cytoplasmic toxicity of mutant huntingtin. *J Cell Biol* *181*, 803-816.
- Wang, W., and Hecht, M.H. (2002). Rationally designed mutations convert de novo amyloid-like fibrils into monomeric beta-sheet proteins. *Proc Natl Acad Sci U S A* *99*, 2760-2765.
- Wei, Y., Kim, S., Fela, D., Baum, J., and Hecht, M.H. (2003). Solution structure of a de novo protein from a designed combinatorial library. *Proc Natl Acad Sci U S A* *100*, 13270-13273.
- Welch, W.J., and Feramisco, J.R. (1984). Nuclear and nucleolar localization of the 72,000-dalton heat shock protein in heat-shocked mammalian cells. *J Biol Chem* *259*, 4501-4513.
- Wen, W., Zhu, W., He, Y., Kochan, N.A., Reppermund, S., Slavin, M.J., Brodaty, H., Crawford, J., Xia, A., and Sachdev, P. (2011). Discrete neuroanatomical networks are associated with specific cognitive abilities in old age. *J Neurosci* *31*, 1204-1212.
- West, M.W., Wang, W., Patterson, J., Mancias, J.D., Beasley, J.R., and Hecht, M.H. (1999). De novo amyloid proteins from designed combinatorial libraries. *Proc Natl Acad Sci U S A* *96*, 11211-11216.
- Williams, S.C. (2013). Alzheimer's disease: Mapping the brain's decline. *Nature* *502*, S84-85.
- Wimo, A., Jonsson, L., Bond, J., Prince, M., and Winblad, B. (2013). The worldwide economic impact of dementia 2010. *Alzheimers Dement* *9*, 1-11 e13.

- Winkler, E., Kamp, F., Scheuring, J., Ebke, A., Fukumori, A., and Steiner, H. (2012). Generation of Alzheimer disease-associated amyloid beta42/43 peptide by gamma-secretase can be inhibited directly by modulation of membrane thickness. *J Biol Chem* *287*, 21326-21334.
- Winklhofer, K.F., Henn, I.H., Kay-Jackson, P.C., Heller, U., and Tatzelt, J. (2003). Inactivation of parkin by oxidative stress and C-terminal truncations: a protective role of molecular chaperones. *J Biol Chem* *278*, 47199-47208.
- Winklhofer, K.F., Tatzelt, J., and Haass, C. (2008). The two faces of protein misfolding: gain- and loss-of-function in neurodegenerative diseases. *EMBO J* *27*, 336-349.
- Woerner, A.C., Frottin, F., Hornburg, D., Feng, L.R., Meissner, F., Patra, M., Tatzelt, J., Mann, M., Winklhofer, K.F., Hartl, F.U., *et al.* (2016). Cytoplasmic protein aggregates interfere with nucleocytoplasmic transport of protein and RNA. *Science* *351*, 173-176.
- Wojcik, C., and DeMartino, G.N. (2003). Intracellular localization of proteasomes. *The international journal of biochemistry & cell biology* *35*, 579-589.
- Wolff, S., Weissman, J.S., and Dillin, A. (2014). Differential scales of protein quality control. *Cell* *157*, 52-64.
- Woulfe, J.M. (2007). Abnormalities of the nucleus and nuclear inclusions in neurodegenerative disease: a work in progress. *Neuropathol Appl Neurobiol* *33*, 2-42.
- Wytttenbach, A., Swartz, J., Kita, H., Thykjaer, T., Carmichael, J., Bradley, J., Brown, R., Maxwell, M., Schapira, A., Orntoft, T.F., *et al.* (2001). Polyglutamine expansions cause decreased CRE-mediated transcription and early gene expression changes prior to cell death in an inducible cell model of Huntington's disease. *Hum Mol Genet* *10*, 1829-1845.
- Xia, J., Lee, D.H., Taylor, J., Vandelft, M., and Truant, R. (2003). Huntingtin contains a highly conserved nuclear export signal. *Hum Mol Genet* *12*, 1393-1403.
- Yam, A.Y., Xia, Y., Lin, H.T., Burlingame, A., Gerstein, M., and Frydman, J. (2008). Defining the TRiC/CCT interactome links chaperonin function to stabilization of newly made proteins with complex topologies. *Nat Struct Mol Biol* *15*, 1255-1262.
- Yamamoto, A., and Yue, Z. (2014). Autophagy and its normal and pathogenic states in the brain. *Annual review of neuroscience* *37*, 55-78.
- Yan, W., Frank, C.L., Korth, M.J., Sopher, B.L., Novoa, I., Ron, D., and Katze, M.G. (2002). Control of PERK eIF2alpha kinase activity by the endoplasmic reticulum stress-induced molecular chaperone P58IPK. *Proc Natl Acad Sci U S A* *99*, 15920-15925.
- Yang, C., Tan, W., Whittle, C., Qiu, L., Cao, L., Akbarian, S., and Xu, Z. (2010). The C-terminal TDP-43 fragments have a high aggregation propensity and harm neurons by a dominant-negative mechanism. *PLoS One* *5*, e15878.
- Yang, C., Wang, H., Qiao, T., Yang, B., Aliaga, L., Qiu, L., Tan, W., Salameh, J., McKenna-Yasek, D.M., Smith, T., *et al.* (2014). Partial loss of TDP-43 function causes phenotypes of amyotrophic lateral sclerosis. *Proc Natl Acad Sci U S A* *111*, E1121-1129.
- Yang, H., Li, J.J., Liu, S., Zhao, J., Jiang, Y.J., Song, A.X., and Hu, H.Y. (2014). Aggregation of polyglutamine-expanded ataxin-3 sequesters its specific interacting partners into inclusions: implication in a loss-of-function pathology. *Sci Rep* *4*, 6410.
- Yano, H., Baranov, S.V., Baranova, O.V., Kim, J., Pan, Y., Yablonska, S., Carlisle, D.L., Ferrante, R.J., Kim, A.H., and Friedlander, R.M. (2014). Inhibition of mitochondrial protein import by mutant huntingtin. *Nat Neurosci* *17*, 822-831.
- Yoneda, T., Benedetti, C., Urano, F., Clark, S.G., Harding, H.P., and Ron, D. (2004). Compartment-specific perturbation of protein handling activates genes encoding mitochondrial chaperones. *J Cell Sci* *117*, 4055-4066.
- Yoshida, H., Matsui, T., Yamamoto, A., Okada, T., and Mori, K. (2001). XBP1 mRNA is induced by ATF6 and spliced by IRE1 in response to ER stress to produce a highly active transcription factor. *Cell* *107*, 881-891.
- Young, J.C., Agashe, V.R., Siegers, K., and Hartl, F.U. (2004). Pathways of chaperone-mediated protein folding in the cytosol. *Nat Rev Mol Cell Biol* *5*, 781-791.
- Young, J.C., Hoogenraad, N.J., and Hartl, F.U. (2003). Molecular chaperones Hsp90 and Hsp70 deliver preproteins to the mitochondrial import receptor Tom70. *Cell* *112*, 41-50.
- Zandomenighi, G., Krebs, M.R., McCammon, M.G., and Fandrich, M. (2004). FTIR reveals structural differences between native beta-sheet proteins and amyloid fibrils. *Protein Sci* *13*, 3314-3321.
- Zeeb, M., and Balbach, J. (2005). NMR spectroscopic characterization of millisecond protein folding by transverse relaxation dispersion measurements. *J Am Chem Soc* *127*, 13207-13212.

- Zeitlin, S., Liu, J.P., Chapman, D.L., Papaioannou, V.E., and Efstratiadis, A. (1995). Increased apoptosis and early embryonic lethality in mice nullizygous for the Huntington's disease gene homologue. *Nat Genet* 17, 155-163.
- Zhai, W., Jeong, H., Cui, L., Krainc, D., and Tjian, R. (2005). In vitro analysis of huntingtin-mediated transcriptional repression reveals multiple transcription factor targets. *Cell* 123, 1241-1253.
- Zhang, K., Donnelly, C.J., Haeusler, A.R., Grima, J.C., Machamer, J.B., Steinwald, P., Daley, E.L., Miller, S.J., Cunningham, K.M., Vidensky, S., *et al.* (2015). The C9orf72 repeat expansion disrupts nucleocytoplasmic transport. *Nature* 525, 56-61.
- Zhang, K., and Kaufman, R.J. (2008). From endoplasmic-reticulum stress to the inflammatory response. *Nature* 454, 455-462.
- Zhang, L., Xu, M., Scotti, E., Chen, Z.J., and Tontonoz, P. (2013). Both K63 and K48 ubiquitin linkages signal lysosomal degradation of the LDL receptor. *Journal of lipid research* 54, 1410-1420.
- Zhang, X., and Qian, S.B. (2011). Chaperone-mediated hierarchical control in targeting misfolded proteins to aggresomes. *Mol Biol Cell* 22, 3277-3288.
- Zhang, Y., Ona, V.O., Li, M., Drozda, M., Dubois-Dauphin, M., Przedborski, S., Ferrante, R.J., and Friedlander, R.M. (2003). Sequential activation of individual caspases, and of alterations in Bcl-2 proapoptotic signals in a mouse model of Huntington's disease. *J Neurochem* 87, 1184-1192.
- Zhao, S., and Ulrich, H.D. (2010). Distinct consequences of posttranslational modification by linear versus K63-linked polyubiquitin chains. *Proc Natl Acad Sci U S A* 107, 7704-7709.
- Zheng, H., and Koo, E.H. (2011). Biology and pathophysiology of the amyloid precursor protein. *Molecular neurodegeneration* 6, 27.
- Zhou, H., and Zhou, Y. (2002). Folding rate prediction using total contact distance. *Biophys J* 82, 458-463.
- Zhou, H.X., Rivas, G., and Minton, A.P. (2008). Macromolecular crowding and confinement: biochemical, biophysical, and potential physiological consequences. *Annu Rev Biophys* 37, 375-397.
- Zhou, Y., and King, M.L. (2004). Sending RNAs into the future: RNA localization and germ cell fate. *IUBMB Life* 56, 19-27.
- Zimmerman, S.B., and Trach, S.O. (1991). Estimation of macromolecule concentrations and excluded volume effects for the cytoplasm of *Escherichia coli*. *J Mol Biol* 222, 599-620.
- Zou, Q., Bennion, B.J., Daggett, V., and Murphy, K.P. (2002). The molecular mechanism of stabilization of proteins by TMAO and its ability to counteract the effects of urea. *J Am Chem Soc* 124, 1192-1202.

## Publications

**Woerner AC**, Frottin F, Hornburg D, Feng LR, Meissner F, Patra M, Tatzelt J, Mann M, Winklhofer KF, Hartl FU, Hipp MS. *Cytoplasmic protein aggregates interfere with nucleocytoplasmic transport of protein and RNA*. **Science**. 2016 Jan 8; 351:173-6.

Comments in Da Cruz S, Cleveland DW. *Cell biology. Disrupted nuclear import-export in neurodegeneration*. **Science**. 2016 Jan 8; 351: 125-126.

Minton K. *Mechanisms of disease: Stopping traffic*. **Nat Rev Mol Cell Biol**. 2016 Jan 17; 2.

Tamburrino A, Decressac M. *Spotlight. Aged and Diseased Neurons Get Lost in Transport*. **Trends in Neurosciences**. 2016 Apr 01; 4: 199-201

Resenberger UK, Harmeier A, **Woerner AC**, Goodman JL, Müller V, Krishnan R, Vabulas RM, Kretzschmar HA, Lindquist S, Hartl FU, Multhaup G, Winklhofer KF, Tatzelt J. *The cellular prion protein mediates neurotoxic signalling of  $\beta$ -sheet-rich conformers independent of prion replication*. **EMBO J**. 2011 May 18; 30(10):2057-70.

Olzscha H, Schermann SM, **Woerner AC**, Pinkert S, Hecht MH, Tartaglia GG, Vendruscolo M, Hayer-Hartl M, Hartl FU, Vabulas RM. *Amyloid-like aggregates sequester numerous metastable proteins with essential cellular functions*. **Cell**. 2011 Jan 7; 144(1):67-78.

Hempelmann F, Hölper S, Verhoefen MK, **Woerner AC**, Köhler T, Fiedler SA, Pflieger N, Wachtveitl J, Glaubitz C. *His75-Asp97 cluster in green proteorhodopsin*. **J Am Chem Soc**. 2011 Mar 30; 133(12):4645-54.

Lörinczi E, Verhoefen MK, Wachtveitl J, **Woerner AC**, Glaubitz C, Engelhard M, Bamberg E, Friedrich T. *Voltage- and pH-dependent changes in vectoriality of photocurrents mediated by wild-type and mutant proteorhodopsins upon expression in *Xenopus* oocytes*. **J Mol Biol**. 2009 Oct 23; 393(2):320-41.

Pflieger N, **Woerner AC**, Yang J, Shastri S, Hellmich UA, Aslimovska L, Maier MS, Glaubitz C. *Solid-state NMR and functional studies on proteorhodopsin*. **Biochim Biophys Acta**. 2009 Jun; 1787(6):697-705.

Pflieger N, Lorch M, **Woerner AC**, Shastri S, Glaubitz C. *Characterisation of Schiff base and chromophore in green proteorhodopsin by solid-state NMR*. **J Biomol NMR**. 2008 Jan; 40(1):15-21.

Lenz MO, **Woerner AC**, Glaubitz C, Wachtveitl J. *Photoisomerization in proteorhodopsin mutant D97N*. **Photochem Photobiol**. 2007 Mar-Apr; 83(2):226-31.